ABSORPTIONSQUERSCHNITTE VON IN DER PHOTOLYSE VON J_2 UND O_3 UND IN DER ATMOSPHÄRE RELEVANTEN JODVERBINDUNGEN

ABSORPTION CROSS SECTIONS FOR IODINE SPECIES OF RELEVANCE TO THE PHOTOLYSIS OF MIXTURES OF I_2 AND O_3 AND FOR THE ATMOSPHERE

Dissertation zur Erlangung des Grades

Doktor der Naturwissenschaften

am Fachbereich Physik

der Universität Bremen

vorgelegt von

Dipl. Ing. (univ.) Dipl. Phys. Peter Spietz

Bremen, März 2005

ABSTRACT

In this study the absorption spectra of iodine species and their absorption cross sections had been studied. To this end two independent set-ups were optimised and synchronised to allow independent static measurements as well as simultaneous time resolved UV-vis molecular absorption and VUV-UV resonance absorption measurements. Molecular absorption measurements were performed with a CCD camera providing time resolved optical multichannel data. The resonance absorption set-up used a fast single channel photo multiplier tube. With the resonance absorption set-up the absorption cross section of the I($^2P_{3/2}$) 183.038nm transition was determined to be $(5.42\pm0.8)\cdot10^{-14}cm^2\cdot atom^{-1}$ at the centre of the line in agreement with previous data. With the molecular absorption set-up the absolute absorption cross section of I_2 was checked in an independent measurement and the uncertainty of the result could be reduced yielding $\sigma_{I_2}(500nm)=(2.18_6\pm0.02_1)\cdot10^{-18}cm^2\cdot molec^{-1}$ in very good agreement with previously published data. Based on all available data a weighted average of $\sigma_{I_2}(500nm)=(2.19_1\pm0.02)\cdot10^{-18}cm^2\cdot molec^{-1}$ is recommended. With the synchronised combined set-up absorption spectra and cross sections of iodine oxides were studied by flash photolysis of mixtures of I_2 and O_3 in bath gases N_2 and O_2. A method based on Independent Component Analysis and Principal Components Analysis and least squares techniques was developed to separate overlapping absorption from different absorbers recorded in time resolved optical multichannel measurements. The method enables the extraction of pure curves of temporal behaviour of optical density and of pure spectra with an accuracy of ±3%. Individual spectra for ground state IO(ν'←0), vibrationally excited IO(ν'←ν"), ν">0, as well as OIO and three further yet unidentified absorbers were obtained. Analysis of the absorption continuum of IO provided evidence for two optically active repulsive states intersecting with the upper IO($A^2\Pi_i$) state. Anomalous behaviour of the IO(2←0) band was observed which could be explained by chemiluminescence from the IO($A^2\Pi_i$), ν'=2 state, but the source for IO in this state remains unclear. During the first stages of reaction the population of IO was found to be strongly inverted with vibrationally excited IO of up to ν"=7 and 25% in ν"=1, while in thermal equilibrium only 4% should be present. This required separate determination of cross sections for ground state and vibrationally excited state IO. The effect of low resolution and coarse binning on apparent optical density and absolute cross sections of different absorption

bands was studied and a method developed to correct corresponding effects in low resolution measurements. Significant non-linear behaviour of apparent optical density with concentration was found for IO(4←1), of relevance to studies of chemical kinetics and cross sections. A method to determine absolute absorption cross sections from curves of temporal behaviour of optical density was developed, which is independent of chemical modelling and chemical kinetics reference data using the principle of conservation of iodine throughout the course of reaction. Absorption cross sections for iodine oxides were determined to be $\sigma_{IO}(4\leftarrow0) = (3.5\pm0.3)\cdot10^{-17}cm^2\cdot molec^{-1}$ at 0.12nm FWHM for ground state IO only, $\sigma_{IO,eff}(3\leftarrow1) = (2.0\pm0.8)\cdot10^{-17}cm^2\cdot molec^{-1}$ at 0.35nm FWHM for an overall cross section for vibrationally excited IO of $\nu''>0$, further a cross section for the IO $\nu''=1$ progression of $\sigma_{IO}(3\leftarrow1) = (4.5\pm0.5)\cdot10^{-17}cm^2\cdot molec^{-1}$ at 0.12nm FWHM, and for OIO of $\sigma_{OIO}(0,5,1\leftarrow0,0,0) = (1.3\pm0.3)\cdot10^{-17}cm^2\cdot molec^{-1}$ at 0.35nm FWHM. For two yet unidentified absorbers cross sections per iodine atom were determined of $\sigma_{"Z"}(340nm) = (1.0\pm0.2)\cdot10^{-18}cm^2\cdot atom^{-1}$ at 1.3nm FWHM and $\sigma_{"Y"}(322nm) = (1 \text{ to } 3)\cdot10^{-18}cm^2\cdot atom^{-1}$ at 1.3nm FWHM. Results for ground state IO and OIO are in good agreement with literature. The other cross sections have been determined for the first time.

ZUSAMMENFASSUNG

In dieser Arbeit wurden die Absorptionsspektren und Absorptionsquerschnitte von Jodverbindungen untersucht, die sowohl für die Atmosphäre als auch in der Photolyse von J_2 in Anwesenheit von O_3 relevant sind. Zu diesem Zweck wurden zwei unabhängige Experimente optimiert und synchronisiert. Zum einen handelte es sich um einen Aufbau für statische und zeitaufgelöste UV-vis Molekülabsorptionsspektroskopie mit CCD-Kamera und zum anderen um einen Aufbau für zeitaufgelöste UV-VUV Resonanz-absorptionsspektroskopie mit Photomultiplier. Beide Aufbauten können sowohl separat als auch simultan synchronisiert zum Photolysesystem betrieben werden. Mit dem Resonanzabsorptionssystem wurde der Absorptionsquerschnitt des $I(^2P_{3/2})$ 183,038nm Übergangs zu $(5.42\pm0.8)\cdot10^{-14}cm^2\cdot atom^{-1}$ im Zentrum der Linie bestimmt. Mit dem Experiment zur Molekülabsorption wurde der Absorptionsquerschnitt des Jodmoleküls J_2 bei 500nm überprüft, wobei die Unsicherheit des Ergebnisses deutlich reduziert werden konnte. Bestimmt wurde $\sigma_{I_2}(500nm)=(2.18_6\pm0.02_1)\cdot10^{-18}cm^2\cdot molec^{-1}$ in sehr guter Übereinstimmung mit vorhergehenden Veröffentlichungen. Auf Grundlage der verfügbaren Daten wird ein gewichtetes Mittel von $\sigma_{I_2}(500nm)=(2.19_1\pm0.02)\cdot10^{-18}cm^2\cdot molec^{-1}$ empfohlen.

Mit dem synchronisierten Aufbau wurden Spektren und Absorptionsquerschnitte von Jodoxiden untersucht. Hierzu wurden Mischungen aus J_2 und O_3 in Anwesenheit von N_2 und O_2 photolysiert und simultane zeitaufgelöste Absorptionsmessungen mit beiden Systemen durchgeführt. Auf Grundlage von Hauptkomponentenanalyse und Analyse von unabhängigen Komponenten (Principal Components Analysis PCA und Independent Component Analysis ICA) sowie Methoden der kleinsten Quadrate wurde ein Ansatz entwickelt, der die Separation von überlappenden Absorptionen verschiedener Absorber innerhalb einer zeitaufgelösten Vielkanal-CCD-Messung ermöglicht. Damit war die Extraktion von Kurven reiner optischer Dichte sowohl reiner Spektren einzelner Absorber mit einer Genauigkeit von ±3% möglich. Spektren für Jodmonoxid im Grundzustand $JO(\nu'\leftarrow0)$, vibrationell angeregtes $JO(\nu'\leftarrow\nu'')$, $\nu''>0$, sowie von Joddioxid OJO und drei weiteren bisher nicht identifizierten Absorbern konnten damit voneinander separiert werden. Aus der Analyse des Absorptionskontinuums von $JO(\nu'\leftarrow0)$ wurde auf die Existenz zweier optisch aktiver repulsiver Potentiale geschlossen, die das $JO(A^2\Pi_i)$ Potential schneiden. Anomales Zeitverhalten scheinbarer

optischer Dichte des JO(2←0) Übergangs wurde beobachtet, welches durch Chemolumineszenz aus JO($A^2\Pi_i$), ν'=2 erklärt werden kann, wobei die Quelle für JO in diesem Zustand unklar ist. Während der ersten Phase nach der Photolyse wurde vibrationell angeregtes JO bis zu ν"=7 beobachtet. JO mit ν"=1 lag bei 25% relativ zu JO mit ν"=0, wohingegen im thermischen Gleichgewicht nur 4% zu erwarten wären. Dies machte die Bestimmung von getrennten Querschnitten für JO, ν"=0 und JO, ν"=1 erforderlich. Im Zusammenhang mit CCD-Messungen wurde der Effekt niedriger Auflösung und groben Binnings auf scheinbare optische Dichte und abgeleitete Querschnitte untersucht und eine Methode zur Korrektur dieser Effekte entwickelt. Für JO(4←1) wurde signifikante Nichtlinearität zwischen scheinbarer optischer Dichte und Konzentration festgestellt, die relevant ist für die Bestimmung von Querschnitten als auch chemischer Geschwindigkeitskonstanten. Zur Bestimmung von Absorptionsquerschnitten wurde eine Methode entwickelt, die unabhängig von chemischen Reaktionsmodellen und Referenzdaten aus der chemischen Reaktionskinetik ist. sie basiert auf dem Erhaltungsprinzip für Jodatome angewendet auf den Zeitraum der chemischen Umsetzung von Jod nach der Photolyse. Absorptionsquerschnitte von Jodoxiden wurden bestimmt zu $\sigma_{JO}(4\leftarrow0) = (3.5\pm0.3)\cdot10^{-17}cm^2\cdot molekül^{-1}$ bei 0.12nm Halbwertsbreite (FWHM) für die JO, ν"=0 Progression, $\sigma_{JO,eff}(3\leftarrow1) = (2.0\pm0.8)\cdot10^{-17}cm^2\cdot molekül^{-1}$ bei 0.35nm FWHM für einen effektiven Querschnitt für die Progressionen ν">0 zusammen, weiterhin für die Progression JO, ν"=1 von $\sigma_{JO}(3\leftarrow1) = (4.5\pm0.5)\cdot10^{-17}cm^2\cdot molekül^{-1}$ bei 0.12nm FWHM, und für OJO von $\sigma_{OJO}(0,5,1\leftarrow0,0,0) = (1.3\pm0.3)\cdot10^{-17}cm^2\cdot molekül^{-1}$ bei 0.35nm FWHM. Für zwei weitere bisher nicht identifizierte Absorber wurden Querschnitte in Einheiten von cm^2 pro enthaltenem Jodatom bestimmt zu of $\sigma_{"Z"}(340nm) = (1.0\pm0.2)\cdot10^{-18}cm^2\cdot Atom^{-1}$ bei 1.3nm FWHM und $\sigma_{"Y"}(322nm) = (1 \text{ to } 3)\cdot10^{-18}cm^2\cdot Atom^{-1}$ bei 1.3nm FWHM. Die Ergebnisse für Grundzustands-JO und für OJO sind in guter Übereinstimmung mit Ergebnissen vorangegangener Studien. Die übrigen Querschnitte wurden in dieser Arbeit erstmals bestimmt.

PROLOGUE

(Not to be taken completely serious. Freely adapted from "The Hitchhikers Guide to the Galaxy" by Douglas Adams, Pan Books Ltd. 1980)

Far out in the uncharted backwaters of the unfashionable end of the Western Spiral arm of the Galaxy lies a small unregarded yellow sun.

Orbiting this at a distance of roughly ninety-two million miles is an utterly insignificant little blue-green planet whose ape-descendant life forms are so amazingly primitive that they still think digital watches are a pretty neat idea.

This planet has a problem, which is this: Most of the people living on it were unhappy for pretty much of the time. Many solutions were suggested for this problem, but most of these were largely concerned with the movements of small pieces of paper, which is odd because on the whole it wasn't the small pieces of paper, which were unhappy.

And so the problem remained; lots of people were mean, and most of them were unhappy, even the ones with digital watches.

Many people on this planet – The Earth, as it is called by its inhabitants - became increasingly of the opinion that they had all made a big mistake in coming down from the trees in the first place. Others even went as far as to state that even leaving the ocean had already been a bad move. Others, less rigorous, didn't go as far back as this and just blamed some outcomes of what was commonly referred to as the industrial revolution (This took place in the 19th (local) century after someone had got nailed to a tree for saying that it might be good for a change to be nice to people). They said that some developments and achievements from this industrial revolution should have been watched with greater care than most of the people until then had cared to do so.

1 INTRODUCTION

With the technical achievements resulting from the 19th century industrial revolution the population of the world increased significantly and an unprecedented wealth and level of standard of living was achieved in the industrialised countries towards the end of the 20th century. As a result of the nature of the dominant economic system, this wealth on a global

scale was and still is far from being evenly distributed. A large number of communities in the developing countries (the so-called "Third World") struggle to reduce poverty and to achieve what they are being shown by the industrialised countries to be a desirable state of development. The "standard of living" in this context is usually measured in the availability of technical improvements, individual mobility and general monetary wealth.

The continuous improvement of standard of living according to this definition has been achieved by an ever-increasing use of natural resources and energy. Towards the end of the 20th century it became apparent that this excessive use leads to a waste of natural resources and to pollution of the environment. In many of the so-called underdeveloped countries, the focus remains on survival and the struggle for higher standard of living ignoring environmental issues. In part of the industrialised world it has been recognised that the waste of resources and the pollution have grown to an alarming degree and that anthropogenic activities considerably disturb and even endanger the sensitive ecosystem of this planet. It is not surprising that such movements developed more or less exclusively in the richer countries of the world and similarly unsurprising is the fact that all these movements have to struggle against strong resistance and inertia of profit oriented forces in society.

It also became recognised that a purely economical point of view and a purely materialistic definition of standard of living is single sided. Alternative ideas appeared which take into account the quality of the surrounding environment as another important parameter in the definition and the quantitative consideration of standard of living. It has to be hoped that these changes in understanding will be sufficient to withstand the traditional economical forces and that in the future they will possibly lead to a new definition of standard of living with an enhanced focus on environmental qualities and fair distribution of wealth.

The awareness of the destructive potential of human activities was partly initiated by the discovery of the Antarctic Ozone hole in 1984 by [Farman et al., 1985]. A drastic change of view took place, as it became apparent that the ozone shield, which protects life on Earth from harmful ultraviolet radiation, was vulnerable to anthropogenic activities. It became clear that the release of seemingly harmless substances at seemingly negligible concentrations could be capable of causing serious, unforeseen and dangerous effects on a global scale. A by-product of this discovery was the recognition that the at that time present degree of understanding of environmental processes in general and of atmospheric processes in particular was insufficient to estimate the possible effects of anthropogenic activities. As a consequence, the efforts to

monitor and understand the environment increased. Observational systems for atmospheric parameters and constituents were proposed to improve the knowledge and the understanding of the relevant physical and chemical processes in the atmosphere.

One type of observational systems, suitable for environmental monitoring are satellite-based spectrometers. GOME-1 (Global Ozone Monitoring Experiment) and SCIAMACHY (Scanning Imaging Absorption spectroMeter for Atmsopheric ChartographY) were selected for flight to observe globally the ozone distribution in the Earth's atmosphere. GOME-1 has been operating in-orbit since its launch on April the 20th 1995 aboard the second European Research satellite, ERS-2, of the European Space Agency ESA. Currently it is still in operation, while suffering from degradation of some of its navigational subsystems and the data transfer capability of ERS-2. SCIAMACHY is a German and Dutch/Belgian national contribution to ENVISAT, which was successfully launched by ESA on February 28th 2002. In addition an operational mission, planned as successor to GOME-1, is in preparation, called GOME-2. The GOME-2 instrument is part of the core payload of the MetOp satellite series, which forms the space segment of the EUMETSAT Polar System (EPS). It is an enhanced version of the GOME-1 instrument. Three identical instruments are planned to be launched successively at five years intervals to enable fifteen years of continuous operation. In addition to ozone a number of further relevant trace gases are aimed at. For GOME-1 and GOME-2 the retrieval of atmospheric trace gases e.g. H_2O, NO_2, SO_2, BrO, OClO, and HCHO is possible. SCIAMACHY has an increased spectral coverage into the near IR. Further trace gases can be monitored extending the list to $O_2(^1\Delta)$, CO, CH_4, and possibly N_2O. In comparison to the GOME instruments the more sophisticated observational geometry of SCIAMACHY also allows a clearer separation of tropospheric and stratospheric contributions of gases.

These technological projects of the 1980s and 1990s were accompanied by enhanced efforts to understand and model the processes governing the physics and chemistry of the Earth's atmosphere. By now, at the beginning of the 21st century, the basic chemical and physical mechanisms causing the antarctic as well as the arctic ozone depletion are much better understood. Chlorine and bromine are the main contributors to that. But the processes leading to ozone losses in the troposphere on a global scale as well as locally in the planetary boundary layer and the potential role of iodine therein are currently still a source of scientific curiosity. Likewise a possible contribution of iodine to aerosol formation in the atmosphere has been recognised and is presently studied and discussed.

The importance of iodine results from its reactivity and from its significant natural occurrence in the troposphere with methyl iodide being the most abundant iodine compound in the marine boundary layer. Along with other iodocarbons like CH_2I_2, CH_2ClI, C_2H_5I, or C_3H_7I it is found in ocean water and the marine boundary layer. They are formed by various types of macroalgea and phytoplankton. As they are of low solubility, supersaturation of the ocean water can occur causing release of these compounds from the ocean to the atmosphere. In the gas phase the photolysis of iodocarbons leads to the release of iodine atoms which mainly react with O_3 to form IO transferring iodine from organic to inorganic compounds. Around IO, OIO and I a considerable number of gas phase and heterogeneous reactions cause a complex cycling of iodine between gas phase, aerosol and possibly particles (**Fig. 1.1**). Removal of inorganic iodine compounds is believed to occur by wet and dry deposition.

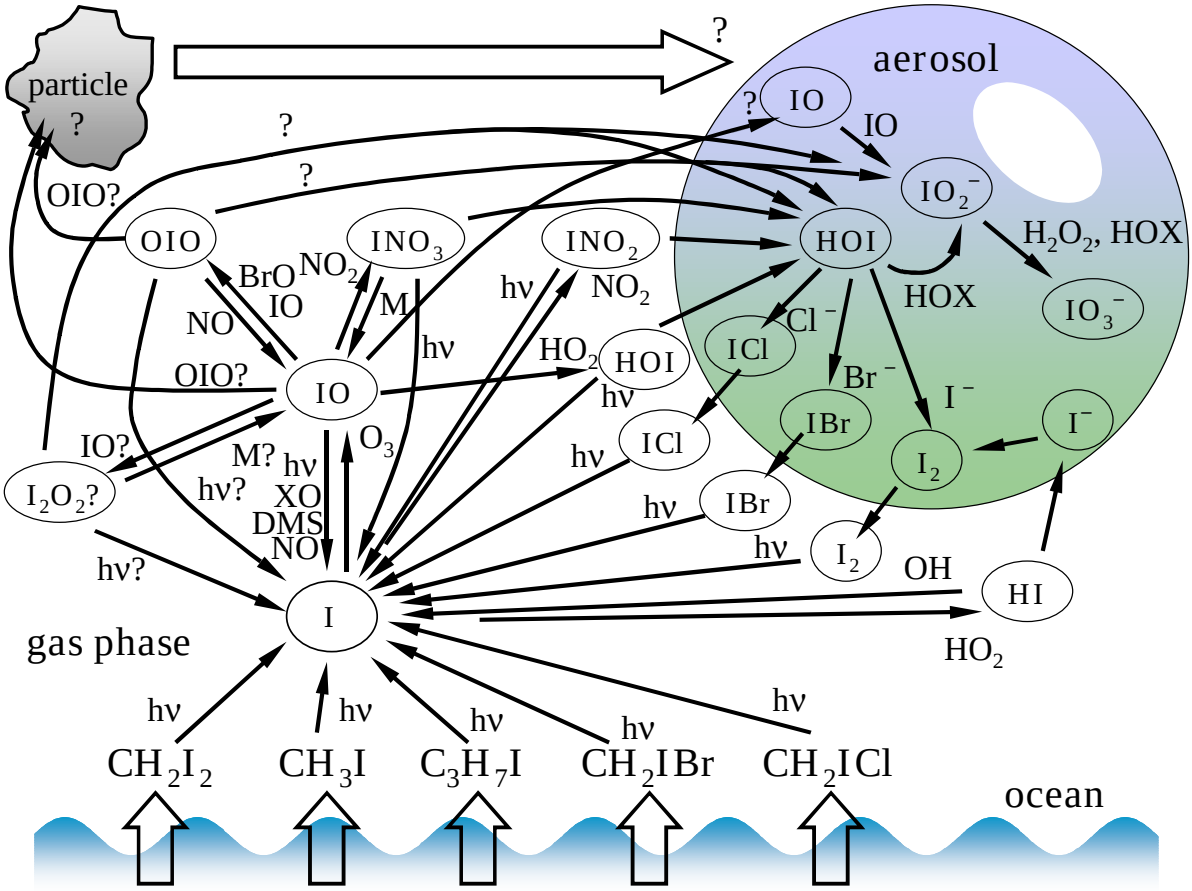

Figure 1.1 Iodine is cycled in the marine boundary layer through a complex scheme of gas phase, liquid phase and heterogeneous reactions. Especially IO and OIO are of interest, as these could open up pathways to particle formation via I_2O_3 and I_2O_4. Also the fate of I_2O_2 – so it exists – needs clarification. The main scheme of pathways is adapted from Glasow and Crutzen (2004). Pathways for IO and OIO to particles to aerosol have been added based on results from this work and recent discussion (J.C. Gómez-Martín, J. Plane, private communication).

Gas phase IO, OIO and I_2 have been observed in the marine boundary layer by Differential optical absorption Spectroscopy [Allicke et al. 1999, Allan et al. 2000, Allan et al. 2001, Saiz-Lopez and Plane 2004]. Also observations of IO in zenith sky measurements above Spitsbergen [Wittrock et al. 2000] and at Neumayer-Station, Antarctica [Frieß et al. 2001] were reported.

In aerosols different inorganic iodine compounds have been found at largely varying proportions [McFiggans et al 2000 and references therein]. Baker et al. [2000] studied aerosol composition and report that iodine is present in aerosol in varying proportions of soluble inorganic iodine, soluble organic iodine and insoluble or unextractable iodine.

A large number of modelling studies have been performed to estimate the partitioning of the iodine species and its contribution to halogen activation and ozone destruction. They indicate a clear potential of iodine for ozone destruction. But a common conclusion of all – early as well as recent studies - was also that sound assessments of the importance of iodine chemistry are impeded by missing knowledge of the iodine precursor fluxes and the significant lack of kinetic and spectroscopic data [Zafiriou 1974, Chameides and Davis 1980, Jenkin et al. 1985, Chatfield and Crutzen 1990, Jenkin 1993, Solomon et al. 1994, Davis et al. 1996, Vogt et al. 1999, Bedjanian and Poulet 2003, von Glasow and Crutzen 2004].

Apart from the impact on ozone chemistry the role of iodine compounds in aerosol formation is currently a source of interest and scientific debate, as aerosol formation in the troposphere has an impact on both regional and global climate. Correlation between low tide and observation of gas phase inorganic iodine compounds and increased particle formation [O'Dowd et al. 2002 and references therein] indicate such a link [Carpenter et al. 1999, Saiz-Lopez and Plane 2004 and references therein]. Again the lack of reliable kinetic data about the formation of aerosol from inorganic iodine compounds I, IO and OIO proves to be limiting. OIO and possibly higher iodine oxides I_xO_y are being discussed as precursors to aerosol formation [Burkholder et al. 2004]. But again solid assessments are limited, as for the absorption cross section of OIO only estimates were available and kinetic data of its formation and consumption was insufficient. Evidence for higher iodine oxides was only speculative without clear identification of spectra and absorbers.

Improved understanding of iodine chemistry in the atmosphere will also facilitate the use of ^{128}I as a tracer to monitor the release from anthropogenic nuclear activities.

At present these open issues are being addressed by the European Union Framework 5 Program THALOZ "Troposphere Halogens – Effect on Ozone", also dedicated "Halogen Sessions" on

different national and international stages like AFOHAL, Rehatrop, and the EGU and last not least small scale bilateral projects like the German-Latvian project "Ozone Halogen (I, Br) Reactions in Stratosphere and Troposphere" LVA 01/003 between the Institute for Atomic Physics and Spectroscopy at the University of Riga and the Institute of Environmental Physics / Institute for Remote Sensing at the University of Bremen.

In the present work the spectroscopy of iodine oxides is studied with the objective to obtain accurate *relative* absorption spectra of IO, OIO and higher iodine oxides and also to determine *absolute* absorption cross sections for them. Accurate spectra are a prerequisite for remote sensing of iodine species in the atmosphere. The determination of absolute cross sections is hoped to contribute to a clarification of the present inconsistencies among available cross section data of IO and OIO in the literature and to obtain sound results for these and possibly higher oxides. Furthermore the experimental data is meant to provide a basis for studies subsequent to this work, which will analyse the chemical kinetics of IO and especially OIO formation and consumption with a focus on higher oxides and aerosol.

An overview over the present understanding of relevant atmospheric chemistry will be given in the next chapter. After a general section the focus will be on iodine chemistry and iodine oxides spectroscopy. Results from laboratory studies defining the present knowledge of cross sections, the mechanism and rate coefficients relevant to the photolysis of I_2 and O_3 will be summarised. This summary will also show the gaps in our knowledge of spectroscopy and chemical kinetics of iodine oxides. As a consequence the objectives for this study will be postulated, which will directly lead to the key concept of this work, which is the principle of *conservation of iodine*. The individual components of the concept starting from the different experiments followed by the different aspects of analysis to the final determination of absolute absorption cross sections via the principle of conservation of iodine will be presented in the subsequent chapters.

2 CHEMISTRY OF THE ATMOSPHERE

2.1 VERTICAL STRUCTURE OF THE ATMOSPHERE AND OZONE LAYER

A basic boundary condition for the chemical and physical processes within the atmosphere is its vertical structure, which is shown in a generalised form in **Fig. 2.1** [Finlayson-Pitts and Pitts 2000]. This structure varies with latitude, season and year. Consequently **Fig. 2.1** shows an averaged and generalised profile, which – in this case – is typical for mid-latitudes. On a logarithmic scale pressure falls nearly linearly with increasing altitude. Temperature shows a more complicated behaviour typical for planets with an energy absorbing ozone layer. Throughout the troposphere (greek: *tropos*: turn, turning, easily changing. Refers to the mixing within the troposphere), it generally falls with increasing altitude from surface values of the order of 290K to tropopause values of roughly 210K. Strong surface heating is caused by absorption of solar radiation.

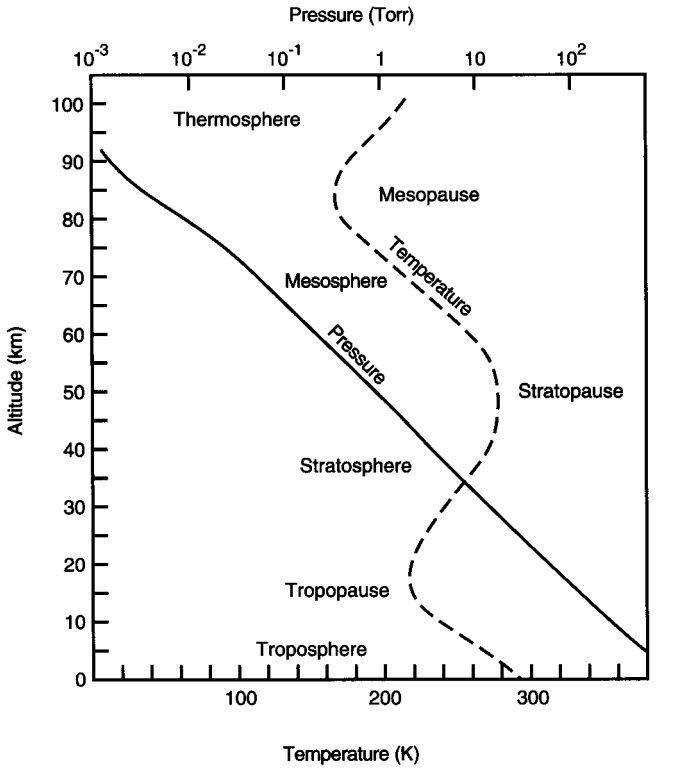

Figure 2.1 The atmosphere is subdivided into different regions depending on their dynamic properties. Shown are typical averaged variations of pressure and temperature with altitude. The different regions are indicated. From [Finlayson-Pitts an Pitts 2000].

As warm air rises, this leads to strong vertical mixing of air masses in the troposphere. Surface emissions reach the tropopause within a few days or even less depending on meteorological conditions. The majority of phenomena responsible for surface weather conditions as clouds, precipitation, and wind take place and are caused by processes in the troposphere. Scavenging of pollutants from the atmosphere by precipitation is a typical property of the troposphere. At the tropopause, the temperature profile changes, now increasing throughout the stratosphere again and reaching its maximum of ca. 280K in the stratopause at about 50km of altitude. This increase of temperature is typical for the Earth's atmosphere and it is not found on planets such as Mars or Venus, [Schubert et al. 1980, Prinn and Fegley 1987]. It is caused by the absorption of radiation in the ozone layer of Earth's atmosphere. The existence of ozone as an atmospheric species had been proposed much earlier by [Schönbein 1840] and its existence in the troposphere was established by chemical methods by [Houzeau, 1858]. In 1881 Hartley published results of an UV-vis spectroscopic study, which showed that ozone should be present in the upper atmosphere [Hartley, 1881]. In the 1920s Dobson developed the ozone spectrophotometer for measurement of atmospheric ozone column density (see Dobson [1968] for a historical overview) and shortly after that his colleague Sir Sydney Chapman proposed a mechanism to explain stratospheric ozone concentrations [Chapman 1930]. The Chapman cycle, as originally proposed, involved the following reactions:

$$O_2 + h\nu \rightarrow O + O \quad \text{(R2.1)}$$

$$O + O_2 + M \rightarrow O_3 + M^* \quad \text{(R2.2)}$$

$$O + O_3 \rightarrow 2\,O_2 \quad \text{(R2.3)}$$

$$O + O + M \rightarrow O_2 + M^* \quad \text{(R2.4)}$$

$$O_3 + h\nu \rightarrow O + O_2 \quad \text{(R2.5)}$$

It was expected that (R2.1) to (R2.5) yield a steady state concentration of ozone in the stratosphere. It is known today that reaction (R2.4) is slow under stratospheric conditions. Based on the exponential increase of O_2 with decreasing altitude and the strong UV-absorptions of O_2 and O_3 it could be concluded that at around 35km the ozone content should reach a local maximum, called the Chapman layer. This is essential for life on Earth as it is known to us, because it absorbs light of harmful wavelengths between 240nm and 290nm (UV-C radiation: 200nm to 280nm) nearly completely. UV-B radiation (280nm to 315nm) up

to 320nm is strongly reduced. The sunlight, which has passed through this atmospheric longpass cutoff filter, is referred to as *actinic radiation*. Thus photochemistry within the troposphere is limited to processes requiring photodissociation energies less than $h \cdot c/290nm \approx 4.3eV \approx 34500cm^{-1}$. Consequently only within the upper section of the stratosphere the photolysis via reaction (R2.1) is possible, because this requires energies corresponding to $\lambda<242nm$. In that case the products are two ground state $O(^3P)$:

$$O_2 + h\nu(\lambda<242nm) \rightarrow 2\,O(^3P) \qquad (R2.1)$$

Photolysis of ozone is somewhat complicated by the fact that different products are possible dependent on photon energy. From $\lambda<310nm$ photon energy is sufficient for the formation of both electronically excited $O_2(^1\Delta_g)$ and $O(^1D)$ via reaction (R2.5). From 310nm to 320nm energy only suffices to form $O(^1D)$ and $O_2(^3\Sigma_g^-)$ and from 320nm to 1180nm both products are in their respective ground states $O(^3P)$ and $O_2(^3\Sigma_g^-)$:

$$O_3 + h\nu(\lambda<310nm) \rightarrow O(^1D) + O_2(^1\Delta_g) \qquad (R2.5a)$$

$$O_3 + h\nu(\lambda<320nm) \rightarrow O(^1D) + O_2(^3\Sigma_g^-) \qquad (R2.5b)$$

$$O_3 + h\nu(\lambda<1180nm) \rightarrow O(^3P) + O_2(^3\Sigma_g^-) \qquad (R2.5c)$$

Any excited $O(^1D)$ will be deactivated to $O(^3P)$ by collisional quenching with N_2 or O_2. The rate coefficient for this is of the order of 10^{-11} $cm^3/(molec.\cdot sec)$ [NIST 1998]. The rate coefficients at 298K for reactions involving $O(^3P)$ according to [NIST 1998] are:

$$O(^3P) + O_2 + M \rightarrow O_3 + M^* \quad [6.0\cdot10^{-34}cm^6/(molec.^2\cdot sec)] \qquad (R2.2)$$

$$O(^3P) + O_3 \rightarrow 2\,O_2 \quad [7.96\cdot10^{-15}cm^3/(molec.\cdot sec)] \qquad (R2.3)$$

$$O(^3P) + O(^3P) + M \rightarrow O_2 + M^* \quad [1.07\cdot10^{-33}cm^6/(molec.^2\cdot sec)] \qquad (R2.4)$$

$O_2(^1\Delta_g)$ has a comparatively long radiative lifetime of the order of ca. 75min [Lafferty et al. 1998, Newman et al. 1999] and it is thought to be collisionally quenched and not to react. The energy released following the photoexcitation and -dissociation of O_3 gives rise to the observed temperature increase in the stratosphere. Reaction (R2.2) also releases excess energy contributing as well to the elevated stratospheric temperature.

As a result of the inverted temperature profile only limited vertical mixing and no precipitation scavenging takes place in the stratosphere (lat. *stratum*: layer). Ignoring chemical reaction the lack of an effective physical removal mechanism results in pollutants having long residence times in the stratosphere. By the Mt. Pinatubo eruption massive particle injections into the stratosphere produced layers in the stratosphere, which could be measured as long as two years after the actual eruption. So absorption of UV radiation results not only in a protective layer against biologically damaging radiation but also determines the temperature structure of the atmosphere and thereby influences its vertical structure.

In the upper end of the stratosphere the O_2 concentration, which falls off exponentially with increasing altitude, becomes too small to produce significant amounts of ozone. Therefore the concentration of O_3 and also the warming effect by the Chapman cycle die off. The temperature profile changes again, now falling again with increasing altitude. The transition region is called stratopause, the region above it, where temperature falls again, is called mesosphere. The mesosphere extends from roughly 50km to 85km. As a result of temperature falling with altitude, vertical mixing becomes significant. Above this region the temperature starts to rise again because of the increasing absorption of short wave radiation by O_2 and N_2 as well as by atomic species. The transition region is called mesopause. The region above it is called thermosphere.

The layered structure of the atmosphere leads to significantly different chemical and photochemical phenomena and characteristics in its different regions.

2.2 OZONE CHEMISTRY OF THE GLOBAL STRATOSPHERE

The existence of an ozone layer in the stratosphere can qualitatively be explained by the Chapman cycle. Chapman explained loss of O and O_3 by (R2.3) and (R2.4). The sum of O and O_3 is called "odd oxygen". In the 1960s it became clear that it did not explain the observed ozone concentrations correctly, which were significantly smaller than predicted by corresponding model calculations. The odd oxygen loss reactions (R2.3) and (R2.4) could not account for the losses required to explain the smaller observations. They should have been a factor of 4 to 5 faster to explain the observed smaller stratospheric concentrations. As the concentrations of potential reaction partners for ozone have to be expected to be small throughout the stratosphere, **catalytic loss mechanisms** were proposed by [Bates and Nicolet, 1950]:

	$X + O_3$	$\rightarrow$	$XO + O_2$	
	$XO + O$	$\rightarrow$	$X + O_2$	
net.:	$O + O_3$	$\rightarrow$	$2\ O_2$	(M1)

A mechanism like this would remove most effectively odd oxygen from the Chapman cycle and would thereby reduce its efficiency of ozone formation. XO could be any radical capable of this catalytic reaction pattern. Bates and Nicolet proposed **hydrogen oxides OH and HO_2 (HO_x)** as candidates for this catalytic cycle. To avoid confusion it has to be pointed out that all these considerations were done having the *global* stratosphere in mind. At that time – prior to the detection of the antarctic "ozone hole" - nothing indicated that any effects in the context of ozone chemistry should be more localised than mere latitudinal structures. Cycles involving **Nitrogen oxides NO and NO_2 (NO_x)** were suggested by Crutzen [1970] and Johnston [1971]. The NO_x cycle proved to be the most important removal mechanism for ozone. The source of NO_x is N_2O, which is transported from the troposphere and which is photolysed and reacts with $O(^1D)$ to form NO. In 1974 it was suggested by [Stolarski and Cicerone, 1974] that also similar catalytic ozone destruction cycles could be possible involving **chlorine**, if there were only sufficient sources of chlorine atoms in the stratosphere. Shortly after their publication it was shown by [Molina and Rowland, 1974] that indeed chlorine from **anthropogenic sources** was capable to reach the stratosphere. They reasoned that chlorofluorocarbons (CFCs) due to the lack of loss reactions and removal processes in the troposphere were sufficiently inert to reach the stratosphere, even if it were after years of slow transport through the troposphere. Different loss processes, which had been studied for CFC-11 and CFC-12 (Freon 11: CCl_3F, Freon 12: CCl_2F_2), only demonstrated the – in terms of industrial usage - superior inertness of these gases with lifetimes of ≈540 years and 1800 years respectively [National Research Council, 1979]. But this technical advantage is at the same time the cause for their destructive role in the atmosphere. Long lifetimes result in their being transported to the stratosphere. Since the wavelength distribution of solar radiation shifts to shorter wavelength with increasing altitude the CFCs eventually become exposed to wavelengths of light which are sufficiently short to photolyse them. These processes are negligible in the troposphere, where the actinic radiation is insufficient to break the bonds of these molecules. Active chlorine and ClO are released into the stratosphere giving rise to a

chlorine catalysed ozone destruction as described by mechanism (M1). The lifetime of CFCs, when considering their stratospheric losses, is 40 to 80 years for CFC-11 and roughly twice as much for CFC-12 [WMO, 1995].

In addition to the release of chlorine from CFCs it soon became clear that also **bromine atoms** could play an important role in stratospheric ozone depletion, as they are also capable of catalytic cycling as in (M1) [Wofsy et al., 1975]. As sources for stratospheric bromine the Halons were identified. These molecules are similar to CFCs, i.e. halocarbons containing bromine and chlorine. Halons are frequently used as fire suppressants wherever the use of water is not advisable, as it is the case in electrical and electronic equipment, especially on aircrafts. The most used compounds are CF_2ClBr (Halon-1211) and CF_3Br (Halon-1301). The Halons are unreactive like the CFCs. They therefore share the same fate of reaching the stratosphere unaltered and there being removed by photolysis or reaction with $O(^1D)$ thereby releasing the halogens Cl and Br. The other source of Br is methyl bromide CH_3Br, which contributes to stratospheric bromine content, even though it is also removed by the tropospheric loss reaction with OH. There are strong natural (release from the biosphere in the ocean and on land) and anthropogenic sources (agriculture). Both are of the same order of magnitude with the natural sources being slightly larger according to [WMO, 1995].

For **hydrogen oxides HO_x** the following cycles are now established to contribute at specific different extent to the observed ozone losses in the global as well as the polar stratosphere (Rate coefficients again [NIST, 1998]):

	$O + OH$	$\rightarrow$	$O_2 + H$	$[3.3 \cdot 10^{-11} cm^3/(molec. \cdot sec)]$	(R2.6)
	$H + O_2 + M$	$\rightarrow$	$HO_2 + M$	$[5.7 \cdot 10^{-32} cm^6/(molec.^2 \cdot sec)]$	(R2.7)
	$HO_2 + O_3$	$\rightarrow$	$OH + 2\ O_2$	$[2 \cdot 10^{-15} cm^3/(molec. \cdot sec)]$	(R2.8)
net.:	$O + O_3$	$\rightarrow$	$2\ O_2$		(M2)

	$O + OH$	$\rightarrow$	$O_2 + H$	$[3.3 \cdot 10^{-11} cm^3/(molec. \cdot sec)]$	(R2.6)
	$H + O_3$	$\rightarrow$	$OH + O_2$	$[2.9 \cdot 10^{-11} cm^3/(molec. \cdot sec)]$	(R2.9)
net.:	$O + O_3$	$\rightarrow$	$2\ O_2$		(M3)

$O_3 + OH \rightarrow O_2 + HO_2$ $[6.8 \cdot 10^{-14} cm^3/(molec. \cdot sec)]$ (R2.10)

$HO_2 + O \rightarrow OH + O_2$ $[5.9 \cdot 10^{-11} cm^3/(molec. \cdot sec)]$ (R2.11)

net.: $O + O_3 \rightarrow 2\ O_2$ (M4)

Generally OH can be produced by reaction of oxygen atoms with methane or water vapour and the photolysis of H_2O:

$O(^1D) + CH_4 \rightarrow OH + CH_3$ $[2.2 \cdot 10^{-10} cm^3/(molec. \cdot sec)]$ (R2.12)

$O(^1D) + H_2O \rightarrow 2\ OH$ $[2.2 \cdot 10^{-10} cm^3/(molec. \cdot sec)]$ (R2.13)

$H_2O + h\nu \rightarrow OH + H$ (R2.14)

While the stratosphere is very dry due to thermal trapping of upwelling water vapour in the cold tropopause, water vapour in the stratosphere is present by the oxidation of CH_4 and the reaction of HO_2 with OH:

$CH_4 + OH \rightarrow H_2O + CH_3$ $[6.3 \cdot 10^{-15} cm^3/(molec. \cdot sec)]$ (R2.15)

$HO_2 + OH \rightarrow H_2O + O_2$ $[1.1 \cdot 10^{-10} cm^3/(molec. \cdot sec)]$ (R2.16)

The **nitrogen oxides chemistry** – abbreviated by NO_x (i.e. the sum of NO and NO_2) - displays a more complicated structure than just a NO_2 driven simple catalytic cycle as (M1) (Rate coefficients again [NIST, 1998]):

$O_3 + NO \rightarrow O_2 + NO_2$ $[1.8 \cdot 10^{-14} cm^3/(molec. \cdot sec)]$ (R2.17)

$NO_2 + O \rightarrow NO + O_2$ $[9.7 \cdot 10^{-12} cm^3/(molec. \cdot sec)]$ (R2.18)

net.: $O + O_3 \rightarrow 2\ O_2$ (M5)

$2 \times (\ O_3 + NO \rightarrow O_2 + NO_2\ )$ $[1.8 \cdot 10^{-14} cm^3/(molec. \cdot sec)]$ (R2.17)

$NO_2 + O \rightarrow NO + O_2$ $[9.7 \cdot 10^{-12} cm^3/(molec. \cdot sec)]$ (R2.18)

$NO_2 + h\nu \rightarrow NO + O$ (R2.19)

net.: $2\ O_3 + h\nu \rightarrow 3\ O_2$ (M6)

	$O_3 + NO$	$\rightarrow$	$O_2 + NO_2$	$[1.8 \cdot 10^{-14} cm^3/(molec. \cdot sec)]$	(R2.17)
	$NO_2 + O_3$	$\rightarrow$	$NO_3 + O_2$	$[3.2 \cdot 10^{-17} cm^3/(molec. \cdot sec)]$	(R2.20)
	$NO_3 + h\nu$	$\rightarrow$	$NO + O_2$		(R2.21)
net.:	$2\ O_3 + h\nu$	$\rightarrow$	$3\ O_2$		(M7)

However reaction NO_2+O_3 has a low rate coefficient and NO_3 is strongly photolysed in daylight. The different forms of NO_x involved in the stratospheric cycles are mainly produced by oxidation of N_2O. This species is unreactive in the troposphere and therefore has a lifetime sufficient to reach the stratosphere. It is biogenically emitted from biological processes in soils and from the oceans. In the stratosphere it is converted to NO by reaction with $O(^1D)$:

	$O(^1D) + N_2O$	$\rightarrow$	$2\ NO$	$[6.7 \cdot 10^{-11} cm^3/(molec. \cdot sec)]$	(R2.22)

[Johnston, 1971] suggested that direct injection of NO_x from supersonic transport aircraft could also constitute a significant source contributing to NO_x driven ozone destruction. Even though the number of supersonic transport aircrafts turned out to be much smaller than originally anticipated, the number of sub-sonic civil transport aircrafts reached a level that NO_x driven ozone destruction in this context again became an issue to be considered.

Chlorine catalysed ozone depletion is possible following the pattern of cycle (M1) (Rate coefficients again from [NIST, 1998]):

	$Cl + O_3$	$\rightarrow$	$ClO + O_2$	$[1.2 \cdot 10^{-11} cm^3/(molec. \cdot sec)]$	(R2.23)
	$ClO + O$	$\rightarrow$	$Cl + O_2$	$[3.8 \cdot 10^{-11} cm^3/(molec. \cdot sec)]$	(R2.24)
net.:	$O + O_3$	$\rightarrow$	$2\ O_2$		(M8a)

Other catalytic cycles involving the self reaction ClO + ClO and the interhalogen reaction ClO + BrO are in principle also possible. But they become meaningful only in the perturbed stratosphere, see below.

Similar as for chlorine, the same pattern (M1) is possible for **bromine** as well, which reaches the stratosphere in sufficient amounts (Rate coefficients again from [NIST, 1998]):

	$Br + O_3$	$\rightarrow$	$BrO + O_2$	$[1.16 \cdot 10^{-12} cm^3/(molec. \cdot sec)]$	(R2.25)
	$BrO + O$	$\rightarrow$	$Br + O_2$	$[4.1 \cdot 10^{-11} cm^3/(molec. \cdot sec)]$	(R2.26)
net.:	$O + O_3$	$\rightarrow$	$2\ O_2$		(M8b)

A common feature of all the "odd oxygen" catalytic ozone destruction cycles is that they require O atoms. As a result these are dominant only at high altitudes and at sufficient solar illumination.

For **iodine** the chemistry is less well understood than for the other halogens bromine and chlorine. In principle also for iodine a mechanism according to (M1) is possible:

	$I + O_3$	$\rightarrow$	$IO + O_2$	$[1.2 \cdot 10^{-12} cm^3/(molec. \cdot sec)]$	(R2.27)
	$IO + O$	$\rightarrow$	$I + O_2$	$[1.2 \cdot 10^{-10} cm^3/(molec. \cdot sec)]$	(R2.28)
net.:	$O + O_3$	$\rightarrow$	$2\ O_2$		(M8c)

While in general for all three halogens Cl, Br, and I catalytic cycles like (M1) are possible, their atmospheric impact varies strongly with their sources, source locations, atmospheric lifetimes and dynamical processes of the atmosphere [WMO, 2003]. For iodine it was speculated, that some amounts of iodocarbons could reach the stratosphere in spite of their short tropospheric life time, if sufficiently fast transport mechanisms would exist [Solomon et al. 1994]. Volatile alkyl iodides of marine origin like CH_3I, C_2H_5I, and CH_2I_2 have tropospheric lifetimes of a few days or much less. Any iodine which would have reached the stratosphere, would enable two more cycles [Bedjanian and Poulet 2003]:

	$IO + HO_2$	$\rightarrow$	$HOI + O_2$	$[8.4 \cdot 10^{-11} cm^3/(molec. \cdot sec)]$	(R2.29)
	$HOI + h\nu$	$\rightarrow$	$OH + I$		(R2.30)
	$OH + O_3$	$\rightarrow$	$HO_2 + O_2$	$[6.8 \cdot 10^{-14} cm^3/(molec. \cdot sec)]$	(R2.31)
	$I + O_3$	$\rightarrow$	$IO + O_2$	$[1.2 \cdot 10^{-12} cm^3/(molec. \cdot sec)]$	(R2.27)
net.:	$2\ O_3$	$\rightarrow$	$3\ O_2$		(M9)

and for X = Br or Cl:

	$IO + XO$	$\rightarrow$	$I + X + O_2$		
	$IO + XO$	$\rightarrow$	$IX + O_2$		
	$IX + h\nu$	$\rightarrow$	$I + X$		
	$I + O_3$	$\rightarrow$	$IO + O_2$	$[1.2 \cdot 10^{-12} cm^3/(molec. \cdot sec)]$	(R2.27)
	$X + O_3$	$\rightarrow$	$XO + O_2$		
net.:	$2\ O_3$	$\rightarrow$	$3\ O_2$		(M10)

In contrast to the formerly estimated ozone removal efficiency of iodine of ca. 1000 times that of chlorine [Solomon et al, 1994] it is currently estimated to range between only 150 and 300. But the estimate is uncertain due to the lack of knowledge on the photochemistry of OIO, the possible existence of the I_2O_2 dimer, its photolytic lifetime and on the heterogeneous chemistry of iodine reservoirs. Also uncertainties in the cross sections contribute to this.

All considerations up to here were made with respect to the global stratosphere. Considering all mentioned mechanisms plus - to a limited extent - the ClO + ClO and ClO + BrO mechanisms (M11) and (M12) leads to a modelled ozone budget, which for the global unperturbed stratosphere is consistent with the observations [Molina and Rowland 1974, Molina and Molina 1987, McElroy et al. 1986]. The research behind all this had started out to merely explain the difference between the ozone budget, as predicted by the Chapman cycle and observations. Its focus changed significantly, when in the course of this research it was recognised that also anthropogenic activities could harm the ozone layer.

2.3 OZONE CHEMISTRY OF THE PERTURBED POLAR STRATOSPHERE

The **hypothesis of anthropogenically caused ozone destruction** caused worldwide concern, because the processes involved indicated a potentially large ozone depletion. The protection of the biosphere from harmful UV-B radiation by the ozone layer could be seriously reduced by these processes. UV-B radiation is sufficiently energetic to damage DNA and thereby cause skin cancer in humans and the degradation of plants with effects in agriculture and a variety of other eco-systems. In 1995, Crutzen, Molina, and Rowland shared the Noble Prize in Chemistry for their contributions to establishing the link between tropospheric processes, emissions to the atmosphere and stratospheric chemistry.

This honour was most likely catalysed by the discovery of the antarctic "ozone hole" by Farman et al., [1985], which caused a drastic change of view. It became apparent that the concern about the release of CFCs, halons and CH_3Br was indeed justified and that a global and vital part of the Earth's atmosphere, the ozone shield, was – beyond previous common belief - vulnerable to anthropogenic activities. This was only possible as a product of different effects. Firstly there was an insufficient understanding of environmental and particularly atmospheric processes, which were being studied by a only small scientific community. Secondly there existed a far-spread public attitude of general believe in technical feasibility. This ignored possible negative by-products of the unthinking use of technological and industrial development. So both the knowledge and a readiness required for estimating effects of anthropogenic activities were underdeveloped.

The observation by Farman et al., which was subsequently supported by satellite observations and other field studies, showed that since the 1970s, each spring-time after polar sunrise the ozone concentrations above the station at Halley-Bay, Antarctica dropped. After the rapid losses the ozone concentrations recovered on a time scale of weeks and months. The observed drop increased from year to year, as can be seen in **Fig. 2.2** [Finlayson-Pitts and Pitts 2000]. It shows a compilation of data including the Farman et al. data and subsequent measurements by Jones and Shanklin [1995]. The extent and rapidity of the observed loss effect were totally unexpected.

Even though there had been a clear increase in stratospheric chlorine and bromine content, the model calculations done around the early 1980s had predicted only small *global* ozone losses. The observations by Farman et al. could not be explained by the chemical models used in these calculations, neither in extent, nor in rapidity, nor in their clear geographical and temporal limitation. The resulting increase in scientific activity led to a much clearer understanding of the different aspects of atmospheric chemistry. The role of dynamics of the atmosphere in the localised occurrence of polar ozone depletion could be identified. The importance of heterogeneous and multiphase processes on liquid and solid surfaces was discovered. These processes are characterised by the so called "perturbed" polar stratosphere during polar winter and spring.

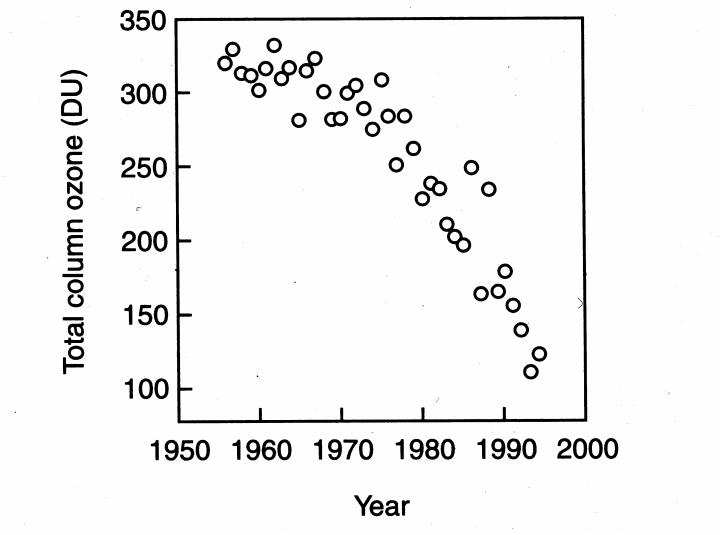

Figure 2.2 From 1957 to 1994 the total column of ozone measured in each year's October above Halley Bay, Antarctica shows a clear and steady decrease of ozone over the years. From [Finlayson-Pitts an Pitts 2000].

During polar winter the stratosphere is pre-conditioned, thereby setting the stage for perturbed ozone depletion chemistry starting at polar sunrise. During polar night radiative cooling of the stratosphere takes place. The resulting temperature gradient causes high atmospheric pressures within the polar region and subsequent strong downward and outward meridional winds leaving the polar region. As in the case of a "normal" atmospheric high pressure area the radial winds are diverted by the Coriolis effect leading to a counter clockwise rotation (southern hemisphere) of the airmasses around the centre near the pole. This large scale circulation of air is commonly referred to as the Polar Vortex [Schoeberl and Hartmann 1991, Schoeberl et al. 1992]. The rotation efficiently separates the inner air masses from the surrounding stratosphere creating a positive feedback effect, as counterproductive warming by mixing with surrounding mid-latitude air masses is suppressed. Under these conditions extreme temperatures can be as low as 185K. At the edges of the vortex wind speeds of up to ≈ 100m/sec ≈ 360km/h can be reached. Inside the vortex the low temperatures enable the formation of crystals in spite of the typically low stratospheric water concentrations of 2-6ppm. A phenomenon observed under such extreme conditions are the polar stratospheric clouds (PSCs). They occur at heights of roughly 20km and can have a quite remarkable appearance of different colours depending on their height and on the presence of other clouds [Sarkissian et al. 1991]. Their formation is still a matter of discussion but the present understanding is that PSC type I are ternary solutions of HNO_3, H_2SO_4, and H_2O. PSC type Ia

are $HNO_3 \cdot 3H_2O$ and PSCs type II are composed of ice crystals. PSCs type I form around 195K in the polar vortex, whereas type II form close to 185K.

Ozone depletion in the vortex depends critically on the existence of PSCs during winter [e.g. Molina et al. 1987, Molina 1991]. PSCs provide a surface on which heterogeneous – not purely gas phase – chemistry takes place. During polar winter on the surface of the PSC crystals a number of heterogeneous reactions are possible, which slowly transfer chlorine from non-reactive reservoir species like $ClONO_2$, HOCl and HCl back to Cl_2, which in contrast to the reservoir species is photolysable:

$N_2O_5 + H_2O$	$\rightarrow$	$2\ HNO_3$	$[1.8 \cdot 10^{-31} cm^6/(molec.^2 \cdot sec)]$	(R2.32)
$ClONO_2 + H_2O$	$\rightarrow$	$HOCl + HNO_3$	$[5.2 \cdot 10^{-31} cm^6/(molec.^2 \cdot sec)]$	(R2.33)
$ClONO_2 + HCl$	$\rightarrow$	$Cl_2 + HNO_3$	$[5.2 \cdot 10^{-31} cm^6/(molec.^2 \cdot sec)]$	(R2.34)
$HOCl + HCl$	$\rightarrow$	$Cl_2 + H_2O$	$[5.2 \cdot 10^{-31} cm^6/(molec.^2 \cdot sec)]$	(R2.35)
$N_2O_5 + HCl$	$\rightarrow$	$ClNO_2 + HNO_3$	$[5.2 \cdot 10^{-31} cm^6/(molec.^2 \cdot sec)]$	(R2.36)

After polar sunrise the Cl_2 molecules are photolysed, releasing chlorine atoms and thereby starting catalytic ozone destruction. Due to the enhanced abundance of chlorine and the low temperatures apart from (M8a) two further mechanisms become important [Molina and Molina 1987]:

	$ClO + ClO + M$	$\rightarrow$	$Cl_2O_2 + M$	$[2.2 \cdot 10^{-32} cm^6/(molec.^2 \cdot sec)]$	(R2.37)
	$Cl_2O_2 + h\nu$	$\rightarrow$	$Cl + ClOO$		(R2.38)
	$ClOO + M$	$\rightarrow$	$Cl + O_2 + M$	$[6.23 \cdot 10^{-13} cm^3/(molec. \cdot sec)]$	(R2.39)
2 x	$(Cl + O_3$	$\rightarrow$	$ClO + O_2)$	$[1.21 \cdot 10^{-11} cm^3/(molec. \cdot sec)]$	(R2.23)
net.:	$2\ O_3$	$\rightarrow$	$3\ O_2$		(M11)

and a mixed BrO-ClO cycle [McElroy et al. 1986]:

	$ClO + BrO$	$\rightarrow$	$Br + OClO$	$[6.77 \cdot 10^{-12} cm^3/(molec. \cdot sec)]$	(R2.40)
	$ClO + BrO$	$\rightarrow$	$Br + ClOO$	$[6.07 \cdot 10^{-12} cm^3/(molec. \cdot sec)]$	(R2.41)
	$ClOO + M$	$\rightarrow$	$Cl + O_2 + M$		
	$ClO + BrO$	$\rightarrow$	$BrCl + O_2$	$[1.03 \cdot 10^{-12} cm^3/(molec. \cdot sec)]$	(R2.42)
	$BrCl + h\nu$	$\rightarrow$	$Br + Cl$		
	$Br + O_3$	$\rightarrow$	$BrO + O_2$	$[1.16 \cdot 10^{-12} cm^3/(molec. \cdot sec)]$	(R2.25)
	$Cl + O_3$	$\rightarrow$	$ClO + O_2$	$[1.21 \cdot 10^{-11} cm^3/(molec. \cdot sec)]$	(R2.23)
net.:	$2\ O_3$	$\rightarrow$	$3\ O_2$		(M12)

A by-product of the heterogeneous activation reactions (R2.32) to (R2.36) is the de-nitrification, i.e. the conversion of NO_x to HNO_3. The general formation of PSCs has a similar effect in that it also removes water and NO_x from the gas phase. If the temperatures are sufficiently low to allow the formation of water ice crystals on the surface of "normal" PSC (type I) crystals, another variety of PSCs is formed (PSC type II). PSC type II crystals can grow sufficiently large to allow even sedimentation from the stratosphere thereby de-hydrating and de-nitrificating the stratosphere even further.

De-nitrification is important, because NO_x is capable of transferring halogens from its active form, XO to a stable reservoir molecule $XONO_2$:

$ClO + NO_2 + M$	$\rightarrow$	$ClONO_2 + M$	$[1.8 \cdot 10^{-31} cm^6/(molec.^2 \cdot sec)]$	(R2.43)
$BrO + NO_2 + M$	$\rightarrow$	$BrONO_2 + M$	$[5.2 \cdot 10^{-31} cm^6/(molec.^2 \cdot sec)]$	(R2.44)

Cl atoms react with methane, CH_4 to form another reservoir species HCl via

$Cl + CH_4$	$\rightarrow$	$HCl + CH_3$	$[1.0 \cdot 10^{-13} cm^3/(molec. \cdot sec)]$	(R2.45)

In contrast, bromine atoms react slowly or not at all with methane:

$$Br + CH_4 \rightarrow HBr + CH_3 \quad [5.6 \cdot 10^{-23} cm^3/(molec. \cdot sec)] \quad (R2.46)$$

HOCl and HOBr are also reservoir species formed by reaction of ClO and BrO with HO_2:

$$HO_2 + BrO \rightarrow HOBr + O_2 \quad [2 \cdot 10^{-11} cm^3/(molec. \cdot sec)] \quad (R2.47)$$

$$HO_2 + ClO \rightarrow HOCl + O_2 \quad [4.99 \cdot 10^{-12} cm^3/(molec. \cdot sec)] \quad (R2.48)$$

As a result of the above reactions and the fact that the bromine reservoirs $BrONO_2$ and HOBr are more photolabile than $ClONO_2$ and HOCl, under non-perturbed stratospheric conditions only a small fraction of chlorine is present as ClO during daytime, but about 50% of bromine as BrO.

2.4 OZONE CHEMISTRY OF THE TROPOSPHERE

As ozone production via the Chapman cycle (R2.1) through (R2.5) is not possible in the troposphere, it was commonly believed until the 1970s that tropospheric ozone has its source in the stratosphere [Junge 1963], which indeed is the case. A study by [Fishman and Crutzen, 1978] showed that 50% of tropospheric ozone can be explained by transport from the stratosphere. They proposed NO_x driven chemistry as a further source for O_3:

$$NO_2 + h\nu\ (\lambda<420nm) \rightarrow NO + O(^3P) \quad (R2.49)$$

$$O(^3P) + O_2 + M \rightarrow O_3 + M^* \quad [6.0 \cdot 10^{-34} cm^6/(molec.^2 \cdot sec)] \quad (R2.2)$$

Parallel to that a competing reaction with NO exists as a sink for O_3:

$$NO + O_3 \rightarrow NO_2 + O_2 \quad [1.8 \cdot 10^{-14} cm^3/(molec. \cdot sec)] \quad (R2.50)$$

In absence of other gases this would quickly lead to a low equilibrium concentration of O_3. Consumption of NO by reaction with HO_2 and other peroxy radicals designated by RO_2 enables a higher equilibrium concentration of O_3 in remote clean troposphere leading to mixing ratios of 20ppb:

$$NO + HO_2 \rightarrow NO_2 + OH \quad [8.1 \cdot 10^{-12} cm^3/(molec. \cdot sec)] \quad (R2.51)$$

$$NO + RO_2 \rightarrow NO_2 + RO \quad (R2.52)$$

NO_x mixing ratios in remote regions are as low as 5-10 ppt, as for example in the Antarctic boundary layer [Jones et al. 1999] and 10-20 ppt in the arctic [Beine et al. 2001]. Provided sufficient NO_x is present, the oxidation of **CH_4 and non-methane hydrocarbons** results in a catalytic chain generating O_3:

	$CH_4 + OH$	$\rightarrow$	$CH_3 + H_2O$	$[6.4 \cdot 10^{-15} cm^3/(molec. \cdot sec)]$	(R2.53)
	$CH_3 + O_2 + M$	$\rightarrow$	$CH_3O_2 + M$	$[4.5 \cdot 10^{-31} cm^6/(molec.^2 \cdot sec)]$	(R2.54)
	$CH_3O_2 + NO$	$\rightarrow$	$CH_3O + NO_2$	$[7.7 \cdot 10^{-12} cm^3/(molec. \cdot sec)]$	(R2.55)
	$CH_3O + O_2$	$\rightarrow$	$CH_2O + HO_2$	$[1.9 \cdot 10^{-15} cm^3/(molec. \cdot sec)]$	(R2.56)
	$CH_2O + h\nu$	$\rightarrow$	$0.5 \text{ x } (HCO + H)$	(50%)	(R2.57a)
		$\rightarrow$	$0.5 \text{ x } (H_2 + CO)$	(50%)	(R2.57b)
	$0.5 \text{ x } (HCO + O_2 + M$	$\rightarrow$	$CO + HO_2 + M)$	$[5.6 \cdot 10^{-12} cm^3/(molec. \cdot sec)]$	(R2.58)
	$0.5 \text{ x } (H + O_2 + M$	$\rightarrow$	$HO_2 + M)$	$[5.7 \cdot 10^{-32} cm^6/(molec.^2 \cdot sec)]$	(R2.59)
	$2 \text{ x } (HO_2 + NO$	$\rightarrow$	$OH + NO_2)$	$[9.5 \cdot 10^{-12} cm^3/(molec. \cdot sec)]$	(R2.60)
	$3 \text{ x } (NO_2 + h\nu$	$\rightarrow$	$NO + O)$		(R2.49)
	$3 \text{ x } (O + O_2 + M$	$\rightarrow$	$O_3 + M^*)$	$[6.0 \cdot 10^{-34} cm^6/(molec.^2 \cdot sec)]$	(R2.2)
net.:	**CH_4 + 6 O_2**	$\rightarrow$	$H_2O + 0.5\ H_2 + CO + OH +$ **3 O_3**		(M13)

Formation of O_3 depends on the regeneration of NO_2, which in turn depends on the availability of hydrocarbons and NO_x. At low $[NO]/[O_3]$ ratios the reaction of HO_2 with O_3 instead of NO will become dominant:

	$HO_2 + O_3$	$\rightarrow$	$OH + 2\ O_2$	$[2 \cdot 10^{-15} cm^3/(molec. \cdot sec)]$	(R2.61)

Under such circumstances the oxidation of hydrocarbons will lead to a consumption of tropospheric O_3 instead of a formation. The threshold NO mixing ratio lies at $3 \cdot 10^{-11}$. Below this mixing ratio O_3 will be consumed. Above it, it will be produced.

Oxidation of CO can also lead to a production of O_3 [Fishman and Crutzen 1978]:

$CO + OH$	$\rightarrow$	$CO_2 + H$	$[1.7 \cdot 10^{-13} cm^3/(molec. \cdot sec)]$	(R2.62)
$H + O_2 + M$	$\rightarrow$	$HO_2 + M$	$[5.7 \cdot 10^{-32} cm^6/(molec.^2 \cdot sec)]$	(R2.59)
$HO_2 + NO$	$\rightarrow$	$OH + NO_2$	$[9.5 \cdot 10^{-12} cm^3/(molec. \cdot sec)]$	(R2.60)
$NO_2 + h\nu$	$\rightarrow$	$NO + O$		(R2.49)
$O + O_2 + M$	$\rightarrow$	$O_3 + M^*$	$[6.0 \cdot 10^{-34} cm^6/(molec.^2 \cdot sec)]$	(R2.2)
$CO + 2\ O_2$	$\rightarrow$	$CO_2 + O_3$		(M14)

As in (M13), production of O_3 is possible only at higher NO_x above mixing ratios of 10ppt [Crutzen and Zimmermann, 1991]. In remote clean troposphere again HO_2 will dominantly react with O_3 instead of NO leading to a consumption of O_3 instead:

$CO + OH$	$\rightarrow$	$CO_2 + H$	$[1.7 \cdot 10^{-13} cm^3/(molec. \cdot sec)]$	(R2.62)
$H + O_2 + M$	$\rightarrow$	$HO_2 + M$	$[5.7 \cdot 10^{-32} cm^6/(molec.^2 \cdot sec)]$	(R2.59)
$HO_2 + O_3$	$\rightarrow$	$OH + 2\ O_2$	$[2 \cdot 10^{-15} cm^3/(molec. \cdot sec)]$	(R2.61)
$CO + O_3$	$\rightarrow$	$CO_2 + O_2$		(M15)

2.4.1 Halogen driven ozone chemistry of the marine boundary layer

A region of special interest is the marine boundary layer during polar sunrise. Here the ozone budget is strongly influenced by halogen chemistry sometimes leading to a complete temporary depletion of surface ozone. These events were sometimes referred to as *tropospheric ozone holes*. The occurrence is linked to localised largely elevated bromine mixing ratios. The process leading to such elevated BrO mixing ratios are often referred to as *bromine explosion.*

During the 1990s strong and sudden increases in BrO mixing ratio were found in the Antarctic [Kreher et al. 1997] as well as in the Arctic [e.g. Barrie et al. 1988, Bottenheim et al. 1990, Haussmann and Platt 1994, Wittrock et al. 1996, Tuckermann et al. 1997, Martinez

et al. 1999, McElroy et al. 1999]. Large polar air masses of elevated BrO were also observed in both hemispheres by remote sensing from satellite [Richter et al. 1998]. They spanned areas of several thousands of square kilometers. [McElroy et al. 1999] proposed that these boundary layer clouds of BrO could contribute to BrO in the free troposphere as well. The occurrence of elevated BrO was always accompanied by elevated losses of O_3. This is indicative of catalytic destruction of O_3 by bromine chemistry.

Elevated iodine and bromine aerosol concentrations were observed in the marine boundary layer after polar sunrise by [Bottenheim et al. 1990, Barrie et al. 1994]. While the occurrences of bromine and iodine are roughly correlated, there exist clear differences in seasonal variation [Barrie et al. 1994] which are not yet clear [Sirois and Barrie 1999]. But the correlation between low ozone events and the occurrences of elevated bromine and iodine is indicative of at least a partial contribution of iodine to low ozone events during polar sunrise [Carpenter 2003]. Significant amounts of reactive IO and OIO in the mid-latitude marine boundary layer were detected by [Allicke et al. 1999, Allan et al. 2000, Allan et al. 2001] using direct spectroscopic measurements. Wittrock et al. [1996] observed IO above Ny Alesund in ground based zenith sky DOAS measurements. Organic precursors were detected by direct in-situ measurements in mid-latitude marine boundary layer by Carpenter et al. [1999].

The mixing ratios observed for bromine present an important question, because even low mixing ratios of the order of ppt can have an effect on the tropospheric ozone budget [Sander and Cutzen 1996]. As sources for tropospheric halogens two mechanisms have been identified. Firstly release from sea salt and secondly the photolysis of organo-halogenated compounds. Sea salt release mechanisms were described e.g. by [Sander and Crutzen 1996] and [Vogt et al. 1996]. Sea salt contains a large fraction of Cl^- (55.7%), some Br^- (0.19%) and very little I^- ($2 \cdot 10^{-5}$%) [Holland 1978]. Holland firstly discussed the possible halogen release from sea salt.

The observed sudden and localised clouds of elevated BrO mixing ratios in the high latitude marine boundary layer can to a certain extent be explained by auto-catalytic release of halogens from sea salt by the following mechanism [Fan and Jacob 1992, Vogt et al. 1996, Tang and McConnell 1996]:

$$
\begin{aligned}
X + O_3 &\rightarrow XO + O_2 \\
XO + HO_2 &\rightarrow HOX + O_2 \\
(HOX)_g &\rightarrow (HOX)_{aq} \\
(HOX)_{aq} + (Y^-)_{aq} + (H^+)_{aq} &\rightarrow (XY)_{aq} + H_2O \\
(XY)_{aq} &\rightarrow (XY)_g \\
XY + h\nu &\rightarrow X + Y \\
\hline
X + HO_2 + (Y^-)_{aq} + (H^+)_{aq} + O_3 &\rightarrow X + Y + H_2O + 2\,O_2
\end{aligned}
\qquad \text{(M16)}
$$

for X and Y = Cl and Br. Release of ClBr or Br_2 would be rapid, as both are highly volatile. Photolysis during daylight followed by reaction with O_3 would reproduce XO as feedback to the auto-catalytic cycle. This mechanisms was verified by laboratory studies by Fickert et al. [1999]. They also reported that release of bromine is favoured over that of chlorine, making chlorine release a by-product of bromine auto-catalytic production. Auto-catalytic release of iodine is unlikely due to the much smaller iodine content. Nevertheless elevated IO concentrations could contribute to auto-catalytic release of bromine, because iodine gas phase reactions are generally faster than those of bromine or chlorine.

Recently, frost flowers have been recognised as the dominant source of sea salt aerosol in the Antarctic. They provide a large effective surface and a reservoir of sea salt ions at significantly elevated concentrations. Such conditions favour heterogeneous autocatalytic reactions as above taking place on their salt-laden ice surfaces. Recent studies comparing ice coverage data with BrO mixing ratios, both from satellite data, provided evidence for a correlation between the two [Kaleschke et al. 2004]. This indicates that indeed frost flowers on newly formed sea ice are the source of bromine found in the bromine events.

The other source of bromine in the troposphere is by degradation or photolysis of halocarbons. They originate naturally from algae and occur as various species: CH_3Br, CH_2Br_2, $CHBr_3$, as well as mixed species as CH_2IBr. But also the corresponding iodine species exist: CH_3I, CH_2I_2, CHI_3, and CH_2ICl. All of them are easily photolysed in the troposphere giving rise to short life times. For brominated hydrocarbons they are of the order of months, while for iodinated hydrocarbons they are of the order of minutes to some days.

So while tropospheric bromine is believed to be dominantly produced by auto-catalytic release from sea salt explaining the localised occurrence of elevated bromine mixing ratios, for iodine the major sources in the marine boundary layer are identified to be iodo-hydrocarbons from marine algae [see Carpenter 2003 for a review]. In coastal tidal regions iodo-hydrocarbons are released by macro algae under conditions of oxidative stress. This is supported by observations which showed clearly elevated mixing ratios for some reactive halocarbons at low tide [Carpenter et al. 1999]. But there is evidence for other offshore sources of halocarbons from both in-situ measurements as well as modelling studies [Carpenter et al. 2000, Carpenter et al. 2001]. This is consistent with micro algae, which inhabit the entire ocean surface and which could be shown to be a significant source of a number of halocarbons [Itoh et al. 1997, Manley and de la Cuesta 1997]. Shipboard measurements gave some evidence for possible production of CH_2I_2 and CH_2ICl by micro algae [Klick and Abrahamsson 1992, Moore and Tokarczyk 1993, Schall et al. 1997] and also for a spring time seasonal maximum in coastal waters [Klick 1992]. But even though laboratory and field data do not give a complete picture yet, the data is sufficiently consistent to consider both macro and micro algae as significant sources for boundary layer iodo-hydrocarbons.

Already in 1980 Chameides and Davis [1980] published an extensive study on the possible role of iodine in tropospheric chemistry. Other studies followed considering its potential with respect to lower stratosphere ozone depletion and again on tropospheric chemistry [Davis 1996]. Given the aforementioned observational data for bromine and iodine reactive species, by now there is increasing evidence that both iodine and bromine play a significant role in tropospheric chemistry in a number of regions. Under tropospheric conditions mechanism (M1) is negligible, because of the lack of free oxygen atoms. Due to the much higher abundance of O_2 as compared to any halogen monoxide XO, reaction with O_2 will be the dominant sink for O.

Therefore mechanisms involving the self reaction of XO (x = Cl, Br, and IO) have to be considered:

$$
\begin{array}{lrcl}
2 \times (& X + O_3 & \rightarrow & XO + O_2) \\
 & XO + XO & \rightarrow & 2\,X + O_2 \\
\hline
\text{net.:} & 2\,O_3 & \rightarrow & 3\,O_2
\end{array}
\qquad \text{(M17)}
$$

as well as interhalogen reactions of the monoxides:

	$X + O_3$	$\rightarrow$	$XO + O_2$	
	$Y + O_3$	$\rightarrow$	$XO + O_2$	
	$XO + YO$	$\rightarrow$	$X + Y + O_2$	
net.:	$2\ O_3$	$\rightarrow$	$3\ O_2$	(M18)

The efficiency of these mechanisms depends on the rates of the self reaction and the interhalogen reaction respectively. They are the rate limiting steps in the mechanisms. Alternative channels of XO+XO as well as of XO+YO need also be considered. Especially those forming the dioxides and possibly the dimer are of importance, as they might open up pathways to aerosol formation via higher oxides or even further O_3 consumption. In this context the observation of Himmelmann et al. [1996] proved to be significant as they reported for the first time unequivocally the existence of OIO as a product from flash photolysis of I_2 in the presence of O_3. The ozone depletion potential of OIO depends critically on the possible photolysis pathways:

$OIO + h\nu$	$\rightarrow$	$IO + O(^3P)$	(R2.63a)
	$\rightarrow$	$I + O_2$	(R2.63b)

Photolysis via (R2.63b) would increase the O_3 depletion potential, because this would enable the following O_3 depleting cycle [Plane et al. 2001]:

2 x (	$I + O_3$	$\rightarrow$	$IO + O_2$)	$[1.2 \cdot 10^{-12} cm^3/(molec. \cdot sec)]$	(R2.27)
	$IO + IO$	$\rightarrow$	$OIO + I$		(R2.64)
	$OIO + h\nu$	$\rightarrow$	$I + O_2$		(R2.63b)
net.:	$2\ O_3$	$\rightarrow$	$3\ O_2$		(M19)

If photolysis takes place via (R2.63a), (M19) would be a null cycle via recycling $O(^3P)$. The photodissociation of OIO is currently a question of ongoing research and discussion. Misra and Marshall [1998] calculated a threshold wavelength of 418nm for photolysis via (R2.63a). The absorption spectrum of OIO is centred around 550nm and the separated spectra

determined in this work clearly die off at 450nm, already clearly in the overlap region with the IO absorption. At 418nm the absorption cross section of OIO therefore is very small, which would indicate only a very small contribution of (R2.63a) to ozone depletion. Ingham et al. [2000] reported that at laser photolysis at 532nm no photo-dissociation of OIO was observed placing an upper limit to the quantum yield of $7 \cdot 10^{-3}$ at that wavelength. Contrasting this, recent laboratory studies by Plane et al. [2001] suggested the possibility of photodissociation via (R2.63a). Maier and Bothur [1997] observed OIO trapped in an argon matrix and reported OIO photolysis at λ>435nm. Therefore the question of photo-dissociation of OIO and the implication on catalytic consumption of O_3 are still an open issue.

Another cycle for iodine dependent O_3 depletion could involve reaction with **HO_2** [Carpenter 2003]:

	$I + O_3$	$\rightarrow$	$IO + O_2$	$[1.2 \cdot 10^{-12} cm^3/(molec. \cdot sec)]$	(R2.27)
	$IO + HO_2$	$\rightarrow$	$HOI + O_2$	$[8.4 \cdot 10^{-11} cm^3/(molec. \cdot sec)]$	(R2.65)
	$HOI + h\nu$	$\rightarrow$	$OH + I$		(R2.66)
net.:	$2\ O_3$	$\rightarrow$	$3\ O_2$		(M20)

At higher concentrations of NO_x a regeneration of I atoms and a formation of NO_2 takes place, compensating the O_3 depletion and making (M21) a null cycle:

	$I + O_3$	$\rightarrow$	$IO + O_2$	$[1.2 \cdot 10^{-12} cm^3/(molec. \cdot sec)]$	(R2.27)
	$IO + NO$	$\rightarrow$	$I + NO_2$	$[2 \cdot 10^{-11} cm^3/(molec. \cdot sec)]$	(R2.67)
	$NO_2 + h\nu$	$\rightarrow$	$NO + O$		(R2.49)
	$O + O_2 + M$	$\rightarrow$	$O_3 + M$	$[6.0 \cdot 10^{-34} cm^6/(molec.^2 \cdot sec)]$	(R2.2)
net.:	$O_3 + O_2 + O$	$\rightarrow$	$O_3 + O_2 + O$		(M21)

Other depletion cycles can by hypothesised:

4 x (	$I + O_3$	$\rightarrow$	$IO + O_2$)	$[1.2 \cdot 10^{-12} cm^3/(molec. \cdot sec)]$	(R2.27)
4 x (	$IO + NO_2 + M$	$\rightarrow$	$IONO_2 + M$)	$[5.9 \cdot 10^{-31} cm^6/(molec.^2 \cdot sec)]$	(R2.68)
	$IONO_2 + M$	$\rightarrow$	$IO + NO_2 + M$	branching: α	(R2.69a)
	$IONO_2 + M$	$\rightarrow$	$I + NO_3 + M$	branching: $1-\alpha$	(R2.69b)
	$IONO_2 + h\nu$	$\rightarrow$	$I + NO_3$	branching: β	(R2.70a)
	$IONO_2 + h\nu$	$\rightarrow$	$IO + NO_2$	branching: $1-\beta$	(R2.70b)
					(M22)

The potential ozone depletion of (M22) depends on the individual branching ratios of (R2.69a,b), (R2.70a,b), and the rate coefficient. These are not or not well determined yet. also the effect of NO_3 photolysis recycling O and therefore O_3 needs to be taken into account. There are some indications for possible contribution of (M22) to boundary layer ozone loss [Carpenter, 2003].

A large number of modelling studies have been performed to estimate the partitioning of the iodine species and its contribution to halogen activation and ozone destruction. They indicate a clear potential of iodine for ozone destruction. But a common conclusion of all – early as well as recent studies - was also that sound assessments of the importance of iodine chemistry are impeded by missing knowledge of the iodine precursor fluxes and the significant lack of kinetic and spectroscopic data [Zafiriou 1974, Chameides and Davis 1980, Jenkin et al. 1985, Chatfield and Crutzen 1990, Jenkin 1993, Solomon et al. 1994, Davis et al. 1996, Vogt et al. 1999, von Glasow and Crutzen 2002, Bedjanian and Poulet 2003].

Apart from the role of iodine in ozone depletion and halogen activation also that in aerosol formation is of concern, as aerosol formation in the troposphere has an impact on both regional and global climate. Correlation between low tide and observation of gas phase inorganic iodine compounds and increased particle formation (O'Dowd et al. [2002] and references therein) indicate such a link (Carpenter et al. [1999], Saiz-Lopez and Plane [2004] and references therein). Hoffmann et al. [2001] suggested polymerisation of IO and OIO to form higher iodine oxides as precursors to aerosol formation. O'Dowd [2001] observed significant bursts of new particle formation during low tide and Hoffmann et al. [2001] suggested that I_xO_y

formation could be the cause to this. Formation of aerosols is a common feature of iodine laboratory experiments, where at high concentration of iodine species in many cases a whitish deposit was observed in the reaction vessels [Cox and Coker 1983, Harwood et al. 1997, Spietz et al. 1998, Bloss 2001]. By standard IR spectroscopy, consideration of the observed needle shaped cristals and the strong hygroscopic character of the deposit obtained from I_2/O_3 flash photolysis experiments, I_2O_5 could be identified to be a product of $IO/OIO/O_3$ chemistry [Spietz 1997]. McFiggans et al. [2000] obtained good agreement between observations of IO in the marine boundary layer [Allan et al. 2000] and a box model including iodine recycling through marine aerosol. They predict an impact of iodine on catalytic O_3 consumption in the boundary layer and a significant enrichment of iodine in marine aerosol. Also de-nitrification by enhanced uptake of $IONO_2$ into aerosols was indicated by their results.

In a number of studies OIO and higher oxides I_xO_y have been implicated in the particle formation in the marine boundary layer [Hoffmann et al. 2001, O'Dowd et al. 2002, Burkholder et al. 2004] but the mechanism is still not understood. Again solid assessments are limited if not impeded, as for the absorption cross section of OIO only estimates were available and kinetic data of its formation and consumption is insufficient. Spectroscopic evidence for higher iodine oxides in literature is only scarce, where a number of featureless absorptions of changing appearance have been reported. A clear identification of spectra and absorbers is missing. Estimation of photolytic stability and lifetimes of higher oxides is not possible. The aspects of iodine aerosol chemistry increased the focus of laboratory studies on the formation and identification of higher oxides. Still the pathway leading from IO and OIO to the end-products, among which up to now only I_2O_5 is clearly identified, is not understood.

In the next chapter the knowledge obtained from laboratory studies of relevance to the atmosphere will be summarised. This will also show the gaps and inconsistencies in our knowledge, which were already found to limit modelling studies and to impede solid assessments of the role of iodine in the different aspects of atmospheric chemistry. This discussion will lead to the objectives and the layout of the present work.

3 AVAILABLE REFERENCE DATA FOR IODINE OXIDES

3.1 ABSORPTION CROSS SECTIONS FOR IO AND OIO

IO emission spectra have been known since the first studies of Vaidya [1937]. Durie and Ramsey [1958] recorded the first absorption spectrum of IO. In [1960] Durie et al. published a thorough study of the emission system of IO, where vibrational and rotational analysis was performed. Since then spectra of iodine oxides and their absorption cross sections have been studied frequently [see **Table 3.1** and also e.g. Vikis and McFarlane 1985, Turnipseed et al. 1995, Himmelmann et al. 1996, Maier and Bothur 1997, Newmann et al. 1998, Atkinson et al. 1999, Ingham et al. 2000, Miller et al. 2001, Miller and Cohen 2003]. OIO was discovered significantly later than IO. Only in 1996 it was discovered by Himmelmann et al. [1996] in Bremen, who first observed its gas phase absorption spectrum in the visible in the photolysis of mixtures of I_2 and O_3. Other absorptions, which could be attributed to other or higher oxides have been reported by different authors, but identification was always tentative or at least not unequivocally [Harwood et al. 1997, Spietz et al. 1998, Bloss 2001, Rowley et al. 1999]. Formation of aerosols as a common feature of iodine laboratory experiments with formation of a whitish deposit was also observed [Cox and Coker 1983, Harwood et al. 1997, Spietz et al. 1998, Bloss 2001]. Molecules of interest are I_2O_2 and I_2O_3, which are likely to be among the reaction products formed in IO and OIO consumption. Such molecules are likely to form the link between primary products IO and OIO and higher oxides as late and possibly final products. Neither the expected intermediate nor the possibly final oxides themselves (with the exception of I_2O_5) have been observed and identified. This also limits our understanding of aerosol formation, which is of interest to the atmosphere, see above.

When considering spectroscopic data available for IO and OIO, a considerable uncertainty if not disagreement among the up to now published results becomes apparent. **Table 3.1** summarises the previously published estimates for the IO(4←0) and for the OIO absorption cross section. For OIO only very few estimates and determinations have been published.

Reference	$\sigma IO(4\leftarrow0)\cdot10^{-17}$ ($cm^2\cdot molec^{-1}$)	$\sigma OIO\cdot10^{-17}$ ($cm^2\cdot molec^{-1}$)	FWHM (nm)	T (K)
Clyne and Cruse, [1970]	0.5	-	0.25	293
Cox and Coker, [1983]	$3.1^{+2}_{-1.5}$ λ=426.9nm	-	0.27	303
Jenkin and Cox, [1985]	2.2±0.5	-	0.27	306
Sander, [1986]	3.1±0.3	-	0.17	298
Stickel et al.,[1988]	3.1±0.6	-	0.3	300
Lazlo et al., [1995]	2.8±0.5	-	0.3	295
Huie et al., [1995]	2.7±0.5	-	0.3	295
Harwood et al., [1997]	3.6±0.5	-	0.14	203-373
Spietz et al., [1998]	3.8±0.2	>0.4 (0,5,1) (range: 2 to 5)	0.27	293
Bloss et al., [2001]	1.9±0.2	$0.87\pm0.15<\sigma_{OIO}<1.29\pm0.22$ (0,5,1)	1.13	295
Joseph et al., [2002]		1.64±0.10 (0,4,1)	0.4 (CRDS)	

Table 3.1: The absorption cross sections $\sigma_{IO}(4\leftarrow0)$ and σ_{OIO} as determined by different authors are shown. The resolution, at which the cross sections were determined, is given as full width at half maximum FWHM.

3.2 CHEMICAL KINETICS REFERENCE DATA

In the same way the published chemical kinetic rate coefficients for the main reactions involved in the formation and consumption of IO and OIO are far from being clearly understood. Determination of rate coefficients and cross sections are often critically linked, as most experiments yield ratios of absolute cross section divided by the rate coefficients of the relevant reactions. In addition to the aforementioned studies, which either focussed on spectroscopic aspects or covered spectroscopic aspects and chemical kinetics simultaneously, also a large number of studies on chemical kinetics of formation and consumption of iodine oxides exist [Turnipseed et al. 1995, Gilles et al. 1997, Turnipseed et al. 1997, Atkinson et al. 1999, Larin et al. 1999, Canosa-Mas et al. 1999,Vipond et al. 2002]. By analogy to the well

established case of chlorine for the self reaction of IO in principle five channels are possible, if different isomeric structures for I_2O_2 are disregarded:

$IO + IO + M$	$\rightarrow$	$I_2O_2 + M$	(R3.1a)
$IO + IO$	$\rightarrow$	$I_2 + O_2$	(R3.1b)
$IO + IO$	$\rightarrow$	$2\,I + O_2$	(R3.1c)
$IO + IO$	$\rightarrow$	$IOO + I$	(R3.1d)
$IO + IO$	$\rightarrow$	$OIO + I$	(R3.1e)

Tab. 3.1 lists rate coefficients published for the IO self reaction. Most publications report a rate coefficient for the overall reaction and a combination of either I-atom producing channels or non-I-atom producing channels. Results for branching ratios are only a few and the agreement is not satisfying. Channel (R3.1a) is frequently considered as a significant source for the I_2O_2 dimer [Sander 1986, Harwood et al. 1997, Bloss et al. 2001] even though up to now no unequivocally spectroscopic evidence for its existence has been published. For channel (R3.1b) Sander [1986] and Laszlo et al. [1995] placed an upper limit of 5% and Harwood et al. [1997] one of 30% of the overall (R3.1) rate. Unpublished work from our lab yielded an upper limit of 7%. Energy considerations showed that this channel is inhibited by an energy barrier [Plane 2003, private communication].

Channel (R3.1d) postulates the existence of IOO, which was never observed except in matrix isolation experiments [Maier and Bothur 1997]. Ab initio calculations and energy considerations showed IOO to be only very weakly bound if stable at all. The only channel of which existence up to now seems to be considerably well established is therefore channel (R3.1e) as a source to the observed OIO. Ab initio calculations by Misra and Marshall [1998] predict OIO to be the major product with $\Delta_f H°(OIO)=76.7 kJ \cdot mol^{-1}$. In time resolved measurements the formation of OIO always follows a pattern which is highly correlated in extent and time to the observed IO concentrations. But still simulations and modelling of observed optical density against time have not yet been able to reproduce the observations. Especially the consumption of OIO, which occurs to be faster than that of IO is still an open question of concern.

Reference	Reaction	rate coefficient [$cm^3 \cdot mole^{-1} \cdot s^{-1}$]
Cox and Coker 1983	$IO + IO \xrightarrow{M} I_2O_2$ $IO + IO \rightarrow I + IOO \rightarrow 2I + O_2$	near gas kinetic collision rate
Jenkin and Cox 1985	$IO + IO \rightarrow$ products	$(2.8\pm0.4)\cdot10^{-11}$ p-depend., 200mbar $(8.0\pm2.7)\cdot10^{-12}$ p-independent
Sander 1986	$IO + IO \rightarrow IOOI^* \xrightarrow{M} I_2O_2$ (a) $\rightarrow I_2 + O_2$ (b) $\rightarrow 2I + O_2$ (c) $IO + IO \rightarrow IOIO^* \rightarrow I + OIO$ (e)	k_{prod}: $5.3^{+4.7}_{-2.6}\cdot10^{-11}$ $(k_c+0.5k_e)/k_{prod}=0.45$ at 28mbar $k_b < 5\%$
Stickel et al. 1988	$IO + IO \rightarrow$ products	k_{prod}: $(6.6\pm2)\cdot10^{-11}$
Jenkin et al. 1991	$IO + IO \xrightarrow{M} I_2O_2$	
Laszlo et al. 1995 Huie et al. 1995	$IO + IO \xrightarrow{M} OIO + I$ (e) $\rightarrow I_2 + O_2$ (b) $\rightarrow 2I + O_2$ (c)	k_{prod}: $(8.0\pm1.8)\cdot10^{-11}$
Harwood et al. 1997	$IO + IO \xrightarrow{M} I_2O_2$ (a) $\rightarrow I_2 + O_2$ (b) $\rightarrow 2I + O_2$ (c) $\rightarrow OIO + I$ (e)	k_{prod}: $(9.9\pm1.5)\cdot10^{-11}$ $(k_a+0.5k_e)/k_{prod}=0.78$ at 1000mbar $k_b<30\%$
Atkinson et al. 1999	$IO + IO \rightarrow$ prod.	$k_{prod.}$: $(10\pm3)\cdot10^{-11}$
Ingham et al. 2000	$IO + IO \rightarrow$ prod.	k_{prod}: $(9.3\pm1)\cdot10^{-11}$
Vipond et al. 2002	$IO + IO \xrightarrow{M} I_2O_2$ (a) $\rightarrow I_2 + O_2$ (b) $\rightarrow 2I + O_2$ (c) $\rightarrow OIO + I$ (e)	k_{prod} : $(9.3\pm1.9)\cdot10^{-11}$ at 2 Torr $k_a\approx0$ at given pressure $k_b\approx0$ $k_c>0.56\pm0.20$ $k_e<0.44\pm0.20$
Bloss et al. 2001	$IO + IO \xrightarrow{M} I_2O_2$ (a) $\rightarrow I_2 + O_2$ (b) $\rightarrow 2I + O_2$ (c) $\rightarrow OIO + I$ (e)	k_{prod} : $(8.2\pm1)\cdot10^{-11}$ $0.42 < k_a/k_{prod} < 0.55$ $k_b/k_{prod} \le 0.05$ $0.07 < k_c/k_{prod} < 0.15$ $0.30 < k_e/k_{prod} < 0.46$
Dillon et al.[a] 2004	$IO + IO \xrightarrow{M} I_2O_2$ (a) $\rightarrow I_2 + O_2$ (b) $\rightarrow 2I + O_2$ (c) $\rightarrow OIO + I$ (e)	k_{prod}: $(9.8\pm1.2)\cdot10^{-11}$ $(k_c+0.5k_e)/k_{prod}=0.4$ at 26.7mbar

Table 3.1 For the self reaction of IO mostly overall rate coefficients have been published, where the more recent determinations differ significantly from the earlier ones. Results on detailed branching ratios are scarce. Different intermediates IOIO and IOOI have been considered. But even though a large branching ratio of approximately 50% is postulated for that channel, spectroscopic evidence for its existence is still missing.)[a]: private communication 2004.

In $I+O_3$ photolysis experiments undertaken in the context of the present work a significant formation of vibrationally excited IO at ν"=1 and 2 was observed at optical densities of up to 40% of that of ground state IO(4←0) absorptions [Spietz and Gómez-Martín, unpublished work]. Harwood [1997] also observed absorptions by vibrationally excited IO in $O+CF_3I$ photolysis, but they reached only less than 10% of the (4←0) transition. The role of these excited species up to then remained unclear.

Further doubts about our present understanding of IO chemistry arise from the contradictory observations of pressure dependence in the temporal behaviour of IO concentration. While in systems without ozone no pressure dependence for the consumption of IO is observed [e.g. Sander 1986, Laszlo 1995], other observations in systems with O_3 give evidence for the existence of pressure dependent reactions of IO consumption [e.g. Cox and Coker 1983 compared to Clyne and Cruse 1970, Jenkin and Cox 1985] as well as possibly its formation [Spietz and Gómez-Martín, unpublished work]. The possible formation of the I_2O_2 dimer is a critical issue in this context. If this channel existed, it would by necessity be pressure dependent. Similarly, reaction of IO and OIO forming I_2O_3 could be a plausible sink for IO and OIO, especially because strong sinks are needed to explain the fast OIO consumption:

$$IO + OIO + M \rightarrow I_2O_3 + M \qquad \text{(R3.2)}$$

Both analogous reactions for bromine [Rowley et al.1996] and chlorine [NIST 1998] are established. But again such a reaction – if significant - would introduce a likewise significant pressure dependence into the consumption of IO. Which is not what has been observed in experiments without O_3.

With respect to the formation of I_2 an IO-catalysed mechanism was proposed by Harwood et al. [1997]:

$$I + IO + M \rightarrow I_2O + M \qquad \text{(R3.3)}$$

$$I_2O + I \rightarrow I_2 + IO \qquad \text{Cl: } [9.6\cdot10^{-11}\text{cm}^3/(\text{molec.}\cdot\text{sec})] \qquad \text{(R3.4)}$$

$$\text{net.:} \quad 2\,I \rightarrow I_2 \qquad \text{(M3.1)}$$

Observations by Bloss et al. [2001] support this prediction. If (R3.4) would be similarly fast as it is in the case of chlorine, (R3.3) would be the rate limiting step once the pressure is

reduced below a certain threshold depending on mixing ratios. Again this would produce a pressure dependence, which is not observed in mixtures without O_3.

In summary our understanding of the mechanism of IO and OIO formation and consumption is far from satisfactory. Even though the role of vibrationally excited IO in its formation appears to be significant, the mechanism remains to be clarified and its impact quantified. While the overall rate coefficient of its self reaction at least among the recent publications seems to converge near 9 to $10 \cdot 10^{-11} cm^3 \cdot molec^{-1} \cdot s^{-1}$ the individual channels can not be called well established. This is severely limiting the possibilities and reliability of determining an absorption cross section for OIO. This even more as the mechanism of OIO consumption remains completely unclear. Whether reaction with itself or with IO, most studies indicate in any case large rate coefficients of the order $10^{-10} cm^3 \cdot molec^{-1} \cdot s^{-1}$. Under such circumstances a determination of cross sections, which has to rely on a knowledge of the chemical mechanism and rate coefficients would be highly dependent on the used kinetic reference data with all its uncertainties. A more independent determination is desirable.

3.3 SPECTRA OF IODINE OXIDES

Considering the available spectra of iodine oxides the situation is likewise far from satisfactory. Comparing the available observational data for the IO absorption spectrum illustrates this (see **Fig. 3.1**). While the band structure of the IO absorption spectrum is always present in the different data sets, still large differences exist about the background on which the banded structure is possibly situated. Some spectra show the IO(4←0) band situated on what appears to be a continuum, others closer to zero background absorption. Some tend towards a negative background indicating clearly problems with either lamp drift or overcorrected background absorptions of other absorbers.

Considering the ratio of the available data relative to an arbitrarily selected one (here the spectrum obtained in this work was used) shows the variations even clearer. While in the continuum region the scatter is only of the order of 20% around the maximum of the continuum, the deviations increase up to 50% towards its UV flank but also in the peaks of the dominant bands to the red. For this comparison the spectra were scaled to each other at the top of the (6←0) transition.

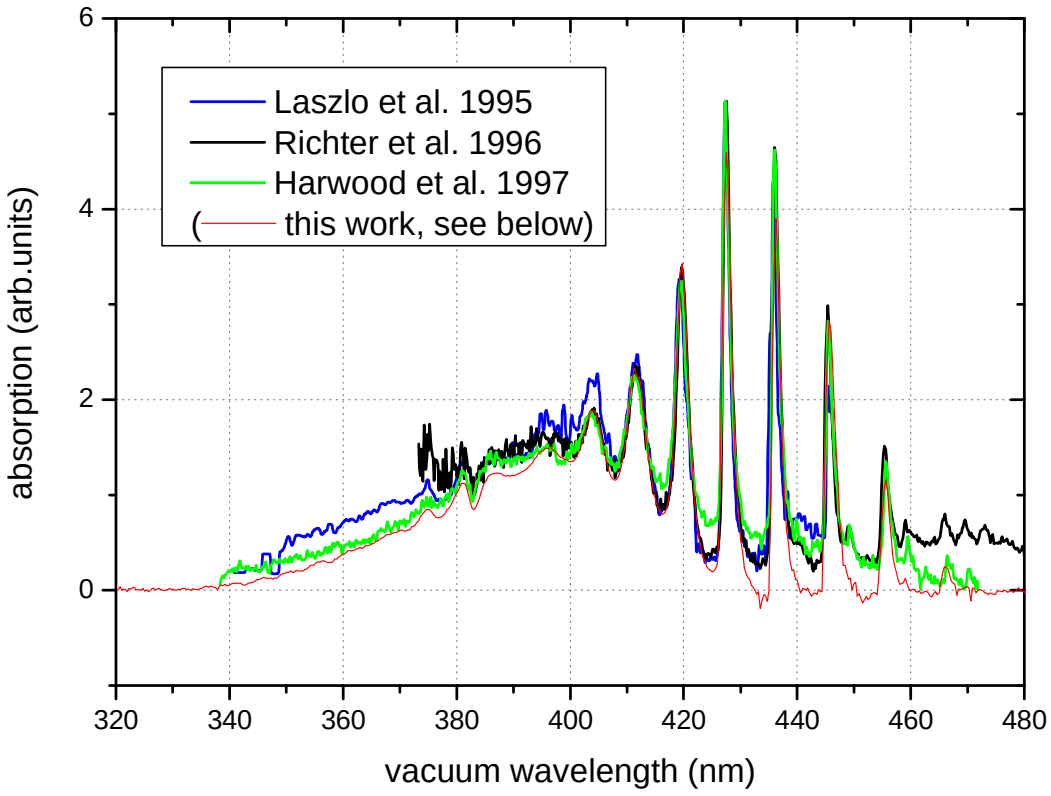

Figure 3.1 For IO a number of previously published spectra exist. They are plotted along with the spectrum obtained later on in this work for reference. All previously published spectra show different amounts of uncorrected background absorptions and fail to determine the ends of the spectrum. There is also disagreement with respect to the height of the bands. The spectrum of Laszlo et al. consists of two sections obtained in different chemical systems ($O+I_2$ first section and $O+CF_3I$ for 430-447nm)

For retrieving atmospheric abundances of IO with Differential Optical Absorption Spectroscopy DOAS [Solomon et al. 1987, Finlayson-Pitts and Pitts 2000], this situation is not satisfying as the uncertainty in differential cross section directly limits the achievable accuracy of the retrieved concentrations. As the available *relative* spectra of IO are scaled to an absolute absorption cross section determined in most cases for the IO(4←0) band, the differential absorption cross section hinges crucially on the correct determination of background absorption. Errors in the differential absorption cross section arising from insufficient separation and drift effects are 13% in the spectrum published by Harwood [1997] (relative to IO(4←0)) and 14% in Laszlo's spectrum [1995] (relative to IO(0-3)). In comparison to the former spectra the one published by Bloss et al. [2001] (not available) displays significantly less background absorption even though in the troughs between the

(4←0) down to the (0←0) a remaining background in their spectrum can not be excluded. Bands from excited IO and the overlapping band from OIO are superimposed.

Similar problems exist for the available OIO data by Himmelmann et al. [1996], Ingham et al. [2000], and Bloss et al. [2000] (not available). In Himmelmann et al. especially on the short wavelength side clear downward features and irregular background disturb the spectrum (see **Fig. 3.2**). The line shaped features can be caused by Xenon lines indicating disturbance of the spectrum by the Xenon photolysis flash tubes or vibrationally excited IO. Part of the neighbouring spectrum of IO is also plotted. From the troughs between IO bands the level of zero absorption can be inferred, as there no or only negligible absorptions exist. Relative to that the OIO spectrum is clearly situated on a background of unidentified origin. Sections of the spectrum tend below the inferred zero line and the background in general is irregular. This disagrees with the relatively regular shape of the analogous OBrO and OClO spectra. The spectrum by Ingham et al. shows similar problems of background with optical density clearly dipping below zero in the NIR. For comparability the spectra were scaled to each other in the region between 520 to 560 nm. In the bottom graph the ratio between the Himmelmann et al. spectrum and that by Ingham is plotted. Apart from the general disagreement in background also isolated line shaped features exist. These can either be caused by Xenon lines in the Himmelmann spectrum or by different contributions from overlapped IO(ν'←0) and IO(ν'←ν''), ν''>0 transitions or by a disagreement in wavelength calibration. The clear downward feature at 484.7nm coincides with the IO(2←1) band illustrating the problem of separation of overlapped spectra.

The temporal resolution of the Himmelmann et al. set-up was severely limited by slow and – even worse – sequential read-out of the used photodiode array. The time shift present within one spectrum was 16µs/pixel and therefore roughly 16ms per 1024 pixel spectrum. The half life time of OIO in the experiments was of the same order of magnitude. Keeping this in mind, it is not surprising that upon closer analysis of the original data the spectrum shows significant negative sections clearly proving the existence of unresolved problems caused by unknown background absorptions. Also traces of I_2 absorption bands can be found due to interference between the sequential read-out and the extraction of the spectrum by subtraction of consecutive spectra.

The existence of higher oxides as products of the IO/OIO consumption reactions in general is out of question owing to the fact that in the consumption of IO and OIO iodine is always lost to

unaccounted sinks. But spectra of products – if observed at all - are scarce, not very accurate and clearly not separated [Cox and Coker 1983, Harwood et al. 1997, Spietz et al. 1997, Bloss et al. 2001].

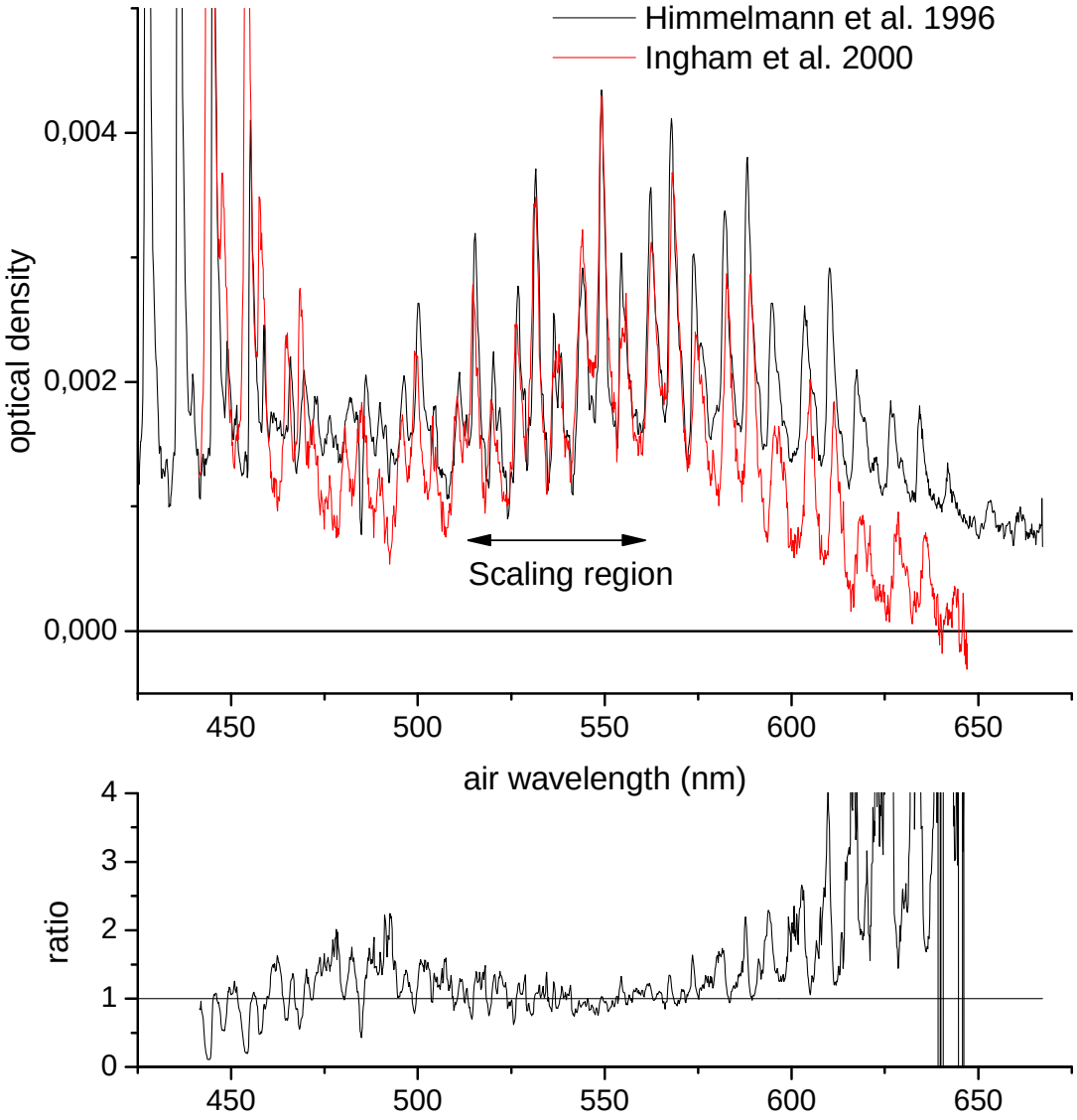

Figure 3.2 To the author's best knowledge only three spectra of OIO have been published. The first by Himmelmann et al. [1996], two others by Ingham et al. [2000] and Bloss et al. [2001]. Unfortunately the latter was not available at the time of publication of the present work. Spectra were scaled to each other in the region between 520 to 560 nm. From the troughs of IO the level of zero absorption can be inferred, as there no or only negligible absorptions exist. Relative to that both OIO spectra are clearly situated on a background of unidentified origin. Sections of the spectrum tend below zero and line shaped features are clearly present.

In preparation to the present work a number of mechanistic studies of IO and OIO formation were performed focussing on the different behaviour of the system under varying conditions of overall pressure, mixing ratios and different bath gases. Both full kinetic models (trying to model IO/OIO formation and consumption in detail) as well as approximate reduced models were extensively tested. A general result of these studies was the inconsistency of results, be it cross sections or rate coefficients or general behaviour of concentrations in time. Also the dependence on different reference data proved to be problematic, in line with the expectation mentioned above.

Therefore efforts were made to develop a method which enables a more independent determination of cross sections. If possible, usage of rate coefficients and assumptions on the chemical mechanism should be avoided as far as possible and cross sections of iodine oxides should be determined in an independent experiment.

3.4 CONCEPT OF THIS WORK

One approach for determining absolute absorption cross sections is to use traces of temporal behaviour of observed absorbers, consider the mechanism of formation and consumption of the main absorbers, which as a first guess could be IO and OIO, and try to reproduce the observed traces of optical density by suitable chemical models. From an idealistic point of view all rate coefficients and all cross sections should be treated as unknown parameters simultaneously to achieve a solution which is as self-consistent as possible. But in such a mechanistic approach the rate coefficients of reactions and the cross sections of absorbers are reciprocally linked. A simultaneous determination is difficult, if not systematically impossible. Also, due to the apparent complexity of the chemical system, such an approach is prone to over-parameterisation.

As a common alternative, estimates for selected rate coefficients and cross sections determined in other studies can be used to reduce the number of free parameters. In many cases this enables determination of estimates for the remaining unknowns. But such a reduced system relies on the accuracy of the formerly determined parameters. The solution is no longer self-consistent and no longer independent of previous determinations of rate coefficients and cross sections. If different estimates exist for the formerly determined parameters, it will be even more difficult to decide, which parameters are to be used as a basis

for the actual study. Such a dependence is undesirable and might even impede a solution. Another simplification could be to modify the mixing ratios and pressures in the experiment trying to favour some reactions over others. Then a simplified mechanism could be tested to explain a reduced set of observations. Continuing iteratively it might be possible to include other absorbers and reactions trying to explain more and more of the observations. But the approximations within such a procedure must not be underestimated, especially not in a complex system.

But given the incomplete understanding of the IO/OIO chemistry as summarised before, such limited approaches, which use part of this available data are not desirable, because they lead to unclear dependencies on the used reference data rather than to independent new results. In conclusion the following requirements were postulated for the present study:

1. Notwithstanding the reliability and validity of the previously determined parameters the objective of the present study was to enable an *independent* determination of sought cross sections for IO, OIO and further higher oxides.
2. Modelling of chemical kinetics was to be avoided. Thereby neither previous determinations of chemical rate coefficients nor mechanistic assumptions would be needed.
3. Estimates for the complete set of cross sections – i.e. of all iodine species formed in the experiment - should be obtained *simultaneously* to ensure their general validity. This would at the same time avoid usage of any previous determinations of any cross sections.

These objectives can be satisfied by a method which in the following is referred to as the method of iodine conservation.

3.4.1 Conservation of iodine atoms

Given a system of n linearly independent equations in n unknowns, it is possible to solve this system for the n unknowns. No further information about the origin of the equations or the parameters in the individual equations is needed. If the number of linearly independent

equations is larger than the number of unknowns, over-determination enables optimisation techniques to determine optimal estimates for the sought unknowns.

This concept can be transferred to the present problem, where for a certain number of absorbers the unknown absorption cross sections are to be determined. This requires a set of observations, from which a set of equations can be deduced. Now consider a flash photolysis experiment, in which the different absorbers are formed and consumed with different rates of formation and consumption. By the flash a certain number of iodine atoms is released via photolysis of I_2. The released iodine atoms are subsequently distributed in varying proportions over

1. free iodine atoms,
2. I_2 molecules, which are possibly formed during the course of reaction, and
3. the different reaction products, i.e. the different iodine oxides formed and consumed during the experiment.

If the number of free iodine atoms and of I_2 molecules is known by measurement as a function of time, the number of iodine atoms as a whole, which are contained in the remaining set of (even unknown) iodine oxides, can be determined. This is a reasonable assumption, because cross sections for both can be determined with high accuracy and reliability in separate static experiments. No complications due to complex chemical mechanisms interfere.

If furthermore the temporal behaviour of optical density of all iodine oxides formed is known, it will be possible to state *for each point in time* t_i a linear equation, which contains

- the optical densities of individual iodine oxides measured at time t_i as coefficients,
- their reciprocal cross section as unknowns and
- the number of iodine atoms contained in all iodine oxides as a whole at time t_i as the constant term.

The different equations describe how iodine is distributed across the different species as a function of time. The number of available data points t_i in time defines the number of equations. The requirement that equations have to be linearly independent limits the number of equations, as especially for later times the curves of decay of different absorbers tend to

become very similar. But during a large part of the experiment containing the largest variations of different absorbers it will be possible to obtain a number of linearly independent equations considerably larger than the number of unknown cross sections. Solution of the over-determined system of equations by ordinary least squares techniques produces optimal estimates for the unknown cross sections *simultaneously* and *consistently*. Conservation of the number of available iodine atoms in time being the key to the system of equations explains the name, which we choose for the method.

Important conclusions:

- *The coefficients in the system of equations are the optical densities of individual iodine oxides. Their origin does not enter into the algorithm. Even their order in time is unimportant. The only purpose of time resolved measurement in this context is to provide a sufficient number of linearly independent equations. Therefore no knowledge of the chemical system nor any chemical kinetics reference data is needed for the solution. This satisfies the second requirement to the method stated above.*
- *Cross sections of iodine oxides are all treated the same and are determined simultaneously and consistently. No a priori determinations are used. This satisfies requirement three.*

Together these two satisfy the first requirement for an independent determination of absorption cross sections. As a clear advantage even absorbers, whose stoichiometry is not yet known, can be included in the system, if their absorption is measured.

The only crucial assumption to the method is that all relevant absorbers are covered by measurement and are included in the system of equations with their corresponding optical density and their unknown cross section. This assumption can be tested by checking the residuals obtained from the least squares solution for systematic behaviour. If any systematic behaviour were present, this would indicate that a relevant absorber is not accounted for in the approach. The method will be presented in more detail in **Chapter 10**.

3.4.2 Experimental Requirements

Given the desired method, the experiment had to be tailored to it. The technique used in the experiments of this laboratory study was fast time resolved molecular and resonance

absorption spectroscopy of flash photolysis experiments. The flash photolysis technique was developed by Norrish and Porter [Norrish and Porter 1949] and successfully applied in many studies of shortlived radicals and their reactions [Norrish 1967, Porter and Wright 1953]. It is well suited to produce large numbers of radicals whose decay is observed subsequent to the flash. In our experiments we photolysed mixtures of I_2 and O_3 in bath gases N_2 and O_2 with broad band Xenon flash tubes. The flash photolysis of such mixtures produces iodine atoms and oxygen atoms in the presence of I_2 and O_3. These components then quickly react on time scales of some hundreds of microseconds to some tens of milliseconds depending on the mixing ratios to form the highly reactive radicals IO and OIO. These in turn were equally quickly consumed by further reactions that under certain conditions finally lead to strong formation of solid deposits indicating the existence of higher iodine oxides as final products.

The *method of iodine conservation* firstly requires a large and simultaneous coverage of as many absorbers as possible. Secondly the short life times of transient iodine radicals requires sufficiently fast time resolved optical detection systems with suitable vibration control systems for the whole optical set-up. For time resolved recording of intensity spectra a spectrometer and a CCD camera (charge coupled device: two-dimensional silicon semiconductor) were combined. The CCD camera was modified to enable time resolved operation. It enables simultaneous multichannel recording of full spectra per time step. Optical throughput of the system was optimised to enable the necessary short exposure times. By applying the Beer-Lambert law directly to the two-dimensional CCD recordings obtained with and without absorbers, optical density was calculated. The result is a matrix, whose entries are optical density as a function of wavelength and time.

The resonance absorption set-up consisted of an electrodeless iodine resonance lamp, a VUV-monochromator and a photomultiplier tube. Set to 183.038 nm it can be used to measure the concentration of ground state $I(^2P_{3/2})$ given a knowledge of the oscillator strength of the 183.038 nm transition. The same holds for metastable $I(^2P_{1/2})$. But his proved to be irrelevant under the chosen conditions of our experiments. Both optical systems were combined in a reaction vessel with two crossed optical axes. Both were synchronised to each other and to the photolysis system.

Because the resonance absorption set-up can be empirically calibrated relative to the I_2-absorption, the necessary a priori data could in principle be reduced to solely the cross section σ_{I_2} of I_2. For this a number of published estimates exist. Being the keystone to the chosen

approach, it was to be determined within this work. Nevertheless also the oscillator strength for iodine atoms I($^2P_{3/2}$) was determined. But at the same time empirical calibration had to be performed to account for characteristics of the set-up.

From the time resolved multichannel optical absorption measurements performed with the CCD the temporal behaviour of optical density of - at best *all* relevant - iodine containing species I_2, IO, OIO, vibrationally excited IO, and other yet unidentified absorbers had to be extracted. A good overview of the absorptions, which were to be expected, had been obtained from the preparatory studies to this work. Likewise for iodine atoms I($^2P_{3/2}$) (ground state) the time dependent concentration was to be determined using resonance absorption.

3.4.3 Data Analysis Requirements

In the same way as the experimental set-up also the methods for data analysis had to be tailored to allow an optimal analysis of the time resolved molecular absorption data. A traditional method in chemical kinetics and spectroscopy is to calculate "intelligent differences" of spectra in order to isolate contributions dominantly caused by one absorber. Similarly traces of temporal behaviour of individual absorbers can be determined, e.g. by "on-peak minus off-peak" differences, which assumes approximately constant background absorption. This method finds its analogy in linear algebra, where a system of linear equations (corresponding to a set of mixed spectra observed at different times or to a set of observed variation of absorbance in time at different wavelengths) is solved by using the subtraction method for "manually" eliminating unknowns. But as the number and the relative magnitude of unknowns in the case of spectroscopy and chemical kinetics is itself not known and background absorptions of traces of other absorbers can not be excluded, this method is always an approximate one. Also it uses only a small fraction of the available data neglecting the major remainder of information contained in the data recording.

Here the introduction of multivariate analysis techniques like Principal Components Analysis and Independent Component Analysis (PCA and ICA) as well as different least squares techniques proved to be most important improvements. Their combination allowed for the first time to extract from overlapping measurements the practically pure curves of optical density versus time of the transient short-lived absorbers IO and OIO, the precursor I_2 plus a number of unidentified products. Vibrationally excited IO was also found to behave differently from ground state IO and corresponding curves were extracted. All extracted

curves are to a high degree free of technical drift effects and of mixing with absorbances of other overlapping absorbers [Gómez Martín et al. 2004]. This is a prerequisite to the application of the method of iodine conservation. The separation method enabled extraction of pure spectra of absorbers as well. They too are to a similar degree free of drift effects and overlapping absorbances. This is a clear and important improvement with respect to the formerly published spectra, refer to the discussion above.

Having determined pure curves of optical density versus time the last step before applying the method of iodine conservation is consideration of possible effects of limited resolution on the observed curves. A time resolved detection system with broad spectral coverage allows simultaneous measurement of multiple absorbers. This enables more accurate determination of absorption spectra and absolute cross sections in terms of coverage of relevant absorbers. The same holds for subsequent studies of chemical kinetics. But as a trade-off to broad spectral coverage, banded spectral features can sometimes be recorded with insufficient spectral resolution and/or insufficiently fine detector binning. This renders the true physical spectrum of recorded intensities changed by instrumental and spectrum specific artefacts. This effect proved to be critical for the IO(4←0) absorption band with respect to apparent magnitude of absorption as well as to linearity between observed optical density and concentration. But other absorptions are affected too. To overcome this problem, an integral approach for the treatment of intensity recordings was developed. Thereby the apparent magnitude of absorption was corrected and the linearity between optical density and absorber concentration was re-established.

Having thus assured that the curves of optical density versus time are free of drift, overlap and resolution dependent effects, the method of iodine conservation could finally be applied to them. Following the concept described in the following chapters time resolved flash photolysis recordings obtained under different chemical conditions and with different spectral coverage were analysed and for the first time produced *separated* spectra of the different species and a *self-consistent* set of absolute absorption cross sections.

The separation of overlapped spectra also enabled analysis of band strength of the IO spectrum, its continuum absorption and of vibrationally excited states. This is also presented.

4 OSCILLATOR STRENGTH OF IODINE ATOMS

Electrodeless Discharge Lamps (EDL) are well known as intense sources of a variety of atomic emissions in the ultraviolet spectral region [Revalde and Skudra 1998, Gross et al. 2000]. Recently, the development and a first study of an inexpensive and convenient EDL iodine line source, powered by radio frequency (RF) were reported [Gross et al. 2000]. For the present study the time resolved CCD set-up designed for molecular absorption was combined with a resonance absorption set-up using the newly developed iodine EDL. Opposed to the arrangement to be used later in the kinetic experiments with I_2 and O_3, here both absorption set-ups were combined along the same axis of the reaction vessel, which guaranteed that both probed the same volume. The second major difference was that here the CCD camera was used for both the molecular as well as the resonance absorption set-up. In the I_2+O_3 photolysis experiments on I_xO_y cross sections a photomultiplier tube was used for resonance absorption for improved sensitivity.

The study could be limited to the I($^2P_{3/2}$) ground state transition at 183.038nm, because it could be shown that metastable I($^2P_{1/2}$) (206.163nm) under the conditions to be used in the experiments on cross section determination was most rapidly quenched by a highly efficient resonant energy transfer to O_2 also used in chemical oxygen iodine lasers COIL. See Marter et al. [1996] and references therein. Absorptions from I($^2P_{1/2}$) in experiments without quenching generally showed a signal to noise ratio of the order of at least 100:1. On these grounds a detection limit of better than 1% relative to the total amount of iodine released by the flash can be inferred for I($^2P_{1/2}$). In the experiments for I($^2P_{3/2}$) as well as in I_2+O_3 mixtures no absorption by I($^2P_{1/2}$) was detected. This justifies the limitation to I($^2P_{3/2}$) with an uncertainty of less than 1%.

A crucial factor in resonance absorption is the determination of the emission line profile of an EDL. This depends on the temperature of the emitting plasma, which in general is not directly accessible. In this study an indirect method was developed using relative absorption of emission and absorption lines of different widths. These lines are assumed to have Doppler broadened line shape. The source temperature can be inferred from different relative absorptions measured at different absorber concentrations. This knowledge was then used to estimate the oscillator strength for the atomic transition I($^2P_{3/2}$) at 183.038nm.

4.1 EXPERIMENTAL

A schematic diagram of the apparatus is shown in **Fig. 4.1**. It comprises a reaction vessel, a flash photolysis system, a UV-visible grating spectrometer, and a CCD camera as detection system. The reaction vessel consists of a double-jacketed quartz tube and is temperature stabilised by a flow of ethanol from a thermostatic bath. The optical windows at the front and back end of the vessel are made from fused silica and are double walled and evacuated for thermal insulation. A 250 W tungsten lamp was used for molecular absorption spectroscopy of I_2 between 350 and 650nm. After having traversed the vessel twice (flip mirror 1 in place and flip mirror 2 flipped aside, see **Fig. 4.1**), the analysis light was focussed onto the entrance slit of a Czerny-Turner spectrometer (Acton Research, 500mm focal length), operated alternatively with a 150 groove·mm^{-1} grating blazed at 300 nm (for tungsten lamp) or a 1200 grvs·mm^{-1} holographic grating (for resonance absorption with iodine EDL, see below). The spectra were recorded by the CCD camera (Roper Scientific) with a 1024×1024 silicon detector chip (SiTE). The CCD can be operated either *statically* recording individual spectra at pre-set times or *time resolved* recording sequences of full spectra at set time intervals. For time resolved mode the chip of the CCD camera is masked by a laboratory-made horizontal slit such that always roughly 5 rows are exposed simultaneously. By shifting all rows step wise from the exposed area down under the mask, time resolved recording of spectra is achieved. Shifting time in the fastest mode is 20µs. By this mechanism each spectrum is exposed during 5 shift intervals and accumulates the temporal variation of signal during this time. This corresponds to a 5-point "moving-average" smoothing of the original temporal behaviour of optical density versus time. The shape of the smoothing kernel function is not rectangular, but determined by the characteristic illumination function on the chip of the CCD. Without correction, the effective resolution in time is therefore limited to roughly 100µs. This is sufficient, if the observed structures change slowly in comparison to this effective temporal resolution. If faster processes were to be monitored, then a deconvolution in time could improve the effective temporal resolution slightly using a *measured* characteristic function of illumination. In the present work, however, all processes of interest were kept sufficiently slow to enable the direct usage of time resolved signals without deconvolution.

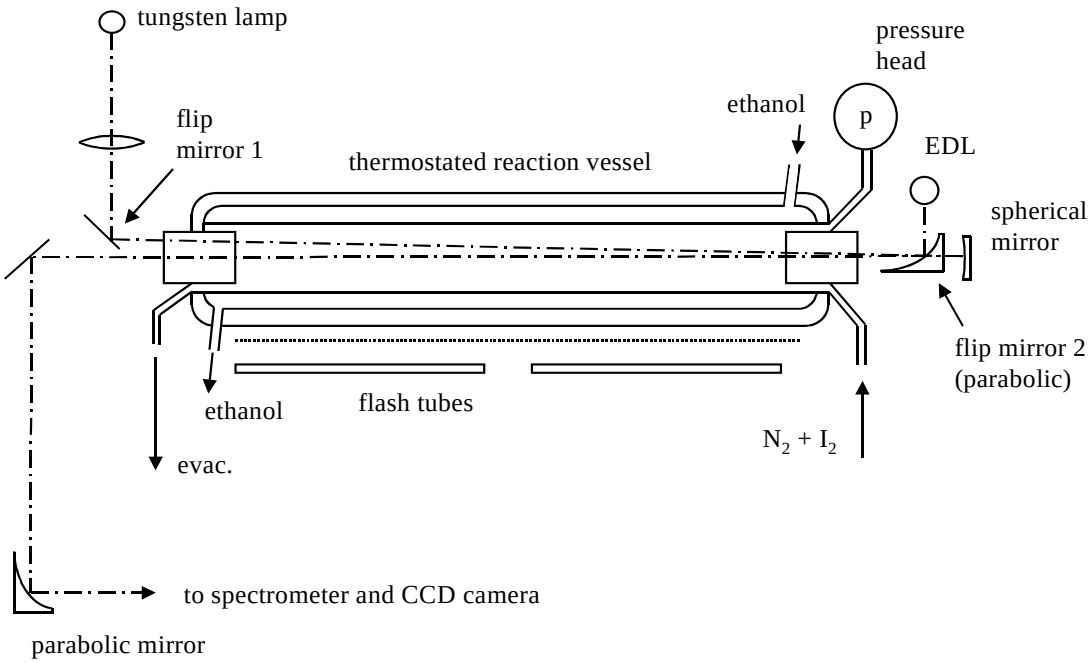

Figure 4.1 A schematic diagram of the apparatus of the combined flash photolysis and resonance absorption set-up is shown.

The reaction vessel is surrounded by a concentrically mounted sheet metal cylinder, containing the two 30cm Xenon flash tubes (Heimann HG9903) of the photolysis flash system. The maximum output of the flash tubes is 160 J per flash at 1500 V discharge each. The energy of the flash can be varied by placing optical filters between the tube and the vessel or by varying the charging voltage of the flash system. In these experiments the typical flash energy was approx. 80 J each. The repetition rate was limited by the readout time of the CCD or the purging time of the vessel – whichever was slower - and was generally of the order of 0.1 Hz.

Iodine atoms were produced in the reaction vessel by photolysis of mixtures of N_2 and I_2 at approximately 17 mbar. The number of iodine atoms produced by each photolysis flash was determined by time resolved measurement of loss of I_2 by absorption spectroscopy. For these measurements the I_2 absorption spectrum between 350 nm and 650 nm was observed using the 150 grvs·mm^{-1} grating and the tungsten lamp. Spectral resolution in this configuration was approximately 0.8 nm full width at half maximum (FWHM). Dispersion was 0.32nm/pix at a geometric width of 0.26µm per pixel. Since a large section of the I_2 spectrum was recorded in these measurements (in contrast to monochromatic measurements as usually recorded by photomultiplier systems), drift effects of the lamp could be minimised. Furthermore a good

signal-to-noise ratio of the time resolved signal was achieved by numerical integration over parts of the observed I_2 absorption spectrum.

For the resonance absorption set-up a radio frequency (RF) powered EDL and generator as described in [Gross et al. 2000] were used instead of the tungsten lamp (flip mirror 2 in place and flip mirror 1 flipped aside, see **Fig. 4.1**). The atomic emission line of iodine at 183.038 nm had been the main focus of this study. Further emission lines in this region are at 178.276 nm, 179.909 nm, 184.445 nm, 187.641 nm, and 206.163nm. The last three of them were also readily observed. To record far UV and vacuum UV (VUV) signals below 240 nm, the entire optical system was enclosed and purged with N_2 to suppress absorption by O_2.

The light of the EDL was passed through the reaction vessel once and then focussed into the spectrometer. It was analysed using the 1200 grvs·mm^{-1} holographic grating. With this grating the dispersion of the spectrometer was sufficient so that the lines under study were well separated even with the entrance slit opened up to 0.5 mm (0.04nm/pix). Thereby throughput of the spectrometer was optimised to compensate for loss of light of the optical system which was due to absorption especially in the far UV and VUV. The line shape itself was not resolved in this setting and only spectrally integrated intensities could be measured:

$$I = \int_{\text{line}} \Phi(\nu)\,d\nu \qquad \textbf{(1)}$$

where $\Phi(\nu)$ is normalised to the integral line intensity I and describes the distribution of intensity over the line profile as a function of frequency ν. With the given grating (1200 grvs·mm^{-1}) and the entrance slit set to 0.5 mm the signal of the individual lines as recorded by the CCD chip was dominated by the spectrometer's characteristic function with a FWHM of approx. 21.5 pixels (≈0.5 mm on chip). The signals recorded by individual pixels were binned in hardware (on chip) and software (post processing) in order to improve the signal to noise ratio. **Fig. 4.2** shows three typical recordings of intensity versus time recorded at 183.038nm at 0.5ms per data point. The three traces were measured at three different concentrations of $[I_2]$. The concentrations of [I] as released by photolysis differ correspondingly. Absorption signals at 183.038 nm as well as at 206.163 nm during photolysis were recorded in time resolved mode (**Fig. 4.2**).

The intensities observed *before* (no iodine atoms ⇒ measured intensity I_0) and *after* the flash (iodine atoms from photolysis ⇒ measured intensity I) provided the data for calculating

absorbance A=ln (I_0/I) or relative absorption Q=(I_0-I)/I_0 (= 1-exp(-A)). The experiments were performed in flow mode. A stable flow of I_2 in N_2 was produced by passing a flow of N_2 through a thermostated glass vessel (T=273.15 K, ice water) containing I_2. This flow could be diluted by an additional flow of pure N_2. Flows were controlled using calibrated mass flow controllers (MKS Instruments). Pressure in the vessels was measured by calibrated capacitance manometers (MKS Instruments). The I_2, resublimed p.a., was obtained from ACROS Organics, C.A.S No.:7553-56-2. The N_2 was obtained from Messer-Griesheim (grade 4.8).

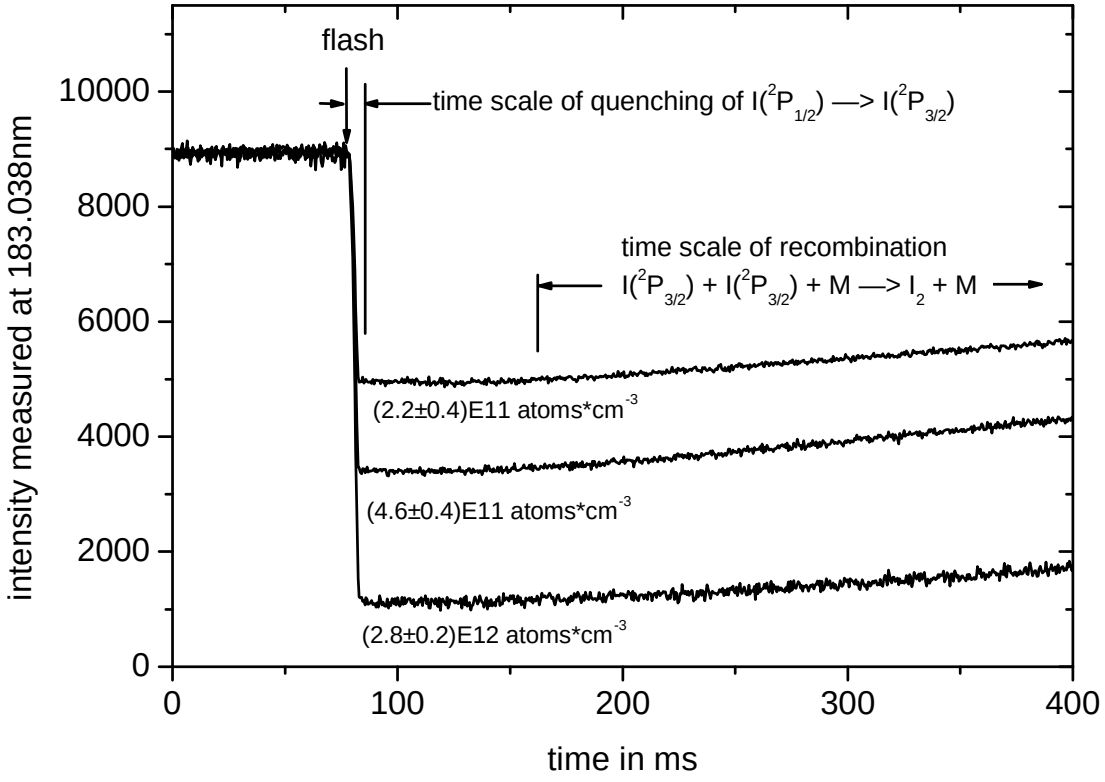

Figure 4.2 Three time resolved intensity measurements at 183.038 nm are shown. They were recorded at three different concentrations of [I_2] with correspondingly different concentrations of [I] (see labels of curves) under otherwise constant conditions. The time scale of the fast quenching of $I(^2P_{1/2})$+M → $I(^2P_{3/2})$+M and that of the recombination of $I(^2P_{3/2})$+$I(^2P_{3/2})$ → I_2 + M are indicated. The intensity I which was used to calculate relative absorption and *effective* absorbance respectively was calculated as an average over the intermediate time interval between 100 and 150 ms. Similarly the reference intensity I_0 was determined using the time interval before the flash.

The design of the EDL has a side arm of 6cm length, which is well separated from the discharge region (**Fig. 4.3**). This side-arm can be temperature-stabilised at different temperatures (see [Revalde and Skudra 1998] and [Gross et al. 2000] for more details) enabling the vapour pressure of iodine in the lamp and discharge volume to be precisely

controlled. This enables the dependence of self-absorption and self-reversal on partial pressure of iodine in the discharge volume to be studied.

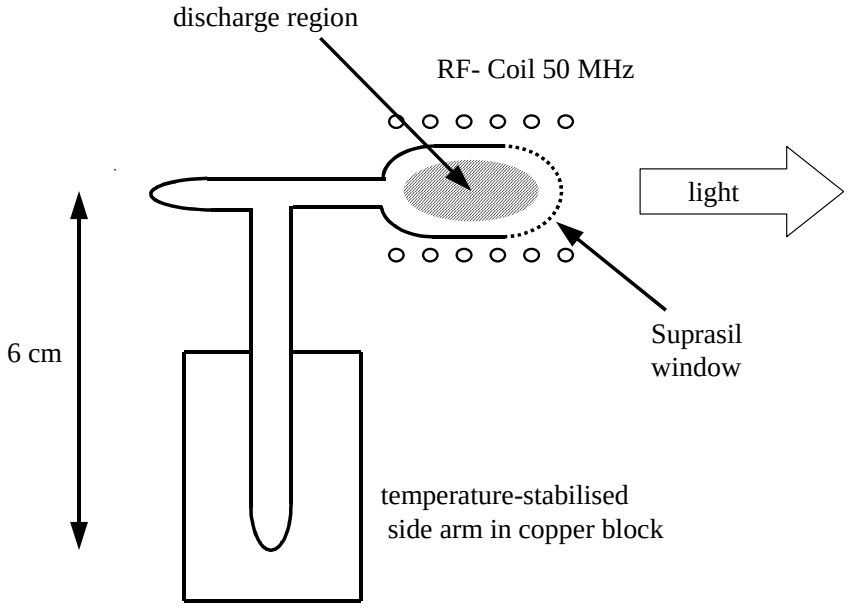

Figure 4.3 The EDL consists of a discharge volume of approx. 18 mm outer diameter and 35 mm length. The discharge volume is connected to a side arm of approx. 6 cm length, which is located in a thermostated block of copper. By thermostating the side arm of the lamp volume the vapour pressure of iodine inside the lamp can be controlled.

4.2 METHODS AND RESULTS

4.2.1 Optimal operating conditions: Minimising self-absorption

The phenomena of self-absorption and self-reversal in atomic line sources result from the simultaneous presence of emitting atoms and lower state atoms capable of absorption within the discharge volume of the lamp. Lower state atoms, which are outside the plasma but still within the lamp volume, have a lower temperature than the emitting atoms within the plasma. Therefore, their absorption line profile is narrower than the emission line profile from the plasma and a self-absorbed or even self-reversed line results. The spatial distribution and the relative concentrations of emitting and absorbing atoms depend critically on the partial pressure of the element (here iodine) within the discharge volume: The higher the partial pressure, the more lower state atoms exist outside the emitting plasma. Revalde and Skudra [1998] examined line shapes emitted by a mercury EDL using a Fabry-Perot interferometer, a comparable type of RF generator, and the same lamp construction as used for our EDL. They showed that, within certain limits, self-absorption can be reduced by the use of stronger RF-

fields, whereby more atoms are transferred into higher states. A more efficient method is regulation of partial pressure of iodine in the lamp via side arm temperature ([Revalde and Skudra 1998], [Gross et al. 2000]). The studies of Revalde and Skudra [1998] demonstrated that self-*reversal* becomes less critical at partial pressures below 10^{-2} mbar, i.e. for I_2 around 263 K. Therefore, in our studies the side arm temperature was varied between ca. 243 K and 268 K corresponding to iodine vapour pressures of the order of 10^{-3} to 10^{-2}mbar.

In our study only the integrated signal of the iodine emission line was measured as defined by **(1)**. Therefore, an indirect method for estimating self-absorption and self-reversal was used. The relationship of Beer-Lambert applies to the absorption of *monochromatic* radiation, i.e.

$$A(\nu) = \ln\left(\frac{I_0(\nu)}{I(\nu)}\right) = \sigma(\nu)\cdot N \cdot L \qquad \textbf{(2)}$$

where $\sigma(\nu)$ is the absorption cross section of the absorber at frequency ν, N is the absorber concentration (molecules per volume) and L is the optical path length within the absorbing gas. $I(\nu)$ and $I_0(\nu)$ are the intensities at frequency ν measured with absorber and without absorber in the vessel respectively. By $A(\nu)$ the Beer-Lambert absorbance at frequency ν is designated. The relationship of Beer-Lambert does not apply to the case of *integrated* signals I and I_0 according to **(1)**. Still under certain conditions a proportional relationship between absorber concentration N and an *effective* absorbance A_{eff}, formally calculated according to

$$A_{eff} = \ln\left(\frac{I_0}{I}\right) \propto N \qquad \textbf{(3)}$$

can be used and has to be calibrated empirically (calibration curve). Here I_0 and I are the measured integral intensities according to **(1)**. If beyond that self-absorption occurs in the lamp, the situation is further complicated. The calibration curve relating the effective absorbance A_{eff} to the absorber concentration N then deviates from straight proportionality displaying an increasingly reduced signal at higher absorber concentrations. In this case it can be shown [Boumans 1972] that deviation from proportionality gets stronger with growing self-absorption of the emission line under otherwise constant conditions.

Consequently, for decreasing side arm temperatures and therefore decreasing self-absorption under otherwise constant conditions, the effective absorbance calculated according to **(3)**

should approach the optimal estimate for a self-absorption-free measurement. Therefore, the concept for assessing self-absorption was:

1. Photolysis of I_2 in N_2 to produce constant amounts of $I(^2P_{3/2})$ and $I(^2P_{1/2})$ in the reaction vessel.
2. Measurement of the resulting effective absorbance $A_{eff} = \ln(I_0/I)$ as a function of side arm temperature, i.e. by varying the extent of self-absorption and self-reversal.

In this chemical system photolysis of I_2 produces iodine atoms in ground state ($^2P_{3/2}$) and metastable state ($^2P_{1/2}$):

$$I_2 + h\nu \rightarrow \alpha \cdot I(^2P_{3/2}) + \beta \cdot I(^2P_{1/2}) \qquad \text{(R4.1)}$$

with $\alpha+\beta=2$ and $h\nu$ designating the photolysing photon. The branching ratio defined by α and β depends on the spectrum of the photolysis flash as well as on the internal energy of the I_2 molecule [Hunter and Leong 1987]. It can be shown that knowledge of α and β is not necessary for our studies. In our experiments the excited metastable iodine atoms $I(^2P_{1/2})$ observed at 206.163nm were most rapidly quenched by collisions (compare also [Gross et al. 2000]). The time scale of this depended on the mixture and was of the order of a few µs up to 100 µs. On the other hand the recombination reaction

$$I(^2P_{3/2}) + I(^2P_{3/2}) + M \rightarrow I_2 + M \qquad \text{(R4.2)}$$

with a rate coefficient k of the order of 10^{-32} to 10^{-29} $cm^3 \cdot s^{-1} \cdot atom^{-1}$ [NIST 1998] is slow and takes place on a time scale of several 100 ms. **Fig. 4.2** illustrates the different time scales of these two effects. The quenching of iodine ($^2P_{1/2}$) was already completed on the intermediate time scale of our experiments while the recombination reaction has not yet changed the concentration of iodine ($^2P_{3/2}$) significantly. Hence both effects were negligible within an interval between roughly 100 to 150 ms on the time axis of **Fig. 4.2**. I_0 was determined by averaging the measured values before the flash while I was calculated as an average over a suitable time interval after the flash and before recombination started to be significant.

For each temperature setting the effective absorbance at 183.038 nm following the photolysis of I_2 and the formation of $I(^2P_{3/2})$ was measured in time resolved mode and averaged over at least 20 consecutive flashes under otherwise identical conditions. The concentration of $I(^2P_{3/2})$ produced by the flash was determined from a knowledge of the photolysis rate of I_2. This had

previously been measured using the absorption of I_2 between 350–650 nm. The I_2 concentration was stabilised to within ±3 % and the flash energy was held constant during these experiments. The yield of $I(^2P_{3/2})$ per flash from I_2 could, therefore, be assumed to be constant within these error limits.

Fig. 4.4, parts a and b, shows six curves of effective absorbance versus side arm temperature as measured at six different absorber concentrations. The six curves are shown three at a time and in the case of **Fig. 4.4b** the lower two curves are translated vertically by +0.25 and +0.45 respectively for clarity. The data clearly displays the expected behaviour. It approaches a limiting maximum value at the lowest side arm temperatures. A further decrease in temperature only decreases the iodine concentration and the emission intensity of the discharge. The minimum temperature that could be reached with the present set-up was approx. 243 K. Optimum operating conditions with minimum self-absorption are already reached at side arm temperatures between 246 K to 248 K. These temperatures correspond to an iodine vapour pressure in the EDL's discharge region of about $2.5 \cdot 10^{-3}$ mbar. Under these conditions self-absorption in the EDL is minimal whilst emission intensity is not yet significantly reduced. The same behaviour was observed for all six individual data sets recorded at six different atomic iodine concentrations in the reaction vessel (ranging from $0.98 \cdot 10^{11}$ atoms·cm^{-3} to $2.8 \cdot 10^{12}$ atoms·cm^{-3}). Accordingly, it is assumed that self-absorption in the EDL can be neglected in the following analysis.

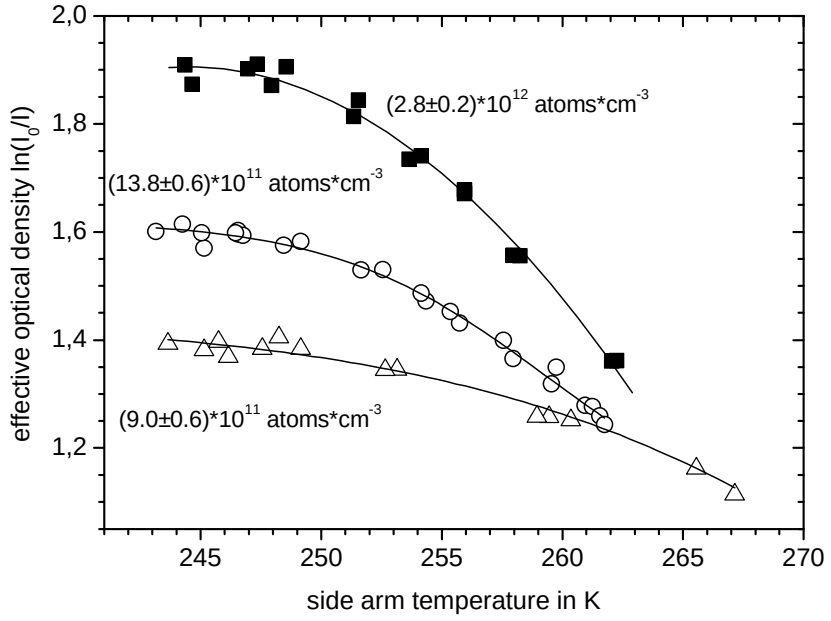

Figure 4.4a See caption **Fig. 4.4b**.

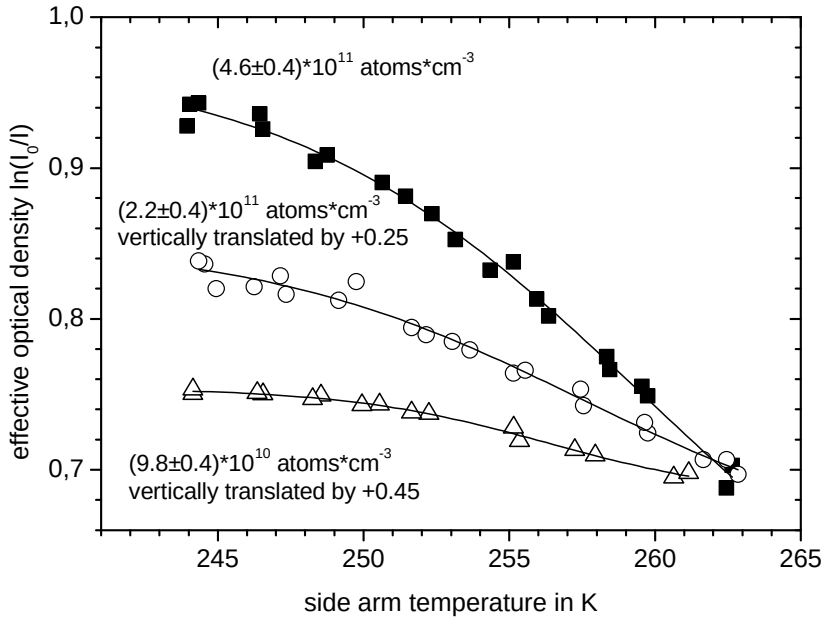

Figure 4.4 The effective absorbance $A_{eff}=\ln(I_0/I)$ for six different absorber concentrations (iodine atoms [I]) in the vessel was determined as a function of side arm temperature under otherwise constant conditions. For clarity the six traces are shown three at a time. In Fig 4b the lower two curves are translated vertically by +0.25 respectively +0.45 for clarity.

4.2.2 Determination of emission temperature in the EDL

From each of the six data sets mentioned above, only the intensities measured under minimal self-absorption conditions (the "low temperature limits") were used for further analysis and, in the next step, line profiles of emission and absorption were taken into account.

At room temperature (≈300 K) the gas mixture in the lamp has a pressure of approx. 3 mbar which corresponds to a concentration of ca. $7.25 \cdot 10^{16}$ molecules·cm^{-3}. The temperature of the plasma is most likely between 700 and 1400 K, when the lamp is in operation. Under such conditions the Lorentz line width is 0.0006 cm^{-1} (at 700 K) to 0.0009 cm^{-1} (at 1400 K) due to pressure broadening in the lamp, whereas the Doppler line width under the same conditions is more than two orders of magnitude larger (about 0.09 cm^{-1} at 700 K to 0.13 cm^{-1} at 1400 K). The Doppler width of the lines in units of wavenumber was calculated by:

$$\delta\tilde{\nu}_D = \frac{\nu_0}{c} \cdot 2 \cdot \sqrt{\ln 2 \cdot \frac{2k_B T}{mc^2}} \qquad \textbf{(4a)}$$

where ν_0 is the frequency of the line, k_B Boltzmann's constant, T the temperature of the gas, m the mass of the emitting atom in kg, and c the velocity of light. Pressure broadening was calculated via the impact approximation, which yields a Lorentz line profile of width (wavenumber):

$$\delta\tilde{\nu}_L \approx \frac{1}{c \cdot \tau_{coll}} \approx \frac{n \cdot A \cdot \bar{v}}{c} = \frac{n \cdot A}{c} \cdot \sqrt{\frac{8 \cdot k_B T}{\pi \cdot m}} \qquad \textbf{(4b)}$$

τ_{coll} is the time between collisions according to gas kinetic theory. It is approximated using the number density of gas particles, n, the cross section for collision, A, and $\bar{v}$ as the mean particle velocity in a gas with Maxwell velocity distribution.

The overall pressure in the reaction vessel (bathgas with I_2) was maintained at about 17 mbar corresponding to $\approx 4 \cdot 10^{17}$ molecules·cm^{-3}, which is roughly six times larger than what is found for the gas in the lamp. The vessel temperature was maintained at room temperature 293 K. Even though this temperature is significantly lower than the temperature in the lamp, the higher concentration led to a larger Lorentz line width of 0.0024 cm^{-1} (293 K) in the vessel. Yet again, similar as in the lamp, the corresponding Doppler line width was more than one order of magnitude larger (0.06 cm^{-1} at 293 K). Therefore both, the emission line profile and the absorption line profile were clearly Doppler dominated.

However, the Doppler width of the emission line in the EDL was larger than that of the absorption line by a factor of approximately 1.5 to 2. Therefore it is expected that the absorbances calculated according to $A_{eff}=\ln(I_0/I)$ and plotted versus iodine concentration N in the reaction vessel do not follow the proportional relationship postulated in **(3)** despite the fact that self-absorption is already minimised and assumed negligible.

The data plotted in **Fig. 4.5** clearly displays this expected behaviour: The deduced effective absorbances show increasingly reduced values for higher concentrations and clearly deviate from proportional behaviour. They are not proportional to the absorber concentration N in the vessel. In view of finally deducing the oscillator strength and in order to understand and analyse this behaviour quantitatively, the concept of relative absorption $Q=(I_0-I)/I_0$ rather than absorbance $A=\ln(I_0/I)$ will be used in the following. These quantities are related according to $Q=1-\exp(-A)$.

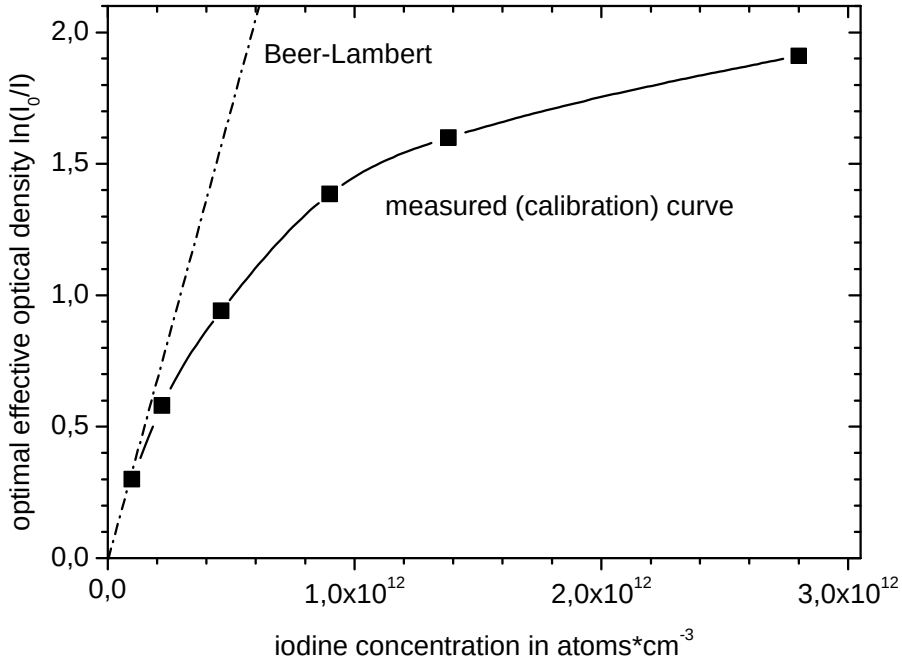

Figure 4.5 The *optimal* effective absorbance $A_{eff}=\ln(I_0/I)$ for T < 245 K is plotted as a function of absorber concentration in the reaction vessel. The straight line represents a Beer-Lambert or an at least proportional relationship between absorbance and absorber concentration. The measured data displays increasingly reduced values for large absorber concentrations deviating from a proportional behaviour.

Relative absorption Q can be expressed in terms of Doppler profiles of emission and absorption lines (see [Mitchell and Zemansky 1972] for a detailed derivation of equations **(5)** to **(7)**):

$$Q = \frac{I_0 - I}{I_0} = \frac{\int_{line} \Phi_0(\nu) d\nu - \int_{line} \Phi_0(\nu) \cdot \exp(-k(\nu) \cdot L) d\nu}{\int_{line} \Phi_0(\nu) d\nu}, \qquad \textbf{(5)}$$

where

$$\Phi_0(\nu) = \Phi_0 \cdot \exp\left(-4 \cdot \ln 2 \cdot \left(\frac{\nu - \nu_0}{\delta\nu_{D,em}} \right)^2 \right) \qquad \textbf{(6a)}$$

represents the emission Doppler profile of maximum intensity Φ_0, width $\delta\nu_{D,em}$ and centre ν_0,

$$k(\nu) = k_0 \cdot \exp\left(-4 \cdot \ln 2 \cdot \left(\frac{\nu - \nu_0}{\delta\nu_{D,abs}} \right)^2 \right) \qquad \textbf{(6b)}$$

designates the absorption Doppler profile of maximum absorption k_0 at the line centre ν_0 and of width $\delta\nu_{D,abs}$ and where L in **(5)** is the optical path length in the absorbing medium. A variable α is introduced (see **(7)** and **(9)**) to express the dependence of Q on emission and absorber temperature. It is defined as the ratio of the Doppler width in emission and the Doppler width in absorption and can be expressed in terms of the two absolute temperatures:

$$\alpha = \frac{\delta\nu_{D,em}}{\delta\nu_{D,abs}} = \sqrt{\frac{T_{em}}{T_{abs}}} \qquad \textbf{(7)}$$

This notation is used in listing the "low temperature limits" from the six data sets expressed in terms of relative absorption $Q(\alpha)$ in **Table 4.1** along with the corresponding absorber concentration N.

Absorber Concentration N [10^{11} atoms·cm^{-3}]	Relative Absorption $Q(\alpha)$ [dimensionless]
0.98 ± 0.1	0.2607 ± 0.0002
2.2 ± 0.4	0.4423 ± 0.0004
4.6 ± 0.4	0.6082 ± 0.0005
9.0 ± 0.6	0.7517 ± 0.0004
13.8 ± 0.6	0.8002 ± 0.0004
28.0 ± 1.0	0.8498 ± 0.0005

Table 4.1: Relative absorption $Q(\alpha)$ at 183.038 nm as a function of absorber concentration N.

The instrument response function and the fact, that the line profiles are not spectrally resolved are taken into account in **(5)** by integrating over the line profiles according to **(1)**. Note that the intensity I measured with absorbing atoms in the vessel is expressed in terms of the incident emission line profile. This is multiplied by a Beer-Lambert factor, which is modulated by the profile of the absorbing line $k(\nu)$. The absorber line profile according to equation **(6b)** contains the maximum value k_0, which is proportional to the absorber concentration N in the vessel:

$$k_0 \propto N \qquad \textbf{(8)}$$

After inserting the expressions **(6a)** and **(6b)** into **(5)** a relationship between the experimentally measured integrated intensities I and I_0 and (via k_0 and relationship **(8)**) the absorber concentration N is defined. Using a series expansion equation **(5)** can be transformed into [Mitchell and Zemansky 1972]:

$$Q(\alpha) = \frac{I_0 - I}{I_0} = \sum_{n=1}^{\infty} \frac{(-1)^{n+1} \cdot (k_0 \cdot L)^n}{n! \cdot \sqrt{1 + n \cdot \alpha^2}} \qquad \textbf{(9)}$$

If α were known, this expression could then be solved for k_0 using $Q(\alpha)$ and L known from the experiment. Yet by reversing the argument we numerically solve equation **(9)** for k_0 using

1. the measured $Q(\alpha)=(I_0–I)/I_0$ and L for the different concentrations in the vessel and
2. a value for α dependent on an assumed (trial) T_{em} (T_{abs} being known)

and then check for the proportionality postulated by relationship **(8)**. If the values resulting for k_0 are not proportional to the known absorber concentration then the value assumed for the emission temperature is not correct. On the contrary: The better the proportionality between k_0 and N, the better the emission temperature is estimated.

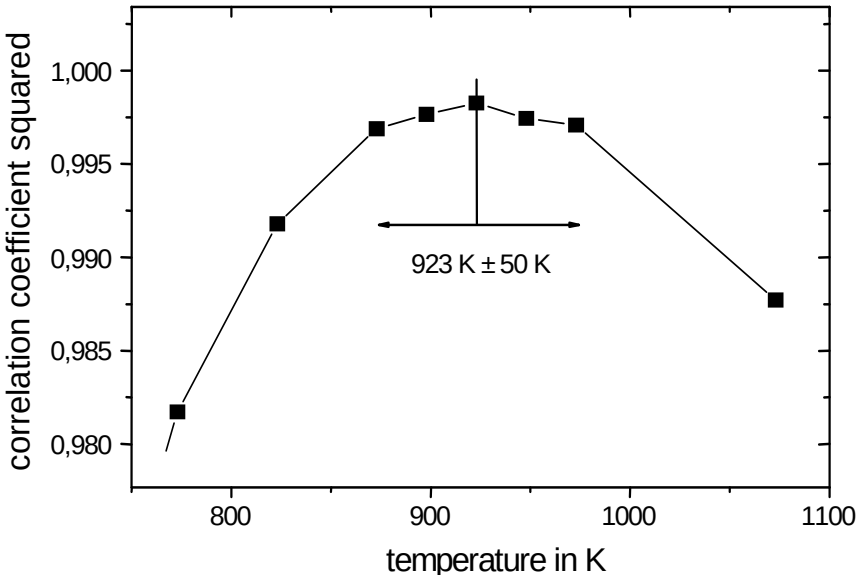

Figure 4.6 The square of the correlation coefficient achieved for a linear fit $k_0=\sigma \cdot N$ (with σ as proportionality constant) is plotted against assumed emission temperature. At T=923 K it clearly reaches a maximum indicating that the proportionality is best and, therefore, the best estimate for the emission temperature is reached. The accuracy is conservatively estimated to ±50 K yielding T_{em}=(923 ±50) K.

This analysis was performed for various values of emission temperatures. The degree of proportionality was estimated by performing a linear fit according to $k_0=\sigma \cdot N$ (with σ as proportionality constant) and by taking the square of the correlation coefficient that resulted from the fit as a measure for proportionality. For $T_{em}=(923 \pm 50)$ K the best correlation was achieved with a maximum correlation coefficient squared of 0.9983. Within the error limits of ±50 K the square of the correlation coefficient significantly decreased to 0.997 (see **Fig. 4.6**). In **Fig. 4.7** k_0 is plotted versus concentration for this optimal estimate as well as for two different values that were assumed for emission temperature in order to further illustrate the method.

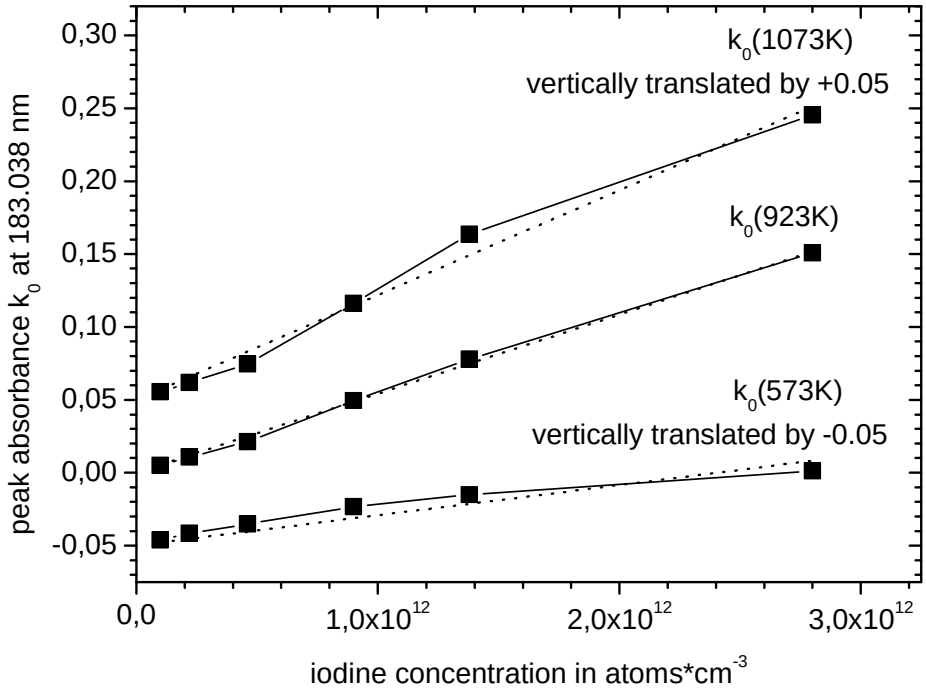

Figure 4.7 The maximum of the absorption profile, k_0, as determined from the measured integral intensities is plotted versus absorber concentration in the reaction vessel. Depending on the source temperature chosen in the determination of k_0 the data for k_0 displays a different curvature. The best estimate for the source temperature is determined by minimising the deviation from proportionality. In addition to the best fit result two other cases at different temperatures are shown to illustrate the method. The latter are vertically translated by +0.05 respectively –0.05 for clarity.

4.2.3 Determination of oscillator strength

The oscillator strength f, the maximum absorption k_0, and the concentration N are related by the following expression [Ingle and Crouch 1988, Thorne et al. 1999, Pinta 1975]:

$$\begin{aligned} f &= \frac{m \cdot c}{2\sqrt{\pi \cdot \ln 2} \cdot e^2} \cdot \delta\nu_{D,abs} \cdot \frac{k_0}{N} \qquad \text{in cgs (Gauss) units} \\ &= \frac{m \cdot c \cdot 4\pi\varepsilon_0}{2\sqrt{\pi \cdot \ln 2} \cdot e^2} \cdot \delta\nu_{D,abs} \cdot \frac{k_0}{N} \qquad \text{in SI - units} \\ &\approx 40.11 \frac{s}{cm^2} \cdot \delta\nu_{D,abs} \cdot \frac{k_0}{N} \end{aligned} \qquad \textbf{(10)}$$

where m is the electron mass, c the velocity of light in vacuum, ε_0 the permittivity of vacuum. Using the proportionality coefficient σ introduced in **(8)** yields:

$$f \approx 40.11 \frac{s}{cm^2} \cdot \delta\nu_{D,abs.} \cdot \sigma \qquad \textbf{(11)}$$

σ was determined by the best linear fit (corresponding to the best estimated source temperature) and relates k_0 and N (see relationship **(8)**). This best fit yielded the estimated source temperature of (923±50) K (see above) and at the same time a proportionality coefficient of

$$\sigma = (5.42 \pm 0.8) \cdot 10^{-14} cm^2 \cdot atom^{-1}$$

where the error limits correspond to the error limits estimated for the emission temperature. Via equation **(4)** the Doppler width $\delta\nu_D$ of the absorption profile at T=293K for an iodine atom ^{127}I had been determined to be 0.0593 cm^{-1} (1.78 GHz), so that the oscillator strength f can be calculated:

$$f = (3.87 \pm 0.57) \cdot 10^{-3}$$

As inferred from the definition of the proportionality coefficient σ and as already anticipated by the use of the Greek letter σ, the proportionality coefficient represents the Beer-Lambert absorption cross section of atomic iodine at the peak of the absorption profile.

4.3 DISCUSSION

Revalde and Skudra [1998] examined a mercury EDL with generator and lamp similar to those used in the present study. They used a Fabry-Perot interferometer to examine the spectral shape of the emission lines. They reported that at mercury partial pressures below 10^{-2} mbar no self-reversal was detectable. In their study the degree of self-reversal was determined by direct measurement of a dip at the centre of the line. Absence of a dip at the line centre indicated absence of self-reversal. Yet the effect of moderate self-absorption (long before self-reversal in the form of a dip at the line centre occurs) cannot be measured by this technique.

In comparison to this, our method using the effect of self-reversal and self-absorption on measured effective absorbances $A_{eff}=\ln(I_0/I)$ according to **(3)** is more sensitive. This is, because even a slightly self-absorbed line (still not self-reversed and still without the development of a dip at the line centre) is already deformed in such a way, that the intensity in the vicinity of the line centre is reduced in comparison to the intensity of the flanks. The absorption of a narrower (colder) absorber line leads to a weaker absorption signal because the intensity of the non-absorbed flanks of the emission line dominates the integrated signal. Following this argument, the method of examining the effect on deduced effective absorbance A_{eff} can be used to assess self-*reversal* as well as the much smaller effect of self-*absorption*. It is a more sensitive method than the direct measurement of self-reversal via the detection of a dip at the line centre.

For this reason, the critical partial pressure reported by Revalde and Skudra [1998] for non self-reversed conditions is considered only an upper limit for conditions, which are free of self-absorption. Hence, their value of 10^{-2} mbar determined under non self-*reversed* conditions for mercury emission and our value of 2.5×10^{-3} mbar for self-*absorption* free (or at least minimised self-absorption) conditions for iodine emission are in rather good agreement.

In the present study we determined the discharge temperature to be $T_{em}=(923 \pm 50)$ K. Clyne and Townsend [1974] report an estimated emission temperature for microwave discharges of approximately 600 K, but this strongly depended on the actual discharge conditions. Due to this major uncertainty they avoided the usage of discharge source temperature by using fluorescence light from a temperature stabilised fluorescence source instead of light emitted directly from a discharge. Skudra (private communication 2001) reports that with the type of EDL used in his as well as in our study, emission temperatures of 800 to 1400 K are expected

depending on generator current and on lamp geometry. In the study of Revalde and Skudra [1998] a strongly self-reversed line profile of mercury 253.7 nm is shown. Estimating a line width (FWHM) in spite of self-reversal by roughly extrapolating the self-reversed line to a more or less non-self-absorbed profile, yields a FWHM value of ca. 0.06–0.07 cm^{-1}, which corresponds to a source temperature of 900–1200K. These temperature estimates are in good agreement considering that the generators and lamps are handmade and therefore not strictly comparable.

To the best of our knowledge there are only two previous publications reporting the oscillator strength for the 183.038 nm transition of iodine. Clyne and Townsend [1974] reported a value of $(1.67\pm0.23)\times10^{-3}$ whereas Lawrence [1967] reported a value that is one order of magnitude larger, $(1.21\pm0.5)\times10^{-2}$. The method applied by Clyne and Townsend is similar to ours. They used the proportionality between known absorber concentration and measured maximum absorption k_0. By using fluorescence rather than a discharge line source they avoided the problem of unknown source temperature and at the same time reduced self-absorption and self-reversal. They used relative intensities of multiplet transitions in the resonance fluorescence light as a diagnostic for the absence of self-reversal. So with both above mentioned methods the measurements define optimum conditions under which an effect of self-absorption can no longer be detected but can not be completely excluded either.

However, in the analysis one significant difference between the two methods remains: If in our measurements a slight self-absorption in the EDL had remained, but was neglected in the analysis, this would show up as a remaining non-proportional behaviour of the deduced k_0 with respect to concentration (see **Fig. 4.7**). As a consequence of the proportionality fit procedure which we used for the determination of the source temperature this would lead to an overestimation of emission temperature. Non-proportionality caused by self-absorption would be misinterpreted as caused by higher source temperature. In that case a slightly broader Doppler profile (determined by the overestimated source temperature) would be used in **(2)** instead of the true self-absorbed emission profile. As a result, the values for k_0, σ and therefore f would be overestimated too. In this view our result should be considered as an upper limit for the oscillator strength.

On the other hand Clyne and Townsend's [1974] data still displays a non-proportionality at higher concentrations. Due to their approach the emission temperature as well as the absorber temperature were known. Therefore, uncertainties in source temperature cannot be

responsible for this deviation. Rather this behaviour might be indicative of a remaining and unaccounted for self-absorption. This then would imply that the inferred oscillator strength was determined for sub-optimal conditions and, therefore, f would be underestimated. This interpretation is further supported by the discussion in their work [Clyne and Townsend 1974], where it is stated, that the iodine emission lines used in their work (178.276 nm and 183.038 nm) were generated by photolysis of ICl with 121.6 nm radiation, which can give excited iodine atoms with significant excess kinetic energy. These lines therefore might be much broader than 300 K Doppler lines, which were assumed in their analysis. This would clearly lead to an underestimation of f values. Following these arguments the discrepancy between Clyne and Townsend's result and ours can be resolved when considering them as upper and lower limits respectively. At the same time the reliability and accuracy of both approaches and methods appears to be well comparable. We come to the conclusion that their result and ours complement each other and, thereby, determine the oscillator strength f more accurately to:

$(1.67\pm0.23)\times10^{-3} < f < (3.87\pm0.57)\cdot10^{-3}$

(Clyne and Townsend) (this work)

Consequently a similar relationship holds for the maximum absorption cross section

$(2.34\pm0.3)\cdot10^{-14}cm^2\cdot atom^{-1} < \sigma < (5.42\pm0.8)\cdot10^{-14}cm^2\cdot atom^{-1}$

(Clyne and Townsend) (this work)

The disagreement between the result of Lawrence [1967] on the one hand and those of Clyne and Townsend and our work on the other hand is not easily understood. When comparing the results of Lawrence with those of Clyne and Townsend it is surprising that their values for bromine lines agree very well, while those for iodine disagree by one order of magnitude. In Clyne and Townsend's work it was shown that this discrepancy could not be explained by broader Doppler profiles as inferred from the generation method of iodine atoms.

4.4 CONCLUSIONS

The optimal operating conditions for an RF powered EDL were determined resulting in minimised self-absorption of emission lines in the experiments of this study. A method was developed to estimate the source's plasma temperature which governs the Doppler line width. The absorption coefficient at the centre of the absorption line and the corresponding oscillator strength for the 183.038 nm resonance absorption transition were determined to $(2.34\pm0.3)\cdot10^{-14}cm^2\cdot atom^{-1} < \sigma < (5.42\pm0.8)\times10^{-14}cm^2\cdot atom^{-1}$ and $(1.67\pm0.23)\times10^{-3} < f < (3.87\pm0.57)\cdot10^{-3}$ with the lower limit determined by Clyne and Townsend and the upper limit from this work.

For the iodine conservation approach the determination of absolute concentration of $I(^2P_{3/2})$ atoms is needed. In principle this could be done by using a (possibly weighted) average of the cross section by Clyne and Townsend and from this work. The discussion above clarified the role of our result with respect to a general estimate of the absorption cross section with a remaining EDL-specific effect, which makes it an upper limit to the true cross section. But with respect to our set-up to be used in the further studies our result can also be directly understood as an empirically calibrated effective cross section, valid for our EDL under the described conditions. In this sense in the following analysis of resonance absorption data our result of $\sigma_{eff} = (5.42\pm0.8)\times10^{-14}cm^2\cdot atom^{-1}$ will be used notwithstanding the fact that the true absorption cross section is expected to lie between Clyne and Townsend's result and ours. But as the measurement's geometry in the experiments to be described below differs significantly from that used here, also a further empirical calibration will be performed as well.

5 ABSORPTION CROSS SECTION OF I_2

The visible and infrared spectrum of I_2 has been studied extensively in the past. With respect to the absolute absorption cross section of I_2 at 500nm, i.e. outside the ro-vibronic region, which reaches from λ>500nm to 650nm, a number of studies had been performed in the past. The first determination of the absolute extinction coefficient of I_2 had been performed by Vogt and Koenigsberger [1923]. Other quantitative studies followed by Rabinowitch and Wood [1935], Kortüm and Friedheim [1947], Sulzer and Wieland [1952], and Tellinghuisen [1973], establishing the latter's result for the cross section as the most reliable one. The recent observation of I_2 in the marine boundary layer by Saiz-Lopez and Plane initiated further studies on the absorption cross section. Studies by Saiz-Lopez et al. [2004] as well as previously unpublished results by Bauer et al. [2004] followed. In recent laboratory studies on the determination of absolute cross sections of iodine oxides as well as related kinetics studies as the European Union project THALOZ [2001], the knowledge of the absolute cross section of I_2 is an important prerequisite to any quantitative analysis adding further to the newly increased interest in I_2. Together with the oscillator strength of $I(^2P_{3/2})$ the absorption cross section of I_2 is the keystone to the method of iodine conservation used in the present work. Therefore efforts were made to confirm the available data on the iodine cross section. The experiment, the analysis and the results will be presented in this chapter.

5.1 EXPERIMENTAL

A schematic diagram of the set-up is shown in **Fig. 5.1**. It is similar to the set-up described in **Chapter 4** and used the same spectrometer and CCD camera as detection system. A different reaction vessel was used made of glass and without thermal insulation or stabilisation. Experiments were performed at room temperature. The length of the vessel was (26.4±0.2)cm. This was the shortest vessel available, thus enabling higher iodine concentrations without too large optical densities. Larger concentrations enabled more accurate measurement of pressure. To avoid I_2 condensation, the partial pressure was always kept below the saturated vapour pressure. The optical windows of the vessel are made from fused silica (50mm dia.). A 150W Xenon arc lamp (Hamamatsu) was used as light source for absorption spectroscopy. The spectrometer was operated with the 150 grooves·mm^{-1} grating

blazed at 300 nm. Spectra were recorded with the CCD camera in static – not time resolved - mode. To enable monitoring of the light source during absorption measurements and thus to account for possible light source drift, a second beam of light was passed parallel to the vessel. With a flip mirror the light was directed either via the vessel or directly from the light source towards the spectrometer.

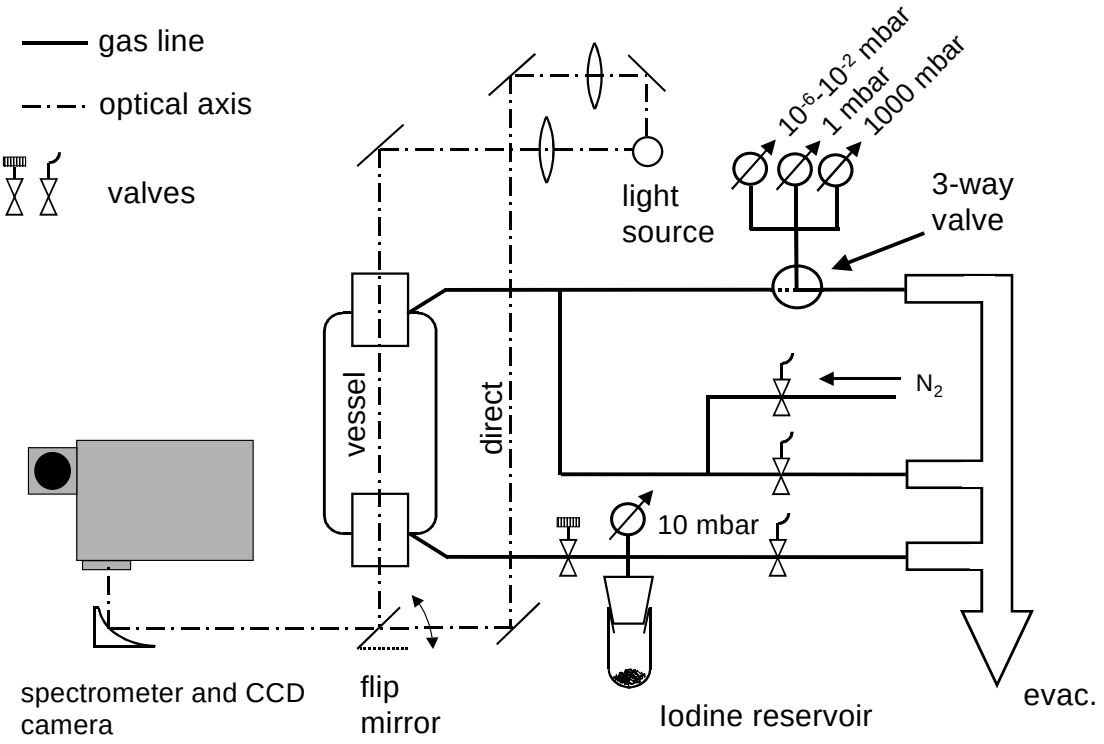

Figure 5.1 In the determination of absolute absorption cross section of I_2 simultaneous measurements of OD and pressure were used. Absorption spectroscopy was performed with a Xenon lamp, a spectrometer and CCD camera. A flip mirror enabled near-real time light source monitoring. Pressure in the vessel was automatically monitored with a 0.001 to 1.0 mbar capacitance barometer.

Pressure in the vessel being the crucial parameter in the determination of concentration it was measured with a temperature stabilised capacitance pressure transducer (MKS Baratron 627B) with 0.001 to 1 mbar range, high linearity, low hysteresis and high reproducibility (specified ±0.12% of reading). Zero point correction was performed with a Penning type pressure head (Edwards, 10^{-3} to 10^{-7}mbar).The temperature of the gas in the vessel, ambient temperature and the temperature of the reservoir were all measured with calibrated 3 wire Pt 100 temperature sensors. The manufacturer's specification for the sensors is ±0.07K. The transducers were calibrated and specified to the same accuracy of ±0.07K. As a conservative error estimate for the temperature measurement 0.5K was assumed based on a comparative measurement. The

vessel was connected to a reservoir, where the iodine was maintained. The pressure in the reservoir was monitored with the same type of temperature stabilised and high accuracy capacitance pressure transducer as the one connected to the vessel, but with 0.01 to 10mbar range. Pressure heads, vessel and iodine reservoir were connected to the vacuum pump such that all could be evacuated independently of each other. During all experiments pressure and temperature readings from al sensors were automatically recorded in sufficiently short time intervals to cover any changes accurately.

5.2 DETERMINATION OF ABSOLUTE ABSORPTION CROSS SECTION OF I_2

The absolute absorption cross section was determined by simultaneously determining optical density via spectroscopic measurement and concentration via pressure and temperature measurement including careful leak rate correction.

5.2.1 Spectroscopic measurements

Each spectroscopic measurement consisted of a recording of the detector's dark signal, followed by repeated alternating measurements of the light source directly and through the vessel respectively. "*Vessel*" measurement and "*direct*" measurement consisted each of a fixed number of accumulations. By the alternating measurement procedure a near-simultaneous recording of both was achieved which enabled a highly effective correction of possible light source drift. Prior to each measurement series the accuracy of drift correction was verified by a set of such measurements without gas in the vessel. In a preparatory experiment within half an hour a light source drift occurred with a trend of the order of 0.02/h to 0.03/h plus irregular scatter of ±0.005, all in units of optical density. The drift was deliberately forced by irregularly venting the xenon arc lamp to create "worst case conditions" for this test. By the described near-real time monitoring the long term drift could in all test measurements be corrected to an irregular scatter in the averaged optical densities of less than ±0.0025 in units of optical density (determined as the standard deviation across a corrected measurement of zero optical density). "Coloured" structures in the uncorrected optical density spectra of empty vessel measurements (caused by light source drift) were to a high degree but not completely removed. As a conservative error estimate for the remaining drift effects an average of the typically found amplitude of the coloured structures of ±0.006 was used. The error of an original measurement was estimated in the sense of a maximal error as the sum of

the determined standard deviation of a corrected empty vessel measurement plus the estimated error from drift. Both statements - scatter of ±0.0025 and ±0.006 conservatively estimated systematic drift - define the general maximum uncertainty of ±0.0085 of determined optical densities with respect to light source drift. Following the described approach, all reference – i.e. empty vessel – and absorption measurements – with I_2 – were performed. It is pointed out that accumulation of deposit on the vessel windows is not corrected by this approach. This is taken into account below.

Wavelength calibration was obtained from measurements of a mercury cadmium line source. Only isolated lines were used for wavelength calibration. Unresolved groups of neighbouring lines were rejected. Wavelength with respect to the 500nm absorption cross section of I_2 is given in standard air. Note: Spectra in the following sections are given in vacuum wavelength for direct comparability with FTS and other spectroscopic measurements and for spectroscopic analysis.

5.2.2 I_2-handling and measurement procedure

In separate preparatory measurements the leak rates of the empty reservoir and the vessel were determined to be 0.3µbar·min^{-1} and 2.1µbar·min^{-1} respectively. In both cases the increase of pressure with time, which was caused by leak rate always displayed a clear linear behaviour on the time scale of our measurements. A linear fit to the vessel's pressure readings covering a 4 hours leak test resulted in a correlation coefficient of R^2=0.99998 between the data points and the linear fit. This justifies extrapolation of the leak rate on the time scale of our measurements.

Prior to each filling both the vessel and the I_2-reservoir containing solid I_2 were evacuated separately to remove any foreign gases due to remaining leaks. After evacuation the reservoir was closed to allow the built-up of gas phase I_2. The vessel was also closed and a number of spectroscopic reference measurements (each a set of *vessel* and *direct* intensity measurements) were performed on the evacuated vessel, providing the error estimate for the spectroscopic measurements and also the ‘empty vessel’ reference for the determination of OD. Parallel to the empty vessel spectroscopic measurements the pressure in the vessel was monitored to check the leak rate of the vessel.

In the next step the I_2-reservoir was connected to allow the I_2-vapour to stream into the vessel. In general the filling proceeded initially through a fast burst resulting from the pressure

gradient between the I_2-filled reservoir and the evacuated vessel. After that, filling proceeded significantly slower dominated by the speed of release from solid to gas phase in the reservoir, where the I_2 vapour was no longer in equilibrium with the solid phase. In the measurement the vessel was preferably filled using the faster initial burst. Thereby it was assured that partial pressure of I_2 was always below saturated vapour pressure and condensation of I_2 thereby minimised.

After filling, the reservoir was disconnected from the vessel and simultaneous pressure readings and spectroscopic measurements were recorded. This filling and measurement procedure was repeated in several steps each time adding some more I_2 into the vessel to collect data for different concentrations. Overall pressures in the vessel were always below 0.7 mbar and well within the range of the 0.001 to 1 mbar pressure transducer. Partial pressure of I_2 was obtained by correcting the time series of overall pressures for leak rate. As justified above, changes in pressure due to leak rate could be assumed to be linear in time with the aforementioned rates. The temperature measurements enabled correction of temperature drifts and conversion to concentration. The partial pressure of I_2 in the vessel was always below 0.35 mbar. The vapour pressure of I_2 at 298K is 0.40 mbar [Chase 1998]. Condensation on surfaces and windows was thereby minimised.

5.2.3 Analysis

In spite of the partial pressure of I_2 being below saturated vapour pressure still wall loss of I_2 occurred in the vessel. It led to a slow but visible reduction of both partial pressure of I_2 as well as of optical density in the spectroscopic measurement. The correlation between both effects was high. Therefore wall loss is automatically compensated in our determination of σ_{I_2}. Nevertheless, due to wall loss also a measurable deposit built up on the windows which was spectroscopically observed. The absorptions of I_2 and deposit were separated by multiple multivariate linear regression of the observed time series of spectra using their different spectroscopic appearance. They were fitted against an average of observed time profiles containing dominantly the deposit's absorption (340 nm to 380 nm) and an I_2 time profile observed at 500 nm. This approach produced the two continuous, smooth and non negative separated spectra of I_2 and the deposit. The fit itself was characterised by high correlation coefficients and residuals distributed normally. This proved the contribution of deposit at 500nm to be negligible, while becoming increasingly important from 485nm (worst case: 3%

relative to optical density of I_2) on to the blue side of the spectrum (20% at 460nm). Consequently the recordings at 500nm can be safely regarded as free of deposit within less than 1% relative to the I_2 absorption. Furthermore, at and below 500 nm the spectrum of I_2 is smooth and free of rotational structure. OD calculated from the pixel outputs is free of instrumental artefacts related to resolution issues. Above 500nm this is not the case, see **Fig. 5.2** and **Fig. 5.3**. Therefore the wavelength of 500nm is well suited for the determination of σ_{I_2}. In the absence of technical imperfections the series of *pure* I_2 OD spectra should vary linearly with partial pressure, i.e. concentration of I_2. The proportionality factor at each wavelength – i.e. pixel - directly determines the sought-for absolute absorption cross section at that wavelength. Therefore the measured OD at 500nm was plotted as a function of partial pressure, i.e. concentration. A linear fit with zero intercept for this OD versus concentration was then performed. This yields the cross section σ_{I_2} at 500nm as the slope of the obtained line.

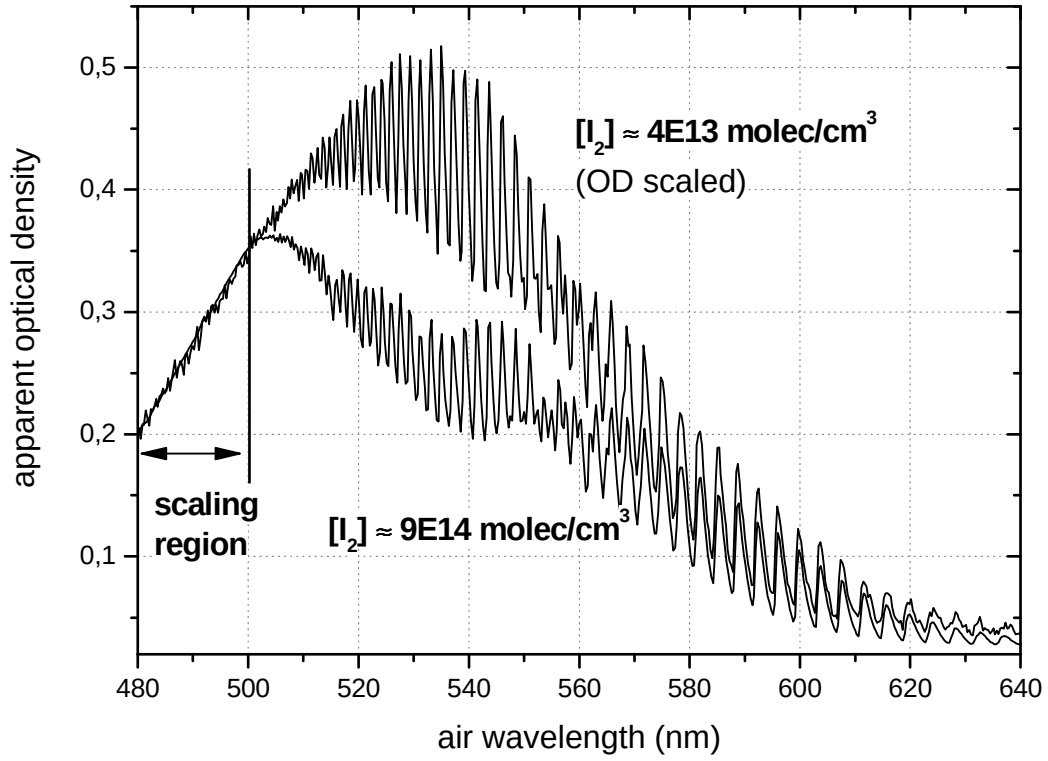

Figure 5.2 Two recordings of I_2 are compared to illustrate the strong non-linear behaviour of apparent optical density of I_2 in the region above 500nm. The spectra were recorded at significantly different concentrations under otherwise constant conditions. In the region below 500nm the spectrum recorded at lower concentration is scaled to the other. Above 500nm the apparent OD of the spectrum of higher concentration clearly grew much slower than in the continuum region below 500nm due to non-linear effects in apparent OD.

5.3 RESULTS FOR THE ABSOLUTE ABSORPTION CROSS SECTION OF I_2

Fig. 5.2 shows the OD of one of the two performed measurement series as a function of concentration and the corresponding linear fit. OD is normalised to unit path length. Each data point is the average of 4 to 6 individual spectroscopic determinations of optical density recorded at a certain I_2 partial pressure. Each spectroscopic determination is the average of 50 individual accumulations of "*vessel*" and "*direct*" as described above. The high quality of both linear fits for the two series was expressed by correlation coefficients of R^2=0.99951 and 0.99846 respectively. In the linear regression the estimated uncertainties of both axes were taken into account [Press et al. 1986]. The uncertainty of concentration was determined after correction of all systematic effects covered by measurement, i.e. leak rate and temperature drift. It therefore contains only the accuracies of the pressure head and the temperature sensor as stated by the manufacturers after error-propagation. The uncertainty of optical density is based on the aforementioned maximum uncertainty of 0.0085 in units of optical density and that of the measured length of the vessel of (26.4±0.2)cm. Note that the uncertainty of 0.0085 is not yet normalised to unit path length.

The error estimate resulting from the linear regression contains both the uncertainty of the observational data *and* the scatter of the individual data points with respect to the linear fit. The estimates for the cross section σ_{I_2}(500nm) obtained from the two series of data are determined as $(2.194\pm0.010)\cdot10^{-18}cm^2\cdot molec^{-1}$ and $(2.158\pm0.018)\cdot10^{-18}cm^2\cdot molec^{-1}$, where the stated uncertainty is that resulting from the linear regression. Using the inverse squared error as weight, a weighted average was calculated from the two results, the error of which being determined by error propagation. This yields $(2.18_6\pm0.009)\cdot10^{-18}cm^2\cdot molec^{-1}$. Apart from that also the uncertainty in wavelength calibration has to be taken into account and – via the estimated derivative of the spectrum at 500nm – converted into an uncertainty of absolute cross section. Assuming an uncertainty of one pixel in wavelength calibration the uncertainty in cross section amounts to $\pm0.012\ cm^2\cdot molec^{-1}$ which is again conservative, as the accuracy of wavelength calibration is of sub-pixel order. To obtain the final uncertainty of the determined cross section this uncertainty is added to that obtained from the linear regression in the sense of a maximum error estimate yielding the final result of our experiments to be $\sigma_{I_2}(500nm)=(2.18_6\pm0.021)\cdot10^{-18}cm^2\cdot molec^{-1}$.

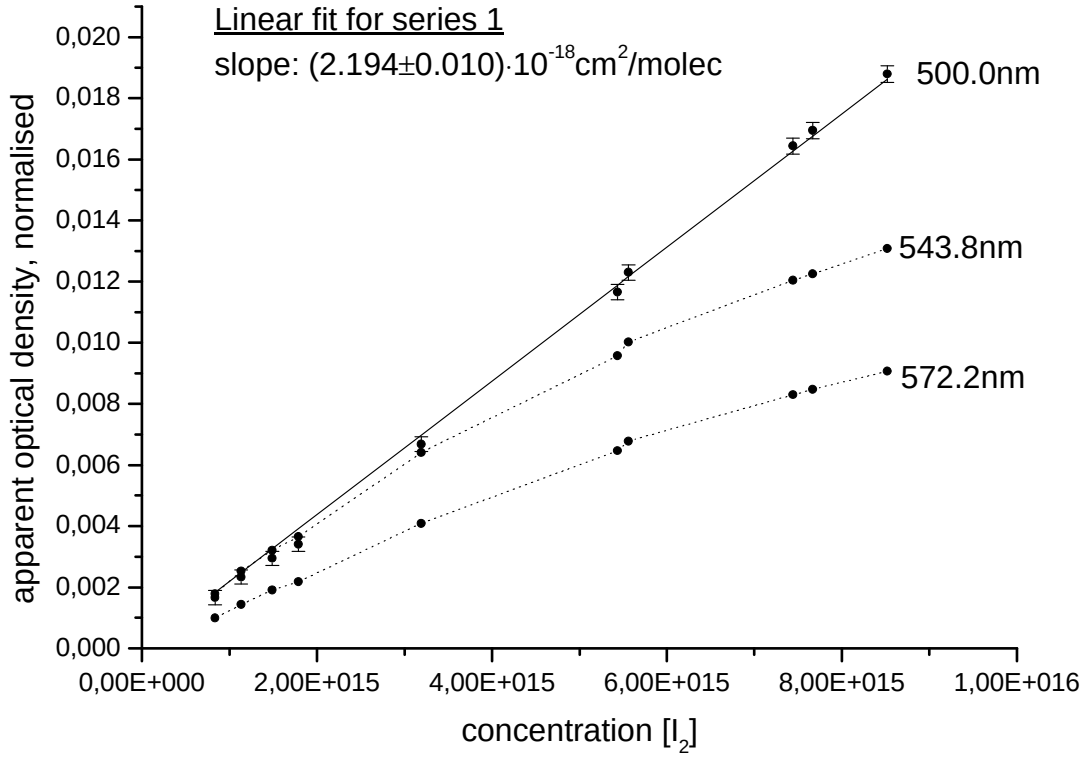

Figure 5.3 The absolute absorption cross section of I_2 at 500nm (in standard air) in the continuous region of its absorption spectrum was determined by simultaneous spectroscopic and pressure/temperature measurement. The graph shows the linear fit of OD against concentration for the first series of measurements. OD is normalised to unit path length. The linear fit produces the estimate for σ_{I2}(500nm). The stated uncertainty is the statistical error estimate from the linear regression based on the input uncertainty estimate for both axes. Data for two other wavelengths from the ro-vibronic region (λ>500nm) is shown, demonstrating the non-linear behaviour of apparent OD in this region due to resolution issues.

5.4 DISCUSSION

The absorption cross section determined in this way is an independent measurement, which did not rely on vapour pressure data. It agrees very well with the recently published results, see **Table 5.1**. The disagreement between data is always well within the stated uncertainties. The determination of Bauer et al. [2004] was also independent of vapour pressure using an approach similar to ours. The careful and extensive study by Tellinghuisen [1973] used vapour pressure data by Stule [1961] and Shirley and Giauque [1959]. Light source drift was compensated by a two beam optical arrangement with beam alternator. The study by Saiz-Lopez et al. [2004] also used vapour pressure reference data to determine absolute cross section, which they measured independently and which agrees well with the previously published data [Chase 1998, Shirley and Giauque 1959].

Based on the results listed in **Table 5.1** a weighted average was calculated, which used the reciprocal squared errors of the individual results as weights:

$$\sigma_{I_2}(500nm)=(2.19_1\pm0.02)\cdot10^{-18}cm^2\cdot molec^{-1}$$

The error of the weighted mean was determined by error propagation. Stated is a 1σ- error.

σ_{I2}(500nm) ($10^{-18}cm^2\cdot molec^{-1}$)	**method**	
2.20±0.07	vapour pressure	Tellinghuisen [1973]
2.29±0.27	vapour pressure	Saiz-Lopez et al. [2004]
2.25±0.09	independent	Bauer et al. [2004]
$2.18_6\pm0.02_1$	independent	this work
$2.19_1\pm0.02$		**weighted average**

Table 5.1 Comparison of results for the absolute absorption cross section of I_2 at λ=500nm. The average was obtained by using the inverse squared error of each individual measurement as a weight. The error was determined by error propagation.

5.5 CONCLUSIONS

The absolute absorption cross section at 500nm (standard air) in the continuum region was determined in an independent measurement. The result of $\sigma_{I_2}(500nm)=(2.18_6\pm0.021)\cdot10^{-18}cm^2\cdot molec^{-1}$ agrees very well with previously published data and the uncertainty could be reduced by more than 50%. A weighted average of $\sigma_{I_2}(500nm)=(2.19_1\pm0.02)\cdot10^{-18}cm^2\cdot molec^{-1}$ of the recent determinations is suggested as the best estimate for the absolute absorption cross section.

6 I_XO_Y SPECTROSCOPY BY SYNCHRONISED MOLECULAR AND ATOM-RESONANCE ABSORPTION

Having determined the oscillator strength of $I(^2P_{3/2})$ and the absorption cross section of I_2 the reference data needed for determination of cross sections of iodine oxides by iodine conservation is available. Synchronous measurements of molecular absorption of precursor molecules and I_xO_y absorbers and of resonance absorption of $I(^2P_{3/2})$ are to be recorded. In this section the set-up used for this type of experiments will be described. An overview of the recorded data-sets will be given. Pre-processing of data, spectroscopic analysis and the final determination of absorption cross sections by iodine conservation will be described in the subsequent chapters.

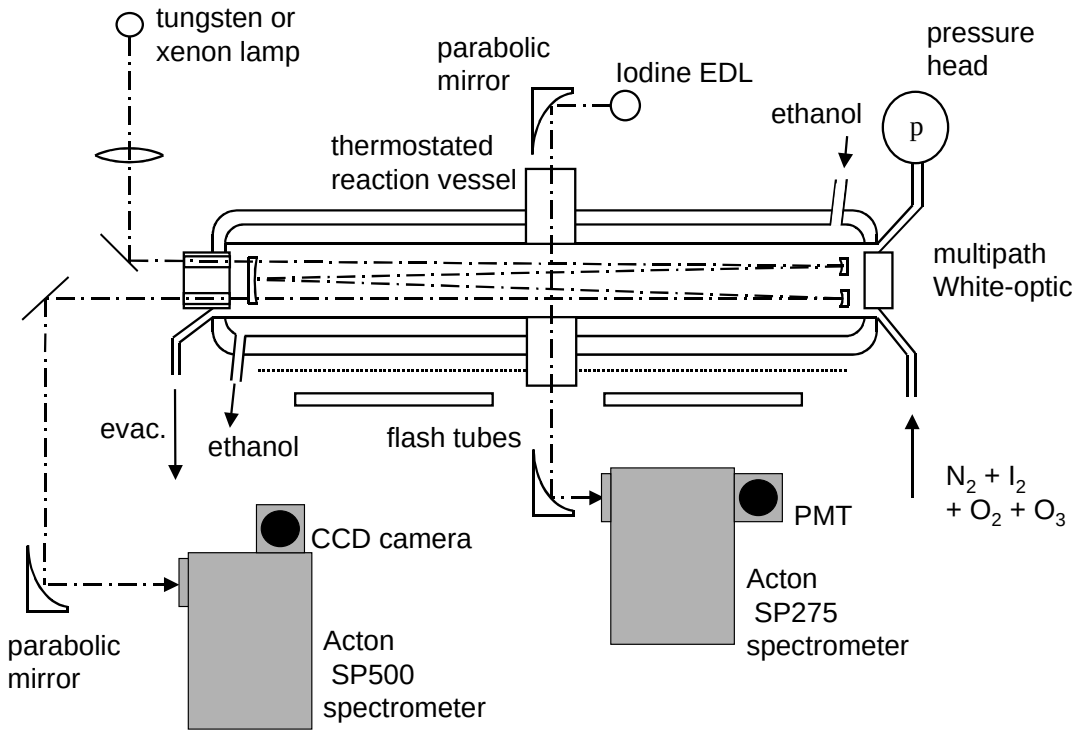

Figure 6.1 For recording of time resolved data for determining spectra and absolute absorption cross sections a synchronised set-up of time resolved molecular absorption spectroscopy and time resolved VUV resonance absorption spectroscopy was used. Molecular absorption spectroscopy was performed with a Xenon lamp, a spectrometer and CCD camera as in the experiments above, but this time in time resolved mode. VUV resonance absorption for iodine atoms was performed with the EDL described in **Chapter 4**. which here is used along the short cross axis.

6.1 EXPERIMENTAL

A schematic diagram of the apparatus is shown in **Fig. 6.1**. It is similar to that described in **Chapter 4**. It comprises a two-axis crossed beams reaction vessel, the same conventional Xenon flash tube photolysis system as above but two independent time resolved absorption spectroscopy detection systems instead of just one. The one for molecular absorption spectroscopy is the same as above (CCD camera for static and time-resolved mode), the other is designed for resonance absorption spectroscopy. Again a different reaction vessel is used specifically designed for this type of synchronised experiment. It has a long axis of 120cm length for the molecular absorption measurement and a short cross axis of 5.5cm length for resonance absorption, where different pathlength compensates different sensitivity. The cross axis is located half way down the long axis of the vessel. The two axes at right angles enable two independent but simultaneous measurements. Opposed to a simple straight vessel without cross axis, in a cross axis vessel inhomogeneities in the photolysis and consequently also in the mixture along the long axis of the vessel can not be excluded. Therefore the resonance absorption signal was always calibrated empirically using photolysis of mixtures of I_2 in N_2 without O_3. For thermal stabilisation and insulation the vessel is constructed with two quartz jackets. The inner one is temperature stabilized by a flow of ethanol from a thermostatic bath. The outer one is evacuated for thermal insulation. Experiments were again performed at room temperature. Along the long axis of the vessel a multiple path optical arrangement is mounted inside the reaction vessel. The optical multi path design is similar to that of White [1942, 1976]. Optical path length within the vessel could be varied in steps of 4.8m up to approximately 24.30m. The optical windows at the entrance and exit of the multi path optics and at both ends of the cross axis are made from quartz and are double walled and evacuated for thermal insulation. For molecular absorption spectroscopy a 150 W Xenon arc lamp was used. Its light was directed along the multi path optics and after having traversed the vessel was focussed onto the entrance of the aforementioned spectrometer and CCD system. For resonance absorption the same RF powered EDL was used as described above. It was located sideways of the vessel. Its light was parallelised by an off-axis parabolic mirror and directed along the short cross axis of the vessel. After having traversed this, it was again focussed by a second off-axis parabolic mirror onto the entrance slit of a second Czerny-Turner monochromator (Acton Research, 275 mm focal length) operated with a 1200 grvs·mm^{-1} holographic grating. Unwanted stray light from imperfect parallelisation was blocked by baffles. The signal was recorded in time resolved mode by a photomultiplier tube

(Hamamatsu, R955) and fast amplification and ADC electronics. Temporal resolution could be as fast as 4μs per data point without electronic artefacts. Separation of lines and usable slit width were similar to the ones described in **Chapter 4**.

Iodine oxides were produced in the reaction vessel by photolysis of mixtures of I_2 and O_3 in bath gases N_2 and O_2 at pressures of the order of 10 to 400 mbar. The experiments were performed in flow mode, as the time scale of reactions was always at least a factor of 30 shorter than that of a single purging time of the vessel. A stable flow of I_2 in N_2 was produced by passing a flow of N_2 through a thermostated and pressure stabilised glass vessel (T=273.15 K, ice water) containing solid I_2. This flow could be diluted by an additional flow of pure N_2. Flows were controlled using calibrated mass flow controllers (MKS Instruments). For some experiments the transport gas was replaced by O_2 to have experiments in pure O_2 as bath gas. Pressure in the vessels was measured by calibrated capacitance manometers (MKS Instruments). The N_2 and O_2 was obtained from Messer-Griesheim (grade 4.8). Ozone was produced by passing a stream of O_2 through a silent discharge. The formation of iodine oxides was initiated by the broad band photolysis of I_2 and O_3. Thus, I and O atoms were formed:

$$O_3 + h\nu \rightarrow O_2 + \delta \cdot O(^3P) + \varepsilon \cdot O(^1D) \quad \text{(R6.1)}$$

$$I_2 + h\nu \rightarrow \alpha \cdot I(^2P_{3/2}) + \beta \cdot I(^2P_{1/2}) \quad \text{(R6.2)}$$

I atoms produced in the excited metastable $I(^2P_{1/2})$ state are rapidly quenched to ground state $I(^2P_{3/2})$ by collision with $O_2(X^3\Sigma^-)$, because of an efficient resonant energy transfer, which is also used in chemical oxygen iodine lasers COIL [Marter et al. 1996 and references therein]. Similarly the $O(^1D)$ excited oxygen atoms are collisionally quenched in an excess of N_2. Both radicals I and O are capable of forming IO via reaction of I with O_3 and O with I_2 respectively. The latter reaction releases additional iodine atoms to react with O_3. Thus, two different sources of IO are simultaneously present in the experiments (Rate coefficients again from [NIST, 1998]):

$$I(^2P_{3/2}) + O_3 \rightarrow IO + O_2 \quad [1.2 \cdot 10^{-12} cm^3/(molec. \cdot sec)] \quad \text{(R6.3)}$$

$$O(^3P) + I_2 \rightarrow IO + O_2 \quad [1.3 \cdot 10^{-10} cm^3/(molec. \cdot sec)] \quad \text{(R6.4)}$$

In order to simplify the chemical system the second IO source was minimised using optical filters (Pyrex) between the flash tubes and the vessel to avoid the photolysis of O_3 below

320nm. Some residual photolysis of O_3 in its Chappuis band still occurs, but as I_2 is in a large excess over oxygen atoms, they scavenge any O atoms quickly. The IO formation due to this process is observed as a – with respect to the temporal resolution of the CCD system and the subsequent formation of IO via (R6.3) - instantaneous initial formation of [IO]. During and following the formation of IO a number of further reactions take place including the self reaction of IO, which is believed to be the main source of OIO. Other products and reaction pathways have not yet been unequivocally determined even though there exist a number of observations and tentative identifications of further absorbers [Cox and Coker 1983, Harwood et al. 1997, Spietz et al. 1998, Bloss 2001].

Time resolved measurements of the described flash photolysis experiments were recorded at effective temporal resolutions mostly ranging between 100µs (20µs/spectrum) up to in some cases 500µs (100µs/spectrum). The CCD system and the photomultiplier tube of the resonance absorption set-up were both synchronised to the flash photolysis system and monitored the molecular species and iodine atoms simultaneously. The time interval covered by the measurement always covered the photolysis flash itself, the subsequent relaxation reaction as well as a sufficiently large interval before the flash containing the light source reference measurement necessary for absorption spectroscopy. Drift effects in the light source output are therefore minimised by the close vicinity of reference and absorption being only a fractions of a second apart.

From the CCD recordings apparent optical densities were then calculated by applying the Beer-Lambert law directly to the pixel read outs taking the averaged pre-flash data as reference $I_0(\lambda)$ and the post flash data as time resolved absorption measurements $I(\lambda,t)$. The intensity recordings of the resonance absorption set-up were converted to concentration following the procedure described in **Chapter 4**. Apparent optical density from the CCD measurement plus iodine atom concentration from resonance absorption provided the basic observational data for each individual experiment to be used in subsequent analysis.

As above, wavelength calibration was obtained from measurements of a mercury cadmium and a mercury line source. Only isolated lines were used for wavelength calibration. Unresolved groups of neighbouring lines were rejected.

6.2 DATA SETS USED IN THIS WORK

Recorded were about 60 datasets to be used in the determination of absolute cross sections. They were centred at 440nm and covered the spectral range from 280nm to 600nm, thus including the short wavelength tails of the UV absorbers, which was important for their separation from the neighbouring IO spectrum. They also covered vibrationally excited IO, I_2 and the largest part of the OIO spectrum. A smaller number of measurements was centred at 500nm and covered the range from 340nm to 660nm including the whole spectrum of OIO up to its NIR end. As these measurements did not contain the for UV absorbers important range between 300 and 340nm, they were of only limited use for the method of iodine conservation and basically provided the spectral information about the NIR side of the OIO absorption. In addition to that also a number of measurements centred at the ozone absorption was taken in order to obtain – if possible - the full spectra of the UV absorbers. But this proved to be difficult and was in most cases impeded by the built up of deposit on the mirrors of the White optic. **Fig. 6.2** shows a typical CCD-recording of a time resolved kinetic experiment. It illustrates the broad spectral coverage of the recordings and the simultaneous measurement of absorptions from different species.

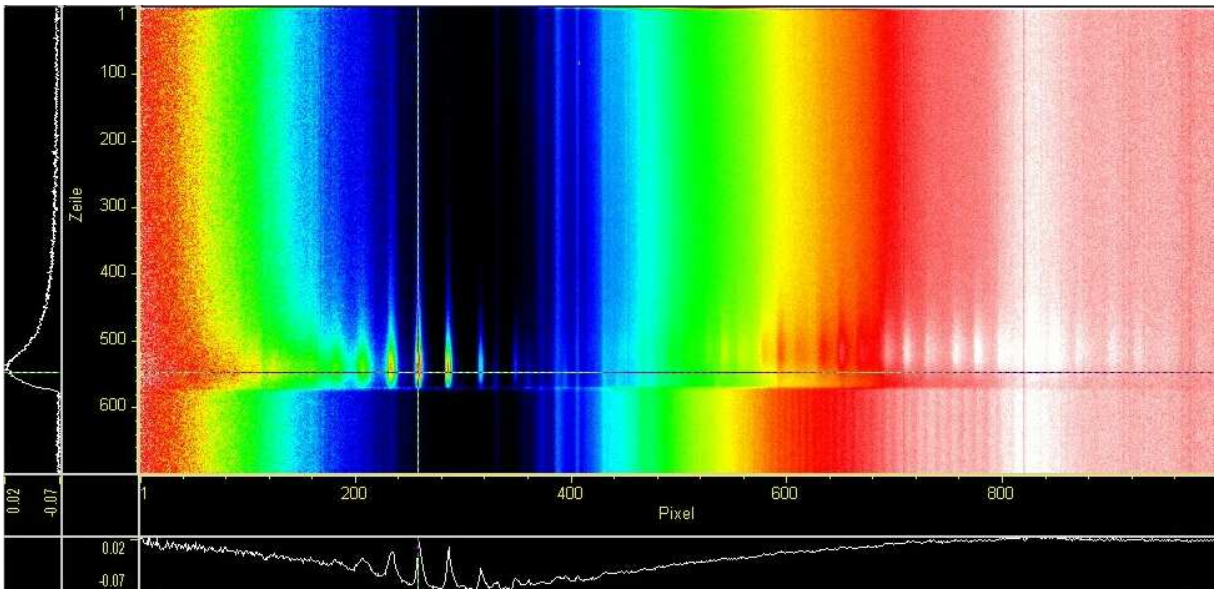

Figure 6.2 A typical CCD recording of a time resolved experiment is shown. Data is already converted to OD. The horizontal axis from left to right corresponds to wavelength (not yet calibrated) while the vertical axis from bottom to top corresponds to time (row numbers in plot are reversed). To the left and at the bottom geometric cross sections through the three dimensional data representation of OD(λ,t) are plotted passing through the IO(4←0) absorption band. The occurrence of the flash near row 580 is marked by the sudden changes of OD. Clearly the absorption bands of IO and IO^* can be seen after the flash and in the wavelength range between pixel 200 to 400. From pixel 500 to 1000 and before the flash the dense bands of I_2 and after the flash the broader ones of OIO are visible.

The data was recorded under various conditions of pressure, mixing ratios and temporal resolution to ensure a general validity of the obtained results. In **Table 6.1** the conditions of experiments, which were used in the method of iodine conservation are listed.

	N exp	**$[O_3]_0$ (molec/cm_3)**	**$[I_2]_0$ (molec/cm_3)**	**P_{vessel} (mb)**	**Buffer**	**Filter**
Group 1	10	$(2.3\pm0.6)\cdot10^{15}$	$(7.6\pm0.9)\cdot10^{12}$	40-400	**N_2**	yes
Group 2 (O_3+hν, Group 1)	6	$(2.6\pm0.6)\cdot10^{15}$	$(5.6\pm0.3)\cdot10^{12}$	40-400	**N_2**	no
Group 3 ($[I_2]_0$, Group 1)	8	$(2.0\pm0.3)\cdot10^{15}$	$(5.4\pm0.3)\cdot10^{13}$	40-400	**N_2**	yes
Group 4 (Buffer, Group 3)	7	$(2.0\pm0.3)\cdot10^{15}$	$(5.4\pm0.4)\cdot10^{13}$	100-400	**O_2**	yes
Group 5 ($[O_3]_0$, Group 3)	6	$(8.2\pm0.9)\cdot10^{14}$	$(4.4\pm0.5)\cdot10^{13}$	40-360	**N_2**	yes
Group 7 (low pressure)	11	$5\cdot10^{14}$-$2\cdot10^{15}$	$1\cdot10^{13}$-$6\cdot10^{13}$	10-40		yes
Group 8 (low pressure, less iodine)	5	$5\cdot10^{14}$-$2\cdot10^{15}$	$3\cdot10^{12}$-$1\cdot10^{13}$	10-40	**N_2**	yes
Group 9 (reproducibility)	6	$(1.04\pm0.15)\cdot10^{14}$	$(5.4\pm0.3)\cdot10^{14}$	40		yes

Table 6.1 Experimental conditions of kinetic datasets used in the method of iodine conservation. Analysed were nine groups with different conditions. In column one it is indicated, which parameter or condition was changed relative to a preceding group. "N exp" is the number of individual experiments. Ozone was varied over nearly one and iodine over two orders of magnitude. Pressure was changed by addition of either O_2 or N_2 as buffer gas with mixing ratios of reactants in the vessel maintained unchanged. "Filter" indicates the usage of an optical filter between flash lamps and vessel

Changes in concentrations of precursors I_2 or O_3 varied the temporal behaviour of concentration of species formed during the course of reaction. By placing a filter between the vessel and the flash lamps the ratio between photolysis of I_2 and that of O_3 could be changed significantly. The filter made of Pyrex reduced O_3 photolysis strongly while at the same time leaving the photolysis of I_2 more or less unchanged. This changed the relative importance of the two sources of IO. Varying the overall pressure has a strong effect on the temporal behaviour of a number of species among which vibrationally excited IO and OIO reacted strongest. But also the formation of higher oxides, which was observed in the UV is affected by pressure. A change of the buffer gas from N_2 to O_2 caused small changes in some species possibly providing insight into the chemical mechanism in a future study of the chemical kinetics of the system.

In summary the available datasets provide a sound basis of measurements of significantly different temporal behaviours of species observed in the photolysis of I_2 and O_3. Widely varied conditions are required to justify the general validity of results. But the variation of temporal behaviour of individual absorbers within an individual data set as well as between different data sets will also play a central role in the separation of spectra, the extraction of separated time curves and in the numerical solution to the method of iodine conservation.

7 SEPARATION OF ABSORBERS

The objective of this chapter is to extract curves of temporal behaviour for all relevant absorbers from their *simultaneous* and therefore overlapped recording in a time resolved CCD measurement. The extracted curves should be as pure as possible to provide the basis for applying the method of iodine conservation. Provided such curves of temporal behaviour it will also be possible - within certain limits - to determine the pure, *separated* spectra of individual absorbers across the full spectral range observed. Both together will enable accurate quantitative analysis of cross sections and chemical kinetics in first place. In second place the spectra obtained in this way will provide the reference spectra needed in general for quantitative spectroscopy of iodine oxides, be it in the field or in the lab.

7.1 SEPARATION OF CURVES OF TEMPORAL BEHAVIOUR FOR INDIVIDUAL ABSORBERS

7.1.1 General procedure

To separate spectra, data analysis methods used in other fields were studied and their potential for adapting them to our needs were explored. Principal Components Analysis (PCA) and Independent Components Analysis (ICA) were found useful for this. Results from this study and details on how these methods are applied properly in the context of time resolved spectroscopy we published in Gómez-Martín et al. [2004].

The key to both methods is the requirement of orthogonality of original "source signals". Source signals or in this context more specifically "source spectra" are the variation of absorption of individual – i.e. separated - absorbers with wavelength. Each source spectrum is regarded as a vector in a multidimensional vector space. The dimension of the vector space is defined by the number of pixels within the spectral window. Mathematically speaking, any set of linearly independent vectors can be transformed into an orthogonal base. But this requires a knowledge of the vectors. In the present case, the vectors are unknown, so a base transformation is not possible and therefore the requirement for orthogonality applies directly to the unknown source spectra.

Tackling the problem pragmatically, orthogonality of two sources means zero scalar product of the spectra of two absorbers – sources - within the considered wavelength interval. It is intuitively clear that this can not be expected automatically and for each spectral interval, as absorption spectra tend to behave differently than e.g. acoustic signals, for which ICA and PCA work fine. Just applying any of the two methods to a time resolved recording of full spectral width will therefore in general produce mixtures of the source spectra. Nevertheless PCA provides a tool for de-noising and for determining the number of relevant sources contained in the data using the relative magnitude of eigenvalues as criterion. Due to the positiveness of absorption, a prerequisite for orthogonality and for the applicability of the methods is centring the data [Gómez-Martín et al. 2004 and references therein]. Having assured this, the issue is to find spectral windows in the recorded data, for which orthogonality is as good as possible fulfilled for the source spectra contained. The better this condition is fulfilled, the better the separation of sources and the better the quality of the separated source spectra will be. The search for suitable spectral windows clearly requires some a-priori knowledge of the spectra. These can be obtained by more "classical" approaches like "on-peak/off-peak"-differences in time and similar empirical methods. Numerical concepts can also be developed helping in this search [Gómez-Martín et al. 2004].

The product of such an analysis in a selected spectral window will be a set of curves of temporal behaviour for the separated absorbers contained in that window plus the corresponding source spectra. Before curves of temporal behaviour and spectra can be further interpreted and analysed, they need to be de-centred again. The set of time curves and source spectra – i.e. absorbers - in that window will in general be a sub-set of the absorbers contained in the full spectral window. The task remains to identify a sufficient number of such windows to extract curves of temporal behaviour for all absorbers relevant on the full spectral range of observational data, the number of which having been determined by PCA. In cases, where no suitable window fulfilling the orthogonality condition of spectra can be found, more classical approaches as scaled differences of superpositions have to be used to iteratively isolate spectra. If one of the absorbers has differential structure, this can be used to remove the structured absorber from any superposition obtained in a different time step. Separation can also be facilitated by firstly removing absorbers, for which a spectrum is known and a time curve can be determined in a different window. This proved to be helpful for the removal of I_2, of which the spectrum under the given spectroscopic conditions could be measured statically before the kinetic experiment.

7.1.2 Separated curves of temporal behaviour

For separation of a curve of temporal behaviour of IO from other absorptions a spectral window from 340 nm to 434 nm was used. PCA determined the number of absorbers in the selected interval to be of the order of 3 or more, but artefacts from deposit, flash and low signal limited the meaningfulness in this case. With curves of temporal behaviour being the only objective of this part of the analysis, the border of the interval was less important than in the case of extracting spectra, where coverage of the whole spectrum by suitable intervals is an issue, see below. In the present context window size could be reduced wherever appropriate to avoid contributions from absorbers which impeded separation. Determination of an appropriate spectral window was not straightforward and had to use a combination of Differential Optical Absorption Spectroscopy DOAS, scaled differences and least squares techniques. It yielded the curve of temporal behaviour of IO with background absorptions from I_2 and two absorptions originating from two yet unidentified higher iodine oxides removed. The latter were temporarily labelled "X" and "Z". Further to the UV and starting from 340 nm with a steep increase a third absorption (labelled "Y") showed up in a number of data sets, which could be separated from the other absorptions. Within the used spectral intervals and with this set of curves the separation in the majority of cases produced source spectra in combination with which the observational data could be explained with residuals distributed normally. This proves that no relevant absorptions were missed in the analysis. In a number of cases this analysis was impeded by the build up of deposit during the photolysis experiments. This usually gradually blocked the UV light with increasing number of flashes and also led to structures in the time resolved data, which did not originate from gas phase chemistry but most likely from photolysis of deposit on mirrors and vessel windows.

Between 480 nm and 600 nm a similar analysis produced the separated curves of temporal behaviour of I_2, OIO and of vibrationally excited IO. Above 480 nm no bands of the IO(ν'←1) progression are contained so that separation yielded temporal behaviour of IO(ν'←2) and higher ν". Opposed to that separation between 425 nm and 480 nm produced curves of temporal behaviour for ground state IO, sometimes an anomalous IO(2←0) (see below for a detailed discussion on this) and IO(ν'←1). Comparison of this and the curve obtained for IO(ν'←2) and higher ν" showed that IO in differently excited states displays a different behaviour in time reflecting different quenching and possibly different rate coefficients in reaction with other molecules.

With respect to conservation of iodine a full set of curves of temporal behaviour consisted of:

1. An absolutely scaled curve of free ground state iodine atoms I($^2P_{3/2}$) recorded in a simultaneous resonance absorption measurement. Empirical calibration was applied obtained from photolysis experiments with I_2 in bath gas without O_3.
2. An absolutely scaled curve of temporal behaviour of I_2 molecules in the photolysed mixture of I_2 and O_3. This was obtained from the above separation.
3. Curves of temporal behaviour of ground state IO, IO(ν'←1), IO(ν'←ν") with ν">1, OIO and the yet unidentified absorptions of "X", "Y", and "Z".

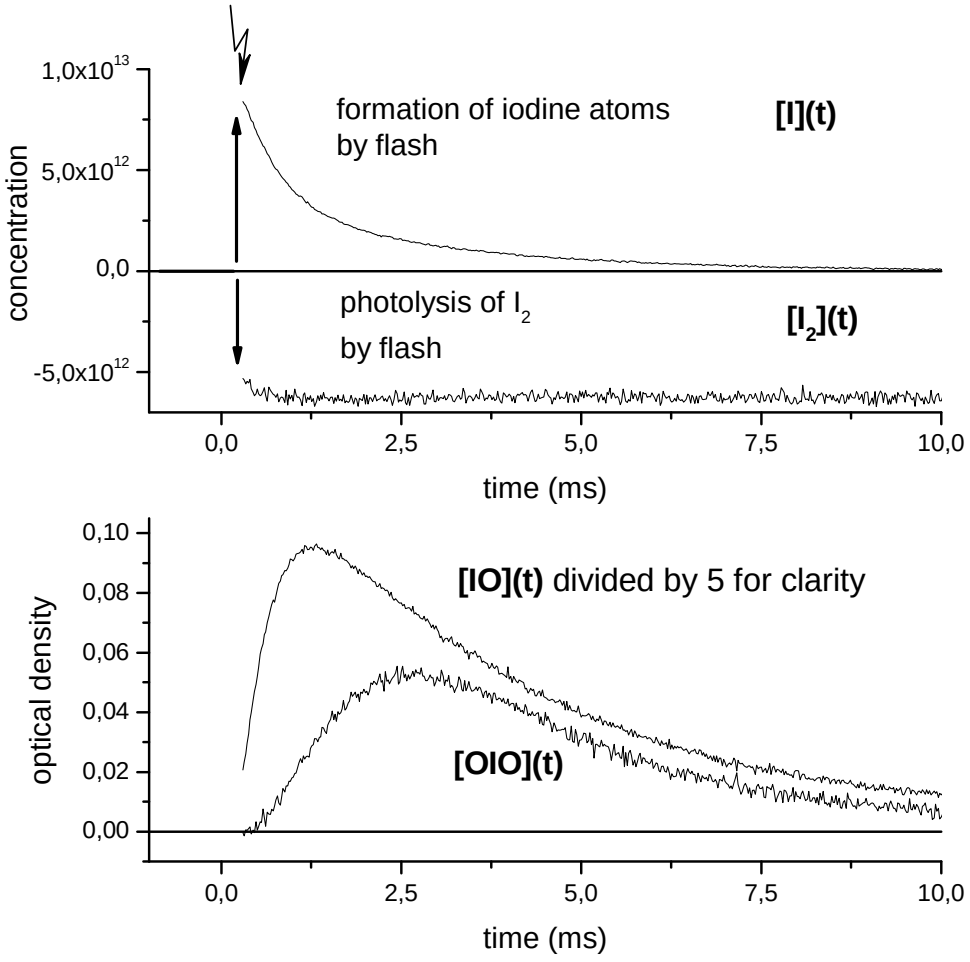

Figure 7.1a Top diagram: The temporal behaviour of free iodine atoms results directly from the simultaneous resonance absorption measurement. It shows the initial formation of iodine atoms by the flash at t=0 and the subsequent consumption. Iodine molecules I_2 are consumed by photolysis and afterwards remain more or less at the same level. Bottom diagram: Formation and consumption of IO and OIO. The curve of IO is downscaled by a factor of 5 for clarity of presentation.

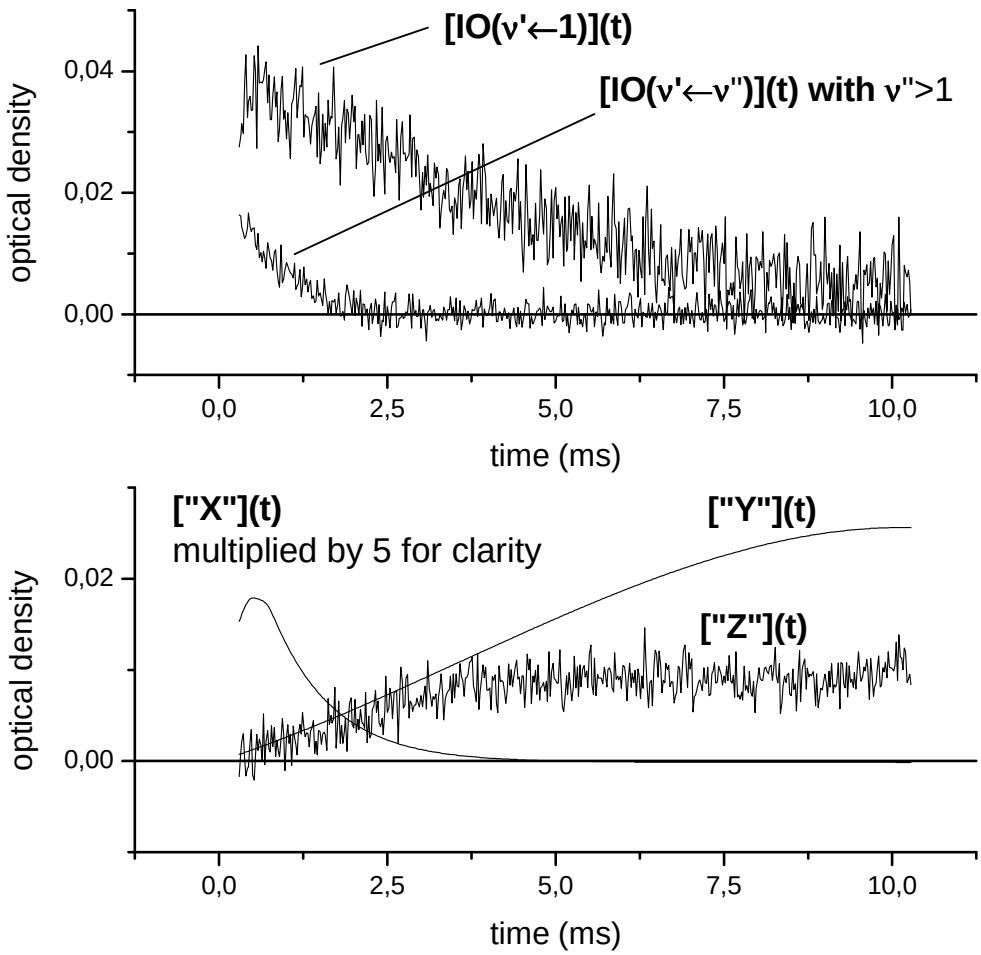

Figure 7.1b Top diagram: Vibrationally excited IO shows clearly different behaviour in the different levels of excitation. The poorer quality of the ν"=1 curve reflects the problems of separation in the region between 420nm and 480nm. Bottom diagram: The curves for "X" and "Y" have been replaced by fitted analytical curves, as their data quality was insufficient for use in the subsequent extraction of spectra. "Z" could be separated from IO without problems. The poorer signal to noise ratio results from the significantly lower signal of "Z", which is only 1/50 of that of IO.

7.1.3 Reliability of an obtained solution and degree of separation

The source spectra are molecule specific and are therefore invariants in the separation. In contrast to that the properties of the individual gas mixtures are solely contained in the curves of temporal behaviour. In this sense the spectra form the link between different data sets. Therefore the quality and the degree of separation can be estimated by comparing the source spectra obtained from the different separations. Deviations between the extracted source spectra indicate incomplete separation. The reproducibility of the main absorbers IO (ground state) and OIO was checked and resulted in a standard deviation of the separated source

spectra of no more than 3% [Gómez-Martín et al. 2004]. This degree of reproducibility in return gives a measure for the degree of separation of the curves of temporal behaviour from other absorbers. For I_2 such a comparison is impeded by non-linear behaviour of apparent I_2 absorption. This is caused by the fact that the rotational lines out of which the I_2 spectrum consists in the visible to NIR range above 500nm are not resolved under the spectroscopic conditions of the experiment [Spietz et al. 2004].

For absorber "Z" the degree of separation is the same as for IO as it was determined in the same separation. For "X" and "Y" it is less, as these were present only under non-optimal spectroscopic conditions (build up of deposit in the same range as "Y") or – in the case of "X" - only very short lived between the photolysis flash and the fast initial formation of ground state IO.

For IO($\nu' \leftarrow \nu''$) with $\nu''>1$ an uncertainty of 10 to 15% can be assumed, as this is the amount of error introduced locally into the superimposed OIO spectrum separated in the same approach. The same is assumed for IO($\nu' \leftarrow 1$).

A further criterion for estimating the quality of the separation is the distribution of the residuals. Systematic features in the residuals indicate insufficient separation. Residuals distributed normally indicate a good quality of the fit.

7.2 Extraction of Full Range Separated Source Spectra

7.2.1 Multiple multivariate regression

In a second step full spectra across the full spectral range can then be obtained by fitting the time resolved data in a multiple multivariate regression against the de-centred curves of temporal behaviour. This approach is based on the fact that time resolved and spectrally multi channel observations of absorption can be interpreted as an expression containing the curves of temporal behaviour $c_j(t)$ and the cross section spectra $\sigma_j(\lambda)$ of absorbers j=1 to n:

$$I(t,\lambda) = I_0(\lambda) \cdot \exp(-L \cdot \sum_{j=1}^{n} c_j(t) \cdot \sigma_j(\lambda)) \qquad \textbf{(1)}$$

where the Beer-Lambert law is used. Rearrangement of this yields:

$$A(t,\lambda) := \ln\left(\frac{I_0(\lambda)}{I(t,\lambda)}\right) = L \cdot \sum_{j=1}^{n} c_j(t) \cdot \sigma_j(\lambda) \qquad \textbf{(2)}$$

In this expression the optical density $A(t,\lambda)$ represents the observational data of optical density as a function of both wavelength and time. The overlapping contributions of individual absorbers are contained in the products of $c_j(t)\cdot\sigma_j(\lambda)$. Without loss of generality it can be assumed, that the data is normalised to unit optical pathlength by dividing the observed optical density by L. Therefore in the following the factor L will be regarded as L=1 and be dropped. In terms of multivariate linear regression the content of equation **(2)** can be expressed in the form of a generative linear model:

$$\mathbf{A} = \sum_{j=1}^{n} \mathbf{c}_j \cdot \boldsymbol{\sigma}_j^T = \mathbf{C} \cdot \mathbf{X} \qquad \textbf{(3)}$$

In this notation $\mathbf{c}_j$ is a column vector containing the temporal behaviour of absorber j with one entry per point in time. $\boldsymbol{\sigma}_j$ is a column vector containing the absorption cross section spectrum of absorber j with one entry per point in wavelength. Matrix **C** – frequently being referred to as the mixing matrix of the system - contains all $\mathbf{c}_j$ as columns while the unknown spectra $\boldsymbol{\sigma}_j$ are contained as rows in matrix **X**. By convention upper case and bold face letters designate matrices and lower case bold face letters designate vectors. Vectors are assumed to be column vectors. Row vectors are obtained by transposition.

The extraction of spectra is equivalent to estimating a set of unknown spectra contained in **X** given the observational data matrix **A** and the mixing matrix **C**. The scaling of the temporal behaviours contained in **C** is arbitrary as any multiplicative factor k possibly contained in any of the $\mathbf{c}_j$ will be directly and automatically compensated by a corresponding inverse factor 1/k in the corresponding estimated spectrum.

Whether a solution to this problem exists or not and how accurate the obtained estimate **X** will be, depends critically on the properties of the mixing matrix **C**. A necessary prerequisite is that the columns of **C** are altogether linearly independent. In terms of numerics: The clearer the linear independence, the smaller the uncertainty in the estimated spectra. But in reverse this also implies that, if two or more absorbers contained in the observational data **A** have similar temporal behaviour or in linear combination make up a curve similar to another absorber, the solution of the above model is limited if not impossible. Such dependences between columns of the mixing matrix are referred to as collinearities.

If collinearities exist in **C**, this will cause at least one of the eigenvalues of the normal matrix $\mathbf{N}=\mathbf{C}^{T}\cdot\mathbf{C}$ to tend to zero. The condition number of the normal matrix **N** - defined as the ratio of the largest to the smallest eigenvalue – will become considerably large. From a numerical point of view the inverse of the normal matrix will be poorly determined. The problem is said to be "ill-conditioned". According to Dahlquist et al. [1974] the errors in the estimated unknowns, which originate from errors in the observational data as well as in the data constituting the mixing matrix **C** (in the present case the curves of temporal behaviour of individual absorbers) are amplified by the condition number of the normal matrix. Clearly in the case of a systematic linear dependence between any set of columns $\mathbf{c}_j$ the condition number will become infinite and the inverse will not exist for the given normal matrix **N**. In case the inverse of **N** exists, the square root of its diagonal elements multiplied by the error of the coefficients of **C** directly equals the standard error of the estimated unknowns. It has to be pointed out that this simplified statement for multiple multivariate regression is only true, if the errors in **C** are constant or, in the lack of a better estimate, are assumed to be constant.

Coming back to the application, the problem of collinearities can to a certain degree be overcome by appropriate selection of sub sets of data, i.e. of appropriate spectral windows. The sub set of data should be selected such that absorptions of one or more absorbers contributing to the collinearities are not contained in the window, i.e. the absorption spectra of these absorbers should be zero within the spectral window. Practically speaking this allows to remove the corresponding columns $\mathbf{c}_j$ of such absorbers from the mixing matrix. The number of unknown spectra within the window is likewise reduced. As a clear drawback this directly reduces the range of the obtained spectra. For the excluded sections another extraction needs to be performed, possibly compromising on quality of the extraction.

7.2.2 Reliability of an obtained solution

In estimating the reliability of an obtained solution, a number of practical criteria are helpful. In first place the aforementioned standard error of the estimated unknowns is a good guideline for estimating the extent of possible collinearities. With respect to the shape of the estimated solutions, the non-negativity condition for individual absorption spectra needs to be checked. As long as emission can be excluded in the chemical system under study, all absorption spectra must be purely positive. If by subtraction of pre-flash absorption of pre-cursors the observational data is centred to pre-flash conditions, also negative absorptions can occur as a result of pre-cursor consumption (e.g. I_2 in **Fig. 7.4**, top graph). But in that case the pre-cursor's absorption spectra must be purely negative. Spectra with mixed positive and negative sections are impossible. Solutions to **(3)** with systematically mixed positive and negative sections in any of the estimated spectra indicate systematic problems in the whole separation as such. Likewise systematic structures in the remaining residuals indicate similar problems while residuals distributed normally are a necessary indicator of a good separation. Similar to the case of separation of curves of temporal behaviour described above, the quality of separation is further verified by comparing spectra obtained from different data sets recorded under significantly different conditions.

7.2.3 Error estimate for obtained spectra

The uncertainty stated for the extracted spectra is based on the estimated error of observations. This was obtained from the absorption measurements recorded during the pre-flash time interval. During that time the absorbance does not change, as no reactions occur. Averaging in time and subtracting the averaged spectrum from all spectra recorded before the flash creates an array of measurements in wavelength versus time, which in an artificial way is free of absorptions. The standard deviation determined in this data array was used as a realistic estimate of the observational error.

This standard deviation was then introduced as the estimated observational error in the extraction of time curves, which used the only for this purpose intermediately determined partial spectra. The time curves were extracted by multiple multivariate linear regression. In this regression two variants of errors were calculated. Firstly the error estimate of the columns of the mixing matrix was used to vary the entries into the mixing matrix into both directions by addition and subtraction of this error. Then the regression was solved for each case. The

effect on the solutions obtained for the different variations was used as an estimate for the error propagated into the estimated unknowns. Secondly an error estimate for the unknowns was determined without an a-priori estimate of the error assuming constant unit weight for all coefficients of the mixing matrix. This error estimate is therefore a purely statistical error estimate based on the condition of the normal matrix. Whichever was larger was used as the conservative error estimate for the resulting unknowns.

All data sets listed in **Tab. 6.1** were analysed in this way, producing for each a set of curves of temporal behaviour of absorbers. The same multiple multivariate linear regression was then used to extract full range spectra or spectra in extended spectral windows. The regression followed the same scheme as above, but now based on the determined time curves and their error estimate. Again the final error was estimated conservatively by choosing the larger of both errors. In the averaging of spectra obtained from different data sets the estimated error was used as a weight and the error of the result was determined accordingly.

7.3 RESULTING FULL RANGE SPECTRA

In the visible and NIR 53 data sets of time resolved flash photolysis recordings were analysed covering two different spectral ranges of 280nm to 600nm and 340nm to 660nm. For the observed unknown absorber, which covers the O_3 absorption, two further data sets were examined covering 210nm to 410nm.

7.3.1 Ground state IO(ν'←0)

Superimposed other absorbers and extraction procedure

From the studies of Durie and Ramsay [1958] and Durie et al. [1960] the position of the IO(0←0) transition is known to be at 465.5nm marking the end of the ground state IO absorption spectrum towards the red side. The observations of Himmelmann et al. [1996] showed that in that region the absorptions of OIO already overlap with those of IO. Furthermore in our studies we observed significant absorptions in the same region clearly arising from vibrationally excited IO(ν'←ν") with ν">0. Depending on the mixtures and on pressure the partitioning between ground state and excited state IO changes significantly. Also the temporal behaviours of concentration of both depend on these conditions and were in all

cases clearly different between the two. This fact makes it necessary to treat ground state and vibrationally excited IO as two individual species rather than a compounded averaged IO spectrum. In the work of Cox and Coker [1982], Stickel et al. [1988], Turnipseed et al. [1995], Himmelmann et al. [1996], Harwood et al. [1997], Ingham et al. [2000] as well as in Bloss et al. [2001] some bands of excited IO are visible in the recorded IO absorptions (compare also **Tab. 10.3**). Relative to the maximum ground state band the excited species reached amplitudes ranging from a few percent up to as much as 15%. If the absolute absorption cross sections of ground state and excited state IO were the same, the content in vibrationally excited IO would directly define a systematic error of the same magnitude in the determination of absolute IO cross section and kinetics. In **Fig 3.1** the up to now published spectra of IO – as far as they were available - are compared. They show significant systematic disagreement and fail to determine the background and the ends of the spectrum. For comparison the spectrum determined in this work is also shown. **Fig. 7.2** shows the ratio of the previously published spectra relative to the present result. The deviations are significant.

As different behaviour in time is the key to separation, it was promising to try a separation of ground state and vibrationally excited IO even though the similarity in shape of the temporal profiles – both displaying similar rise and decay times – is a limiting factor with respect to collinearity. The temporal behaviour of overlapping OIO always showed a slower formation than the IO species. Contribution of I_2 present in the same region is unproblematic as the temporal behaviour of I_2 is totally different from that of the transient absorptions of the iodine oxides.

If collinearities caused problems, a limitation of the spectral window to 467nm on the red side always was a suitable measure, just including the last band of ground state IO(0←0). Collinearities caused by vibrationally excited IO could also be reduced and even avoided by analysing only data sets obtained at high pressures, in which excited IO was significantly reduced by collisional quenching. Towards the UV the IO absorption ends in the vicinity of 320 to 330nm. Varying the UV side of the extraction interval helped to verify this. Starting from 460nm towards the UV the smooth absorption of "Z" becomes more and more important, which slowly rises in time indicating that it is caused by a product of the IO and OIO consumption mechanism. Its temporal behaviour could be obtained directly from the range around 320nm, where no other absorptions were detected in our analysis. In some cases its contribution did not become important above 420nm due to the flat tail of its spectrum.

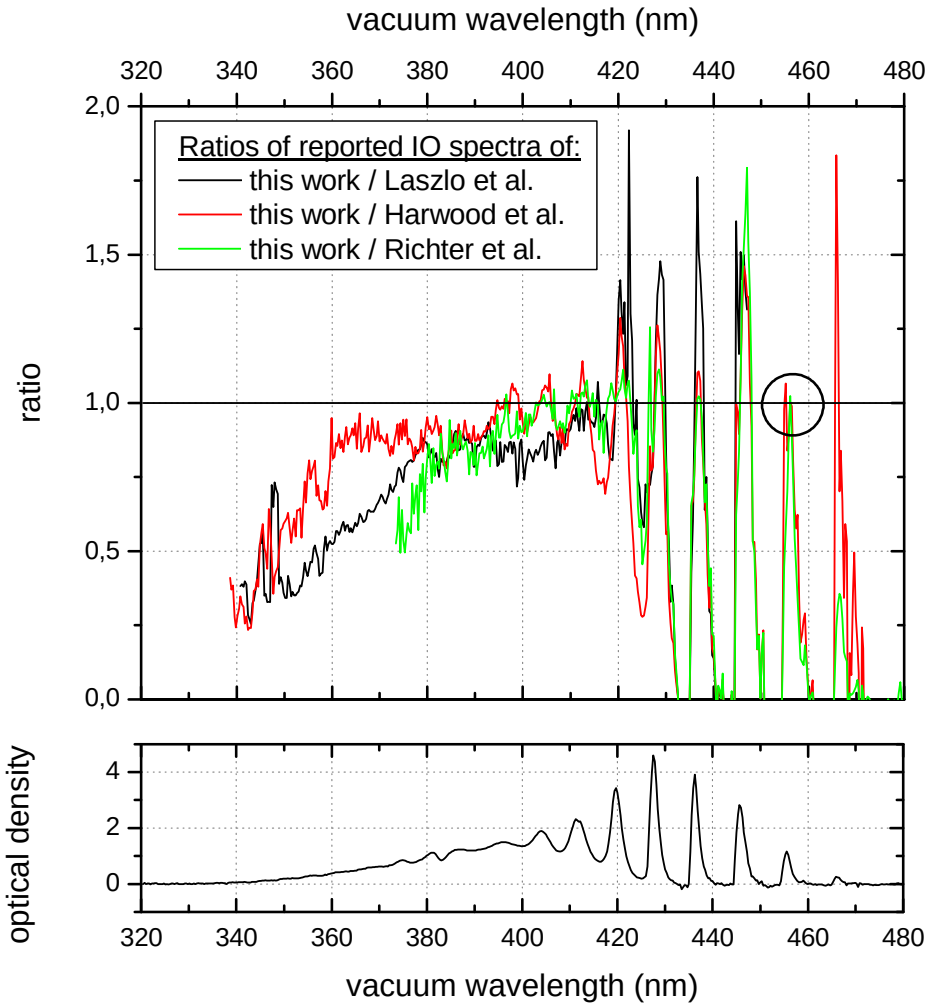

Figure 7.2 To quantify the deviations between the previously published spectra more clearly, the ratio between the spectrum determined in this work and each previously published spectrum is considered. Prior to that all spectra were scaled upon each other in the top of the IO(0←1) band (circle). The deviations are large ranging from about 20% in the continuum region to even larger deviations in the region of the peaks. A large part of these deviations also originates from contradictions in the wavelength calibration of up to 0.5nm.

In **Fig. 7.3** the spectrum obtained for ground state IO is plotted. It is free of negative absorptions proving that no systematic problems in the extraction exist. The UV-end of it is clearly determined. Superimposed to the continuum absorption bands of small amplitude are visible, which increase in amplitude near 380nm. From thereon to the red the progression of (ν'←0) bands becomes dominant, while the continuum absorption dies of near 430 nm. From the (4←0) band to the red all troughs between bands return to zero. The (2←0) band displays an anomalous behaviour to be discussed below.

Anomalous behaviour of IO(2←0)

A further aspect to be taken into account in the extraction is the apparent behaviour of the IO(2←0) absorption band. In a large number of our measurements this band shows a significantly different temporal behaviour than all other bands of ground state IO. Also the peak height of the band appears reduced in comparison to the whole progression, deviating from a common envelope. This was roughly approximated by a gaussian for bands IO(0←0) to IO(5←0). The effect is strongest in low pressure experiments and decreases systematically with increasing pressure. Strong UV-photolysis (experiments with no filters between vessel and flash lamps) enhances the effect.

Extraction of spectra could only be achieved by further subdividing the extraction window such that in one version the (2←0) was included and in another not. This provided clear separation of the band from the other ground state bands. In **Fig. 7.3** the extraction for IO(v'←0) (top) along with the separately extracted IO(2←0) band (bottom) is shown. Traces of the IO(3←0) are extracted along with the IO(2←0). In the bottom graph the relative error for the extracted spectrum is plotted.

The temporal behaviour of the IO(2←0) deviates strongest from that of the other ground state bands before and around the time of maximum concentration. Later on the deviation dies off. Even without knowing the origin of the observed deviation, it is nevertheless possible to estimate the correct peak height of IO(2←0) relative to that of IO(4←0). This is achieved by determination of the ratio between the tail of temporal behaviour of IO(2←0) relative to that of IO(4←0). Assuming that in the tails the deviation has died off, the ratio directly yields the desired ratio between peaks. In the top graph of **Fig. 7.3** both an extraction containing IO(2←0) with reduced peak height due to incomplete separation and one with corrected peak height are plotted. After correction IO(2←0) fits well within a common envelope.

Uncertainty and reproducibility

For the spectrum of IO the obtained relative error from above 360nm was generally less than 2.5%. Within the band maxima is of the order of 1 to 2 %. Between the bands, where the absorption goes to zero, the *absolute* error is of the order of 0.5 to $2 \cdot 10^{-3}$ in units of optical density compared to 0.45 in the band maximum. It increases systematically within the range, where the most serious collinearities between the different species occur.

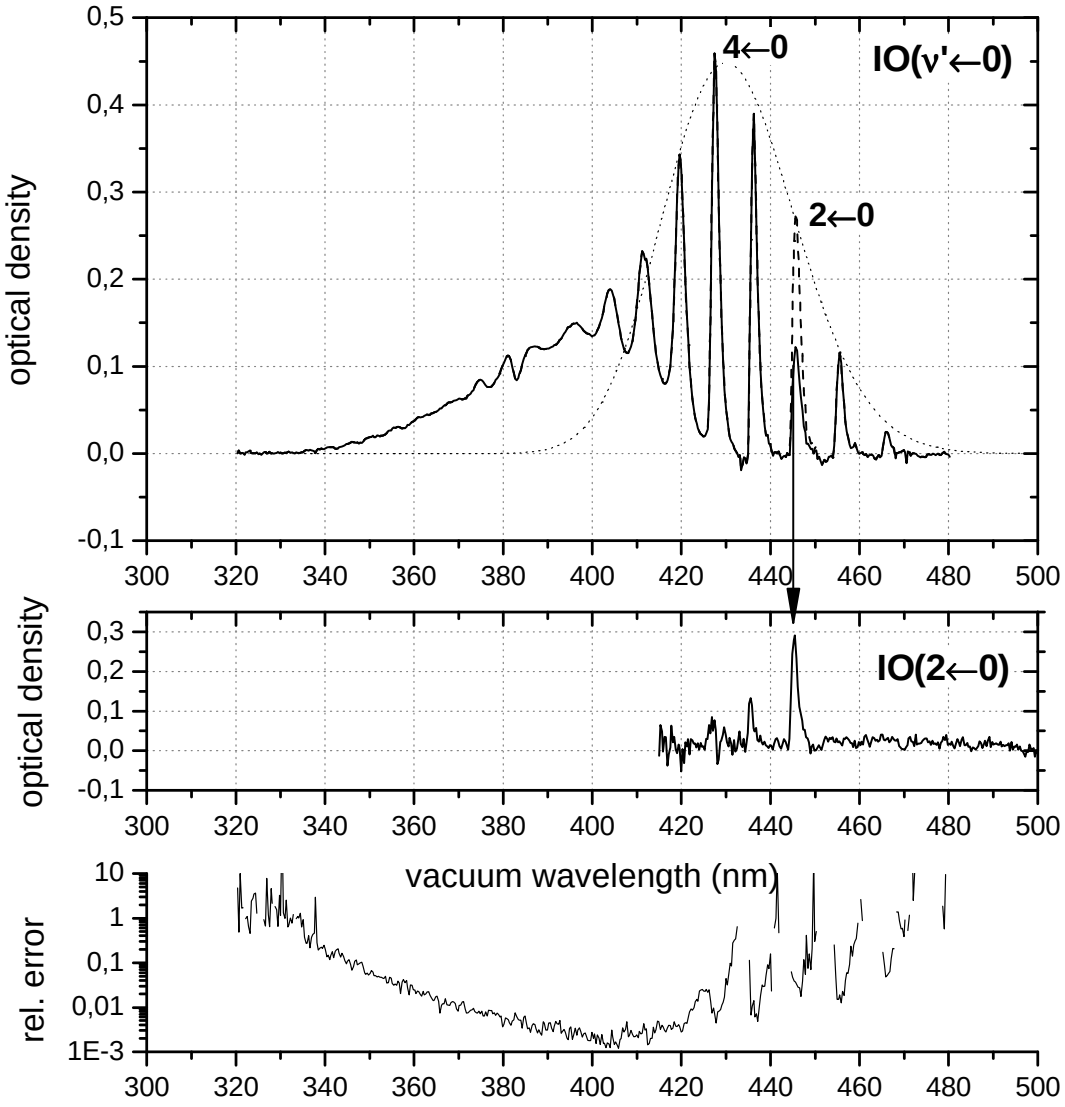

Figure 7.3 The extracted spectrum of ground state IO is plotted (top diagram) including the apparently reduced IO(2←0) band before and after correction. The UV end of the spectrum is clearly determined showing also structures in the continuum range. From the (4←0) to the red all troughs between bands return clearly to zero. The relative error of the spectrum is shown in the bottom diagram ranging around 1% for the largest part of the continuum and the band peaks. In the middle diagram the extraction for the irregularly behaving bands IO(2←0), IO(3←0) is plotted.

Also to the red of the IO(4←0) and in the neighbouring troughs the signal tends to be slightly negative due to imperfect separation from excited IO. These systematically negative sections are in the worst case no more than 4% compared to the neighbouring band.

The reproducibility of the separations and extractions of spectra from the more than 40 data sets was very high. Systematic contradictions occurred whenever the spectral window for the separation or extraction was inadequately chosen and included absorptions causing

collinearity or being unaccounted for by the chosen curves of temporal behaviour. Another reason for systematic deviations between extractions was the build up of deposit during the flash photolysis experiments. The deposit increased within the accumulations from flash to flash and also was changed by the flash itself. In such cases the spectral window had to be reduced on the UV side. Nevertheless in some extractions systematic deviations remained even though the UV tail of the spectrum returned properly to zero. Only in the comparison of different extractions the contradictions showed up and were always located on the UV flank of the IO continuum. Nevertheless all spectra were introduced into the averaging for the final spectrum, because the origin of the deviations could not unequivocally be attributed to a gross error. But as their estimated errors were generally poorer due to the lower quality of the extraction, they entered with a lower weight into the final averaging.

Wavelength calibration

The calibration of wavelength axis had been obtained by calibration to the known positions of mercury and cadmium lines from a line source. Used were only lines well separated from others under the low resolving spectroscopic conditions of the experiment. All wavelength are converted to vacuum wavelength. The accuracy of the calibration was always better than 1 pixel, which is 0.32nm per 0.26µm geometric pixel size with the 150 grooves·mm^{-1} grating. This was also verified by the wavelength offsets found between spectra of IO obtained from different data sets. The scatter in wavelength was always of the order of in the worst case 0.2nm and of 0.1nm and less normally. The calibration in the ground state bands was verified by comparison to the Cavity Ring Down (CRD) spectra reported by Newman et al. [1998]. Their (vacuum) CRD spectra were convoluted and integrated (binned) to the resolution and detector geometry of our measurements and used as a calibration standard within the interval covered by them. Deviations between our spectrum and the convoluted bands from Newman et al. ranged from -0.08 to +0.07 nm for the isolated (0←–0) to (4←–0) bands. The (5←–0) band was ignored, as it is likely to be distorted by the neighbouring IO continuum absorption. The instrument's function used in the convolution was only an approximate gaussian. Therefore the differences between the convoluted CRD spectra and our spectrum were not used for re-calibration. The differences lying clearly below 0.1 nm justify a conservative (but nevertheless sub-pixel) estimate of wavelength uncertainty of 0.2 nm.

If the effects of resolution and binning are not taken into account, the apparent positions of band maxima will differ more or less strongly depending on the difference in resolution and binning, e.g. IO(4←0) in the CRDS study by Newman et al. at 427.2nm (vac.) versus 427.5nm (vac.) from this work at 1.3nm FWHM. This is explained by the fact that lower resolution and binning always cause the peak of an asymmetric band to being eroded away from the steepest ascent. This can be verified by corresponding simulations and was also verified by the convolution and binning of the data of Newman et al.

7.3.2 Vibrationally excited IO(ν'←ν") with ν">0

Superimposed other absorbers and separation procedure

In the spectral window from 467nm to 600nm (the red end of the observational window) the contributions of vibrationally excited IO(ν'←ν"), ν">0, of OIO and of I_2 could be separated with a good quality and low errors wherever the spectrum has significant absorption. Collinearities with ground state IO were avoided, as the IO(0←0) at 465.5nm was excluded from the spectral window. By limiting the spectral window to 480 to 600nm this could be improved even more, because then IO(ν'←1) with its different behaviour was excluded. Especially the low pressure data sets containing the largest concentrations of excited IO yielded clear spectra. For the bands falling between those of ground state IO, the separation proved to be more difficult, as there the similarity of temporal behaviour of ground state IO in general, that of IO(2←0) and that of excited IO produce collinearities and imperfect extraction of individual spectra. On the other hand the temporal behaviours were sufficiently different to inhibit a reduction of free parameters. In this interval the noise in the extracted spectra is larger and negative traces of ground state IO remain. Below 440nm again the absorption of absorber "Z" needs to be taken into account. But in a number of data sets in the separations with PCA/ICA as well as in the extraction with multivariate regression a further absorption, labelled "X", proved to be significant and was in many fits extracted together with excited IO as a single spectrum with acceptable residuals. The new absorption displays a smooth continuum located in the region of the ground state IO continuum and shows a temporal behaviour similar but not completely the same as that of excited IO.

The temporal resolution of our set-up is defined on one hand by the shifting time per row of the CCD chip and on the other hand by the characteristic function in time (defined by the masking of the chip and the vertical slit width of the mask). The characteristic function has a

half width of 5 to 7 pixels in different regions of the chip. The variations are caused by mechanical imperfections of the laboratory-made masking of the chip. The difference between excited IO and the found absorption is visible only in a time interval of 10 to 12 pixels in time – roughly twice the width of the instrument's characteristic function in time – and very close to the flash. The large remainder of both curves is nearly identical. Therefore it is possible that the observed continuum belongs to excited IO. But on the other hand it can not be excluded that it originates from a further not yet identified species. This will be decided after further analysis of spectra, see below (**Chapter 8**). The full spectrum obtained by joining the three different sections is shown in the middle diagram of **Fig. 7.4**. The top diagram shows an original mixed spectrum for comparison and orientation. In the bottom graph the obtained relative uncertainty is plotted.

Uncertainty and reproducibility

The reproducibility of the spectrum was highest in the range from 480 to 600nm. The shape of the bands and zero absorption in the troughs was always reproduced. Depending on the mixture changes in relative height between groups of bands from different ν" occurred. When the window was extended down to 467nm and below, the different behaviour of IO(ν'←1) and IO(0←0) reduced the reproducibility in that traces of ground state IO appeared in the spectrum or a continuous background disturbed the spectrum. In the continuum in spite of the low signal to noise the reproducibility was good. Based on the error estimate the uncertainty of the spectrum is approximately 2 to 3% in the peaks. In the continuum range it is of the order of 5 to 10%. Between the bands the *absolute* error is of the order of 2 to $5 \cdot 10^{-4}$ in units of optical density.

Wavelength calibration

The wavelength calibration for vibrationally excited IO is the same one obtained from the line source measurements, as described for ground state IO.

Assignment of transitions

In 1958 [Durie and Ramsay 1958] recorded bands of IO in *absorption*, but in those measurements apart from the absorption transitions from ground state only the IO(2←1) was visible. Durie et al. [1960] carefully examined the *emission* spectrum of IO using a 21ft grating spectrometer in second or higher order and observed a large number of transitions from vibrationally excited IO.

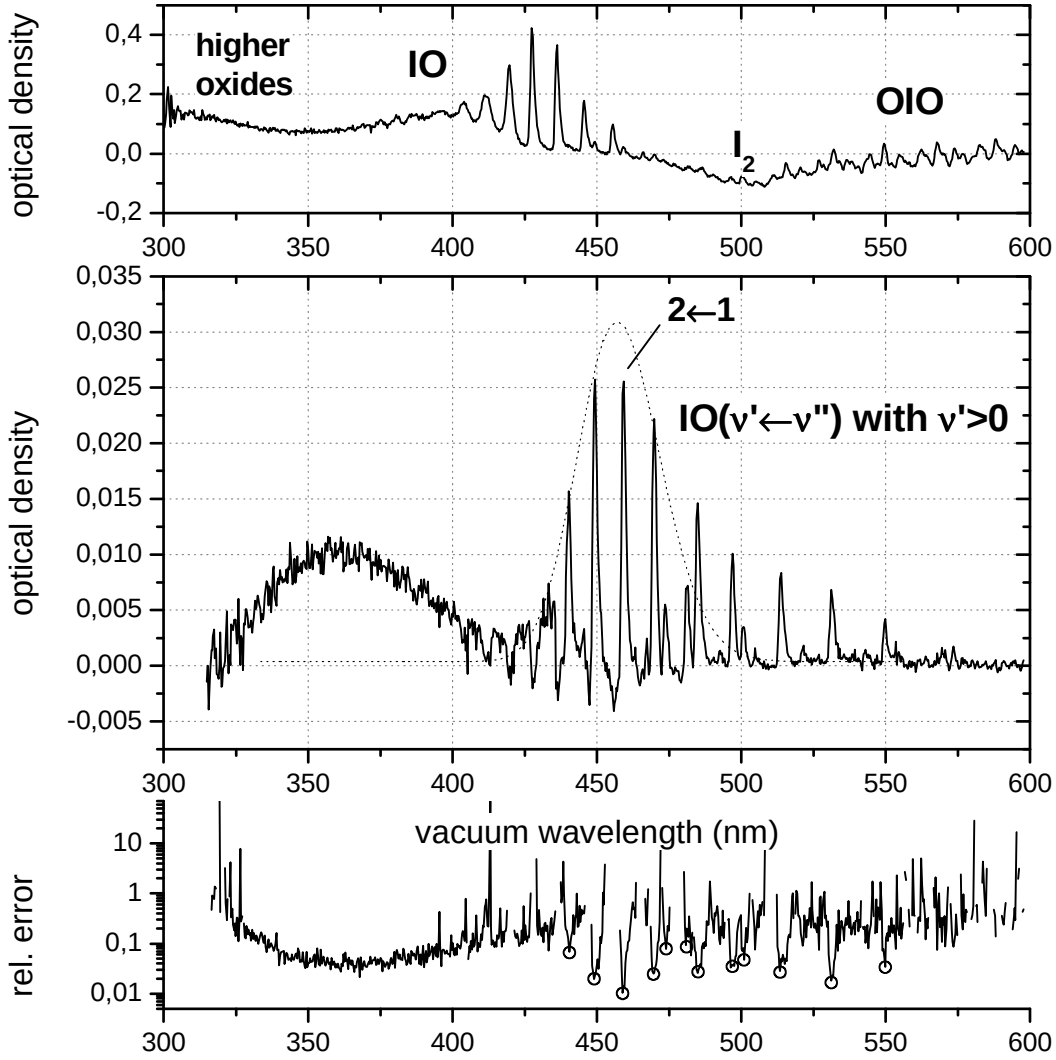

Figure 7.4 The full spectrum of vibrationally excited IO obtained by joining the three sections from the three extraction intervals is shown in the middle diagram. In an original mixture its spectrum is covered by spectra of ground state IO, higher oxides, I_2 and OIO (top diagram). The (2←1) band again shows an apparently reduced height. The relative uncertainty of the extracted spectrum in the continuum range is of the order of 5 to 10% while in the peaks it decreases to 2 to 3% (bottom diagram, open circles). Between the bands the *absolute* error is of the order of 2 to $5 \cdot 10^{-4}$ in units of optical density. The assignment of the continuous absorption to excited IO is not unequivocal as the width of its temporal behaviour is of the order of the width of the detector's characteristic function in time. It could also be caused by a further yet unidentified species.

They performed a thorough rotational and vibrational analysis, which enabled determination of the band *origins* – i.e. that transition within a vibrational band, where J'=0 and J''=0 - of both ground state and vibrationally excited IO. From the band origins they determined vibrational constants for IO, with residuals generally better than 0.005nm. Only overlapped bands were reproduced with larger residuals of 0.02 to 0.03nm.

In our low resolution measurements for the first time a large number of vibrationally excited bands are observed in absorption. In our extracted absorption spectrum 22 bands of excited IO out of 34 observed by Durie et al. [1960] in emission are present. **Fig. 7.5** shows our spectrum of transitions from vibrationally excited levels with the assignments according to Durie et al. As our measurements were aimed at broad and simultaneous spectral coverage, high resolution was not the point of our work. Therefore our spectra can not compete in resolution with their work. Given the limited resolution of 1.2nm FWHM and 0.35nm per pixel of our measurements, our band *heads* are in reasonable agreement with their accurate band *origins*.

Examination of band height of individual progressions shows that in the IO(ν'←1) similar as in the ν''=0 series again the transition leading to the $A^2\Pi_{3/2}$, ν'=2 appears to be reduced in comparison to the neighbouring bands of the same series (see **Fig. 7.4** and compare also **Fig. 3.1**). This indicates that the observed anomaly is linked to the $A^2\Pi_{3/2}$, ν'=2 state. A closer examination of temporal behaviour was impeded by collinearities and by the for our set-up too short time scale of formation and consumption of these excited species.

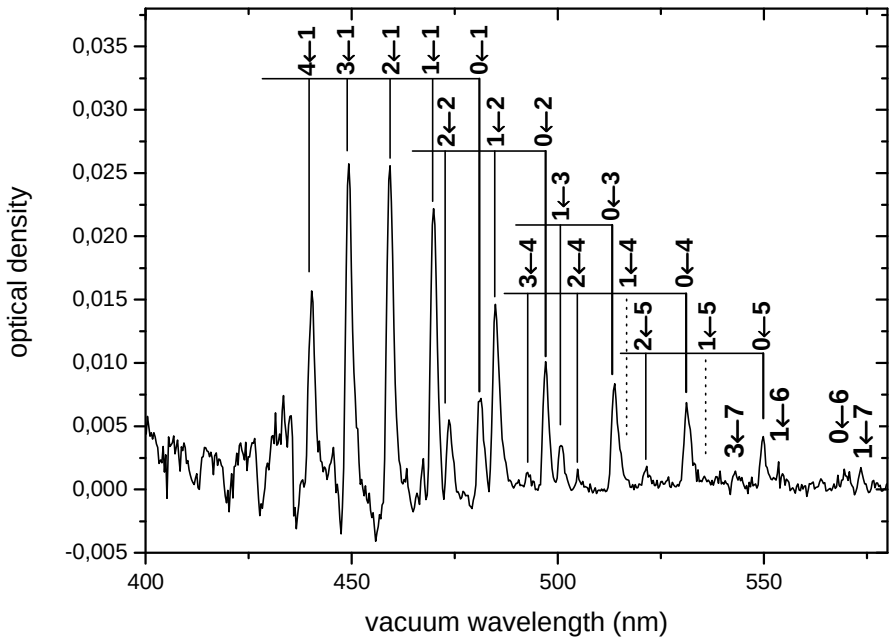

Figure 7.5 The observed bands are identified using the assignations made by the high resolution study of Durie et al. [1960], who observed the emission spectrum of IO using a 21ft spectrograph in orders 2 or higher. While the IO(ν'←ν'') for ν''=1 shows the first four transitions clearly, it is remarkable that for higher progressions dominantly the (0←ν'') occurs in the spectrum. As it will turn out later (**Chapter 8**), this directly reflects the relative magnitude of Franck-Condon factors.

The second interesting feature of the observed hot bands of IO is the strong and regular presence of the IO(0←ν") transitions. Starting with the barely visible (0←6) the bands increase steadily until the (0←2), before decreasing in the (0←1) again.

7.3.3 OIO and higher iodine oxides

In a similar way also a spectrum for OIO and spectra of higher iodine oxides were extracted from the available data. Even though purposefully obtained from the same data and the same simultaneous analysis, for formal reasons their analysis will be presented elsewhere [Goméz-Martín, PhD thesis, in preparation]. For reference, the spectra are shown in **Fig. 7.6** and **Fig. 7.7**. The UV absorption was separated from the underlying ozone absorption using DOAS in the Hartley band and multiple multivariate linear regression approach. There is evidence that the obtained spectrum is a superposition of two absorbers.

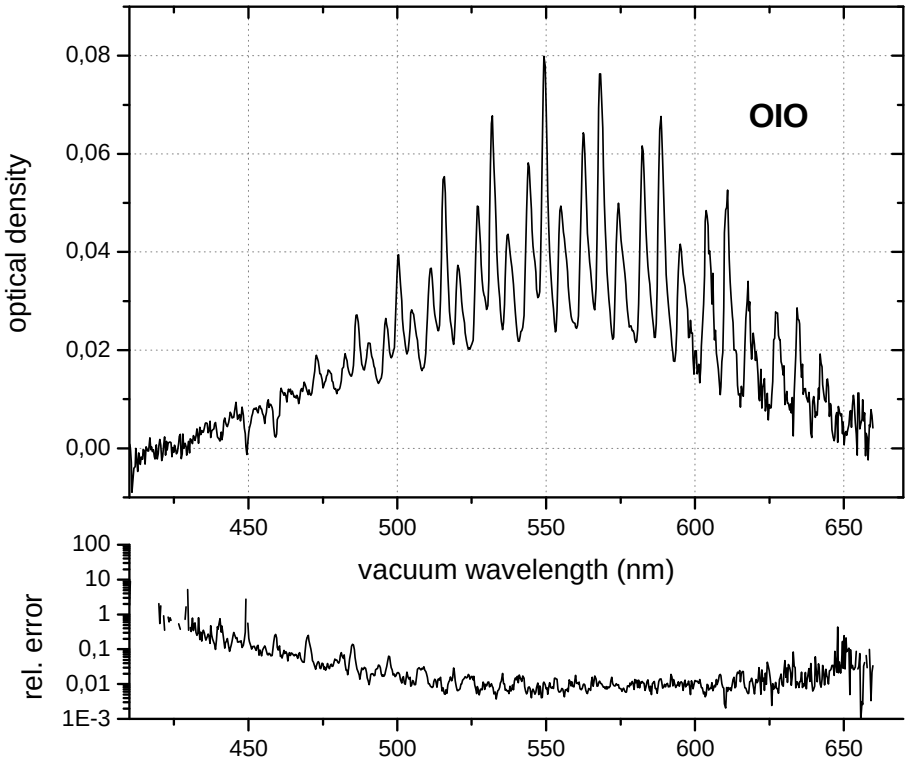

Figure 7.6 The spectrum of OIO was also extracted from different windows and then joined to form a contiguous spectrum. On both sides, the blue as well as the NIR side it shows clearly the end of the absorption and a smooth return to zero.

This is in agreement with the aforementioned extraction of absorbers "Y" and "Z" identified in the UV region of IO. The dotted lines indicate two gaussians, which were fitted to the spectrum. Their shape and position are the result of constraining the fit to two gaussian curves. As this is an oversimplifying approximation, shape and position of these gaussians have to be considered with care.

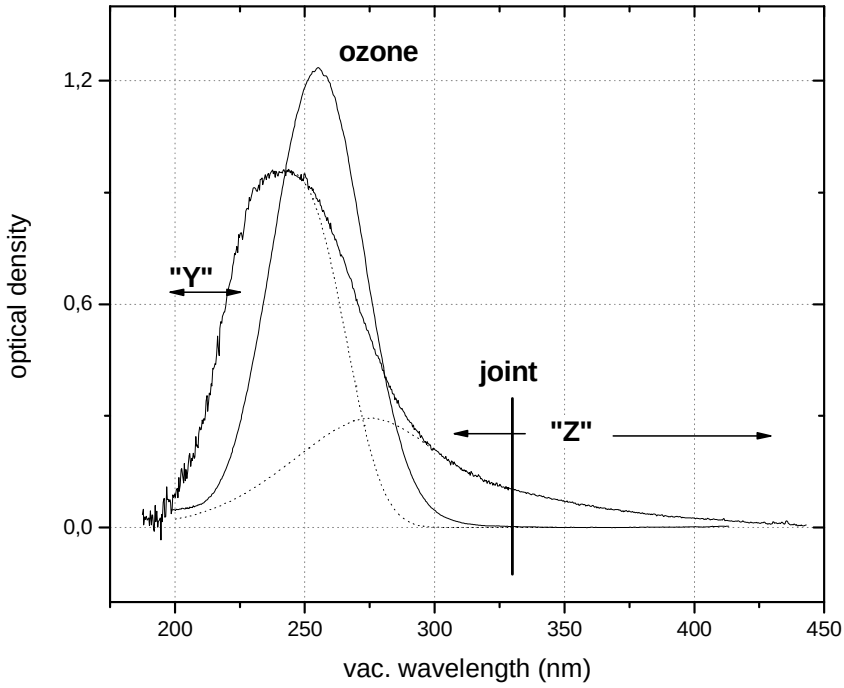

Figure 7.7 A UV absorption was separated from the ozone spectrum. There is evidence that the obtained absorption consists of absorbers "Z" and "Y", as temporal behaviour is slightly different in different regions. Due to collinearity, separation was not possible and only an approximate combined spectrum could be extracted. For illustration two gaussians were fitted under the determined spectrum.

7.4 SUMMARY AND CONCLUSIONS

Multivariate statistical analysis methods Independent Component Analysis ICA and Principal Component Analysis PCA combined with multiple multivariate regression techniques were applied to time resolved optical multi channel recordings obtained with a CCD camera. In these recordings absorbance of different species was superimposed to each other. By use of the mentioned methods it was possible to separate curves of temporal behaviour of individual absorbers from this mixed observational data. This analysis was performed for all data sets in **Tab. 6.1**. The obtained curves of temporal behaviour provide the necessary data for applying

the method of iodine conservation for determining absorption cross sections for all observed absorbers simultaneously. This will be presented below in **Chapter 10**.

In a similar way as for the curves of temporal behaviour also and for the first time the overlapped spectra of IO(ν'←0), IO(ν'←ν") with ν">0, and OIO could be separated from each other and from other underlying absorptions of other iodine oxides. This was accomplished by multiple multivariate regression techniques using the curves of temporal behaviour. The separated spectra could be shown to be free of other absorptions to better than ±3%. The relative error of spectra in the regions with non-zero absorption is of the order of 1 to 2 % for the main absorbers IO and OIO as well as for the band peaks of vibrationally excited IO. With this data now highly accurate reference spectra for these species to be used in quantitative spectroscopy and Differential Optical Absorption Spectroscopy are for the first time available. Three further absorbances labelled "X", "Y" and "Z" have been extracted from the data recorded in the 280 nm to 600 nm window. In the analysis of the UV datasets in the region from 340nm down to 210nm a spectrum could be separated from the spectrum of ozone, which is likely composed of absorbances "Y" and "Z". These are likely to being caused by I_2O_2 and I_2O_3, as they are plausible products in the course of reaction, see (R3.1a) and (R3.2). Other candidates are I_2O_4 or IO_3. The former from reaction OIO + OIO +M and the latter from $I + I_2O_3 \rightarrow I_2 + IO_3$. In any case the observed absorbers are possibly the missing link to formation of higher oxides and aerosol. But identification as well as determination of their mechanism of formation and consumption will have to be performed within a dedicated careful study of chemical kinetics. This is beyond the scope of this work. Such a study will nevertheless use the curves of temporal behaviour obtained in this work.

The origin of absorbance "X" will be studied in the following spectroscopic analysis (**Chapter 8**), as this provides a handle to decide, whether "X" is caused by vibrationally excited IO or by another unidentified molecule.

8 SPECTROSCOPIC ANALYSIS AND DISCUSSION

8.1 ABSORPTION CONTINUUM OF GROUND STATE IO(ν'←0)

The extraction of a full range spectrum for ground state IO being practically free of other absorptions, for the first time enables a clear statement about the shape and the extent of the continuum absorption. This starts around 330 nm and extends to the (4←0) band. Important are the band structures, which are superimposed to it. Among these the localised increase of amplitude near 380 nm is of special interest. Given the high quality of extraction it is promising to examine the origin of the observed continuum absorption. The presence of a continuum absorption indicates the existence of at least one repulsive potential intersecting with the upper binding electronic A $^2\Pi_i$ potential of the IO molecule. Such a repulsive potential will lead to predissociation in the bound states. The degree of predissociation of individual states is determined by the overlap of state functions of binding and repulsive potential at the given energy level and by the coupling mechanism between them. Life times in rotational states will be reduced and rotational lines within the vibrational bands be broadened. Rotational lines are Lorentz shaped, whose characteristic are strong wings. A superposition of a dense set of broadened lorentzian lines will produce a band shape, which in the wings is dominated by lorentzian behaviour. Near the band centre the intensity distribution of rotational transitions will dominate its shape. For bands broadened by predissociation it is reasonable to approximate them by a Lorentz profile.

Examination of the bands of ground state IO shows the expected behaviour (**Fig. 7.4**): From (0←0) to (4←0) the bands display an asymmetry with pronounced steep flanks towards the blue. In the troughs absorption returns to zero. But starting with (5←0), band shape steadily becomes more symmetric, width increases and height decreases and wings become more prominent. The troughs between bands (starting between ν'=4 and 5) no longer return to zero. This supports the expectation that at least part of the continuum is caused by overlap of bands, which are broadened by predissociation. At and around the (10←0) band (380 nm) the width of bands reduces significantly and height is increased again. Broadening of the vibrational bands and therefore predissociation of the corresponding upper states must be smaller than in the neighbouring states. Further towards the UV broadening increases again, with no further visible changes.

The occurrence of a region of less predissociation near (10←0) indicates that at least two repulsive potentials, which intersect with the IO(A $^2\Pi_i$) potential, must be of relevance to the observed continuum absorption. One coupling dominantly to states from ν'=5 to approximately ν'=9 and another coupling dominantly to states ν'>10. This is in agreement with findings by Newman et al., who concluded from their ab initio work on ClO and from Wigner-Witmer correlation rules that a larger number of repulsive potentials is likely for IO. With respect to the interpretation of our observation in principle also a second interpretation is possible, which involves only one repulsive potential. This had to couple more strongly to higher states near the inner turning point of vibration and to lower states near the outer turning point. Coupling to the intermediate states then would be smaller. This possibility can be discarded, because the width of the state function of the ground state with ν''=0 is too narrow to couple to the upper state near its *outer* turning point (see below and **Fig. 8.6**).

8.1.1 Simulation of observed continuum: Multi-parameter fit

To get an insight into the origin of the observed continuum and of the broadening of bands, it was examined, how the observed spectrum can be reproduced based on different assumptions. To this end two hypotheses were considered as a starting point:

Hypothesis 1: The observed continuum is caused solely by overlap of broadened vibrational bands from bound-bound transitions. Where predissociation and therefore broadening is strong, the band shape is approximated by a Lorentz profile. If necessary, asymmetric band profiles will be allowed. The latter is likely for the (5←0), (10←0) and possibly ν'=10±1.

Hypothesis 2: The observed continuum is caused by overlap of broadened vibrational bands from bound-bound transitions and two continua originating from bound-free transitions into the repulsive state. As above, asymmetric profiles will be allowed, where necessary.

Multi-parameter-fitting routines were used to test the two hypotheses. With both it was possible to reproduce the shape of the observed continuum with reasonable residuals, see **Fig. 8.1** and **8.2**. But the magnitude of individual bands relative to each other is far from satisfying. In case 1 the bands located near the maximum of the continuum absorption near

24000 cm^{-1} up to the sharp (10←0) structure are very strong. Then the strength of the modelled bands drops abruptly and stays low until the high wavenumber end of the spectrum. The blue flank of the asymmetric (10←0) band makes up the dominant part of the continuum between 26200 cm^{-1} to 30000 cm^{-1}. Its symmetry is reversed with respect to the other bands, which is unlikely in view of the rotational constants of the different bands. In the second case the gaussian continua contribute most to the observed continuum. But as a consequence the fit lets the (7←0) band drop abruptly, while allowing subsequent bands to rise again. In both cases the behaviour of bands appears to be unsystematic.

It has to be concluded that fitting the observed continuum by individual band profiles with or without additional gaussian continua is in any case overparameterised. But the problem can be constrained by considering the fact that the area under each band is proportional to the Franck-Condon factor of the corresponding transition.

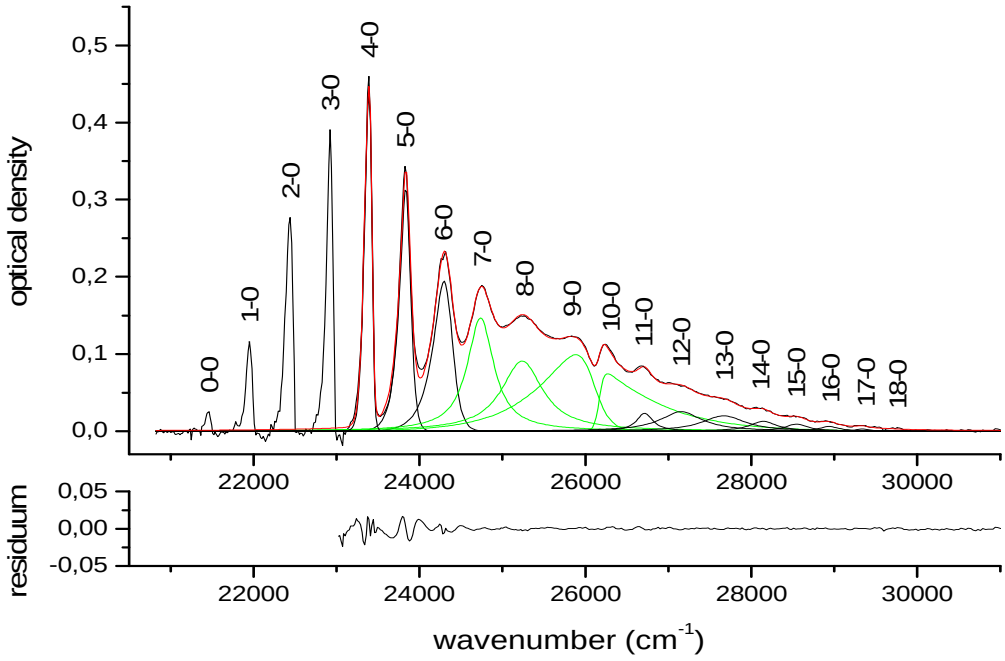

Figure 8.1 The continuum of ground state IO was reproduced by solely using Lorentz as well as asymmetric band profiles. No bound-free transitions were considered. The continuum is produced by the overlap of broadened bands. The main contributions to the continuum originate from the green bands. Clearly (9←0) and (10←0) are exaggerated by the fit.

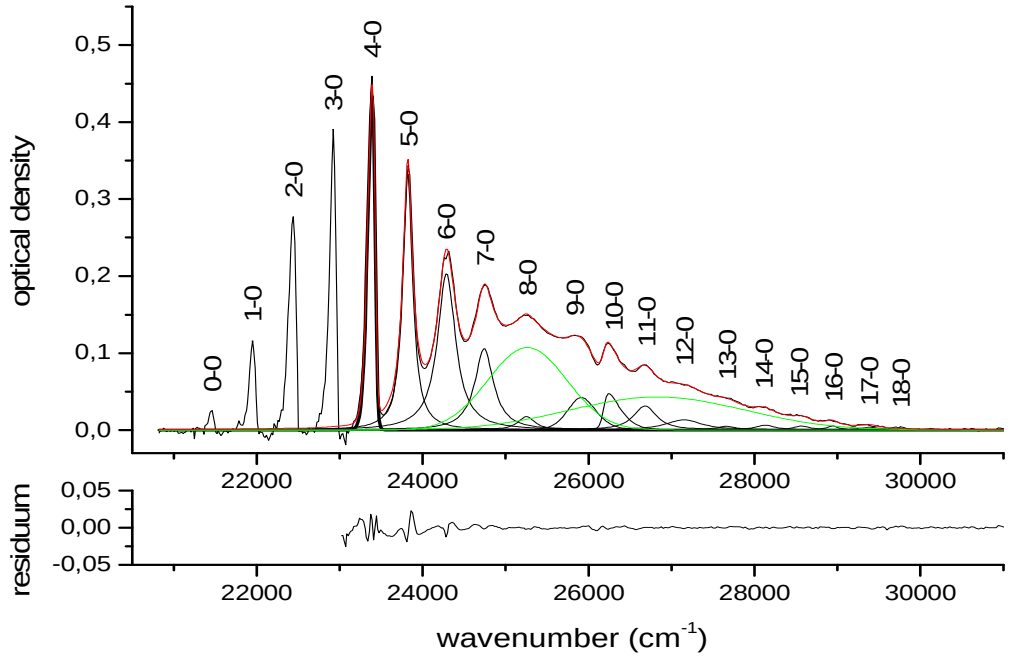

Figure 8.2 The continuum of ground state IO was reproduced by Lorentz shaped bands (some asymmetric) plus two bound-free transitions modelled by two gaussian continua (green). As in **Fig. 8.1** the continuum is reproduced very accurately. But this time the fit makes bands drop significantly at (7←0). At larger ν' they rise again.

Calculation of Franck-Condon factors to constrain multi-parameter fit

Franck-Condon factors for IO have been published by Rao et al. [1974]. They were calculated based on r-centroids and RKR potentials up to ν'=4. In the present context Franck-Condon factors also for ν'>4 are needed, where systematic behaviour as a function of ν' is of primary concern. Therefore Franck-Condon factors were calculated in Morse-approximation. As the *shape* of the Morse potential – apart from r_0, which defines position - is defined by only two parameters D_e and β [Morse 1929, Herzberg 1950], there is a choice, which empirical parameters to use in its definition:

$$V(r) = \alpha \cdot \left(1 - \exp\left[-\beta \cdot (r - r_0)\right]\right)^2 \qquad \textbf{(4)}$$

where α and β can be expressed either as a function of D_e and ω_e or as a function of ω_e and $\omega_e x_e$:

$$\alpha = D_e \quad \text{and} \quad \beta = \sqrt{\frac{2 \cdot \pi^2 \cdot c \cdot \mu}{D_e \cdot h}} \cdot \omega_e \qquad \textbf{(5a)}$$

or

$$\alpha = \frac{{\omega_e}^2}{4 \cdot \omega_e x_e} \quad \text{and} \quad \beta = \sqrt{\frac{8 \cdot \pi^2 \cdot c \cdot \mu \cdot \omega_e x_e}{h}} \qquad \textbf{(5b)}$$

Eigenvalues to the radial Schrödinger equation with Morse potential are of the form:

$$E_\nu = \omega_e \cdot \left(\nu + \frac{1}{2}\right) - \omega_e x_e \cdot \left(\nu + \frac{1}{2}\right)^2 \qquad \textbf{(6)}$$

This solution is exact in the Morse approximation. From experiment, parameters D_e, ω_e, $\omega_e x_e$, and possibly $\omega_e y_e$ are available. So in any case the empirical $\omega_e y_e$ is an approximation to experimental data, which goes beyond the term value approximation of the Morse potential. It therefore does not find its representation in the Morse potential approximation. But usually it is only small and becomes important only at considerably high levels of vibration. In the present case the value available from Durie et al. was neglected.

Definition of the Morse potential by dissociation energy D_e and ω_e **(5a)** was not used, as this would distort the potential in the region of the lower and mid vibrational levels. The agreement in the outer section – assured by D_e - would have been of no interest for the present considerations. **Fig. 8.3** illustrates the differences between empirical energy levels and those obtained by a Morse potential which is defined via D_e and ω_e. If instead, definition via ω_e and $\omega_e x_e$ with the results from Durie et al. [1960] **(5b)** is used, it is guaranteed that the term values, the turning points and the shape of the state functions for low to mid vibrational levels agree with experimental data. Only the small effect of $\omega_e y_e$ is neglected. In consequence also the determination of Franck-Condon factors is in corresponding agreement with experimental data. Following this argument, Franck-Condon factors were calculated in Morse approximation, where the Morse potential was defined via ω_e and $\omega_e x_e$ **(5b)**. For IO($\nu' \leftarrow 0$) they are plotted in **Fig. 8.4** as open circles. They show a clear systematic behaviour, which originates from the difference in internuclear equilibrium distances between the X and A states.

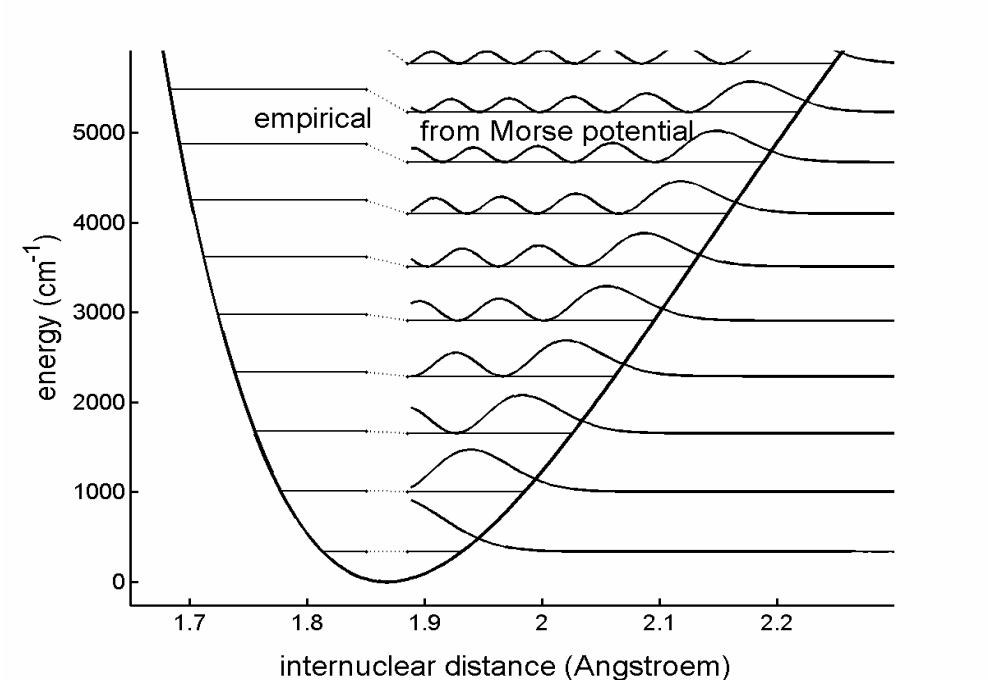

Figure 8.3 The Morse potential for IO(A $^2\Pi_i$) was calculated via eq. **(5a)** based on dissociation energy D_e and vibrational frequency ω_e. In this approximation energy levels and probability density functions were calculated (right). Energy levels are compared to those determined by ω_e and $\omega_e x_e$, which are a good approximation to the experimentally determined levels (left). Energy levels already from $\nu'>4$ are clearly underestimated by a Morse potential defined via **(5a)**. Likewise turning points of state functions and consequently also Franck-Condon factors will be systematically wrong. This can be improved by defining the Morse potential via **(5b)**.

These approximate but with respect to their systematic behaviour nevertheless correct Franck-Condon factors can now be compared to the band strengths obtained from the multi-parameter fits based on hypothesis 1 and 2, see **Fig. 8.4**. It is obvious, that neither of the two at least roughly approximates the expected systematic behaviour.

Discarding hypothesis 1 therefore implies that the observed continuum *has to contain* contributions from bound-free transitions. Discarding hypothesis 2 implies only that the strength of bound-free continua as obtained from the corresponding fit is overestimating their true strength.

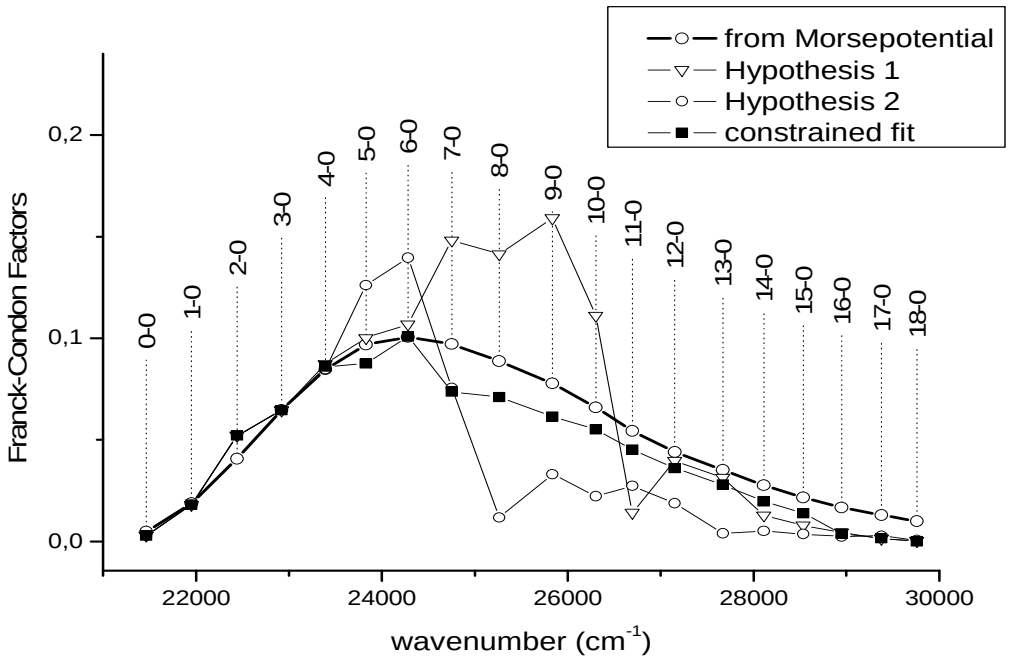

Figure 8.4 Frank-Condon factors were calculated in Morse approximation **(5b)** for transitions from IO(X $^2\Pi_i$), ν''=0 to IO(A $^2\Pi_i$), ν'=0 to 18. They are compared to the integrated band strength of bands obtained from multi-parameter fitting according to hypotheses 1 and 2. Neither of them reproduces the systematic behaviour of the calculated Franck-Condon factors. The integrated band strengths were scaled to the calculated Franck-Condon factors using their ratio in the (3←0) transition. This band is outside the continuum area. Band strengths obtained from a constrained fit are also shown. They fall systematically low compared to the calculated values but follow the expected systematic behaviour much closer.

Results from constrained multi-parameter fit: Evidence for two bound-free transitions

To estimate the strength of the continua of the bound-free transitions, the band strength of bound-bound transitions (ν'←0) with ν'=0 to 18 was constrained to the systematic behaviour of the calculated Franck-Condon factors. The result is shown in **Fig. 8.5**. The structure near the (10←0) transition is somewhat more poorly reproduced, because in this fit only Lorentz profiles were allowed within the continuum. This was required by the limited flexibility of the constraints procedure of the used fitting routine. Nevertheless the observed continuum as a whole is reproduced accurately with only small residuals.

The properties of the deduced bound-free transition continua are summarised in **Tab. 8.1**. They differ significantly in strength, i.e. area under the curve. Band strength was scaled relative to the calculated Franck-Condon factors for the bound-bound transitions. As they originate from the IO($X^2\Pi_i$) at ν''=0, their origin in terms of internuclear distance is the equilibrium distance of the ground state. This is listed in **Tab. 8.1** as well [Durie et al. 1960].

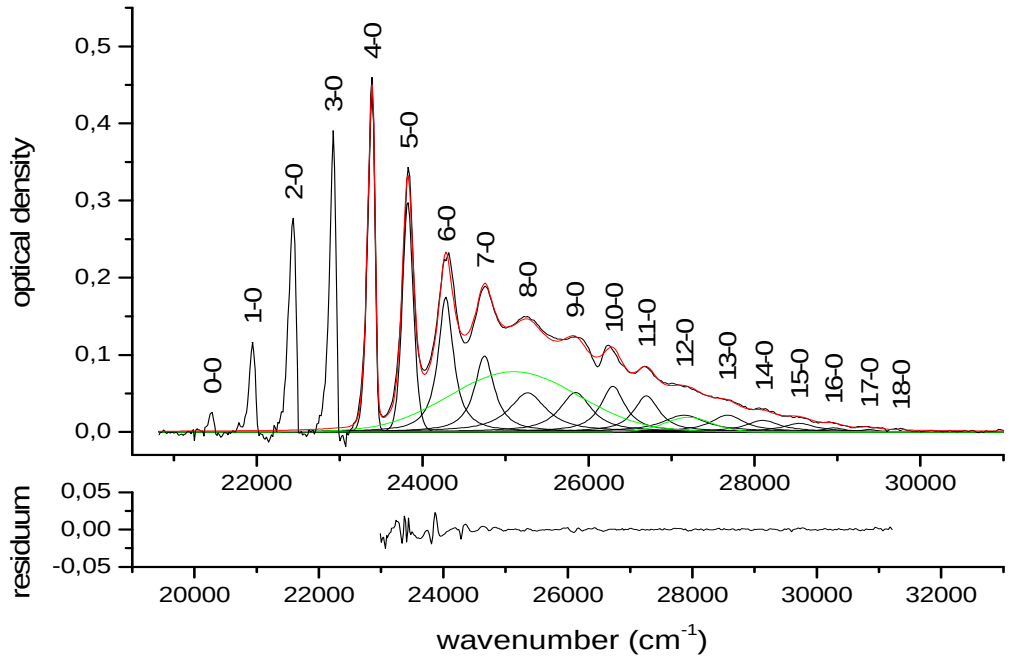

Figure 8.5 The continuum of ground state IO was reproduced by Lorentz shaped bands, whose band strength was constrained to the systematic behaviour of the calculated Franck-Condon factors, see **Fig. 8.4**. In addition, two gaussian continua (green) representing two hypothetical bound-free transitions had to be included to reproduce the observed continuum.

	area [cm^{-1}]	**centre [cm^{-1}]**	**halfwidth [cm^{-1}]**	**origin: r_e ($X^2\Pi_i$) [Å]**
bound-free 1	0.258 ± 0.008	25100.6 ± 18	1543.8 ± 37	ν"=0 1.8676
bound-free 2	0.023 ± 0.002	27201.6 ± 27	570.4 ± 55	ν"=0 1.8676

Table 8.1 Two bound-free transitions are inferred from the constrained fit to the observed absorption continuum of ground state IO. A strong one with its maximum located near the (8←0) transition and a weaker one nearly coinciding with (12←0). Stated uncertainties are those, which resulted from the constrained fit. They indicate the stability of the fit. Realistic estimates of uncertainty are most likely larger. Band strength estimates (area) obtained from the area under the gaussians are scaled relative to the calculated Franck-Condon factors of the bound-bound transitions.

8.1.2 Deducing repulsive states from observed continua

By the internuclear equilibrium distance at ν"=0 and the centre of a spectroscopically found bound-free continuum one point of the corresponding repulsive potential is determined. With the reflection method according to Condon [Herzberg 1950, p. 392, Sulzer and Wieland 1951] it is furthermore possible to construct a tangent to the repulsive potential in that point. By neglecting curvature of the repulsive potential it is possible to correlate the symmetric bell

shaped ground state ν''=0 state function to the observed bell shaped continuum. This makes use of the fact that the state function of the repulsive potential can be regarded as approximately constant with energy. Note that in comparing the wavenumber axis of the spectrum to that of term energies the energy of the lower level (ν''=0) needs to be taken into account. Applying the reflection method to the half width points of both found continua, two points of the tangent were determined. In **Fig. 8.6** the potential curves of IO($X^2\Pi_i$) and IO($A^2\Pi_i$) are plotted (Morse approximation **(5a)**, therefore D_e is correct) along with their energy levels according to Morse approximation **(5b).** Therefore term energies are correct. The tangents obtained by the reflection method are plotted, as well as levels with ν'=0, ν'=2 and ν'=3. The latter are indicated, because the corresponding bands (0←–0), (2←–0) and (3←–0) according to Newman et al. [1998] show the least predissociation. Without considering any details of coupling mechanism this indicates, that the repulsive potential either does not intersect with these levels at all or that the overlap integral of state functions is low.

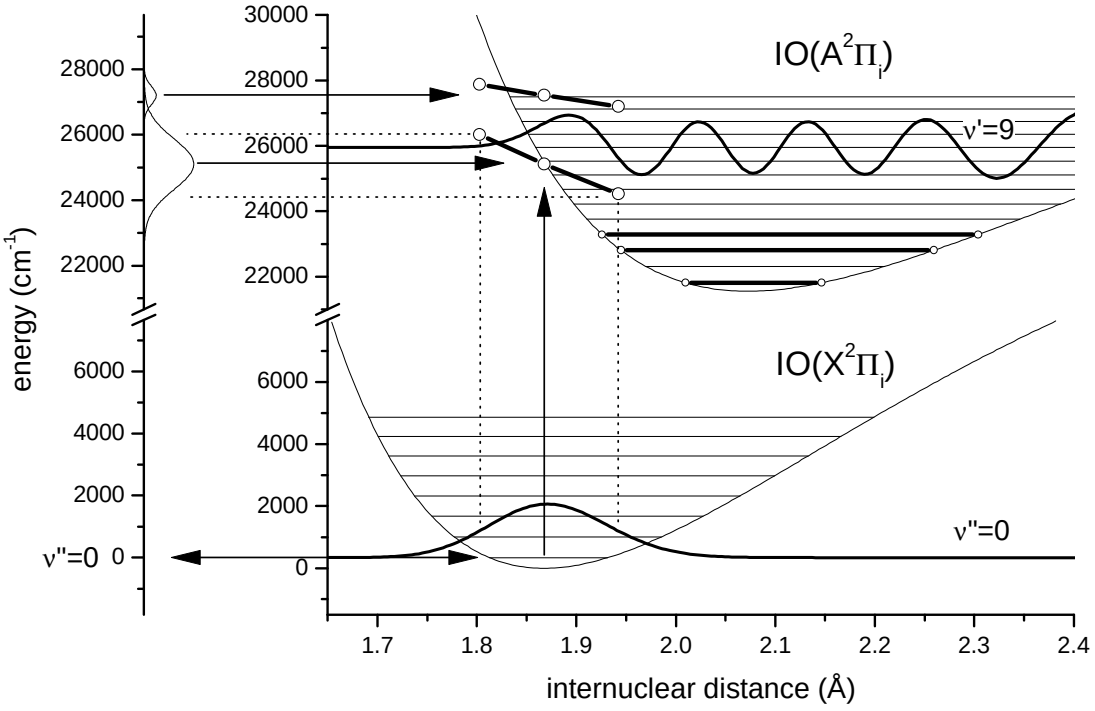

Figure 8.6 By use of the reflection method two tangents to the hypothesised repulsive potentials were constructed (solid black lines, open circles). Their origin from the observed continua (left graph) and the state function at ν''=0 is indicated. Please note the break of the vertical axis from 8000 to 21000 cm^{-1}. Levels ν'=0, 2 and 3 show the least predissociation according to Newman et al. (solid black line, open circles). Therefore the repulsive potentials should either not intersect with them at all or only in a way that the overlap integral nearly cancels.

Considering the inclination of tangents and the energy level of possible dissociation products $I(^2P_{3/2})+O(^3P)$ and $I(^2P_{1/2})+O(^3P)$ enables a plausible association of both, compare **Fig. 8.7**. There an exponential decay was fitted to the tangents and the corresponding atomic asymptote. Intersection of the lower repulsive potential in the middle of levels ν'=2 and ν'=3 seems to fit to their observed low predissociation. Newman et al. proposed that the low predissociation of ν'=2 may be a fortuitous near cancellation of the overlap of bound and repulsive state wavefunctions at that energy. Level ν'=1 intersects near a turning point, where overlap of state functions will be large leading to large predissociation, as observed by Newman et al. Levels ν'>3 intersect closer to the inner turning points, where the state function has increased values and overlap is likely to rise again. ν'=0 does not intersect at all with the hypothetical repulsive potential, why overlap of state functions has to be small. This again is in agreement with the observations of Newman et al., who report, that the (0←0) band shows small predissociation.

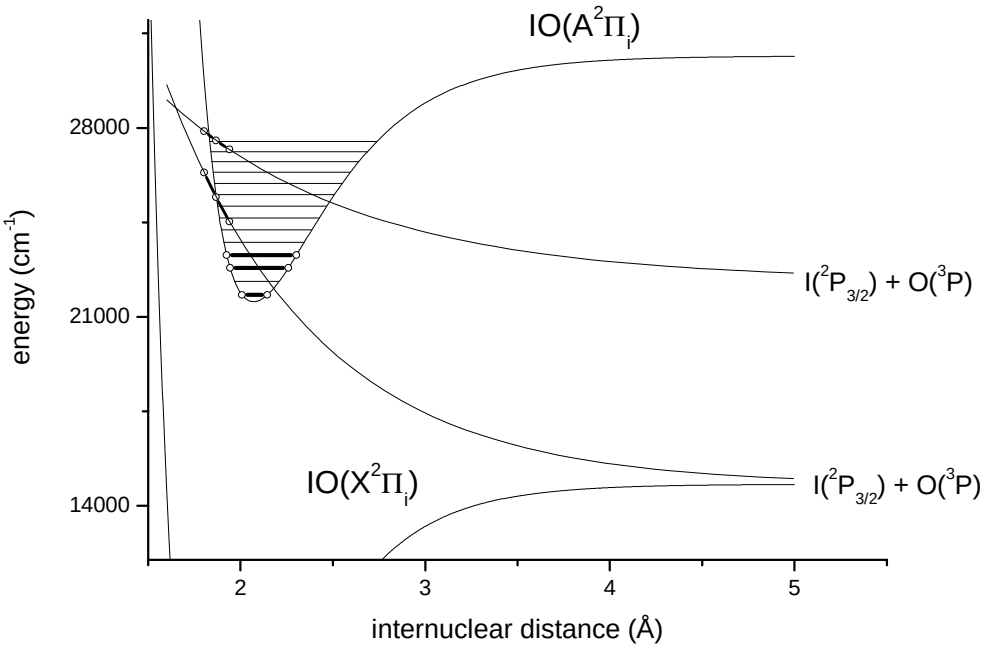

Figure 8.7 The tangents constructed by the reflection method were extrapolated to plausible dissociation products. This extrapolation is based solely on geometric considerations and illustrates that the inclination of both tangents is plausible. Also intersection of the lower repulsive potential in the middle of levels ν'=2 and ν'=3 seems to fit to their observed low predissociation. Level ν'=1 intersects near a turning point indicating large predissociation, as observed. Levels ν'>3 intersect closer to the inner turning points, where the state function has increased values. At ν'=0 overlap should be small, again in agreement with observation by Newman et al.

8.2 Absorption Continuum Extracted Simultaneously with Vibrationally Excited IO(ν'←ν"), ν">0

8.2.1 Observed continua in context of repulsive states found in IO(ν'←0)

Along with IO(ν'←ν"), ν">0 a continuum absorption was extracted. The assignment of which to excited IO is not unequivocal as the width of its temporal behaviour is of the order of the width of the detector's characteristic function in time. It could also be caused by a further yet unidentified species. Having found evidence for two repulsive potentials based on the observed continuum of ground state IO, it is possible to check, whether the continuum in the ν">0 extraction plausibly fits to one or both of these repulsive states or not. Apart from the clear continuum with maximum at ca. 28000 cm^{-1} there is some weak evidence for a further smaller one below (4←1). Both were fitted by a gaussian, see **Fig. 8.8** and then considered in the scheme of the reflection method, see **Fig. 8.9**.

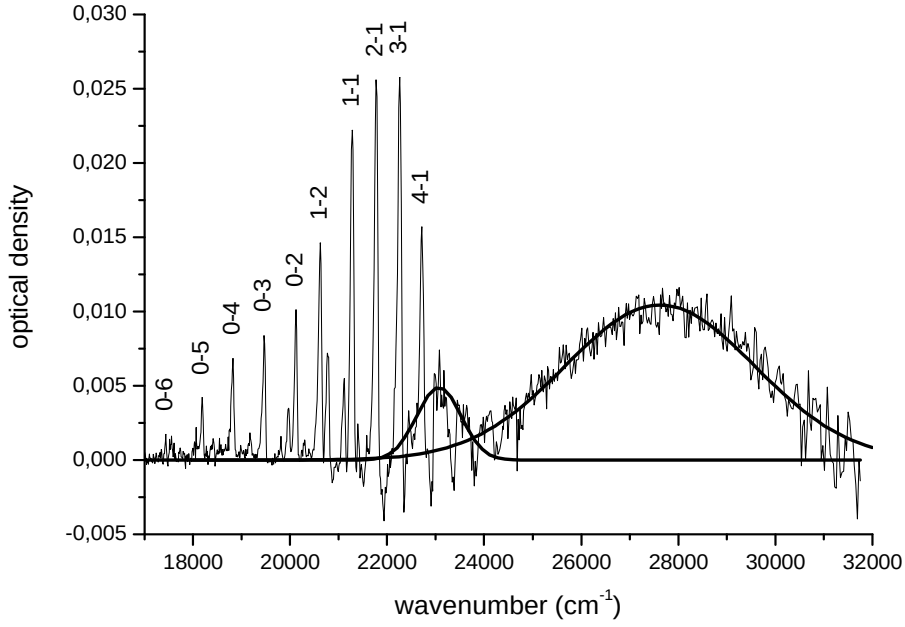

Figure 8.8 Along with IO ν">0 a strong continuum was extracted of unclear origin. Near (4←1) possibly a second smaller continuum is present, which is hidden in residuals of incomplete extraction of ground state IO. Both were fitted to gaussians to introduce them into the reflection method to examine, in how far they fit into the picture of found repulsive states.

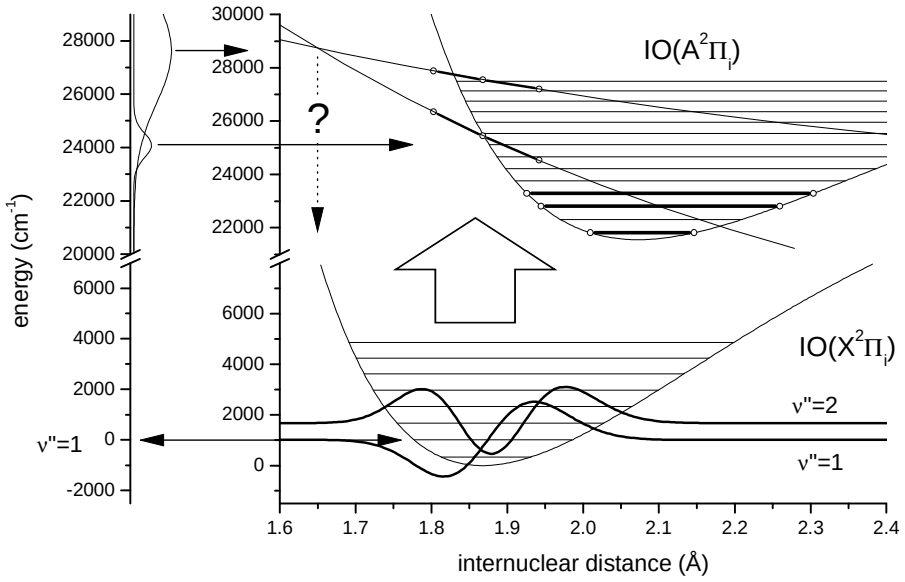

Figure 8.9 In a qualitative way the reflection method is considered for the continua from **Fig. 8.8**. Only the small continuum near 24000 cm^{-1} fits to originating from ν"=1 or 2. The stronger one with its maximum near 28000 cm^{-1} would require transitions from ν">10. Band strength would have to be of the same order as for ν"=1 to explain the observed strength of continuum. This is in contradiction to observations. Only ν" up to 7 was observed. Occupation of higher levels should be negligible. It has to be concluded that the larger continuum does not originate from vibrationally excited IO but probably from another yet unidentified molecule labelled "X" (see above).

But in contrast to the case of ground state IO, ν"=0 here the state functions from ν"=1 and 2 are no longer simply bell shaped, but display clear structures. The shape of a corresponding continuum could only be inferred, if either the shape of the state function in the repulsive state were known to calculate overlap integrals for each energy and thereby to construct the resulting continuum. As the objective here is only a qualitative check, no efforts were made to determine the state function. Or the state function in the repulsive state had to be significantly narrower than that of the bound states. In that case "reflection" could be viewed as scanning the bound state's state function by a narrow delta peak. This would mirror the shape of the bound state's state function into a corresponding continuum. The repulsive potential in the present case is of small inclination, why its state function will be broad. Therefore it is not possible to infer the shape of the expected spectrum in this way. But still a check is possible, whether the continua are located at energies, which plausibly fit to positions of the repulsive states and the state functions of ν"=1 or 2 or not (**Fig. 8.9)**. For the small continuum energies fit to bound-free transitions from ν"=1 or 2 to the lower of the two repulsive states (large open arrow). Transitions to the upper repulsive state would fall into the flank of the larger observed continuum and would be covered by this. Their existence can not be excluded. But for the

large continuum the situation is different. Its maximum lies too high to fit to either of the two repulsive states. According to the reflection method it would have to originate from levels ν">10. The highest observed level of vibrationally excited IO in our spectra was ν"=7. Therefore it is concluded that the observed large continuum *does not* belong to the spectrum of vibrationally excited IO but rather to a further yet unidentified species.

8.2.2 Source of continuum absorption at 28000 cm^{-1}: Spectroscopic evidence for IOO

Due to the temporal behaviour of optical density it must be one of the earliest products formed after photolysis, as for its extraction the curve of temporal behaviour of vibrationally excited IO of levels ν">1 or that of unknown absorber "X" was used, see **Fig. 7.1b**. Reactants at such an early state are basically I, O, I_2, O_2, and O_3. Sources of IO are the reactions:

$$I(^2P_{3/2}) + O_3 \rightarrow IO + O_2 \qquad \text{(R6.3)}$$

$$O(^3P) + I_2 \rightarrow IO + O_2 \qquad \text{(R6.4)}$$

In analogy to the other halogens Cl and Br the following reaction could be possible:

$$I(^2P_{3/2}) + O_2 + M \rightarrow IOO + M \qquad \text{(R8.1)}$$

Based on ab initio calculations [Misra and Marshall 1998] it is predicted to be only very loosely bound and has to be expected to be highly reactive as well. Especially reaction with free iodine atoms is a likely candidate, again in analogy to the other halogens. Due to weak bonding and to the chaperone needed in (R8.1) its temporal behaviour should show a pressure dependence. It should have an impact on the observed behaviour of IO.

8.3 Franck-Condon Factors for IO from Measurement

With the extracted spectra for ground state and excited states of IO relative band strengths were determined by integration of individual bands. Within each progression (common ν") all bands have the same temporal behaviour. Therefore the extraction of spectra from the overlapped time resolved data does not influence their relative band strength. Correct scaling of band strengths within one progression is preserved. But not between different progressions, because different progressions will in general have different temporal behaviour. As the spectrum for vibrationally excited IO was obtained for all ν">0 in one extraction and without discrimination between different ν", in the resulting spectrum the relative scaling between

progressions is not preserved. Because of that, band strength obtained for bands of *different progressions* is not comparable. Integrated optical density as a measure of band strength can be related to Franck-Condon factors (see Herzberg [1950]):

$$\int_{\text{band}\,nm} A(\lambda) = \frac{8\pi^3 \nu_{nm}}{3hc} \cdot N_m \cdot \left|\mathbf{R}_{nm}\right|^2 = \frac{8\pi^3 \nu_{nm}}{3hc} \cdot N_m \cdot \left[\int_{r=0}^{\infty} \varphi_n(r) \cdot \mathbf{R_{nm}} \cdot \varphi_m(r)\, dr\right]^2 \qquad \textbf{(7a)}$$

Using the Franck-Condon principle, the dependence of $\mathbf{R}_{nm}$ on r can be neglected so that by ignoring all other factors a proportionality between band strength and the squared overlap integral, i.e. the Franck-Condon factor for transition n→m is obtained:

$$\int_{\text{band}\,nm} A(\lambda) = \frac{8\pi^3 \nu_{nm}}{3hc} \cdot N_m \cdot \overline{\mathbf{R}}_{nm}^{\,2} \cdot \left[\int_{r=0}^{\infty} \varphi_n(r) \cdot \varphi_m(r)\, dr\right]^2 \propto \left[\int_{r=0}^{\infty} \varphi_n(r) \cdot \varphi_m(r)\, dr\right]^2 \qquad \textbf{(7b)}$$

As the scaling of band strengths between different progressions is not preserved by our extraction method, which produced the spectra, the relative band strengths within each band were scaled to the Franck-Condon factors published by Rao et al. [1974] for each progression. **Fig. 8.10** compares their values to those obtained from our measurements. Results for ν''=0, ν'>4 are those obtained earlier from the constrained fit to the IO(ν'←0) continuum absorption. All others were obtained by direct integration of optical density across the band and subsequent scaling to the values by Rao et al. Also shown are the Franck-Condon factors obtained from our calculations based on a Morse potential approximation, see **(5a)** and **(5b)**. In general the systematic behaviour of band strength obtained from our spectra is in good agreement with the ones predicted by Rao et al. Results are listed in **Tab. 8.2** and **Tab. 8.3**.

The results for ν''=0 agree well for ν'≤4 (scaling was performed for ν'=3) with both the results by Rao et al as well as those from Morse approximation. But for larger ν' – where no results by Rao et al. exist – our estimates for Franck-Condon factors obtained from the constrained fit fall systematically below those from Morse approximation. This indicates some unresolved issues either in the constrained fit or in the Morse approximation. The former is quite likely, as the constrained fit is still prone to uncertainties. Also the estimated factors do not behave as smoothly as one would expected.

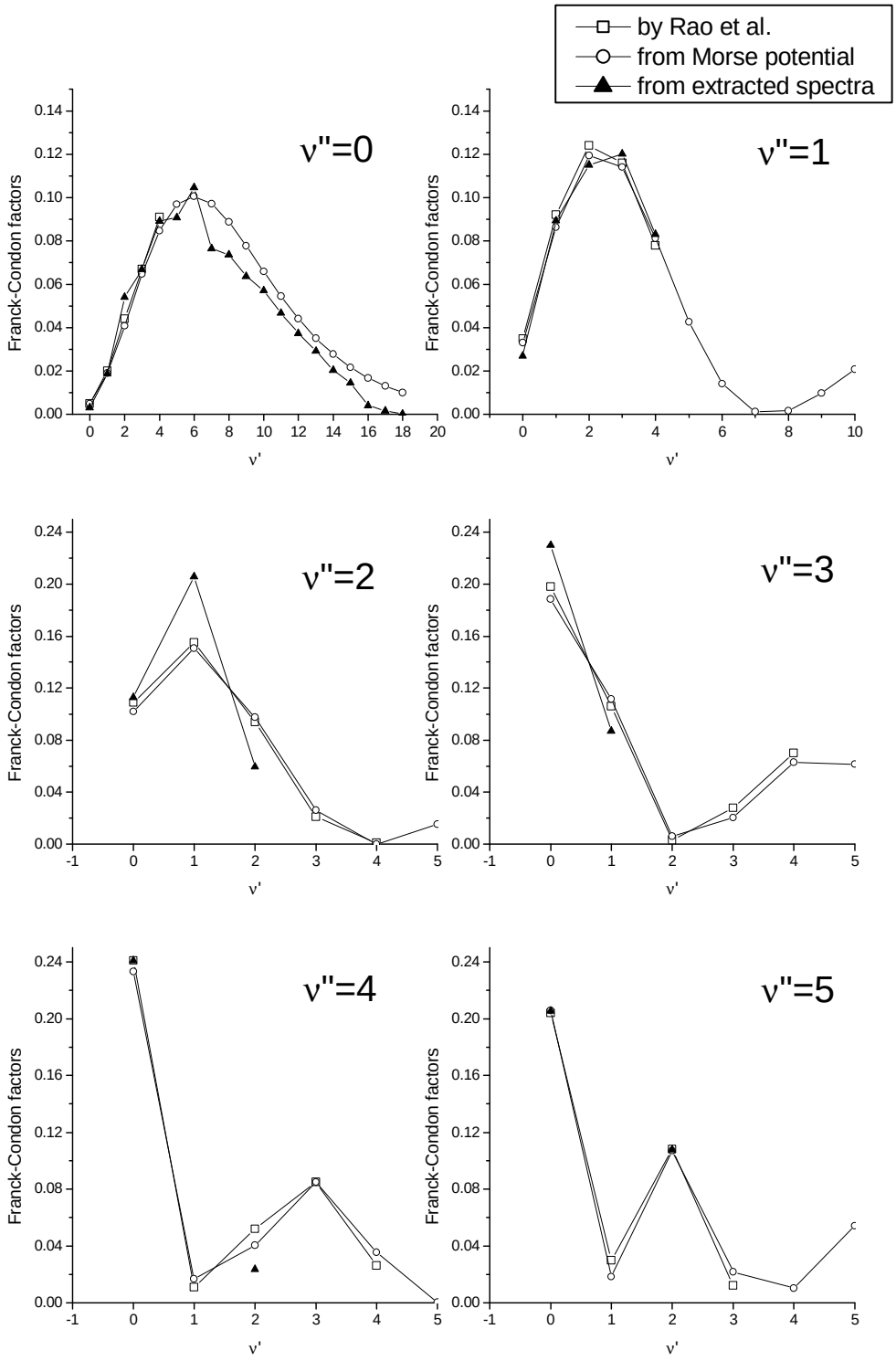

Figure 8.10 In our spectra of ground state and excited IO band strength was estimated by integration across individual bands. After appropriate scaling they could be compared to Franck-Condon factors published by Rao et al. as well as to those obtained in Morse approximation (see above). The agreement is good. For $\nu''=0$, $\nu'>4$ inconsistencies remain between the results from a constrained fit and a Morse approximation.

	ν'←0	ν'←1	ν'←2	ν'←3	ν'←4	ν'←5
ν'=0	0.005 0.0049 0.0031	0.035 0.033 0.027	0.109 0.102 0.113	0.198 0.188 0.230	0.241 0.233 0.241	0.204 0.206 0.206
ν'=1	0.02 0.019 0.019	0.092 0.086 0.089	0.155 0.15 0.20	0.106 0.11 0.09	0.011 0.017 --	0.03 0.018 --
ν'=2	0.044 0.041 0.054	0.124 0.120 0.115	0.094 0.098 0.060	0.003 0.006 --	0.052 0.040 0.024	0.108 0.107 0.108
ν'=3	0.067 0.065 0.067	0.116 0.114 0.120	0.021 0.026 --	0.028 0.020 --	0.085 0.085 --	0.012 0.022 --
ν'=4	0.091 0.085 0.089	0.078 0.081 0.083	0.001 0.00001 --	0.07 0.06 --	0.026 0.036 --	 0.010 --

Table 8.2 Franck-Condon factors for IO are listed. First entry per cell by Rao et al. [1974], second from Morse approximation and third from integrated band strength from our measurements (only bands outside of continuum absorption). The latter were scaled to the values of Rao et al. using the averaged ratio within each progression (same ν"). The uncertainty is estimated to be ±10% for all ν"=0 and 1 and for all ν'=0. For all others ±30%.

	Morse	from fit
ν'=5	0.0969	0.0907
ν'=6	0.1006	0.1047
ν'=7	0.0972	0.0765
ν'=8	0.0888	0.0736
ν'=9	0.0778	0.0637
ν'=10	0.0659	0.0572
ν'=11	0.0544	0.0468
ν'=12	0.0441	0.0374
ν'=13	0.0351	0.0291
ν'=14	0.0277	0.0205
ν'=15	0.0216	0.0145
ν'=16	0.0168	0.0041
ν'=17	0.0130	0.0017
ν'=18	0.0100	0.0001

Table 8.3 Same as **Tab. 8.2**, but for ν"=0 with results from Morse approximation and from integrated bands from constrained fit. The uncertainty in the values obtained from the constrained fit for ν">4 is estimated to be of the order of 30% based on **Fig. 8.10**.

For ν"=1 the agreement between all three series of Franck-Condon factors is strikingly good, while for larger ν" – due to the smaller number of data points available – the agreement is less clear. But still the systematic pattern is followed closely by the estimates obtained from

integrated bands. The magnitude of Franck-Condon factors of (4←0) compared to (2←1) and (3←1) can also give a measure for the relative magnitude of absorption cross section of these bands, because they all are outside of continuum regions and therefore have similar shape. This comparison indicates that the maximum cross section in the ν"=1 progression will be roughly 30% higher than that of the (4←0) band.

8.4 ANOMALOUS BEHAVIOUR OF IO(2←0)

8.4.1 Hypothesis: Chemiluminescence from IO($A\,^2\Pi_i$) at ν'=2 and ν'=3

The observed different temporal behaviour of the IO(2←0) and in parts also of the IO(3←0) can be explained in terms of chemiluminescence. In that case it has to be assumed that a considerable number of IO molecules is formed in the IO($A^2\Pi_i$), ν'=2 and ν'=3 with sufficient life time for subsequent radiative transition to the ground state. Chemiluminescence would partly compensate the absorption from those ground state bands. This hypothesis is completely in line with the structure found for these bands in the cavity ring down spectroscopy measurements reported by Newman et al. [1998]. Their measurements showed clear rotational structure and smallest predissociation for the (2←0) transition and slightly larger for the (3←0) transition. All other bands but the IO(0←0) are without rotational structure and are strongly predissociated. IO molecules formed in the $A^2\Pi_i$ state at ν'≠2 and ν'≠3 will therefore dissociate rather than relax by radiative transition.

8.4.2 Possible source of IO in $A^2\Pi_i$ state

The comparison of temporal behaviour of IO(2←0) and the remaining IO(ν'←0) bands shows that the source of IO($A^2\Pi_i$) as the origin of chemiluminescence is strongest during the initial period while towards the end both curves (after appropriate scaling) coincide accurately (see **Fig. 8.11**). Reversing the argument and subtracting the scaled IO(2←0) from the IO(4←0) produces a time curve which is a direct measure for the presence of chemiluminescent IO relaxing from the upper $A^2\Pi_i$ state.

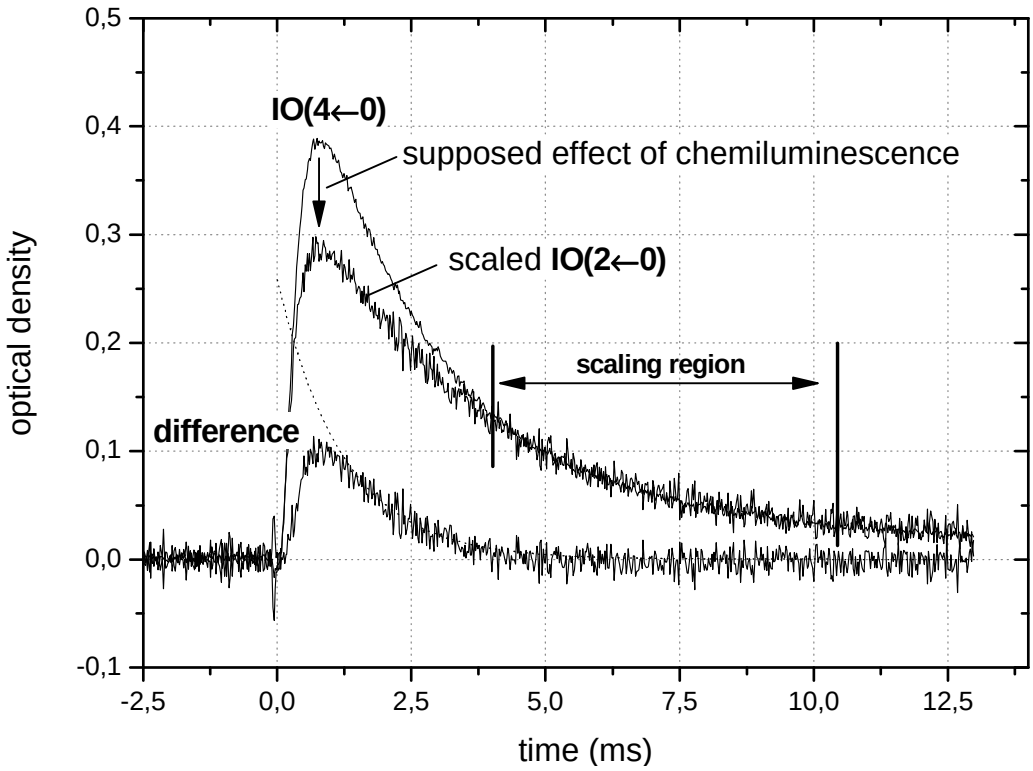

Figure 8.11 The curve of temporal behaviour of IO(2←0) was scaled to that of IO(4←0) in the indicated region. Clearly the apparent difference is strongest during the first 3 to 4 ms. Subtracting one from another produces a curve describing the temporal behaviour of the effect. The deviation can be understood in terms of chemiluminescence from the IO($A^2\Pi_i$), ν'=2 band, which shows the least predissociation [Newman et al. 1998]. Chemiluminescence would partly compensate the absorption from IO(2←0).

The lifetime of IO in the IO($A^2\Pi_i$) state with ν'=2 or ν'=3 with respect to radiative relaxation to the ground state is of the order of 10 to 100 picoseconds, while the chemical lifetime of IO with respect to self reaction or other consumptive reactions is of the order of milliseconds. Therefore the curve – if it indeed were chemiluminescence – would be a direct measure of the kinetics of formation of IO($A\ ^2\Pi_i$) without interference of any secondary chemistry. The decay of its time curve follows a clear first order (**Fig. 8.12**). This makes both O + I_2 with [O]<<[I_2] as well as I + O_3 with [I]<<[O_3] likely candidates for a pseudo first order formation of IO in the $A^2\Pi_i$ state. The energy at the minimum of the IO($A\ ^2\Pi_i$) potential well is 21557.81 cm^{-1} [Durie et al. 1960, NIST Online Databases 2003]. Comparing this to the available energy, which is released in the respective reactions of formation clearly proves that only O(^{1}D) + I_2 is capable to form IO in the $A\ ^2\Pi_i$ state. The enthalpies of formation, which were used in this calculation, are listed in **Tab. 8.4**.

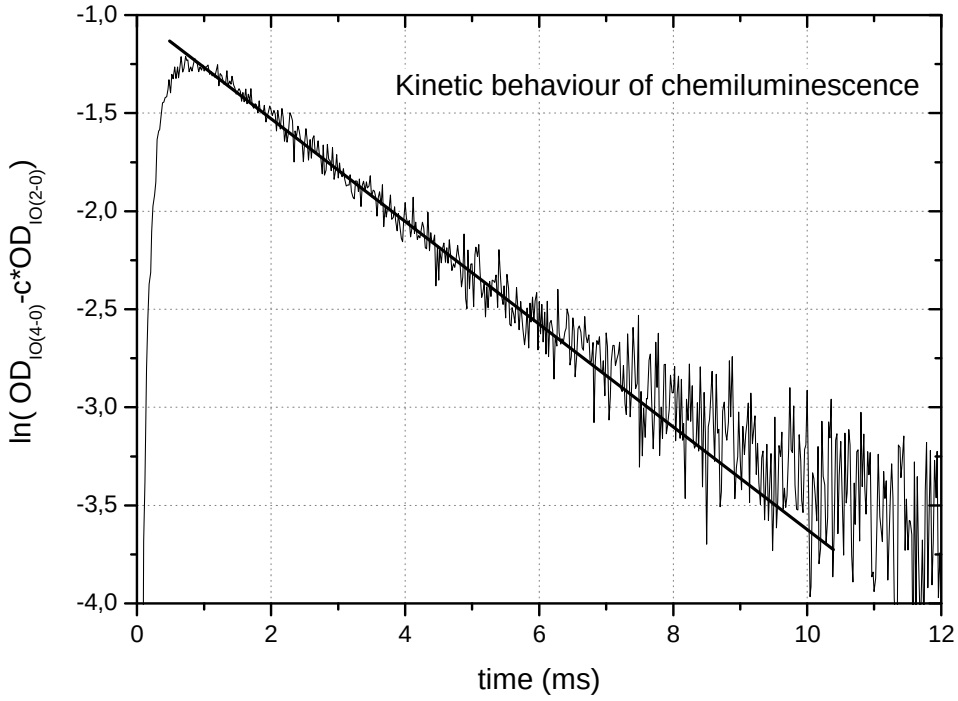

Figure 8.12 Interpreting the difference between IO(4←0) and a scaled (2←0) curve of temporal behaviour as a decay curve displays a clear first order behaviour. This indicates that the source of hypothetical chemiluminescence could be a reaction with pseudo first order kinetics.

The available results for the enthalpy of formation of IO are somewhat critical, as depending on the different reference data the available energy either suffices to form IO in the $A^2\Pi_i$ state or falls too low. The latter is true for the value reported in Lide [1993], for which the energy would be too low by roughly 3200 cm^{-1}. The critical threshold for $\Delta_f H°$ of IO(X $^2\Pi_i$) lies at 136.6 kJ/Mol. Three more recent results including the review by Chase [1996] indicate a value which allows direct formation in the upper IO(A $^2\Pi_i$) state at low vibrational levels, see **Fig. 8.13**. One at (135±4)kJ/Mol is just above the threshold while the error limits reach below the threshold.

In case the enthalpy of formation of IO would be larger than the threshold value, a gap of roughly 2000 cm^{-1} (≈24kJ/Mol) could be bridged by vibrational energy from the I_2 molecule. After the flash I_2 is likely to exist for a limited time at vibrational levels of the order of 20 to 25 providing energy of 2000 to 2500 cm^{-1}. This would then introduce a first order pressure dependence due to quenching of $I_2(20<v''<25)$.

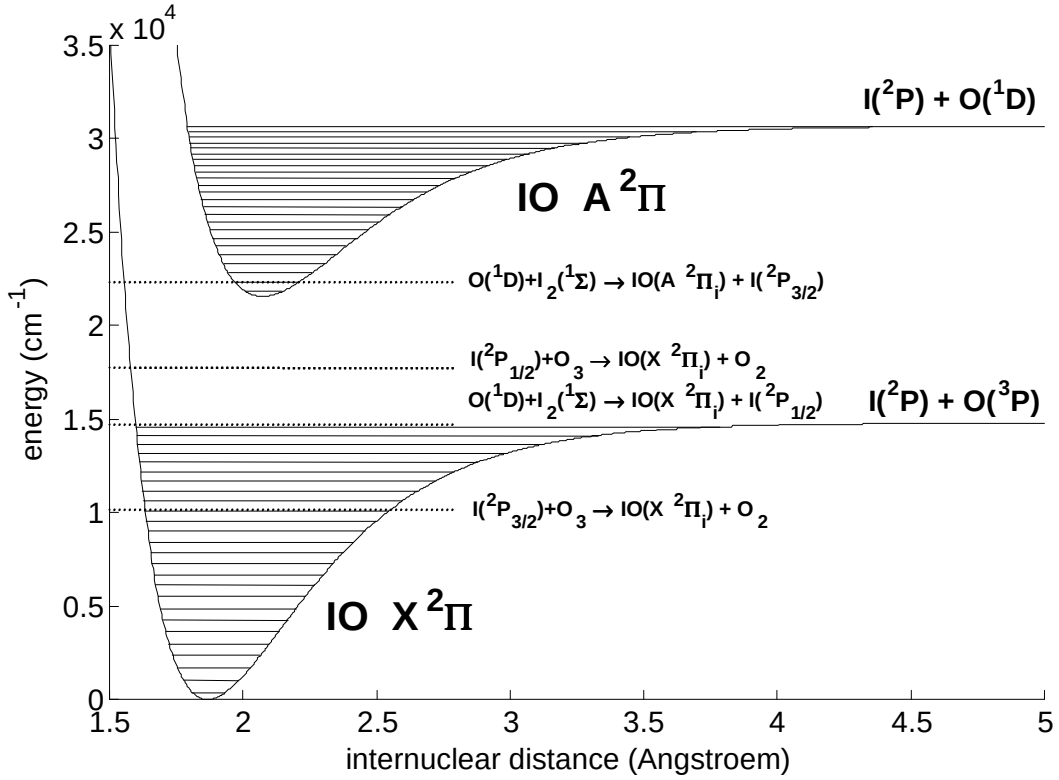

Figure 8.13 Based on enthalpies of formation the different source reactions for formation of IO are considered. Only $O(^1D) + I_2 \rightarrow IO(A^2\Pi_i) + I(^2P_{3/2})$ provides enough energy to produce IO in the upper electronic A state. Levels were calculated with $\Delta_f H_{298}$ for IO by Chase [1996].

All other possible sources of IO do not provide sufficient energy for the formation of IO in the A $^2\Pi_i$ state. In terms of enthalpies, chemiluminescence, which was indirectly inferred by our observations most likely results from the reaction of $O(^1D) + I_2 \rightarrow IO(A^2\Pi_i) + I(^2P_{3/2})$.

This is further supported by the fact that the dissociation products of $IO(A^2\Pi_i)$ are $I(^2P)$ and $O(^1D)$ as reported by Durie and Ramsay [1960]. Reversing their argument, which used the Wigner-Witmer correlation rules, makes $O(^1D)+I_2(^1\Sigma)$ the most likely source of $IO(A^2\Pi_i)$.

Chemiluminescence was directly observed by Miller and Cohen [2001], who used reaction $O+I_2$ at pressures at and below 1 mbar as source for IO and who used the brightness of chemiluminescence as a diagnostic of successful IO production. In their experiment oxygen atoms were produced in an O_2 discharge. At the reported low pressures a large fraction of O atoms had to be expected in $O(^1D)$.

molecule	$\Delta_f H_{298}$ [kJ/Mol]	$\Delta_f H_{298}$ [cm^{-1}]	Reference
$I(^2P_{3/2})$	106.8	8928	IUPAC 2003
$I(^2P_{1/2})$	197.6 (=106.8 + 90.9)	16518	Okabe 1978
I_2	62.42	5216	IUPAC 2003
IO(X)	(175.1) **128±13** 135±4 120±5 115.9	(14637) **10700±1087** 11285±334 10031±418 9688	(Lide 1993) **Chase 1996**[a] in Chase 1996[b] in Chase 1996[b] Bedjanian et al. 1997
$O(^3P)$	249.18	20831	IUPAC 2003
$O(^1D)$	438.9	36689	IUPAC 2003
O_3	142.7	11929	IUPAC 2003

Table 8.4 Enthalpies of formation are listed, which are relevant to the reactions $O+I_2 \rightarrow IO+I$ and $I+O_3 \rightarrow IO+O_2$. [a]: Extensive literature review. [b]: Results for IO, which were communicated after the review by Chase was accepted for publication. The results are not considered in the recommended value by Chase. In our considerations the recommended value of 128 kJ/Mol was used.

In our experiments the source of $O(^1D)$ is the photolysis of O_3 by the photolysing flash predominantly at λ<320nm. Even with filters (Pyrex) between the vessel and the flash lamps, a photolysis rate for O_3 of the order of 0.1% could not be avoided. At $[O_3]$ of the order of 10^{15}molec/cm^3 this produces $O(^1D)$ of the order of 10^{12}molec/cm^3. This is of the same order of magnitude as the observed IO concentration. Without filters the formation of $O(^1D)$ is by more than one order of magnitude larger producing significant amounts of $O(^1D)$. In so far the hypothesis of $O(^1D)+I_2$ as source of $IO(A\ ^2\Pi_i)$ is consistent with the observations and the conditions of our experiments as well as with energetical and configurational arguments.

But there is one flaw to it. Quenching of $O(^1D)$ with N_2 takes place at a rate of $2.6 \cdot 10^{-11}$ cm^3·molec^{-1}·sec^{-1} (and $4.05 \cdot 10^{-11}$ cm^3·molec^{-1}·sec^{-1} with O_2). At an overall pressure of 40 mbar concentrations of $[N_2]$ and $[O_2]$ were both of the order of 10^{17} molec/cm^3. This gives $O(^1D)$ a lifetime of less than a microsecond. This is in direct contradiction to the hypothetical chemiluminescence which lasts over milliseconds, while the radiative relaxation of $IO(A^2\Pi_i)$ takes place on a timescale of 10 to 100 picoseconds.

As an alternative hypothesis it could be considered that non-linear effects in the apparent optical density cause the apparent different behaviour of the IO(2←0) and (3←0) bands. IO concentrations in our experiments were of the order of 10^{12} to 10^{13} molec/cm^3 and the maximum cross section in the rotational lines of IO(2←0) is of the order of $7 \cdot 10^{-17}$ cm^2/molec [Atkinson et al. 1999]. This yields a maximum optical density around 1.0. Saturation effects in optical density therefore have to be excluded. Non-linearity in apparent optical density due to low resolution and coarse binning is clearly present at the order of 16% (see **Chapter 9**), but is not large enough to explain the observed anomalous behaviour of the IO(2←0) band.

In **Tab. 10.2** previous publications with information on cross section spectra are listed. In the clear spectra published by Laszlo et al. [1995], Ingham et al. [2000] and Bloss et al. [2001] the relative strength of bands of ground state IO can be compared clearly and they do not show a reduced (2←0) band in O+I_2 and O+CF_3I experiments. But it is not clear at which time after the initial formation the spectra were recorded. In the only other spectrum recorded in O+CF_3I [Harwood et al. 1997] no clear statement can be made.

On the other hand the available spectra from I+O_3 systems other than the present work are not clear on this. The spectra published by Clyne and Cruse [1970] and Cox and Coker [1983] are sequential recordings and a strong scatter of relative band strength indicates drift effects. A comparison of band strengths is limited. The spectrum by Himmelmann et al. [1996] does not show a strongly reduced (2←0). But the spectrum was recorded in sequential readout mode with 16ms time lag between the first (UV) and the last (NIR) pixel. Due to that it might be that the early phenomenon of reduced peak height of IO(2←0) was missed. Again a clear statement is not possible. So the spectra available in literature do not provide further information about the presence and possible origin of the discussed effect. Even though chemiluminescence could provide an explanation, the source of IO($A^2\Pi_i$) remains unclear and requires further investigations.

8.5 SOURCE OF VIBRATIONALLY EXCITED IO

With respect to the formation of vibrationally excited IO a number of observations are reported in literature. Clyne and Cruse [1970] produced IO in a pure I+O_3 system and observed absorption bands of IO(ν'←1), which were about one-third the intensity of the strongest ν"=0 band. This is similar to what we observe in our experiments. They concluded

from their observations that at least one third of IO molecules from $I(^2P_{3/2}) + O_3$ are initially formed at ν">0. This conclusion they based on the observed relative strength of absorption bands and an assumption on likely Franck-Condon factors of involved bands. Our consideration of Franck-Condon factors (see above) showed that the maximum absorption cross section in the (ν'←1) progression has to be expected roughly 30% higher than that of (4←0). This reduces concentration of excited IO from estimated one-third to one-fourth that of ground state IO. This magnitude underlines the need to account for vibrationally excited IO in the determination of cross section of ground state IO and other species, whenever observations close to the initial formation – here: the flash - are being considered.

Another important conclusion is that with approximately one-fourth of IO being vibrationally excited with significant absorptions from ν" as high as 7, the partitioning is far from thermal equilibrium. By the Boltzmann distribution only a fraction of 4% is to be expected in ν"=1. For ν">1 the fraction is below 0.5%, see **Fig. 8.14**. The population is strongly inverted.

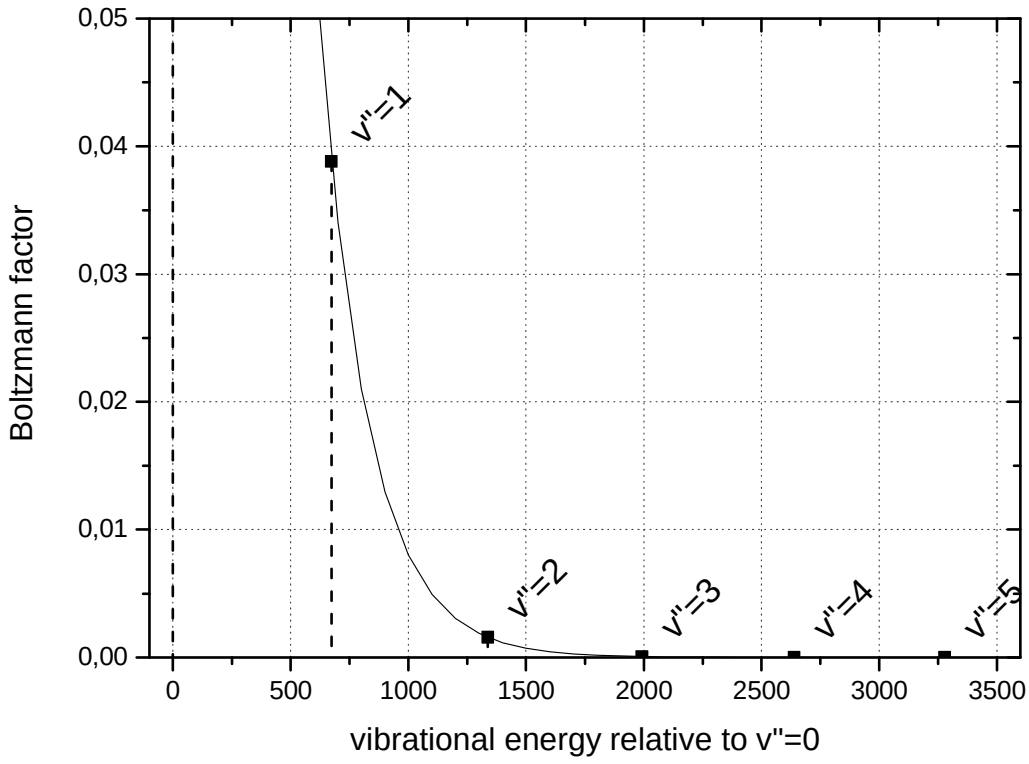

Figure 8.14 The Boltzmann distribution is shown indicating the fraction IO molecules to be expected in excited states ν">0. Already at ν"=1 this fraction amounts to no more than 4% with fractions at ν">1 being negligible. This proves that population in our experiments is strongly inverted.

At thermal equilibrium optical density of (2←1) and (3←1), i.e. the strongest transitions from ν"=1, should not exceed 4/3 * 4% ≈ 5.3% that of (4←1), where the relative magnitude of Franck-Condon factors was used. It remains to be clarified, in how far in our experiments population of IO tends to thermal equilibrium at later times after the flash or not. The permanent presence of ozone and the continuous formation of I by self reaction of IO make it likely that the population will remain inverted throughout the whole time of reaction, due to continuous formation of excited IO by $I+O_3$.

Clyne and Cruse referred to work by McGrath and Norrish [1958], who reported production of ClO and BrO at ν">0 from reaction of Cl and Br with O_3. Cox and Coker [1983] also used the $I+O_3$ system and in their spectrum some structures similar to excited IO are visible. Stickel et al. [1988] observed bands of excited IO in a mixed system with both sources $I+O_3$ and $O+I_2$ present in their system. Turnipseed et al. [1995] reported excited IO in LIF experiments using the $I+O_3$ system. But on the other hand also in experiments using $O+I_2$ or $O+CF_3I$ as a source of IO some vibrationally excited IO was reported, but it seems that the signal is usually weaker than in the $I+O_3$ experiment, see **Tab. 10.2**. In general all reactions discussed in context of **Fig. 8.13** provide enough energy to produce IO in vibrationally excited states. Apart from that also energy transfer from $O_2(^1\Delta_g)$ or $I(^2P_{1/2})$ to $IO(X^2\Pi_i)$ was proposed by Miller at al. [2001] as a source of vibrationally excited IO.

In our experiments – depending on the filters between the flash tubes and the vessel – the sources of IO from $I+O_3$ and $O+I_2$ were simultaneously present, but to different extent. And in all experiments, especially at lowest pressures strong signals of vibrationally excited IO were observed. In all cases the formation of vibrationally excited IO preceded that of ground state IO and especially the bands of ν">1 decayed much faster due to quenching (see **Fig. 7.1b**). Energy transfer from $O_2(^1\Delta_g)$ could also be a likely source in our experiments while transfer from $I(^2P_{1/2})$ is not relevant. This is rapidly converted to $I(^2P_{3/2})$ by energy transfer to O_2, see **Chapter 4**.

Considering spectra shown in previous publications it has to be noted that in their recording the focus most likely was on a large (ground state) IO signal. Therefore it is possible that they missed the larger initial burst of vibrationally excited IO. In so far a quantitative statement about the possible source of excited IO based on available spectra is not possible.

8.6 SUMMARY

By multiple multivariate regression techniques discussed in the preceding chapter the overlapped spectra of IO(ν'←0), IO(ν'←ν") with ν">0, and OIO(ν_1',ν_2',0←0,0,0) had been separated from each other and from other underlying absorptions of other iodine oxides. As these spectra are free of other absorption to within ±3% for the first time an analysis of band strength of ground state IO and vibrationally excited IO was possible. The continuum absorption of ground state IO could be resolved into overlapped bands of bound-bound transitions and two bound-free transitions. From the contribution of bound-free transitions to the observed absorption continuum the existence of two optically active repulsive states intersecting with the IO($A^2\Pi_i$) potential was inferred. By means of the reflection method tangents were determined to the two repulsive potentials. Correlating the tangents to likely dissociation products gave a plausible rough picture of the shape of the repulsive states. The resulting intersections with bound states within IO($A^2\Pi_i$) are in plausible agreement with observations on predissociation of states by Newman et al. obtained by cavity ring down spectroscopy. From a comparison of found repulsive states to continua extracted simultaneously with bands of vibrationally excited IO, ν">0 it has to be concluded that the stronger one of these continua can not be attributed to IO(ν'←ν"), ν">0. It has to be attributed to a new yet unidentified molecule with similar temporal behaviour as excited IO. A likely candidate for this is IOO. Relative band strength was determined for ground state and vibrationally excited IO. Comparison to Franck-Condon factors published by Rao et al. as well as obtained from a Morse approximation shows a good agreement between the experimental values obtained from our spectra and the predicted ones. The anomalous behaviour of IO(2←0) was studied. It could be explained by hypothetical chemiluminescence from IO($A^2\Pi_i$), but the source of which remains unclear. The source of vibrationally excited IO was discussed with $I+O_3$ being likely to be strong, but according to literature other reactions as $O+I_2$ and $O+CF_3I$ should produce IO at ν">0 as well.

9 EFFECT OF RESOLUTION AND BINNING

Before the method of iodine conservation can be applied, possible effects of limited resolution on the observed curves of optical density versus time have to be considered. A time resolved detection system with broad spectral coverage, as it is used in the present study, allows simultaneous measurement of multiple absorbers. This is an important prerequisite to the method of iodine conservation to be used in the following chapter for the determination of absolute absorption cross sections. It also enables more accurate determination of chemical kinetics. But as a trade-off to broad spectral coverage, banded spectral features can sometimes be recorded with insufficient spectral resolution and/or insufficiently fine detector binning. This renders the true physical spectrum of recorded intensities changed by instrumental and spectrum specific artefacts. In the present chapter it is demonstrated that in the case of a "well-behaved" – i.e. free of ro-vibronic structure – absorption band like the iodine monoxide IO(4←0) transition, these effects can easily change the apparent peak absorption up to 30 to 50%. This is illustrated in **Fig. 9.1**. Also deviations from the strict linearity (Beer-Lambert's law) between absorber concentration and apparent , i.e. pixelwisely calculated optical density are found. Estimates for absolute cross sections obtained by iodine conservation – as well as by any other method - would be rendered instrument dependent and due to non-linearity even erroneous by these effects.

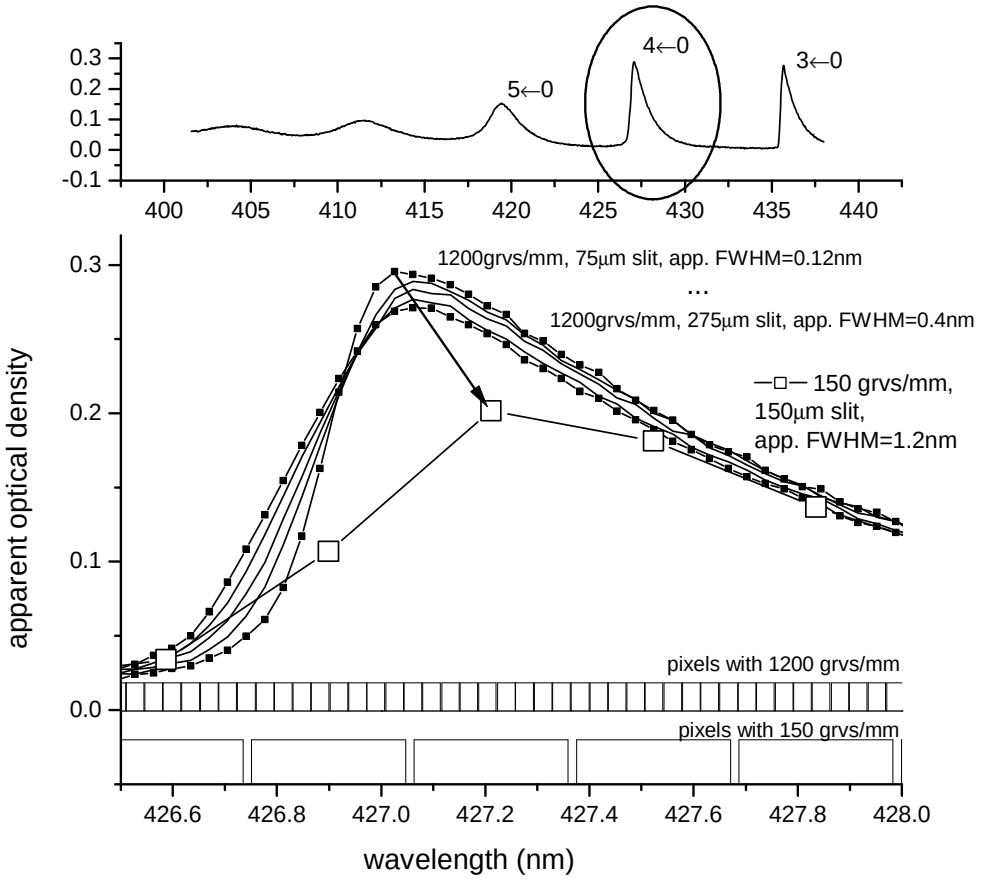

Figure 9.1 In the top graph a section of the iodine monoxide absorption spectrum is shown, as obtained from intensity measurements recorded with a 1200 grvs·mm^{-1} grating (→0.04nm/pix), 75μm slit at effective FWHM of 0.12nm. The IO(4←0) absorption transition is indicated, which will be used as test spectrum throughout this work. The bottom graph shows the shape of this transition, as it is obtained under different spectroscopic conditions. Spectral width of pixels – i.e. size of bins - is indicated by the two different bar plots (top row: 1200 grvs·mm^{-1}, 0.04nm/pixel, bottom row: 150 grvs·mm^{-1}, 0.32nm/pixel). Clearly lower resolution as well as more coarse binning change the apparent shape and the height of the absorption spectrum. Wavelength is in standard air.

To overcome this problem, an integral approach for the treatment of intensity recordings was developed. Thereby the linearity between optical density and absorber concentration is re-established. The method is validated using artificial test data as well as experimental data of the IO(4←0) absorption transition, obtained in the context of I_2/O_3 photochemistry studies. The agreement is accurate to within ±2% (test data) and ±3% (experimental data) supporting the validity of the approach.

9.1 BACKGROUND TO THE PROBLEM

9.1.1 Measurement of intensity spectra

To start with, the determining factors in the recording of intensity spectra are examined. On one hand the spectroscopic part is to be considered and on the other hand the detector part of the set-up. An atomic emission line shall be focussed into a spectrometer. The shape of the line, as it emerges from the spectrometer, describes the spectrometer's characteristic function, or shorter – but less accurately - the instrument's function. Neglecting technical imperfections it is characterised by linear dispersion and spectral resolution of the spectrometer. Linear dispersion is defined by the spacing of the grating's grooves and the focal length of the spectrometer. Knowing both parameters, linear dispersion can be rigorously determined. Spectral resolution - loosely speaking – measures, how a monochromatic line is smeared out when imaged into the spectrometer's focal plane. It is determined by the number of grooves, which are *illuminated* (i.e. which contribute to the diffraction), by the selected order of diffraction, and by the width of the entrance slit of the spectrometer. The number of illuminated grooves depends on the filling of the spectrometer's field of view. This is usually not easily characterised impeding comparability of different experiments. The (rectangular) entrance slit, which is illuminated homogeneously, is imaged by the spectrometer's optics to a rectangle in the focal plane. The augmentation of the spectrometer's optics determines the width of this image. Its edges are smeared out by diffraction. The image – its cross section in dispersion direction (intensity vs. wavelength) being the characteristic function - is recorded by a multichannel detector placed in the focal plane of the spectrometer. Depending on the size, spacing and number of detector pixels, the continuous spectrometer's function is converted to a discrete set of points. This process is often referred to as "sampling". This is incorrect and misleading in the context of multichannel semiconductor detectors. Due to the finite pixel's width, the signal incident on the detector is not sampled but *spectrally integrated* or *binned* on the pixel. This is illustrated in **Fig. 9.2**. Accordingly the recording process should more accurately be referred to as *spectral binning*. This nomenclature will be used throughout this work.

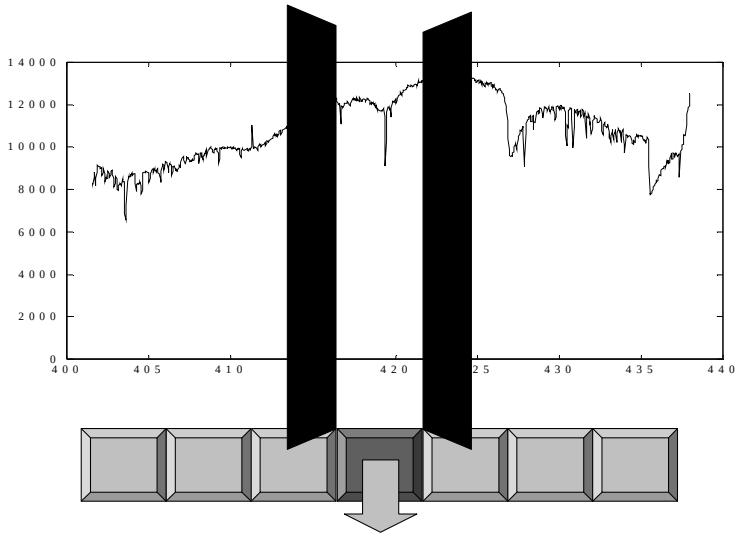

$$I_i = \int_{\lambda_i}^{\lambda_{i+1}} I(\lambda)\, d\lambda$$

Figure 9.2 The process of integrating intensities on a finite-sized semi conductor pixel is illustrated. The dark "blades" indicate the right and left borders of the pixel in analogy to the blades of the slit in a single channel detector experiment. The intensity distribution incident on the pixel (indicated by the spectrum behind) is integrated within the limits of the pixel as defined by the geometry of the pixels and linear dispersion. This integrated intensity is the output signal of the pixel of the multichannel detector.

The width of the spectral interval binned in a pixel will in the following be referred to as the spectral width of the pixel. It is determined by the geometric width of the pixel multiplied by linear dispersion (assuming a rectangular characteristic function of the pixel's sensitivity itself). As the blind spacing between pixels is usually small, it will be neglected here.

If the spectrometer's function (continuous valued in wavelength λ) is covered by a sufficient number of pixels so that its true shape is resembled closely, the *spectral binning* is sufficiently fine. If this is not the case, the *binning* is too coarse (commonly: *undersampling*). The discrete output will in any case be more or less distorted with respect to the true spectral signal. This also needs to be considered e.g. in the characterisation of a spectrometer's characteristic function. When fitting an analytical line shape function to the observed discrete data, the integrating nature of the recording process has to be taken into account. In the same way discrete recordings of any non-monochromatic spectrum are affected. It is intuitively clear that the instrument's effects depend on the *spectral width of the spectrum's features themselves* with respect to the instrument's characteristics. The effect and therefore the errors will be the more serious, the "narrower" the spectrum's structures are with respect to the pure instrument's characteristics.

9.1.2 Deduced quantities

In a measurement the *intensity* of spectra is recorded as primary data. In contrast to that, variables like spectra of optical density or absolute absorption cross section or chemical rate coefficients determined from time resolved measurements are *deduced quantities*. As soon as the effect of the instrument characteristics on shape and absolute value of the measured *intensity* spectra can no longer be neglected, any deduced quantity will be affected and possibly erroneous as well, unless the said effects are properly taken into account.

Often – as in the present CCD measurements - an approximation is used, where Beer-Lambert's law **(1)** is applied pixel by pixel to the detector's output (spectrally binned intensity signals) producing an *apparent* optical density. The approximation is in that *integrated* and *convolved* intensities rather than the theoretically required continuous-valued intensity distributions are used. This approximation impedes the linearity between absorber concentration and apparent optical density due to the – rigorously speaking - *incorrect usage of the Beer-Lambert law*. This must not be mixed up with non-linear effects caused by saturation of unresolved, strong rotational lines of large optical density in low resolution measurements. Likewise, non-linear effects as reported by e.g. Notholt et al. [1991] or Volkamer et al. [1998] are only partially linked to resolution issues. They require their own consideration, as those measurements were made with a Fourier Transform Spectrometer based on a different measurement and analysis process.

The consequences of non-linearity are numerous: It impedes the accurate determination of absolute absorber concentrations using absorption cross section spectra obtained under different conditions. It also impedes the *quantitative* comparability of absolute absorption cross sections determined under different conditions. The situation is similarly problematic for rate coefficients, when determined from time resolved measurements of *apparent optical densities*. They are prone to being erroneous from the same non-linear behaviour of *apparent* optical density with respect to absorber concentration.

The objective of this chapter is to improve this situation. This can be achieved, if a method is established, which either takes into account the effects of different conditions and especially the integration of signals on the pixels – the spectral binning - in a rigorous way or which is independent of them. Thereby the accuracy of spectroscopic measurement of molecule concentration, absolute absorption cross sections as well as of chemical kinetics rate coefficients will be improved.

9.2 PHYSICAL AND MATHEMATICAL BACKGROUND OF OPTICAL MULTICHANNEL ABSORPTION SPECTROSCOPY

9.2.1 Beer-Lambert law for continuous valued intensity

The main idea of absorption spectroscopy is to compare intensity recordings $I_0(\lambda)$ without an absorber to such recordings $I(\lambda)$, in which an absorber is present. Applying the Beer-Lambert law to these recordings produces a quantitative relationship between absorber concentration and - via the absorber cross section - the optical density $A(\lambda)$ obtained from the experiment:

$$L \cdot \sigma(\lambda) \cdot [M] = A(\lambda) = \ln\left(\frac{I_0(\lambda)}{I(\lambda)}\right) \qquad \textbf{(1)}$$

Here $A(\lambda)$ designates optical density, L is the optical pathlength (the geometric distance the light travelled through the absorbing gas), $\sigma(\lambda)$ is the absorber cross section, and [M] the absorber's concentration. Any multiplicative dependency between incident intensity and the detector's output cancels in this approach. Nevertheless, linearity between incident intensity and detector output is a necessary prerequisite. Equation **(1)** constitutes a linear relationship between the product $L \cdot \sigma(\lambda) \cdot [M]$ on one side and optical density $A(\lambda)$ on the other side. $A(\lambda)$ is directly accessible in the experiment via $I_0(\lambda)$ and $I(\lambda)$. The crucial and implicit assumption is that the intensities $I(\lambda)$ and $I_0(\lambda)$ are defined as *continuous* functions of wavelength λ. Mathematically speaking this is only true for infinitely high spectral resolution and infinitely fine spacing of detector elements. In practice it has to be examined, under which circumstances this requirement can be relaxed in an approximate way without having to expect the aforementioned non-linearity effects. Alternatively it could be examined, what different analysis method has to be used, which operates on non-continuous and pixelwise integrated intensity signals. This is, what is going to be presented below.

9.2.2 Beer-Lambert law vs. binned intensities on coarse pixels: A contradiction

For a real, finitely spaced multichannel detector with finitely sized pixels, a measurement corresponds to a pixelwise integration of the spectrally resolved incident intensity $I(\lambda)$:

$$I_i = \hat{I}_i \cdot (\lambda_{i+1} - \lambda_i) = \int_{\lambda_i}^{\lambda_{i+1}} I(\lambda)\, d\lambda \qquad \textbf{(2)}$$

where λ_i and λ_{i+1} are the borders of pixel number i measured along the wavelength axis of the incident spectrum. I_i denotes the integrated intensity, as it is measured on that pixel (units of intensity times wavelength)and $\hat{I}_i$ refers to the intensity normalised to the spectral width of the pixel (units of intensity). Normalisation has to be considered as soon as measurements recorded under different spectroscopic conditions need to be compared.

If the spectrum, as it emerges from the spectrometer, can not be assumed to be fully resolved relative to the spectral width of the pixels, the convolution of the true $I(\lambda)$ with the spectrometer's characteristic function $S(\lambda)$ has to be taken into account:

$$I_i = \hat{I}_i \cdot (\lambda_{i+1} - \lambda_i) = \int_{\lambda_i}^{\lambda_{i+1}} \int_{-\infty}^{+\infty} S(u) \cdot I(\lambda - u)\, du \cdot d\lambda \qquad \textbf{(3)}$$

When relative measurements of intensity I_i and intensity $I_{0,i}$ as in the case of optical densities according to Beer-Lambert are being considered, it is tempting to use a ratio Q_i of intensities based directly on the integrated detector signals. The corresponding *apparent* optical density $A_{app,i}$ would then be:

$$\begin{aligned} A_{app,i} = \ln(Q_i) &= \ln\left(\frac{I_{0,i}}{I_i}\right) = \ln\left(\frac{\int_{\lambda_i}^{\lambda_{i+1}} \int_{-\infty}^{+\infty} S(u) \cdot I_0(\lambda - u)\, du \cdot d\lambda}{\int_{\lambda_i}^{\lambda_{i+1}} \int_{-\infty}^{+\infty} S(u) \cdot I(\lambda - u)\, du \cdot d\lambda}\right) \\ &= \ln\left(\frac{\int_{\lambda_i}^{\lambda_{i+1}} \int_{-\infty}^{+\infty} S(u) \cdot I_0(\lambda - u)\, du \cdot d\lambda}{\int_{\lambda_i}^{\lambda_{i+1}} \int_{-\infty}^{+\infty} S(u) \cdot I_0(\lambda - u) \cdot \exp(-L \cdot \sigma(\lambda - u) \cdot [M])\, du \cdot d\lambda}\right) \end{aligned} \qquad \textbf{(4)}$$

where **(1)** and **(3)** were used. Accordingly, $A_{app,i}$ and Q_i would be discrete quantities defined per pixel. They depend on the width of the integration's interval, i.e. the spectral width of the

detector pixels, the spectrometer's characteristic function $S(\lambda)$ and the incident intensity $I_0(\lambda)$. **(4)** is highly non-linear in the instrument and experiment depending data $I_0(\lambda)$ and $S(\lambda)$. Both *do not cancel* from the ratio. Because of that, the apparent optical density $A_{app,i}$ *does not* constitute an original quantity of the studied absorption phenomenon, but is affected by instrumental and experimental artefacts. In contrast, in the case of fully resolved and continuous valued intensities, all experiment dependent quantities cancel:

$$\begin{aligned} A(\lambda) &= \ln(Q(\lambda)) = \ln\left(\frac{I_0(\lambda)}{I(\lambda)}\right) \\ &= \ln\left(\frac{I_0(\lambda)}{I_0(\lambda)\cdot\exp(-L\cdot\sigma(\lambda)\cdot[M])}\right) = \ln\left(\frac{1}{\exp(-L\cdot\sigma(\lambda)\cdot[M])}\right) \end{aligned} \qquad \textbf{(5)}$$

Only the parameters describing the absorption phenomenon remain. Comparison of **(4)** and **(5)** shows clearly, that *in general* $A_{app,i}$ can not be expected to approximate the correct *continuous* optical density $A(\lambda)$ unless convolution can be neglected *and* binning is close to continuous. This is only possible if both the intensities $I(\lambda)$ and $I_0(\lambda)$ and the absorption spectrum $\sigma(\lambda)$ vary slowly with wavelength relative to the width of $S(\lambda)$ and the spectral width of the pixels. Only then, spectral mixing by the spectrometer's function becomes unimportant and the on-pixel integration approximates the continuous valued incident spectra sufficiently.

Reversing the argument, it has to be concluded that in pixelwise calculation of *apparent* optical densities $A_{app,i}$ the instrumental artefacts will be strongest, where the intensity spectrum or the cross section or both show the strongest variations with wavelength. This is confirmed by simulations shown in **Fig. 9.3**. There, an *apparent* optical density $A_{app,i}$ was simulated for the IO(4←0) absorption transition using spectrometer's functions of different width for convolution. This transition was chosen because it can be regarded as "well behaved" in that it is free of ro-vibronic structure [Newman et al. 1998] and is comparatively broad with a FWHM of roughly 0.9 nm. The spectrometer's function was assumed to be gaussian shaped. The width ranged from 0.0nm (i.e. no convolution) up to 1.4nm FWHM (spectroscopic, not Gaussian 1/e width).

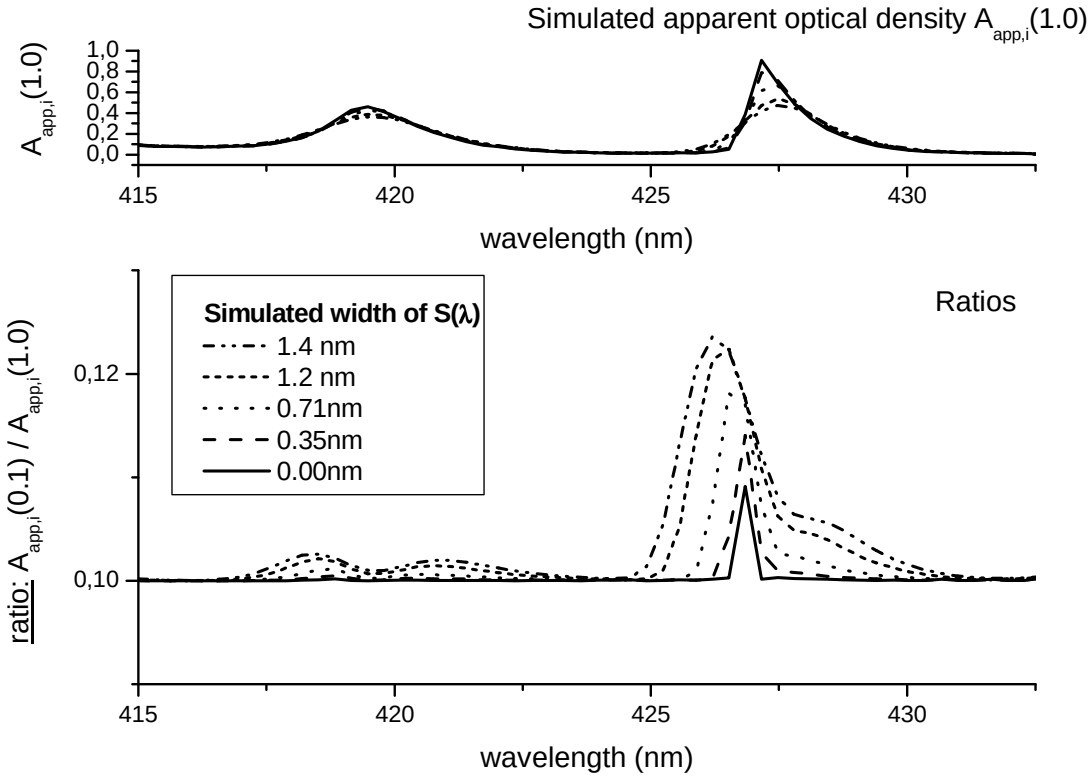

Figure 9.3 Apparent optical density A_{app} was simulated for the IO absorption spectrum for different width of the spectrometer's function S(λ) at a linear dispersion of 0.32nm/pixel. The width of S(λ) is given in the sense of a FWHM. The true quantities $I_0(\lambda)$ and $\sigma(\lambda)$ were approximated by finely binned high resolution measurement data (comp. **Fig. 9.1,** top). True optical density was assumed to be 1.0 in the peak of the IO(4←0) band. Similar spectra were calculated with true $A(\lambda_{max})$=0.1. The upper diagram shows the influence of the spectrometer's function on A_{app} (for true $A(\lambda_{max})$=1.0). Below, for each spectrometer's function the ratio between $A_{app}(0.1)$ for true $A(\lambda_{max})$=0.1 and $A_{app}(1.0)$ for true $A(\lambda_{max})$=1.0 is plotted. In the ideal case, the ratio should be just a horizontal line at 0.1. The clear deviation from this line results from the non-linear structure of **(4)**. As expected, the deviations are strongest, where the spectrum shows the strongest variation with wavelength. Wavelength is in standard air.

Spectral binning was simulated by numerical integration across the fixed spectral width of the pixels (0.32nm per 0.26µm geometric pixel size). Calculations followed **(4)**. The true continuous valued $I_0(\lambda)$ and $\sigma(\lambda)$ were approximated by finely binned high resolution measurement data (1200grvs·mm^{-1}, 75µm slit width, 0.035nm per 26µm pixel size, 0.12nm apparent FWHM determined without interpolation). True optical density $L\cdot\sigma(\lambda)\cdot[M]$ was assumed to be 1.0 in the peak of the IO(4←0) band at 427.2nm. In the upper diagram the influence of the width of the spectrometer's function on $A_{app,i}(1.0)$ is shown for orientation. To check the linearity, a second set of spectra of apparent optical density was calculated at 0.1 true peak absorption designated as $A_{app,i}(0.1)$, thereby covering a reasonable interval of optical density, i.e. concentration. The lower graphs in **Fig. 9.3** show the ratios of the two

sets. Without non-linear effects, the ratio between spectra recorded at different absorber concentration should produce a horizontal line at intercept 0.1. The graphs show a clear deviation of up to 20% from this expected straight line. The deviations are strongest for strongest convolution. And the strongest deviations occur, where the original spectrum has its steepest flank at the band heads. To reduce this effect, the spectrometer's function must be more narrow than the spectral width of the pixels, because then spectral mixing will basically take place within the spectral interval of a pixel – cross pixel mixing would be neglectable. But even for a zero-width spectrometer's function, i.e. fully resolved spectra, the non-linear behaviour does not disappear from the ratio. The residuals then have to be the result of the finite width of the integration interval.

In some applications a strategy to resolve problems of insufficient binning is to reduce spectral resolution, i.e. to use a broader spectrometer's function. The above considerations show, that to a certain degree this strategy forces a trade-off on linearity. Similar to the discussed effect of the steep flanks of the absorption spectrum $\sigma(\lambda)$, any sharp variations in the light source spectrum $I_0(\lambda)$ will have the same effects. This is the background for the so-called "I_0-effect" in differential optical absorption spectroscopy (DOAS) measurements (compare [Johnston 1996, Richter 1997] and references therein), where Fraunhofer lines in the solar spectrum create artefacts in absorption spectra measured in the atmosphere.

To avoid the complications caused by dividing integrated recordings I_i and $I_{0,i}$, an alternative mathematical relationship between the product of $L \cdot \sigma(\lambda) \cdot [M]$ and the measured quantities I_i and $I_{0,i}$ needs to be found. It should take into account the *integral nature of the pixel signals* I_i and $I_{0,i}$ as expressed in **(2)** and should under certain conditions become independent of the spectrometer's function and convolution contained in **(3)**.

Motivated by the signal's integration on the pixels, it is tempting to use intensities, which are *integrated across a certain wavelength interval*, i.e. which are summarised pixel readouts. As a consequence, the full incident intensity within the considered interval will be used, no matter what the individual pixel signals had been. Spectral mixing due to a spectrometer's function of finite width will be without effect within the interval of integration. At the boundaries spectral mixing will occur across roughly as many pixels, as make up the width of the spectrometer's function. Light from outside the selected spectral interval will be mixed across the boundary into the interval and vice versa. This will be without effect, if the intensity within this cross-boundary mixing area – with and without absorption - does not

change significantly or if the mixing area is small relative to the width of the spectral interval as a whole. The processing of such integrated intensities must then establish a mathematical link to the in this context sought physical quantities, which are contained in the product of $L \cdot \sigma(\lambda) \cdot [M]$.

This concept is partly motivated by a similar approach, which is used in resonance absorption spectroscopy. There also integrated intensities are considered, because the atomic lines under study are in general far smaller than the resolution of the used spectrometers (see **Chapter 4** and references therein). In the analysis of resonance absorption data, the line shapes of absorber and emitter are introduced in the form of analytical line shape functions, which are justified by atomic physics, compare equations **(4-1)** and **(4-4)**. The approach developed here follows the same line of thinking. But instead of analytical atomic line shapes, an approximation to the true molecular absorption spectrum as well as the true incident light source spectrum has to be used. Such can be higher resolved and finer binned recordings from another measurement. These in the following will be referred to as the necessary *a-priori spectra*. The method will make use of numeric integration of multichannel measurements, why in the following it will be referred to as "Multichannel Integrated Absorption Spectroscopy", or – more shortly – "MIntAS".

9.3 INTEGRAL APPROACH TO COARSELY BINNED MEASUREMENT DATA

An integral of intensity is considered, denoted by $I(\lambda_1,\lambda_n)$, covering n pixels where the integral is determined across a spectral interval of wavelength λ_1 to λ_{n+1} (refer to **(2)**). The interval is selected such that it firstly covers the spectral feature under study – e.g. the rotational-vibrational absorption band – completely. Secondly it has to be assured, that the aforementioned cross-boundary mixing is of negligible magnitude. The integration then corresponds to the sum over a *number of pixels*, namely from 1 to n. For the intensity measured *without absorber* one gets:

$$I_0(\lambda_1,\lambda_n) = \int_{\lambda_1}^{\lambda_{n+1}} I_0(\lambda)\,d\lambda = \sum_{i=1}^{n} \int_{\lambda_i}^{\lambda_{i+1}} I_0(\lambda)\,d\lambda = \sum_{i=1}^{n} I_{0,i} \qquad \textbf{(6)}$$

The same expression for the case of intensity measured *with absorber* reads:

$$
\begin{aligned}
I(\lambda_1,\lambda_n) &= \int_{\lambda_1}^{\lambda_{n+1}} I(\lambda)\,d\lambda \\
&= \int_{\lambda_1}^{\lambda_{n+1}} I_0(\lambda)\cdot\exp(-L\cdot\sigma(\lambda)\cdot[M])\,d\lambda \\
&= \sum_{i=1}^{n}\int_{\lambda_i}^{\lambda_{i+1}} I_0(\lambda)\cdot\exp(-L\cdot\sigma(\lambda)\cdot[M])\,d\lambda \\
&= I(\lambda_1,\lambda_n,L,\sigma(\lambda),[M])
\end{aligned}
\qquad \textbf{(7)}
$$

Here the fact was used that for continuous functions of wavelength λ the usage of the Beer-Lambert law **(1)** is rigorous and correct. Therefore $I(\lambda)$ can be expressed as a function of $I_0(\lambda)$ and the parameters defining the absorption process, contained in the product $L\cdot\sigma(\lambda)\cdot[M]$. But the relationship is complicated by the fact that the exponential is contained within an integral expression.

9.3.1 Definition of observable D as absolute absorption

With **(6)** and **(7)** now a quantity has to be defined, which can be deduced from the observational data $I_0(\lambda_1,\lambda_n)$ and $I(\lambda_1,\lambda_n,L,\sigma(\lambda),[M])$. The objective is to establish a mathematical link between this observational data and the parameters L, $\sigma(\lambda)$, and [M]. A reasonable choice is the difference between $I_0(\lambda_1,\lambda_n)$ and $I(\lambda_1,\lambda_n,L,\sigma(\lambda),[M])$. To distinguish it from relative quantities as used in the context of the Beer-Lambert law or in resonance absorption it is referred to as *absolute absorption D*:

$$
\begin{aligned}
D(\lambda_1,\lambda_n,L,\sigma(\lambda),[M]) &= I_0(\lambda_1,\lambda_n) - I(\lambda_1,\lambda_n,L,\sigma(\lambda),[M]) \\
&= \int_{\lambda_1}^{\lambda_{n+1}} I_0(\lambda)\,d\lambda - \int_{\lambda_1}^{\lambda_{n+1}} I(\lambda,L,\sigma(\lambda),[M])\,d\lambda \\
&= \int_{\lambda_1}^{\lambda_{n+1}} I_0(\lambda) - I(\lambda,L,\sigma(\lambda),[M])\,d\lambda \\
&= \int_{\lambda_1}^{\lambda_{n+1}} I_0(\lambda)\cdot(1-\exp(-L\cdot\sigma(\lambda)\cdot[M]))\,d\lambda
\end{aligned}
\qquad \textbf{(8)}
$$

Given that cross boundary mixing can be neglected, this expression is correct for any number of pixels. The difference D on the left introduces the observational data from the experiment, i.e. the difference of sums of pixel signals:

$$D(\lambda_1, \lambda_n, L, \sigma(\lambda), [M]) = \sum_{i=1}^{n} I_{0,i} - \sum_{i=1}^{n} I_i \qquad \textbf{(9)}$$

The integral on the right side of **(8)** introduces the true continuous valued functions of absorber cross section $\sigma(\lambda)$ and light source intensity $I_0(\lambda)$ as well as the parameters L and·[M]. In contrast to the common usage of the Beer-Lambert law in the approximate pixelwise formulation, here not a single value of absorption cross section per pixel is involved, but the true shape of absorption cross section across the full interval under study and as a continuous function of wavelength λ.

For signal to noise reasons the variable of interest in quantitative absorption spectroscopy or in chemical kinetics is in many cases the absorption at the peak of an absorption band. Having this in mind, the analogy to resonance absorption can be further exploited: *There* also an integral across a combined emission-absorption structure is recorded. For both the emission line as well as for the absorption line the line profile is approximated by a mathematical function based on a-priori knowledge. The unknown is the peak value of the absorption line profile. Following this line of thinking, the absorption cross section $\sigma(\lambda)$ can be split into its peak value σ_{max} and its spectral band shape $\sigma_{norm}(\lambda)$, which in its peak is normalised to unity:

$$\sigma(\lambda) = \sigma_{max} \cdot \sigma_{norm}(\lambda) \quad \text{with} \quad \max(\sigma_{norm}(\lambda)) = 1 \qquad \textbf{(10)}$$

So $\sigma_{norm}(\lambda)$ can now be interpreted as the true and a-priori known shape of the absorption band as measured in a higher resolved and more finely binned measurement. The product $L \cdot \sigma_{max} \cdot [M] = A_{max}$ then consequently correspond to the unknown peak absorption, which is to be determined from the integrated observational data D obtained from a lower resolved and more poorly binned measurement. Inserting **(10)** into **(8)** and reordering the factors yields:

$$D(\lambda_1, \lambda_n, L, \sigma(\lambda), [M]) = \int_{\lambda_1}^{\lambda_{n+1}} I_0(\lambda) \cdot (1 - \exp[-(L \cdot \sigma_{max} \cdot [M]) \cdot \sigma_{norm}(\lambda)]) \, d\lambda \qquad \textbf{(11)}$$

Completing the analogy to resonance absorption the continuous valued intensity spectrum $I_0(\lambda)$ on the right side corresponds to the a-priori known emission line shape. Therefore $I_0(\lambda)$ also needs to be known a-priori and in higher resolution and better binning, same as for $\sigma_{norm}(\lambda)$. How to obtain this will be considered below.

So for now the task remains to solve **(11)** for the product $L\cdot\sigma_{max}\cdot[M]$. After Taylor series expansion of the exponential function, consideration of on-pixel integration as in **(7)** and a rearrangement of the summations, the following expression results:

$$\begin{aligned} D(\lambda_1,\lambda_n,L,\sigma(\lambda),[M]) &= \sum_{p=1}^{\infty}(L\cdot\sigma_{max}\cdot[M])^p\cdot\sum_{i=1}^{n}\int_{\lambda_i}^{\lambda_{i+1}} I_0(\lambda)\cdot(-1)^{p+1}\cdot\frac{\sigma_{norm}(\lambda)^p}{p!}\,d\lambda \\ &= \sum_{p=1}^{\infty}(L\cdot\sigma_{max}\cdot[M])^p\cdot C_p \end{aligned} \qquad \textbf{(12)}$$

This is a polynomial expression of variable $L\cdot\sigma_{max}\cdot[M]$ and coefficients C_p, which depend on $I_0(\lambda)$ and $\sigma_{norm}(\lambda)$. In the present form the latter two and therefore the C_p are not yet accessible.

9.3.2 Role and origin of $\sigma_{norm}(\lambda)$ and $I_0(\lambda)$

One of the objectives is to establish a mathematical link between absorption cross section measurements of different resolution and binning. Therefore it is reasonable to approximate the continuous $\sigma_{norm}(\lambda)$ in **(12)** by a discrete, pixelwisely calculated absorption $\sigma_{norm,\,j}$, (j=1,..,m and m>n) from a higher resolved and more finely binned measurement. This implies the extraction of the peak absorption $L\cdot\sigma_{max}\cdot[M]$ with respect to this higher resolved $\sigma_{norm,j}$ from the lower resolved and more coarsely binned observable D. The approach is rigorous in the sense that it establishes an "upward compatibility" between different measurements. The better the true $\sigma_{norm}(\lambda)$ is approximated by $\sigma_{norm,\,j}$, (j=1,..,m and m>n), the closer the determined σ_{max} will approximate the true peak value $\sigma(\lambda_{max})$. The true $\sigma(\lambda_{max})$ is the upper limiting value of this upward compatible approximation series of σ_{max}. (Note: Quantities expressed as a continuous function of wavelength λ (as "$\sigma(\lambda_{max})$") are understood as true quantities. Opposed to that "σ_{max}" is the result of the discrete treatment of the problem.)

Similarly, also the light source signal $I_0(\lambda)$ needs to be approximated at the same spectral resolution and binning as $\sigma_{norm,\ j}$. Putting it in a practical way: From the *measured*, lower resolved and more coarsely binned $I_{0,i}$ (with i=1,..,n<m), now an *artificial*, higher resolved and more finely binned $I_{0,j}$ (with j=1,..m and m>n) needs to be derived. To avoid confusion: $I_0(\lambda)$ is the intensity spectrum as it was present in the experiment, in which the low resolution and coarsely binned observable $D(\lambda_l,\lambda_n,L,\sigma(\lambda),[M])$ was determined. (Note: Subscript i is used to indicate the less well resolved and binned measurement with i=1,..,n. Subscript j designates the better resolved and finer binned measurement with j=1,..,m, *with m>n*).

9.3.3 Numerical aspects of approximating the a-priori needed $\sigma_{norm}(\lambda)$ and $I_0(\lambda)$

Without loss of generality it can be assumed that the binning of $I_{0,j}$ as well as $\sigma_{norm,\ j}$ can be interpolated such, that the *pixel borders* of the more coarsely binned measurement $I_{0,i}$ coincide with *data points* of both $I_{0,j}$ and $\sigma_{norm,\ j}$. In that case it is assured that each pixel of $I_{0,i}$ is always covered exactly by a corresponding set of points of $I_{0,j}$ and $\sigma_{norm,\ j}$. This facilitates numerical treatment of the differently resolved and binned datasets. The number of data points of the higher resolved and finer binned dataset (m) will then depend on the pixel number m_{pix} of the more coarsely binned measurement as $m = n \cdot m_{pix} + 1$.

The reference $I_{0,j}$ at points j of the true $I_0(\lambda)$ could be determined by interpolating the coarse measurement $I_{0,i}$ onto the finer grid of $\sigma_{norm,j}$. This will be applicable, if the light source's spectrum is sufficiently smooth within the region under study and on-pixel integration can be neglected. This for example would be a possible approximation for the smooth spectrum of a Tungsten Halogen lamp. If spectral features, which are narrow in comparison to the spectrometer's function and the spectral width of the pixels – as, e.g. emission lines in some regions of a Xenon arc lamp's spectrum, Fraunhofer lines in the solar spectrum, or any other sharp features created by the spectroscopic set-up itself - are contained in the light source's spectrum, a different approach has to be used. In that case a higher resolved and more finely binned light source spectrum $\hat{I}_{0,k}$ from a completely different measurement but of the same type of light source has to be used, which has to be interpolated onto the grid of $\sigma_{norm,\ j}$. The result designated by $\hat{I}_{0,j}$ then has to be scaled and fitted to the measured $I_{0,i}$ to account for different experiment conditions. This procedure will yield the necessary artificial spectrum $I_{0,j}$. In the scaling and fitting process again the integral nature of pixel signals $I_{0,i}$ has to be

taken into account. In this approach – similar as in the case of $\sigma(\lambda)$ - the discrete intensity spectrum $\hat{I}_{0,k}$ has to be used as an approximation to the true continuous valued light source spectrum. Assuming that the interpolation onto the correct grid has already been done, the fitting of $\hat{I}_{0,j}$ to the experiment's conditions can for example be done by a polynomial approach and a simple trapezoidal numerical integration:

$$I_{0,i} = \Delta\lambda \cdot \sum_{j} \frac{I_{0,j} + I_{0,j+1}}{2} = \Delta\lambda \cdot \sum_{j} \frac{\hat{I}_{0,j} \cdot P(\lambda_j) \; + \; \hat{I}_{0,j+1} \cdot P(\lambda_{j+1})}{2} \qquad \textbf{(13)}$$

for each pixel i=1,...,n, where the summation index j covers all fine pixels falling into the coarse pixel i. The difference between the two light source measurements is taken into account by introducing the scaling polynomial $P(\lambda_j)$ of variable λ_j. The coefficients of this polynomial can be determined such that for each pixel i=1,..,n equation **(13)** is fulfilled in an optimal way in the sense of a least squares fit.

Inserting the thus obtained discrete variables $I_{0,j}$ and $\sigma_{norm,j}$ as an approximation to the continuous valued $I_0(\lambda)$ and $\sigma_{norm}(\lambda)$, the coefficients C_p in **(12)** can themselves be approximated:

$$\begin{aligned} C_P &= \sum_{i=1}^{n} \int_{\lambda_i}^{\lambda_{i+1}} I_0(\lambda) \cdot (-1)^{p+1} \cdot \frac{\sigma_{norm}(\lambda)^p}{p!} \; d\lambda \\ &\cong \Delta\lambda \cdot \frac{(-1)^{p+1}}{p!} \cdot \sum_{j=1}^{m-1} \frac{I_{0,j} \cdot \sigma_{norm,j}^p + I_{0,j+1} \cdot \sigma_{norm,j+1}^p}{2} \\ &= C_p\left(I_{0,j}, \sigma_{norm,j}\right) \end{aligned} \qquad \textbf{(14)}$$

where the summation over pixels i followed by integration from λ_i to λ_{i+1} is replaced by numerical integration across the whole interval using the finer sampled data points j=1,..,m. Inserting the coefficients $C_p(I_{0,j},\sigma_{norm,j})$, **(12)** can be solved for the variable $A_{max}:=L\cdot\sigma_{max}\cdot[M]$. Depending on the actual task the result can then be used to determine σ_{max} as a function of known concentration [M] or [M] as a function of known σ_{max}. But according to the fundamental theorem of algebra, a polynomial expression of degree n has the same number of roots. Therefore the solution of **(12)** is not unambiguous.

9.3.4 Strategies for finding the correct root

To find the correct – i.e. physically meaningful - root, in a first step all imaginary roots can be rejected. In the calculation itself the number of remaining real roots might depend on the numerical conditions and indirectly thereby on the selected maximum degree of the series expansion. At which order the series expansion can be truncated without loss of accuracy depends on the coefficients as well as on the machine precision. The truncation order has to be determined accordingly. The identification of the correct real root is facilitated by remembering, that the product $L \cdot \sigma_{max} \cdot [M]$ corresponds to the Beer-Lambert optical density observed at λ_{max} at the top of $\sigma_{norm}(\lambda)$:

$$A_{max} = L \cdot \sigma_{max} \cdot [M] \approx L \cdot \sigma(\lambda_{max}) \cdot [M] = A(\lambda_{max}) \qquad \textbf{(15)}$$

Varying the absorber's concentration and thereby the observational input D will cause the true Beer-Lambert optical density $A(\lambda_{max})$ to vary in the same systematic manner. According to **(15)** the physically meaningful solution A_{max} has to vary in the same systematic way. The other real roots will in general not vary in the same way. In case that **(12)** is applied to time resolved measurements, the temporal variation of D(t) provides exactly such a criterion. The physically meaningful root $A_{max}(t)$ will have to show the same systematic temporal behaviour as the time dependent observable D(t), as it directly depends on the time varying concentration [M](t). Once the physically meaningful root $A_{max}(t)$ is identified, this will directly correspond to a peak optical density as it would have been recorded under high resolution and fine binning conditions of $\sigma_{norm,j}$. Non-linear behaviour with respect to absorber concentration, as it has to be anticipated for the coarsely binned *apparent* optical density data, will be as much corrected for, as the more finely binned $\sigma_{norm,j}$ is free of this effect. If $\sigma_{norm,j}$ is sufficiently well resolved and sufficiently finely binned, the non-linearity between absorber concentration and optical density will be fully removed.

9.4 VALIDATION USING ARTIFICIAL TEST DATA

To validate the method described above, discrete experimental data was simulated as described in the context of **Fig. 9.3**, see above. Used were the same *measured* finely binned high resolution intensity spectrum $I_{0,j}$ and the same likewise *measured* IO absorption spectrum $\sigma_{norm,j}$ as approximations to the physically true quantities $I_0(\lambda)$ and $\sigma(\lambda)$. True peak optical

density $\sigma_{norm,max}$ was set to 1.0 (at λ_{max}=427.2nm). From this base data via **(4)** the simulated experimental $I_{0,i}$ and I_i as well as $A_{app,i} = \ln(I_{0,i}/I_i)$ were calculated. Different spectroscopic conditions were simulated by varying the width of the (gaussian) spectrometer's characteristic function $S(\lambda)$ from 0.0nm (i.e. no convolution, fully resolved, but nevertheless binned) up to 1.4nm FWHM (spectroscopic, not Gaussian 1/e width). Pixel width and linear dispersion were kept constant at 0.32nm per 26µm pixel width. For all cases also a shift in wavelength relative to the detector was simulated. 10 shifts of 0.1 pixel each were applied. In **Fig. 9.4** – among other results - the effect of instrumental characteristics on the peak value of *apparent* optical density $A_{app,i}$ is shown (filled squares, $A_{app,max}$). $A_{app,max}$ is plotted as a function of wavelength shift. From left to right each subplot resembles one set of shifts, each subplot at one specific spectrometer's function. For fully resolved intensity spectra (leftmost, "0.0nm FWHM") the influence of wavelength shift shows the largest effect on $A_{app,max}$ of up to 13%. With increasing width of the instrument's function this effect reduces, as sharp features in the spectra are "smeared out". As a trade-off, $A_{app,max}$ more and more underestimates the true peak absorption of 1.0 falling seriously off to values around 0.5 at 1.4nm FWHM. The latter correspond to coarse but nevertheless realistic measurement conditions. An apparent shift of the maximum position as a function of FWHM is also observed across as many as six pixels (≈1.8nm).

For validation of MIntAS, the artificial datasets of $I_{0,i}$ and I_i were subjected to the MIntAS method. If it worked correctly, the true maximum optical density of 1.0, which was used in the creation of the test data, should be reproduced. To examine the effect of the a-priori data $I_{0,j}$ and $\sigma_{norm,j}$, differently well resolved data was used for them. As the ideal case, a set of $I_{0,j}$ and $\sigma_{norm,j}$ recorded under *the same spectroscopic conditions* as the initially assumed "true" quantities was used as MIntAS a-priori data (0.12nm FWHM, 0.32nm per 26µm pixel width). This should reproduce the original maximum optical density of 1.0 exactly. But also two sets of significantly less well resolved signals were used (0.35nm FWHM and 0.62nm FWHM, both 0.32nm per 26µm pixel width). The results from these three MIntAS retrievals are shown in **Fig. 9.4** as three different rows of open circles.

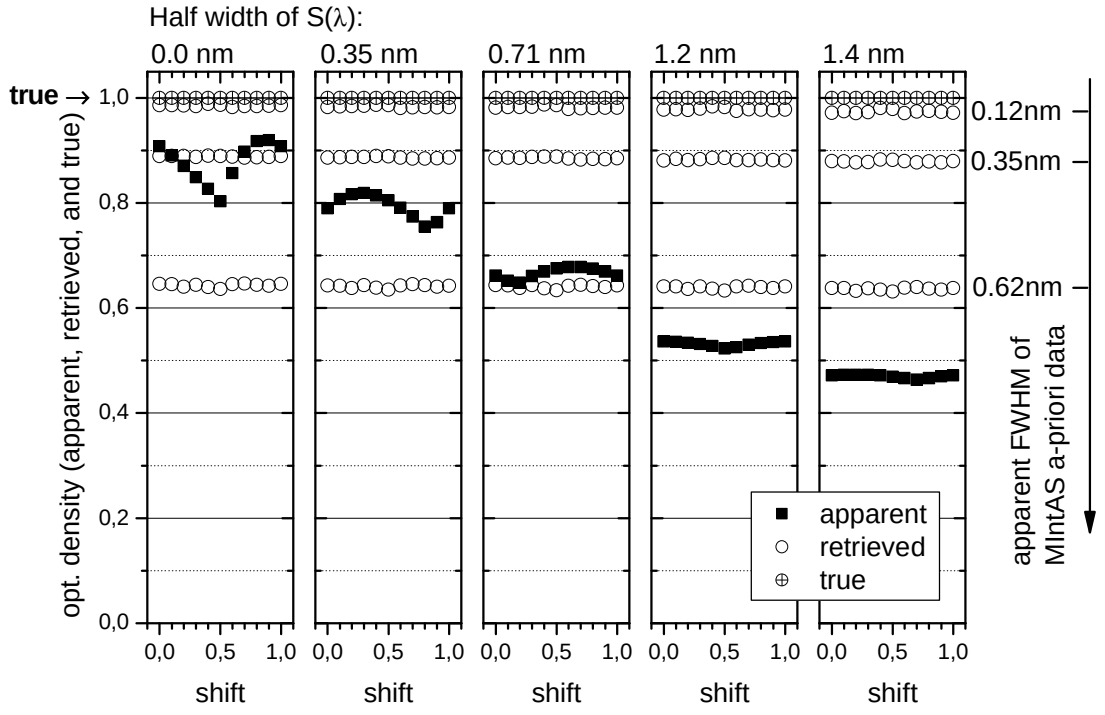

Figure 9.4 Simulated peak absorption $A_{app,max}$ of the IO(4←0) transition is shown (filled squares). True peak absorption was set to 1.0. $A_{app,max}$ was calculated for five spectrometer's functions (five subplots from left to right) and depending on a wavelength shift relative to the detector (0.0 to 1.0 pixels in steps of 0.1 pixel, bottom axis). The spectrometer's functions differed in half width as indicated above. Pixel size of 0.32nm spectral width per 0.26µm geometric width was constant for all. The variation of $A_{app,max}$ with pixel offset becomes smaller with increasingly coarse spectrometer's function. At the same time the true peak absorption of 1.0 is more and more underestimated. Open circles show three series of MIntAS retrieved peak absorptions A_{max} obtained for three different a-priori spectra labelled by their measured FWHM (right side). In each subplot the effect of pixel offset is corrected by MIntAS. For a high resolution a-priori spectrum the underestimation is removed to within ±2% by MIntAs (top row of open circles).

As a first result it can be stated that the dependence on wavelength shift, which was present in the peak value $A_{app,max}$ (filled squares) is no longer present in the MIntAS-retrieved results. This is reasonable, as the MIntAS-approach uses a wide spectral interval instead of just a single pixel to retrieve the absorption at the peak wavelength. It should therefore be independent of sub-pixel wavelength shifts.

With respect to the maximum value itself the results are more complex. For a-priori data sets of the same resolution and binning (1200grvs·mm^{-1}, 75µm slit width → 0.04nm/pix and FWHM=0.12nm) the retrieved peak absorption in one case lies systematically 2% low (shown in **Fig. 9.4**, open circles, top row) while in others (not shown) similarly systematically between this and 2% high. This is most likely due to uncorrected background absorptions in

the a-priori data. Based on that the systematic uncertainty for this specific retrieval is estimated to ±2%. Within this 2% uncertainty any underestimation due to low resolution and coarse binning is successfully corrected by MIntAS for all simulated datasets (0.0nm, 0.35nm, 0.71nm, 1.2nm, and 1.4nm FWHM of spectrometer's function, horizontal label axis).

When less well resolved and less finely binned data was used (1200grvs·mm^{-1}, 240µm slit width → 0.04nm/pix and FWHM=0.35nm as well as 300grvs·mm^{-1}, 100µm slit width → 0.16nm/pix and FWHM=0.62nm: both open circles, middle and bottom row), the retrieved data itself more and more underestimated the initially selected true peak absorption of 1.0. This leads to the at first sight strange effect that MIntAS in some cases produces smaller values than those obtained in the simulated measurement for $A_{app,max}$ themselves. The reason for this behaviour lies in the fact, that the MIntAS approach fits an integrally determined absolute absorption "under a given curve" of assumed "true" absorption cross section (the a-priori data). If $A_{app,max}$ – the measurement – resulted from a better resolved and more finely binned measurement than the a-priori cross section spectrum used in MIntAS, the same amount of absolute absorption (determined from $A_{app,i}$) can be fitted under a less high (because less resolved and therefore wider) a-priori cross section profile $\sigma_{norm,j}$. Therefore the retrieved A_{max} from MIntAS turn out smaller than the $A_{app,max}$. This demonstrates, that this method of transforming absorption measurements from one set of conditions to another works in both directions: "upwards" as well as "downwards". A critical issue in the a-priori cross section spectrum used in the MIntAS retrieval is the possible presence of a systematic and uncorrected background absorption. The same is true of the observational data $I_{0,i}$ and I_i, from which the peak absorption A_{max} is to be retrieved by MIntAS. This illustrates the need of truly separated absorber spectra as obtained in **Chapter 7**.

9.5 Validation Using Low Resolution and Coarsely Binned Time Resolved Measurements of Iodine Monoxide IO

The data used for validation was recorded using the CCD set-up described in **Chapter 6**. The absorption spectra recorded for iodine monoxide IO were centred around the IO(4←0) absorption transition. Different combinations of grating and entrance slit width were used to study the effect of resolution and binning on the shape and size of the apparent IO optical density, i.e. $A_{app,i}$. During these series of measurements the chemical conditions and therefore the IO concentration was maintained constant. By regularly repeated measurements under

identical spectroscopic conditions this stability was checked and could be shown to be better than ±2.5%/h. Using these stability check measurements, any detected drifts in the chemical system could be corrected. Thereby it was assured that the deduced apparent optical density $A_{app,i}$ of the IO absorption was only changed by effects of resolution and binning. The peak absorption under highest resolution (IO(4←0) nearly fully resolved, 1200 grooves·mm^{-1} → 0.04nm/pix, effective FWHM=0.12nm) amounted to 0.29 in units of (apparent) optical density. All apparent peak values $A_{app,max}$ were normalised relative to that obtained with 1200grvs·mm^{-1} and 150µm entrance slit (producing 0.23nm FWHM), which were the conditions of the stability check measurements. Therefore a larger number of measurements existed for these specific conditions, which enabled averaging and reduction of scatter.

In **Fig. 9.5** the normalised peak values of apparent optical density thus determined are plotted (open circles). They show the expected increase of peak absorption $A_{app,max}$ when resolution and linear dispersion were increased. The averaged reference value at 0.23nm FWHM is indicated by a large open circle with a centred cross. The reduction of peak absorption between highest resolution (1200 grooves·mm^{-1}, 75mm slit → 0.12nm FWHM) and lowest resolution (150 grooves·mm^{-1}, 75mm slit → 0.96nm FWHM) amounted to approx. 36%. This is less than in the simulated data. But there the true peak absorption was assumed to be 1.0, which is roughly 3 times higher than in the true measurements considered here. Therefore any effects of the non-linear character of **(4)** should be significantly stronger than in the more moderate measurement's case.

To validate the MIntAS method, from a measurement of IO recorded under same chemical conditions, but under low resolution and coarse binning (150grvs·mm^{-1}, 100µm entrance slit width corresponding to 0.32nm/pixel and 1.2nm FWHM) the peak absorptions were retrieved with MIntAS using differently well resolved and differently binned spectra as a-priori spectra. Background absorbers in the a-prior spectra were corrected by subtracting any absorption showing up in the trough to the red side of the IO(4←0) transition. This simple method could be used, because the IO(4←0) absorption transition in our experiments was considerably free of other absorber background and because the IO absorption itself in the trough is negligible. Nevertheless for a more accurate analysis the separation of absorbers following the methods described in **Chapter 7** and Gómez-Martín et al. [2003] is recommended.

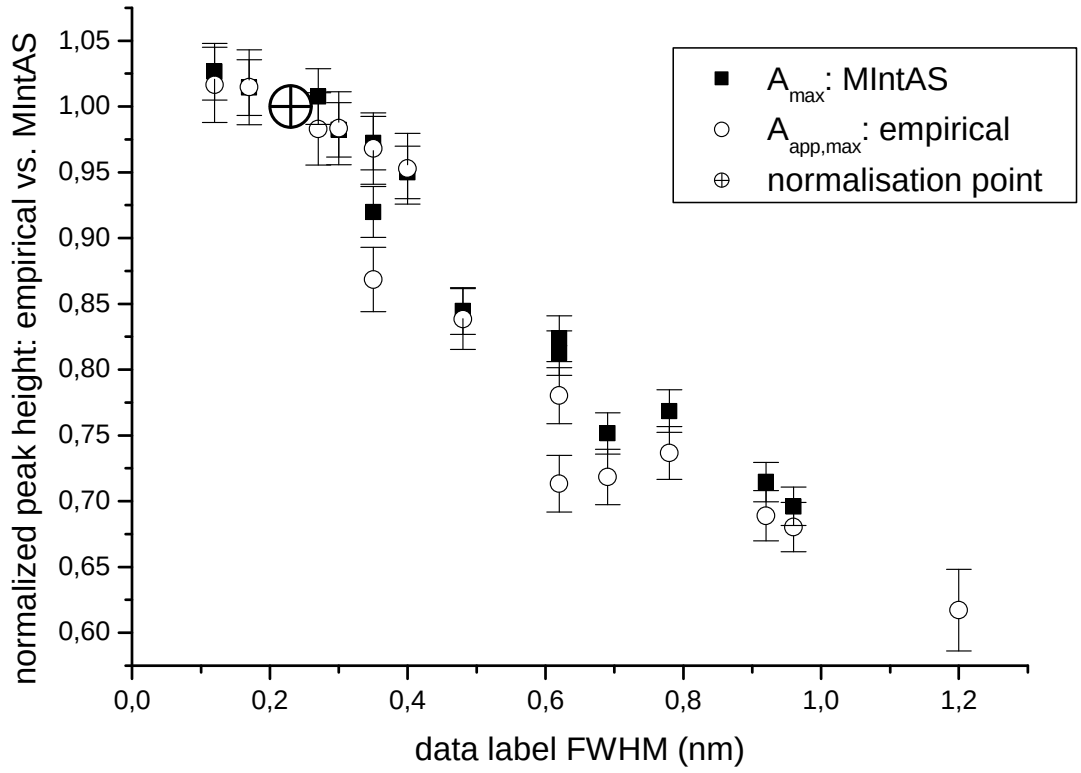

Figure 9.5 The apparent peak absorption of the IO(4←0) absorption band under different spectroscopic conditions was determined. Firstly by direct measurement yielding $A_{app,max}$, where the chemical conditions were maintained constant (open circles). And secondly by retrieving peak absorptions A_{max} from a low resolution, coarsely binned measurement relative to different higher resolved, finer binned a-priori spectra using the MIntAS retrieval method (filled squares). All values normalised relative to the corresponding value obtained at 0.23nm FWHM. The error bars were determined as the standard deviation of the scatter of data points after systematic data behaviour had been removed by a suitable polynomial fit. They are of the order of 2,1% (MIntAS) and 2,8% (direct measurement). The agreement between MIntAS and measured peak absorptions is for all but two data points well within the error limits supporting the validity of the MIntAS method. On average the remaining disagreement between both methods is of the order of 3.1%.

The peak absorptions retrieved by MIntAS were again all normalised relative to the 0.23nm FWHM retrieval and are plotted in **Fig. 9.5** as filled squares. The error bars in both cases were determined as the standard deviation of data points after systematic behaviour had been removed by subtraction of a suitable polynomial. For the 1200grvs·mm^{-1} measurements the normalised MIntAS retrieved A_{max} coincide quite accurately with the $A_{app,max}$ data determined experimentally. For 300grvs·mm^{-1} as well as for 150grvs·mm^{-1} the MIntAS retrieved A_{max} lie slightly but systematically higher than the empirically determined values, but the agreement for all but two data points is still within the error limits. On average the disagreement is of the order of no more than 3.1% and the systematic behaviour of peak absorption is clearly reproduced validating the MIntAS approach. The remaining discrepancy could be caused by insufficient correction of background absorber in the MIntAS low resolution input spectrum.

9.6 APPLICATION TO TIME RESOLVED MEASUREMENTS OF IODINE MONOXIDE IO IN THE CONTEXT OF CHEMICAL KINETICS

Having in this way gained confidence into the method, it is applied to time resolved measurement of IO, to check the influence of non-linearity on deduced kinetic constants. An analysis method in chemical kinetics is to determine the behaviour of absorber consumption ("decay") with respect to certain models reflecting specific forms of reactions and conditions. Such are pseudo first order or second or higher order consumption. In that context the data is plotted logarithmically or inverse resp., as in that case the observational data should result as a straight line if the assumed (tested) consumption characteristics are correct (i.e. first or second order resp.). A simple and straightforward approach (Refer to Laidler [1987] for further details on chemical kinetics methods). But both logarithmic as well as inverse representations have their own typical sensitivities to disturbances in the observational data, especially towards the end of consumption traces, where concentration of the absorber under study becomes small. Such disturbances could be either a remaining, uncorrected background absorption or a non-linear behaviour due to insufficient resolution and/or binning.

The simulation of apparent optical density $A_{app,i}$ had shown that this does not necessarily depend linearly on absorber concentration (compare context of **Fig. 9.3**, see above). In the simulations the deviation from linearity reached the order of 3% when comparing true optical density of 0.1 and 1.0 for the IO(4←0) absorption transition. This indicates the order of magnitude to be expected of such effects. As in this context non-linearity due to resolution and binning is to be evaluated, care had to be taken to avoid disturbances from remaining background absorbers. Therefore in time resolved measurement data the IO absorption was separated from any other absorbers using the methods described in **Chapter 7** and Gómez-Martín et al. [2003]. A full dataset of $A_{app}(\lambda,t)$ as a function of pixels and time steps was obtained by suitable multiplication of the separated pure time curve and pure spectrum of IO. The separated absorption of IO was free of other absorptions with an accuracy of better than ±3%. Using this, *absolute absorption* D(t) – now as a function of time - for IO(4←0) was calculated according to **(9)** via $I_{0,i}(t)$ and $I_i(t)$, which only contained absorption due to IO. The a-priori spectra for MIntAS were the ones described in **Section 9.5**.

The combination of separation methods and MIntAS is not fully consistent, because the separation methods are based on the assumption that overlapping absorbers are present as linear combinations of their individual optical densities. Yet in the context of MIntAS this

linearity is explicitly questioned. The fact that the separation of absorbers can be achieved at a high accuracy without systematic residuals supports the assumption that for *separation* the non-linearity is only a minor issue. But after separation and subsequent application of MIntAS, it is difficult to distinguish to which degree the tested chemical kinetics fits are influenced by the inconsistent combination of methods or by non-linearity due to insufficient resolution and binning. To overcome this, MIntAS is applied using *differently finely binned high resolution* a-priori spectra. If a non-linearity due to insufficient resolution and/or binning is present, it should depend systematically on the degree of resolution and binning present in the a-priori spectrum. **Fig. 9.6** shows the ratios between different MIntAS retrieved $A_{max}(t)$ from time resolved measurements, which used differently high resolved a-priori spectra (150gvrs·mm^{-1}, 75µm slit, 0.96nm FWHM to 1200grvs·mm^{-1}, 50µm slit, 0.11nm FWHM) on one hand and the apparent $A_{app,max}(t)$ from a low resolution and coarsely binned measurement of the IO(4←0) transition (150grvs·mm^{-1}, 100µm slit, 1.2nm FWHM) on the other hand. To enable quantitative comparison the ratios have been normalised by the average value calculated from the last 100 time steps.

The top graph shows the variation of maximum optical density in time (apparent $A_{app,max}(t)$ and selected MIntAS retrieved $A_{max}(t)$). The bottom graph shows the ratios themselves. The curved shape of the ratios demonstrates that indeed there is a non-linearity present between absorber concentration (approximated by the MIntAS retrieved $A_{max}(t)$) and apparent optical density $A_{app,max}(t)$. The graphs also prove that non-linearity depends on resolution and binning, because the effect increases systematically with increasing resolution and binning in the a-priori data. Non-linearity caused by the inconsistency of methods can therefore be excluded. Non-linearity reaches as much as 5% in the top absorption at $A_{max}(t)$ of already 0.6 in reasonable agreement with the simulations above. Non-linearity is most likely caused by the steep flank at the band head of the (4←0) transition, which is not sufficiently resolved in the coarse measurement (150grvs·mm^{-1}, 100µm slit, 1.2nm FWHM). **Fig. 9.6** shows further that already at optical densities of slightly more than 0.1 the non-linearity under the mentioned spectroscopic conditions is of the order of 0.5%. This emphasizes the necessity of checking resolution and binning relative to the spectral feature under study.

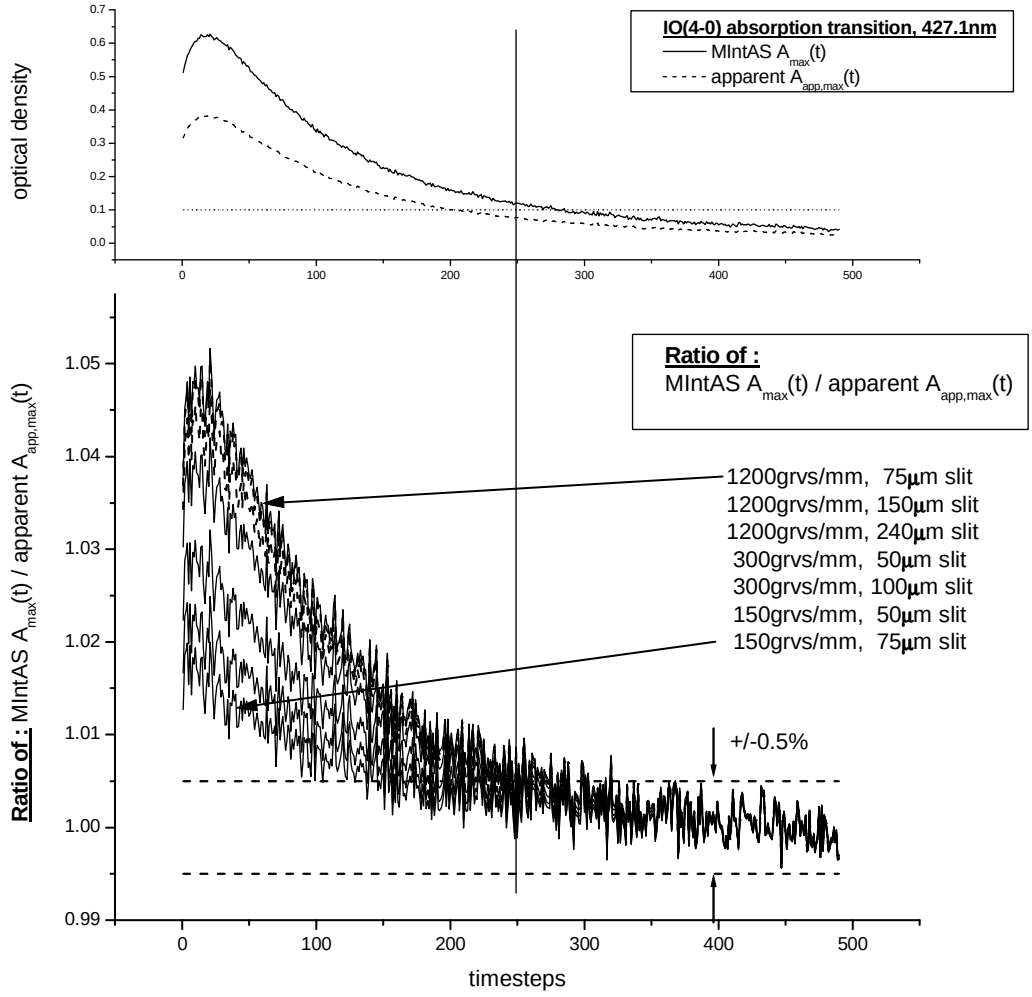

Figure 9.6 The ratios between different MIntAS retrieved optical densities $A_{max}(t)$ from time resolved measurements $I_{0,i}(t)$ and $I_i(t)$ of the iodine monoxide IO(4←0) absorption transition are shown. Differently high resolved a-priori spectra were used (150gvrs·mm^{-1}, 75µm slit, 0.96nm FWHM to 1200grvs·mm^{-1}, 50µm slit, 0.11nm FWHM) to retrieve peak absorptions from the low resolution data (150grvs·mm^{-1}, 100µm slit, 1.2nm FWHM). To enable quantitative comparison the ratios have been normalised by the average value calculated from the last 100 time steps. The top graph shows the variation of optical densities $A_{app,max}(t)$ and one selected $A_{max}(t)$ with time. The curved shape of the ratios indicates clearly a non-linearity between absorber concentration (approximated by the MIntAS retrieved $A_{max}(t)$) and apparent $A_{app,max}(t)$. The systematic increase of this effect with increasing resolution and binning proves that this non-linearity depends on insufficient resolution and binning and not on inconsistency between separation and MIntAS method.

The critical issue is now, in how far the found non-linearity affects the determination of rate coefficients for chemical kinetics studies. To this end an apparent optical density $A_{app,max}(t)$ and a MIntAS retrieved $A_{max}(t)$ are each treated as it would be the case in a kinetic analysis. For each of them firstly the natural logarithm – assuming a test for pseudo first order behaviour of the observed consumption – and then secondly the derivative of this logarithm of optical density was calculated. Compare Laidler [1987] for details on chemical kinetics

analysis. In case the observed decay followed indeed pseudo first order kinetics, a straight line would be expected. The slope of this line would be the quantity of interest. It would directly yield the rate coefficient for the underlying consumption reaction.

In the same way for both apparent optical density $A_{app,max}(t)$ as well as MIntAS retrieved $A_{max}(t)$ firstly the inverse – assuming a test for second order behaviour of the observed consumption – and then secondly the derivative of this inverse were calculated. Again the slope – the derivative – is the quantity of interest. As above, in case the observed decay followed indeed second order kinetics, a straight line would be expected. The slope of this line would directly be equal to the ratio of the rate coefficient of the consumption reaction and the absorption cross section of the absorber under study.

Because in the present case the observed decay follows neither first nor second order due to the specific chemical conditions of the experiment, only the different slopes of the curved plots can in a generalised way be used as a measure for the effect of non-linearity, compare **Fig. 9.7** and **Fig. 9.8**. There in the bottom graph the logarithmic and inverse optical densities are plotted respectively. In the top graphs the corresponding derivatives are shown. The degree to which the derivatives in each case differ between that of $A_{app,max}(t)$ and that of MIntAS retrieved $A_{max}(t)$ expresses the effect of non-linearity on the rate coefficient and ratio of rate coefficient upon cross section, respectively. For the pseudo first order analysis the effect is only minor and reaches no more than 2%, (**Fig. 9.7**). But in the case of a second order analysis the difference in the derivatives reaches as much as 50% (**Fig. 9.8**). If the effect of low resolution and coarse binning in the observational data was neglected in such a kinetic analysis, the error of a deduced rate coefficient or ratio of rate coefficient and cross section would be of exactly the same extent. This clearly demonstrates the necessity of taking resolution and binning effects in studies of chemical kinetics into account.

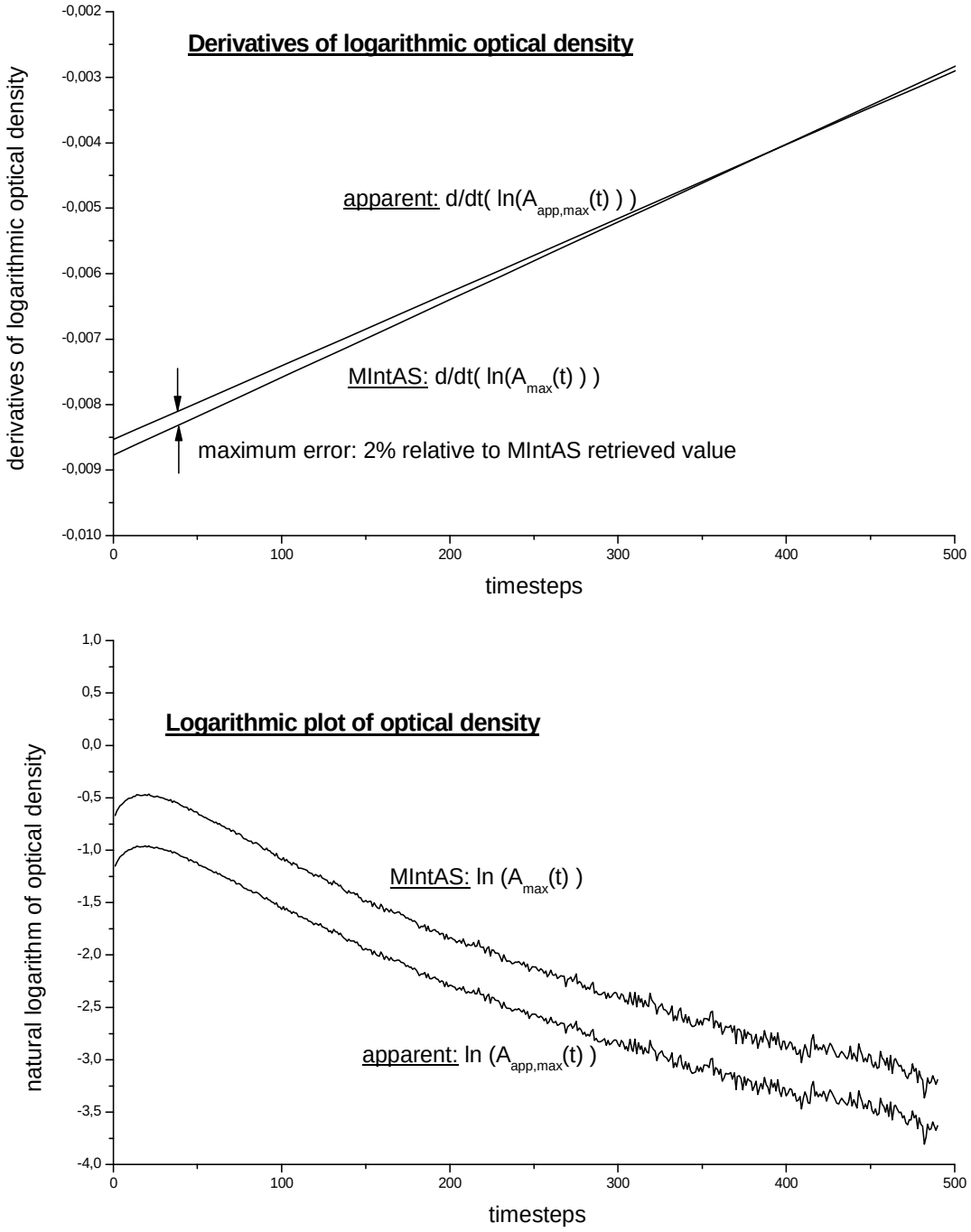

Figure 9.7 In the context of chemical kinetics a test for pseudo first order consumption kinetics is performed by analysing the natural logarithm of optical density (bottom graph) and its derivative (top graph). If the consumption followed pseudo first order consumption, then a straight line would result from the logarithmic data. Its slope would directly yield the rate coefficient of consumption. Due to the chemical conditions in the present experiment this is not fulfilled. Nevertheless *in a generalised way* this approach can be used for estimating the effect of non-linear $A_{app,max}(t)$ versus MIntAS retrieved $A_{max}(t)$ on such an analysis. Here the systematic difference in the derivative is only minor and of the order of 2%.

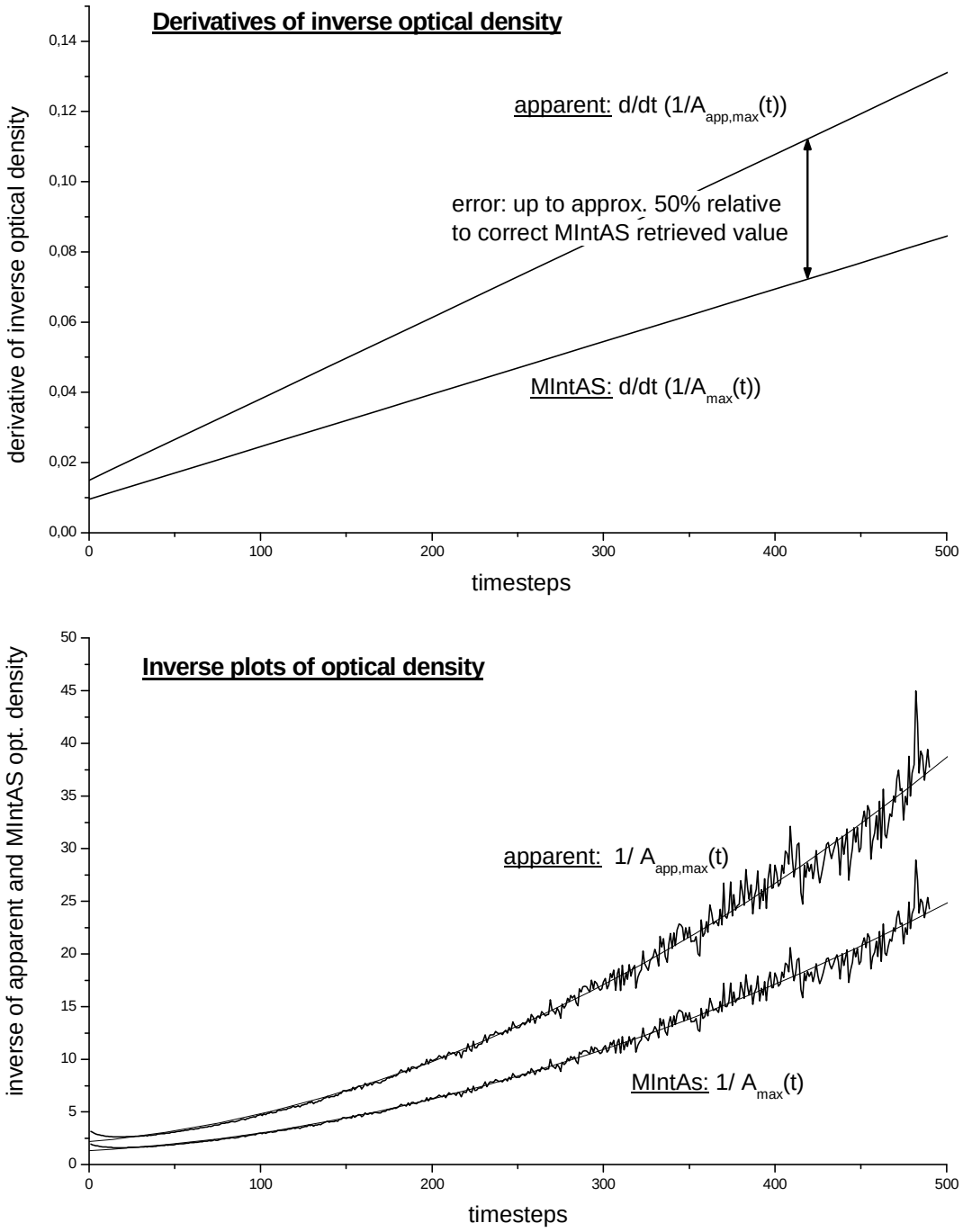

Figure 9.8 Similar as in **Fig. 9.7** a test for second order consumption is illustrated, which requires the inverse of optical density. The slope of inverse optical density yields a measure for the ratio of cross section and rate coefficient. Again the condition itself is not met due to the chemical conditions of the experiment. The inverse of optical density is not linear. Nevertheless the different behaviour of $1/A_{app,max}(t)$ and $1/A_{max}(t)$ can be used as a measure for the effect of non-linearity in $A_{app,max}(t)$ on such an analysis. The deviation amounts to as much as 50% in the derivatives. This would directly be the error of the deduced ratio of rate coefficient upon cross section, if the effect of insufficient resolution and binning was neglected.

9.7 CONCLUSIONS WITH RESPECT TO THE PRESENTED METHOD

The process of recording intensity spectra under low resolution and coarsely binned conditions and their analysis was studied. The effects of coarse spectroscopic conditions on apparent – i.e. pixelwisely calculated - optical density A_{app} has been estimated using simulated but nevertheless realistic test data. A method – in this context introduced as MIntAS: "Multichannel integrated absorption spectroscopy" - was developed which takes the spectroscopic conditions into account. It enables the determination of peak optical densities A_{max} relative to a higher resolved, finer binned and a-priori known absorption spectrum. It thereby provides a means for quantitative comparison of cross section measurements performed under different spectroscopic conditions. The method was successfully validated using simulated test data as well as experimental data. Effects of low resolution and/or coarsely binned spectroscopic conditions on chemical kinetics analysis have also been estimated. This was done using the comparatively "well-behaved" but nevertheless steeply flanked iodine monoxide IO(4←0) absorption transition as test data. In apparent $A_{app,max}$ a non-linearity of approx. 5% was found, which is due to insufficient resolution and too coarse binning. A typical 2^{nd} order chemical kinetics analysis would be sensitive to such a non-linearity causing an error in the deduced rate coefficient or ratio of rate coefficient and absolute cross section of up to 50%. This underlines the importance of taking spectroscopic conditions in chemical kinetics into account even though the initial effect might seem negligible. For molecules of finer structured spectra stronger effects have to be expected and it has to be anticipated that already the determination of concentrations could be disturbed by non-linearity of apparent optical density. In the context of atmospheric remote sensing with ground based or satellite based instruments such candidates could be NO_2 or – especially of interest in the context of iodine chemistry - the measurement of I_2 in the marine boundary layer.

9.8 APPLICATION OF MINTAS IN PREPARATION TO THE METHOD OF IODINE CONSERVATION

The MIntAS method now provides a tool for correcting profiles of optical density versus time for instrument dependent scaling and non-linearity to ensure the validity of the method of iodine conservation. Absorptions to be considered are the IO(4←0) transition, the absorptions of vibrationally excited IO and that of OIO. According to our findings in **Chapter 7** all other

absorptions within this system are either smooth and without ro-vibrational structure or – as in the case of I_2 – can be observed in the continuous parts of their absorption spectra.

So now the MIntAS method has to be applied to the typical "full scale" time resolved measurements. These were normally recorded under broad spectral coverage (150grvs·mm^{-1}, 100µm slit, 1.2nm FWHM). Separation of absorbers was achieved according to **Chapter 7**.

9.8.1 Ground state IO(4←0)

For the method of iodine conservation coarsely binned low resolution data (150grvs·mm^{-1}, 100µm slit, 1.2nm FWHM) was recorded. For the IO(4←0) transition it was shown that the effect of insufficient resolution and coarse binning has in first approximation a significant scaling effect on absolute cross section as well as – in second approximation – a clear non-linearity of up to 6% affecting the applicability of the concept of conservation of iodine. MIntAS could be successfully applied to the IO(4←0) transition. Comparison of the apparent peak height (150grooves·mm^{-1}, 100µm slit, 1.2nm FWHM) and the MIntAS corrected one (a-priori spectrum: 1200 grooves·mm^{-1}, 75µm slit, 0.12 nm FWHM) provides a rough measure of the effect of resolution and binning. The factor between them was determined to be

$$c_{IO} = 1.64 \pm 0.04$$

which implies an underestimation of the IO(4←0) peak absorption of 61% (relative to MIntAS a-priori spectrum) due to limited resolution and binning. Consequently all IO(4←0) data to be used in the method of iodine conservation is pre-processed by MIntAS using an a-priori spectrum recorded with the stated resolution and binning of 1200 grooves·mm^{-1}, 75µm slit, 0.12 nm FWHM. With respect to this a-priori spectrum both scaling and non-linearity are thereby taken into account. Cross sections obtained from this procedure are therefore comparable to the results obtained by Sander [1986]. Spectroscopic conditions in his experiments were characterised by an apparent FWHM of 0.17nm. According to **Fig. 9.5** the remaining systematic difference between results obtained under apparent FWHM of 0.12 nm and 0.17 nm is of the order of no more than 2%. Beyond that the comparability could only be limited, if - in spite of similar FWHM - the shape of the spectrometer's characteristic function differed significantly between his and our experiments.

9.8.2 Vibrationally excited IO

Due to the similar shape of the absorption in principle the same effects have to be anticipated for the vibrationally excited species of IO as for the ground state. For excited species IO(ν'←1) a sufficiently accurate separation of absorbers in low resolution measurements (150grvs·mm^{-1}, 100µm slit, 1.2nm FWHM) was achieved only for a few data sets. The separation is limited by the collinearities described in **Chapter 7**, which exist between curves of temporal behaviour of ground state and vibrationally excited IO. Therefore the effect of resolution and binning on excited IO is only studied for this selected data. Furthermore with respect to MIntAS it is not distinguished between IO(ν'←1) and IO(ν'←ν") with ν">1. The scaling factor determined here will be applied to both.

Finer binned high resolution recordings as a-priori spectra for MIntAS were obtained with 1200grooves·mm^{-1}, 240µm slit, 0.35nm FWHM. For signal-to-noise considerations the entrance slit in these measurements had to be opened further, thereby reducing the effective resolution. In these measurements the bands of ground state and excited state IO are well separated, so that for the a-priori spectra no separation techniques was needed. For the two bands IO(3←1) near 449 nm and IO(2←1) near 459nm MIntAS was applied to the data set which shows the best separation of ground state and excited IO. The shape of the bands of excited IO in both data sets (low resolution/coarsely binned and high resolution/finer binned) is more or less recognizable but clearly dominated by strong noise (**Fig. 9.9**). When comparing the two bands, the correlation coefficient between the bands is no better than 0.94 for the low resolution bands and even worse at 0.87 for the higher resolved ones. The signal-to-noise ratio is no more than 10. For the selected transitions the ratio between MIntAS and apparent optical density is 1.97 and 1.67 respectively. The difference reflects the inaccurate determination of the shape of the bands in both the MIntAS input as well as the a-priori data set. Independent of that for both bands a non-linear behaviour of apparent optical density of 1% is observed, see **Fig. 9.10**. With respect to iodine conservation the contribution of excited IO to the overall budget of iodine is smaller than that of ground state IO. The highest sensitivity of the conservation approach is in the first time interval containing the strongest dynamics of the individual absorbers. Therefore it is justified to neglect the non-linear behaviour of excited IO of only 1% opposed to 6% non-linearity in the case of ground state IO. In that case the effect of resolution and binning reduces to a mere scaling between

coarsely binned low resolution data on one side and the finer binned high resolution a-priori data on the other side.

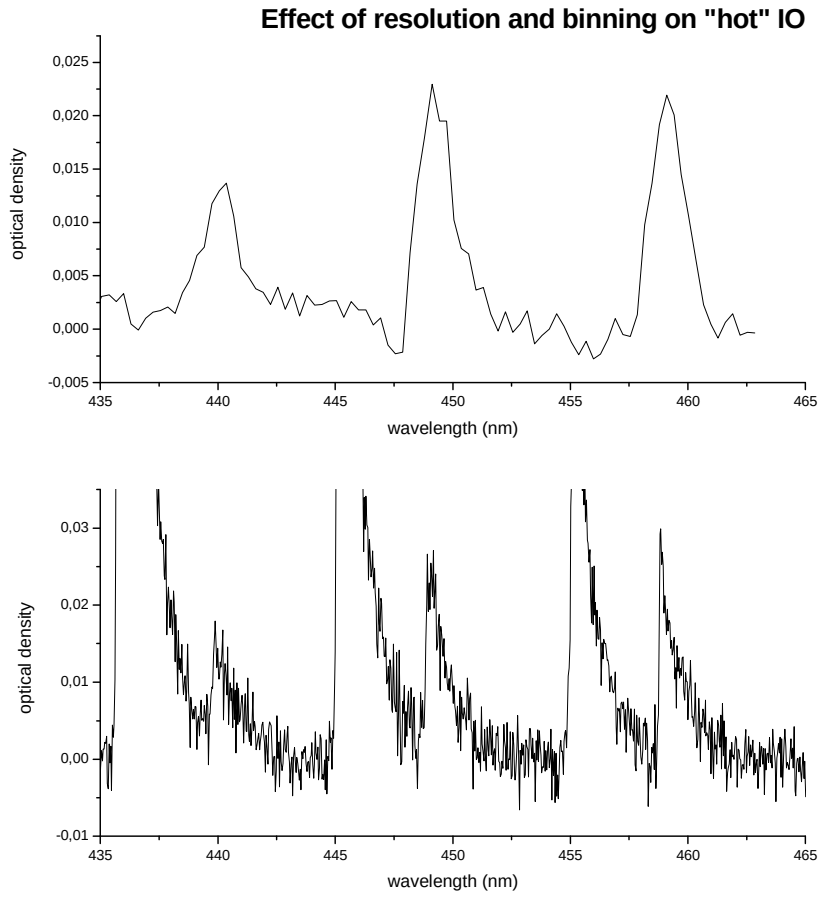

Figure 9.9 The absorption spectrum of vibrationally excited IO(ν'←1) is shown under different resolution. Top: 150grooves·mm^{-1}, 100µm slit, 1.2nm FWHM. Bottom: 1200grooves·mm^{-1}, 240µm slit, 0.35nm FWHM. In the top graph excited IO was already separated from ground state IO(4←0) absorbance. In the bottom graph excited and ground state IO are both shown. For usage in MIntAS the IO(4←0) bands can clearly be manually suppressed as they are well separated from IO(ν'←1). Wavelength is in standard air.

In the lack of better data the scaling between apparent and MIntAS retrieved peak absorption is averaged for the two available calculations. The accuracy is estimated by the standard deviation between the two:

$$c_{IO^*} = 1.8_2 \pm 0.2_1$$

As a consequence, wherever excited IO will have to be considered in the method of iodine conservation, it will be introduced as the curve of apparent optical density versus time without MIntAS correction. Any resulting apparent cross section will then be corrected by the scaling factor determined here.

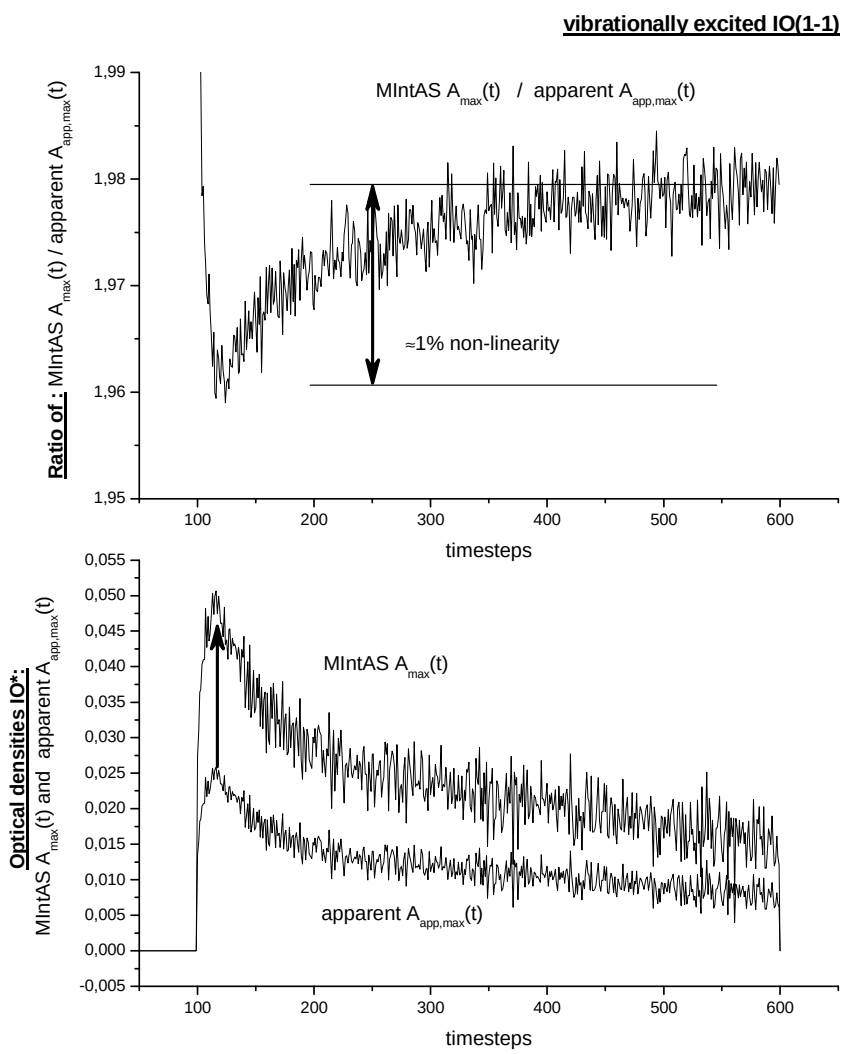

Figure 9.10 Applying MIntAS to vibrationally excited IO(1←1) (spectroscopic conditions as in **Fig. 9.9**) shows a strong dominant increase of maximum absorption by a factor of 1.97 and a slight non-linearity of 1%. The range before the maximum is reached should not be considered in this context to avoid confusion of MIntAS non-linearity and time resolution issues of the CCD. The curves for the IO(2←1) are very similar.

9.8.3 OIO

In the same way as for ground state and excited IO the effects of resolution and binning have to be considered for OIO. But in contrast to the sharp band head structure of the former two, the absorption spectrum of OIO displays a more moderate shape (**Fig. 9.11**). The flanks of the OIO(5,1,0←0,0,0) absorption transition at 549.1 nm are even in low resolution experiments (150 grvs·mm^{-1}, 100µm slit → 1.2nm FWHM) still of the order of 4 to 5 pixels wide while under similar conditions for the IO(4←0) transition the band head side was covered by no ore than 2 to 3 pixels. This indicates that resolution and binning effects should be less critical for OIO than for IO.

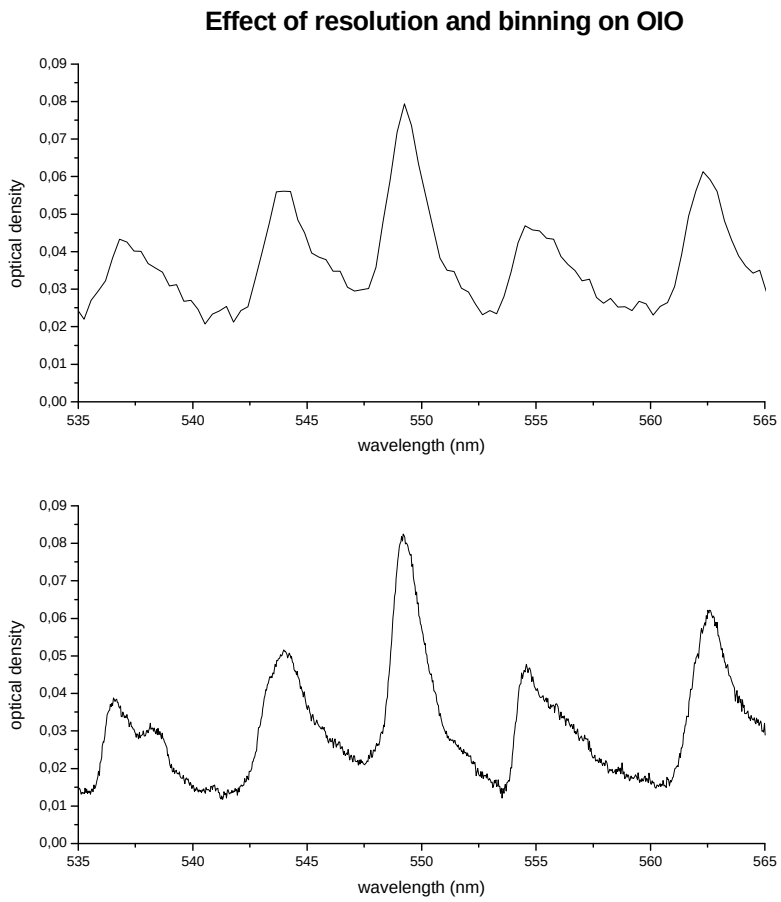

Figure 9.11 In the top graph the low resolution spectrum of OIO around the OIO(5,1,0←0,0,0) transition is plotted. Spectroscopic conditions were 150 grooves·mm^{-1} grating, 100µm slit → 1.2 nm FWHM. In the bottom graph the same section is shown under higher resolved conditions of 1200 grooves·mm^{-1} grating, 240µm slit → 0.35nm FWHM. The structures are less steep than in the case of IO so that less effects of resolution and binning can be expected. Wavelength is in standard air.

Application of MIntAS to the OIO apparent optical density is complicated by the overlap with excited IO as well as molecular iodine I_2. Stepwise separation of spectra has to be performed first. Secondly the broad shape of the OIO spectrum as such limits the applicability of MIntAS. In the IO spectrum the absorption returns more or less to zero between the absorption bands providing clear horizontal sections of the spectrum. This is a pre-requisite – along with the flatness condition of the light source's spectrum – for neglecting cross boundary mixing in MIntAS. In contrast to this the OIO spectrum does not show these horizontal troughs. Therefore cross boundary mixing at the borders of the MIntAS interval will affect the correction more strongly than it is the case for IO.

Application of MIntAS to different individual as well as combined bands of the OIO spectrum around its (5,1,0←0,0,0) absorption transition at 549.1nm firstly showed that no significant

non-linearity is present (**Fig. 9.12**). If indeed a systematic inclination of the ratio between MIntAS retrieved peak height and apparent peak height was observable, it was only in one case around 0.003, in all other cases between 0.001 and 0.002 or even less across the whole time interval from peak to 90% decay. Therefore it is fully justified to neglect non-linearity in OIO in the method of iodine conservation.

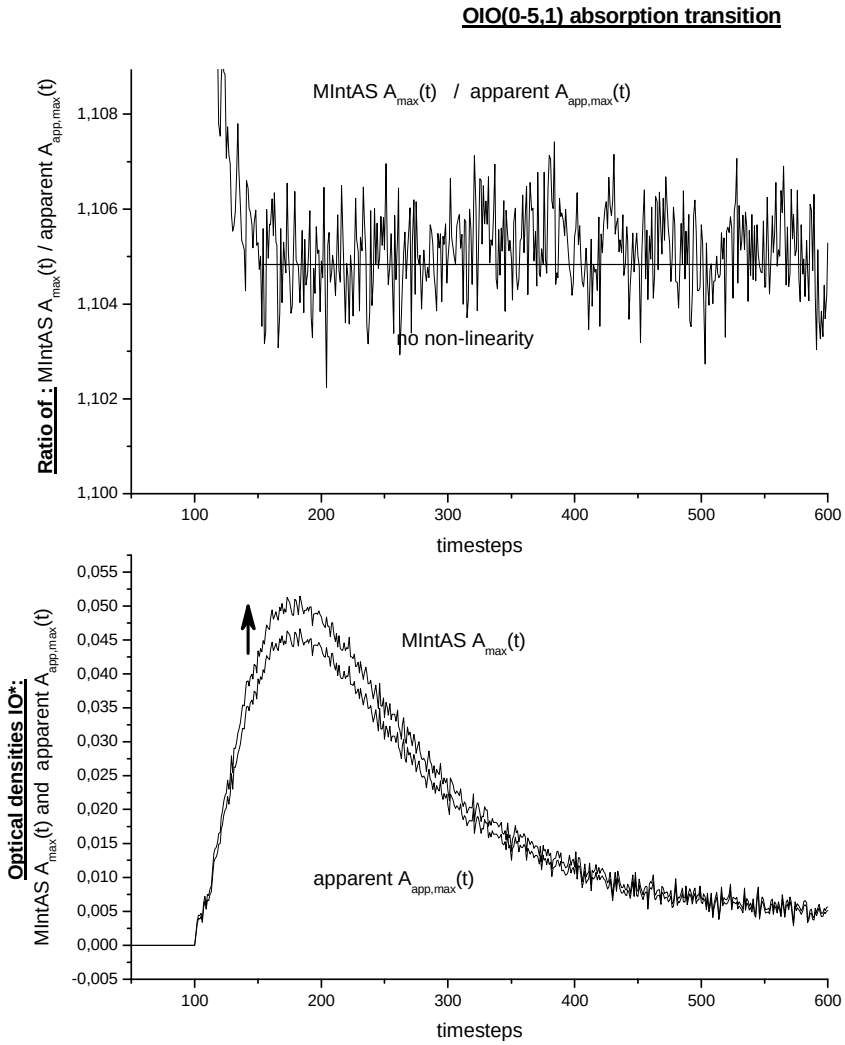

Figure 9.12 For OIO the effect of non-linearity due to insufficient resolution and binning is negligible and – if detectable at all – of the order of 0.1%. Also the scaling factor to correct between the two sets of spectroscopic conditions (see **Fig. 9.11**) is smaller than in the case of IO.

For the OIO(5,1,0←0,0,0) transition the scaling factor between coarsely binned low resolution measurements (150 grvs·mm^{-1}, 100µm slit → 1.2 nm FWHM) relative to the finer binned high resolution ones (1200 grvs·mm^{-1}, 240µm slit → 0.35nm FWHM) was determined to be:

$$c_{OIO,MIntAS} = 1.12 \pm 0.05$$

This result was obtained from four different runs of MIntAS applied to different intervals across the OIO(5,1,0←0,0,0) transition, see **Tab. 9.1**. They show a systematic effect of interval width, reflecting most likely the non-negligible cross boundary mixing. The result is the averaged (and standard deviation) of the four individual results.

left boundary	**right boundary**	**scaling factor**	**non-linearity**
547.85 nm	551.27 nm	1,07	none
547.23 nm	553.44 nm	1,12	noisy 0.001
546.92 nm	553.75 nm	1,13	clear 0.002
553.44 nm	560.28 nm	1,18	noisy 0.0015
	average:	**1.12±0.05**	

Table 9.1 Scaling factors and non-linearity obtained from MIntAS for different intervals.

Similar as for IO also for OIO an empirical determination of scaling of the peak absorption was performed. The analysis of this empirical data yielded a scaling for the same spectroscopic conditions of

$$c_{OIO,emp} = 1.21 \pm 0.1$$

The large uncertainty reflects the low signal-to-noise ratio in these measurements, which was due to technical difficulties in the experiment. The tendency for both MIntAS and empirical scaling is similar, but the agreement is rather poor and just within the error limits. For the method of iodine conservation the scaling is estimated by the weighted mean of the two determinations, as both are based on a likewise limited data base:

$$c_{OIO} = 1.14 \pm 0.05$$

Similar as in the case of vibrationally excited IO the curve of apparent optical density versus time will be introduced into the method of iodine conservation without MIntAS correction. Any resulting apparent cross section will then be corrected by the scaling factor determined here.

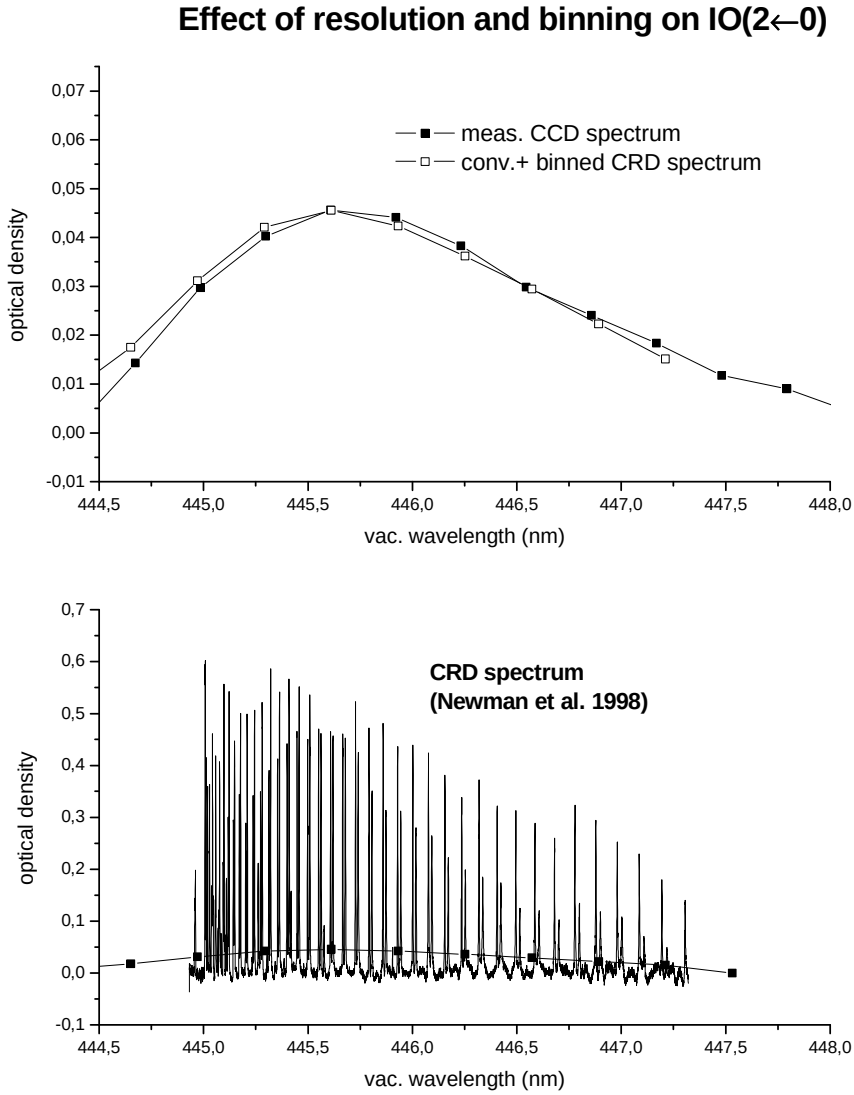

Figure 9.13 To test the MIntAS approach further, it was applied to the IO(2←0) band, which consists of fully separated rotational lines. A CRD spectrum by Newman et al. [1998] is plotted in the bottom graph. A convoluted and binned spectrum is shown in the same diagram (both to scale). The reduction in amplitude is due to the effect of low resolution and binning. In the top graph a measured low resolution CCD spectrum is shown (filled squares). For comparison the convoluted and binned CRD spectrum is plotted as well (open squares). Wavelength in vacuum.

9.8.4 IO(2←0)

The IO(2←0) is of special interest in this context as it is known to consist completely of separated rotational lines. This was determined by the already earlier mentioned CRD spectra obtained by Newman et al [1998]. Therefore it is a welcome test for the method of MIntAS to our measured low resolution data for this band using the high resolution CRD spectrum of Newman et al. as an a-priori MIntAS input spectrum. **Fig. 9.13** shows the low resolution CCD measurement of the IO(2←0) band (filled squares) along with a spectrum (open squares),

which is determined by convoluting the CRD spectrum by Newman et al. with an instrument's function of 1.2nm FWHM and subsequently binning the convoluted spectrum to a detector with pixels of 0.32nm spectral width (top graph). In the bottom graph the original spectrum CRD spectrum of Newman et al. is shown (background removed).

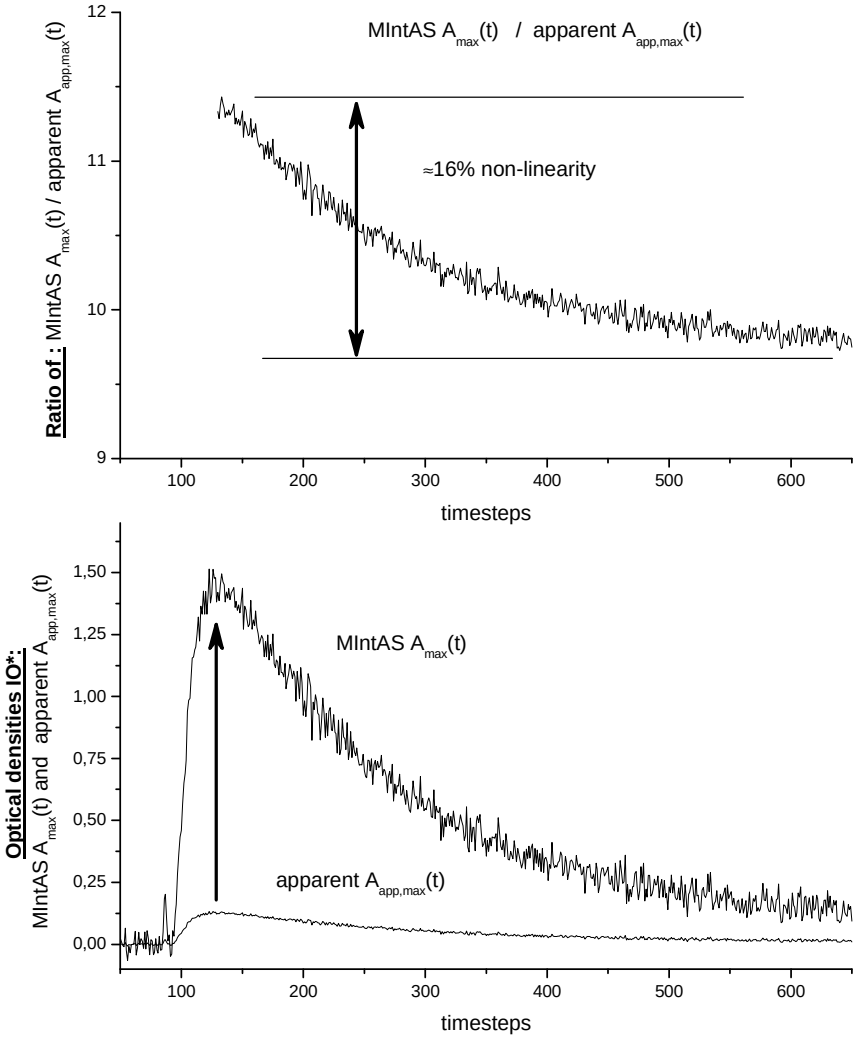

Figure 9.14 The effect of low resolution and coarse binning is strongest for the IO(2←0). The non-linearity increases to 16% no longer justifying the approximate separation into a scaling factor and a remaining non-linearity. Only in terms of magnitude the scaling gives a rough orientation in how much an absorption will be reduced. This factor in the present case is 10.6±3. It compares well with 9.9±1 determined in the reverse direction by convolution and binning of the CRDS spectrum.

Applying MIntAS to the low resolution time resolved CCD measurement with the CRD spectrum as a-priori input corrected the curve of apparent temporal behaviour and produced the curve shown in **Fig. 9.14**. The non-linearity in this case is of the order of 16% and the scaling (as a rough average ignoring the non-linearity) is of the order of 10.6±3. This compares well with the down scaling obtained when convoluting and binning the CRD

spectrum to the spectroscopic conditions of our low resolution spectra, which yielded a factor of 9.9±1. This agreement also validates the MIntAS approach, which in a way is the reverse of convolution and binning given the a-priori knowledge of the higher resolved spectrum and avoiding the knowledge of the instrument's function.

9.9 CONCLUSION

Based on MIntAS and on – where available – empirical data, for an exemplary set of curves of apparent optical density of absorbers the non-linear effects due to resolution and binning were determined. Where the non-linearity is small, only a correction factor was determined. The results for scaling and non-linearity are summarised in **Tab. 9.2**.

species	FWHM		scaling	non-linearity	OD range at HiRes
	LoRes	HiRes			
IO(4←0)	1.3nm	0.12nm	1.64 ± 0.04	6%	0.1-0.6
IO(2←0)	1.3nm	CRDS	11±3 (MIntAS) 9.9±1 (conv.+bin.)	16%	0.01-0.12
IO(1←1) and IO(2←1)	1.3nm	0.35nm	1.82 ± 0.21	1%	0.02-0.05
OIO(5,1,0←0)	1.3nm	0.35nm	1.14 ± 0.05	0.1%	0.01-0.05

Table 9.2 MIntAS results for all absorbers under study are shown. For IO(2←0) the scaling was also determined by the reverse calculation via convolution and binning. The good agreement supports the validity of the MIntAS method. The scaling factors apply for true OD at high resolution within the given range.

These results then define the strategy for applying iodine conservation as the next step of analysis. For ground state IO(4←0) all data is to be pre-processed by MIntAS to correct both non-linearity and scaling. For vibrationally excited IO and OIO non-linearity was found to be of negligible importance. Therefore for the latter two only an effective scaling factor was determined. For them iodine conservation will be applied to the original coarsely binned low resolution measurement data thereby providing cross section results which underestimate the true cross section. The scaling factor determined here will enable the correction of these results to an effective higher resolution.

10 ABSOLUTE ABSORPTION CROSS SECTIONS BASED ON IODINE CONSERVATION

The objective of this work is to determine absolute absorption cross sections as independent as possible of any a-priori data or assumptions. And to determine them consistently. Having now determined and verified the oscillator strength of I($^2P_{3/2}$) and the absorption cross section of I_2, having also achieved separation of spectra and of curves of temporal behaviour of apparent optical density for all observed absorbers and having further corrected the observations of apparent optical density where necessary for low resolution and coarse binning, now the necessary data is provided for applying the method of conservation of iodine atoms to this system. As the preparatory processing has been done in the preceding sections, in the following the term "time curves" or "curves of temporal behaviour of OD" will always relate to the separated and where necessary MIntAS corrected curves of temporal behaviour.

10.1 IODINE CONSERVATION

10.1.1 General

The key to the concept of iodine conservation is the assumption, that all relevant atoms and molecules containing iodine – be it the precursors or be it any product of reaction after photolysis – are accounted for by measurement of a curve of temporal behaviour of OD of that corresponding absorber. Starting with the initial precursor concentration $[I_2]_0$ and based upon all absorbers found within this study, for each following time step t_i the distribution of the initial content of iodine over the individual absorbers can be described:

$$2[I_2]_0 = 2[I_2](t_i) + [I](t_i) + [IO](t_i) + [IO_{v''=1}](t_i) + [IO_{v''>1}](t_i) + [OIO](t_i) + \\ + [X](t_i) + [Y](t_i) + [Z](t_i) + ... \qquad \textbf{(1)}$$

The open end of **(1)** indicates the possibility of missing and not yet accounted for absorbers. The symbolic $IO_{v''=1}$ and $IO_{v''>1}$ designate IO in vibrationally excited states of IO(v'←1) and IO(v'←v'') with v''>1 respectively. Using the known cross section of I_2 and the known oscillator strength of I($^2P_{3/2}$) – or the empirical calibration of resonance absorption -, the temporal behaviour of iodine contained in free atoms and in I_2 molecules during the course of

reaction after photolysis can be determined by direct observation. In the same way the initial amount $[I_2]_0$ of I_2 is known from the spectroscopic measurement. For the remaining absorbers not concentration but OD at a given wavelength is observed. This transforms **(1)** into:

$$2[I_2]_0 - 2[I_2](t_i) - [I](t_i) =$$

$$\frac{OD_{IO}(\lambda_{IO}, t_i)}{\sigma_{IO}(\lambda_{IO})} + \frac{OD_{IO(v''=1)}(\lambda_{IO(v''=1)}, t_i)}{\sigma_{IO(v''=1)}(\lambda_{IO(v''=1)})} + \frac{OD_{IO(v''>1)}(\lambda_{IO(v''>1)}, t_i)}{\sigma_{IO(v''>1)}(\lambda_{IO(v''>1)})} + \frac{OD_{OIO}(\lambda_{OIO}, t_i)}{\sigma_{OIO}(\lambda_{OIO})} +$$
$$\frac{OD_X(\lambda_X, t_i)}{\sigma_X(\lambda_X)} + \frac{OD_Y(\lambda_Y, t_i)}{\sigma_Y(\lambda_Y)} + \frac{OD_Z(\lambda_Z, t_i)}{\sigma_Z(\lambda_Z)} \qquad \textbf{(2)}$$

Here it is assumed that all relevant absorbers are contained, why the open end of the sum is dropped. This includes a necessary approximation with respect to vibrationally excited IO, for which it is known, that vibrational levels of up to ν''=7 have been observed in the experiment. Temporal behaviour was clearly different already between ν''=1 and ν''=2. Strictly speaking the same has to be assumed for ν''>2 even though separation of different curves of temporal behaviour was not possible due to collinearity. Therefore treatment of IO(ν'←ν''), ν''>1 as a single species IO(ν''>1) is a necessary approximation. But the effect should be small, as IO(ν''>1) is present only at very early times of reaction. It is further assumed that all optical density data is normalised to unit path length, why the factor L, which has its origin in the Beer-Lambert law is dropped from the equation.

10.1.2 Linear model

In equation **(2)** the concentrations on the left and the temporal behaviour of ODs on the right are known by observation. Unknowns are the absorption cross sections on the right, which link the observed OD to concentration. It is now possible to state the problem in a form suitable for a least squares linear model, also referred to as multivariate linear regression:

$$\mathbf{y} = \mathbf{A}\cdot\mathbf{x} + \boldsymbol{\varepsilon} \qquad \textbf{(3)}$$

As introduced in **Chapter 7** bold face lower case letters indicate column vectors. Bold face capital letters indicate matrices. In this notation vector **y** contains the observational data for data points t_1 to t_n, i.e. **y** is a column vector of length n. In the same way the system matrix or

mixing matrix **A** consists of n rows containing the observed OD at time t_i. The vector of unknowns **x** contains the reciprocal of the sought absorption cross sections. **ε** is a vector of same dimension and size as the observational vector **y** and contains the error terms:

$$\begin{bmatrix} 2[I_2]_0 - 2[I_2](t_1) - [I](t_1) \\ 2[I_2]_0 - 2[I_2](t_2) - [I](t_2) \\ \dots \\ \dots \\ 2[I_2]_0 - 2[I_2](t_n) - [I](t_n) \end{bmatrix} =$$

$$\begin{bmatrix} OD_{IO}(\lambda_{IO}, t_1) & OD_{IO(v''=1)}(\lambda_{IO(v''=1)}, t_1) & \dots & OD_Z(\lambda_Z, t_1) \\ OD_{IO}(\lambda_{IO}, t_2) & OD_{IO(v''=1)}(\lambda_{IO(v''=1)}, t_2) & \dots & OD_Z(\lambda_Z, t_2) \\ \dots & \dots & \dots & \dots \\ \dots & \dots & \dots & \dots \\ OD_{IO}(\lambda_{IO}, t_n) & OD_{IO(v''=1)}(\lambda_{IO(v''=1)}, t_n) & \dots & OD_Z(\lambda_Z, t_n) \end{bmatrix} \cdot \begin{bmatrix} \frac{1}{\sigma_{IO}(\lambda_{IO})} \\ \frac{1}{\sigma_{IO^*}(\lambda_{IO^*})} \\ \dots \\ \dots \\ \frac{1}{\sigma_Z(\lambda_Z)} \end{bmatrix} + \boldsymbol{\varepsilon}$$

(4)

Assuming n time steps and u unknowns the dimension of **A** is n x u. A necessary requirement to this system of equations is that they all together form a set of linearly independent equations. As soon as more time steps and therefore equations than unknowns are involved – i.e. n>u - the system is in principle over-determined. In the absence of systematic numerical problems like collinearity (see **Chapter 7**) it will be solvable to yield estimates for the sought cross sections. The in the sense of minimized least squares optimal solution is given by:

$$\mathbf{x} = (\mathbf{A}^T \cdot \mathbf{A})^{-1} \cdot \mathbf{A}^T \cdot \mathbf{y} \qquad \textbf{(5)}$$

It is important to note that in this context the purpose of a time resolved measurement is only to provide a sufficient number of linearly independent equations: One for each step in time. The order of observations defined by time t_i of their recording is not of importance and is disregarded. The model is solvable also if all individual equations (rows) in **(4)** were arbitrarily mixed. This illustrates the difference of this method in comparison to kinetic models, where the temporal behaviour of observations is the key to determining rate coefficients as well as – if possible – cross sections.

10.1.3 Advantages of the approach

The important advantages of this approach are clearly its independence of mechanistic hypotheses and kinetic reference data. The only reference data which is required is the absorption cross section of I_2 and the oscillator strength of $I(^2P_{3/2})$. The former was checked within the present work and its uncertainty could even be further reduced by our determination. The latter was also determined and inhomogeneities were accounted for by additional empirical calibration. A second advantage is the fact, that the approach enables *simultaneous* and *consistent* determination of cross sections of all different species observed in the experiment. This is an important improvement with respect to most previous studies, which had to determine selected cross sections under idealized conditions ignoring others and which then had to approximate other cross sections iteratively. Errors in the reference data and in the determination of the first cross section within the iterative chain propagate into the last estimates producing increasing uncertainties for the results determined at the end of the chain. Also such approaches usually had to rely on kinetic reference data. Therefore the resulting estimated cross sections are not independent estimates. Both are not the case in the present approach. A third advantage of the approach, which is closely linked to the fact that all observed absorbers are simultaneously contained, is the increased coverage in time. Within the iterative approaches always only a limited time window of data containing either the earliest products – usually the more or less instantaneous production of IO and OIO – or only the decay of an absorber can be used. Full temporal coverage usually has to be avoided because of the content of other products or their kinetics have to be modelled with multi-parameter kinetic mechanisms bearing the problem of over-parameterisation. In the present approach the number of unknowns is limited to the absorption cross sections while the later products of reaction are included. By this it becomes possible to use also observations from later times within the course of reaction. Thus the data quality of the obtained results is improved by an increased averaging effect.

A remark with respect to the up to now unidentified absorbers is necessary here: Because the stoichiometry of these absorbers is not known, their cross sections resulting from the method of iodine conservation will be cross sections not per molecule but per iodine atom. Once the stoichiometry of the molecule is identified by kinetic or other considerations, their absorption cross sections can be converted to cross sections per molecule by multiplying them by the number of iodine atoms contained in the specific molecule.

10.2 APPLICATION OF THE MODEL AND RELIABILITY OF SOLUTION

The crucial assumption behind the method of iodine conservation is that all absorbers relevant in the system under study are accounted for. Depending on the complexity of the chemical mechanism the number of different product molecules increases with time. Therefore this assumption will become more and more difficult to fulfil the larger the time interval of data is, which is introduced into the model. But in reverse, this limitation is also an important means for checking the reliability of the model: As long as no systematic structures occur in the residuals $\boldsymbol{\varepsilon}^T=[\varepsilon(t_1),...,\varepsilon(t_n)]$, the used data complies with the assumption. As soon as systematic structures occur in the residuals, these can even indicate, where and what kind of absorber is missing, as the systematic shape of the residuals will mirror quite closely the temporal behaviour of the absorber, which is not included in the model.

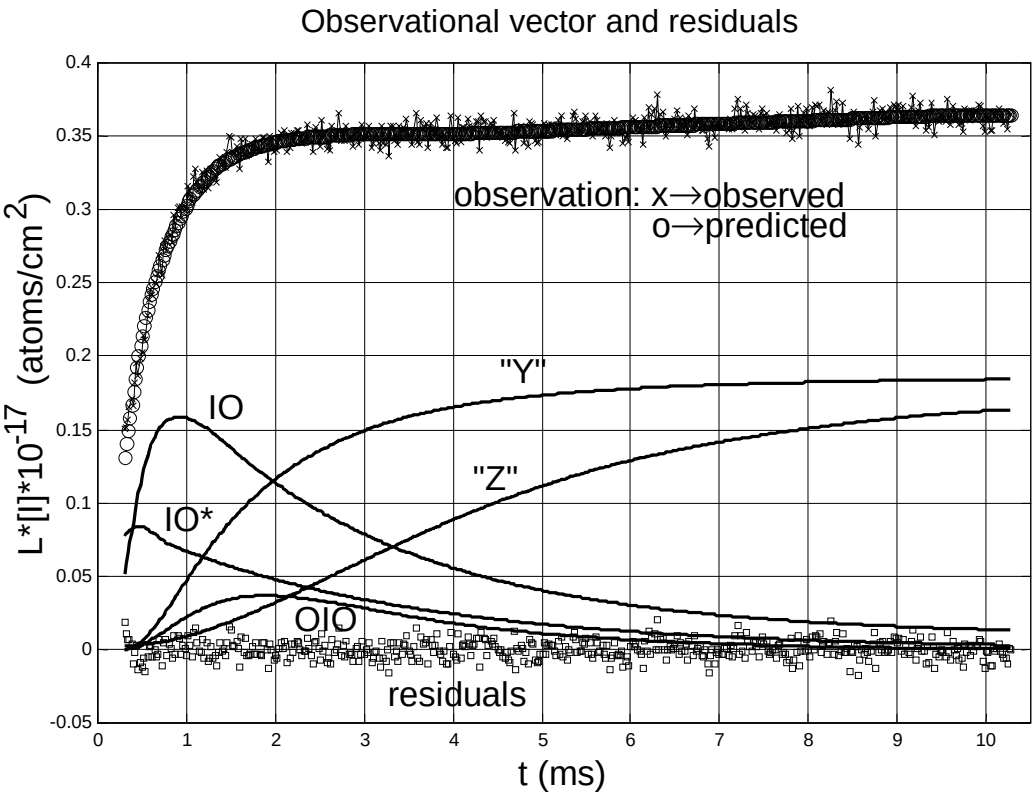

Figure 10.1 Within the concept of iodine conservation the curves of optical density of individual absorbers are regarded as a measure of their iodine content (curves in the lower half: IO, IO*, OIO, Y, Z, with IO*: vibrationally excited IO, see below). Their sum must equal the observations for each point in time (top curve, symbol 'x'). The multivariate linear regression reproduced the observations accurately (top curve, open circles). At the bottom the residuals are plotted which are free of systematic structure. This supports that all relevant absorbers are contained in the model.

In the same way any artefacts present in a curve of temporal behaviour used for an absorber will cause similar systematic structures in the residuals. This could be the case in time intervals close to the flash, where issues of temporal resolution relative to fast initial formation of IO or its excited species might be of importance. **Fig. 10.1** shows the solution to a considerably large time window. The residuals are distributed normally (bottom graph) supporting the assumption that all relevant absorbers are accounted for. The two curves of observation **y** and prediction (top) coincide accurately so that even with different choice of symbols the discrimination between the two is difficult. In between, the curves of iodine content for all absorbers are plotted. Their sum results in the model prediction plotted above.

As a further measure to account for the possibility of unaccounted missing absorbers or artefacts, the following strategy was used for applying the above linear model: A starting point in time was chosen which was assumed to be sufficiently remote from the flash to be free of artefacts. Starting from there, an initial time window was selected and with the data from that window a first solution to the model **(4)** was calculated. Then the interval was increased by a certain number of data points and a new solution to **(4)** was calculated. This procedure was repeated with step by step increased time window, until the whole time interval of available data was covered. This produces a series of estimates for the sought absorption cross sections, one per chosen time interval. Plotting the sets of results for absorption cross sections obtained in this way against the length of the used time interval as independent variable provides a measure for the dependence of the obtained results on the used data interval. In the ideal case the solutions should produce a horizontal graph for each absorber's cross section. This criterion is referred to as "convergence against horizontal plateaus". Two reasons could cause deviations from this. Firstly if the time interval does not contain significant information about one or more absorbers (because their OD is zero or close to zero within the selected interval), the normal matrix of the system will become poorly conditioned or even singular. The results will show significant scatter and unsystematic behaviour. This can be clearly seen in **Fig. 10.2**, where for a selected data set up to a time window length of roughly 25 to 30 pixels the solutions behave erratic or are at least not constant. Also the estimated error for these solutions is in many cases clearly larger. From window size 30 to 45 the results for all absorbers behave in a good manner constant, indicating that all absorbers are well defined by the observational data. Beyond window size of 45 the solutions for OIO and absorbers "Z" and "Y" start to deviate again indicating that some further absorption might be missing.

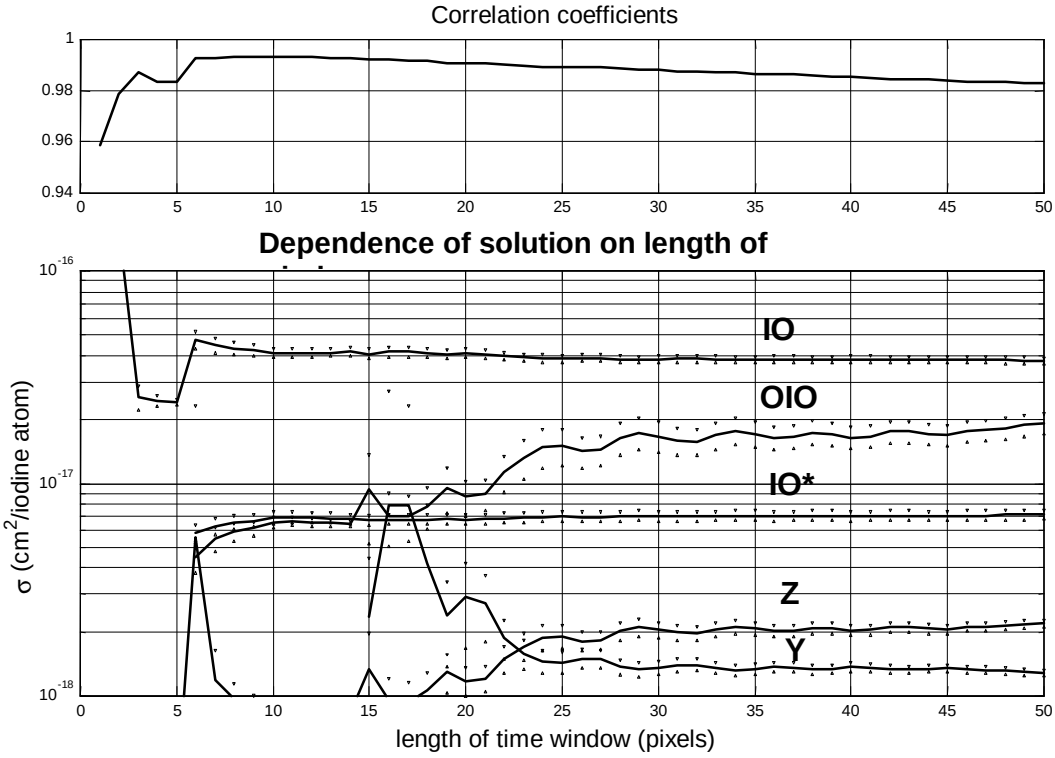

Figure 10.2 An example for applying the method of iodine conservation to a data set is shown. For different sizes of time windows solutions to the iodine conservation model were calculated. From left to right each "column" of points represents one individual solution of **(4)**.The obtained cross sections are plotted against the length of the used time window providing a measure for the consistence of the obtained solutions. For window length between 30 to 45 pixels the solutions are to a considerable degree constant "converging against horizontal plateaus" indicating the absence of collinearity and the absence of missing absorbers.

10.2.1 Results

As in the case of *multiple* multivariate linear regression, the condition of the normal matrix $\mathbf{N}=(\mathbf{A}^T\cdot\mathbf{A})$ is the key to whether the system can be solved or not. One aspect of this was already discussed in the context of the time window being too short. The other aspect is the problem of collinearities as it was discussed earlier in the context of the extraction of spectra. But there it was possible to avoid collinearity to a certain extent by selecting appropriate windows in wavelength and thereby reduce the number of curves of temporal behaviour used in the mixing matrix. In the context of iodine conservation this strategy is not possible, as neglecting an absorber would violate the key assumption that all relevant absorbers are covered.

However, in the analysis of our data it was found that collinearity impedes the solution of the system, if IO($\nu'\leftarrow 1$) and IO($\nu'\leftarrow\nu''$), $\nu''>1$ and "X" are contained simultaneously, because

their temporal behaviours are very similar. Also collinearity between ground state IO and IO at ν"=1 occurred. As a consequence two out of the three IO(ν'←1) and IO(ν'←ν"), ν">1 and "X" have to be dropped from the approach. With respect to IO(ν'←1) and IO(ν'←ν"), ν">1 this is not satisfying, but acceptable, as it can be expected that by summing up both in a common variable IO^* this will only mix different vibrational states of the same species. This will in any case still be an improvement upon the up to now common practice, where ground state and vibrationally excited IO are treated as one absorber. Also the effect of different temporal behaviour will affect mainly early time intervals, so that testing the convergence to horizontal plateaus according to **Fig. 10.2** provides a measure to estimate the reliability of this approximation. To overcome collinearity problems between ground state IO and any of the excited species of IO alternatively either IO(3←1) or IO(1←2) were used. Whenever both possibilities produced a set of results, cross sections for the remaining absorbers were averaged. If only one version produced results, these were used.

But with respect to "X" it is disappointing, that due to collinearity it has to be excluded. This even more, as it was found to be a new and yet unidentified species in our reactive system. Similarly also for in this way reduced data sets still collinearity caused problems. They could be identified to being linked to OIO and "Y". Dropping either one from the set of absorbers solved at least the problem of collinearity without making a statement about physical meaningfulness of the solution. Both absorbers appear to be likewise important. OIO is among the earliest products and has the stronger absorption. On the other hand for one data set convergence with reasonable results was achieved with "Y" being included. This data set is the one, which is shown as an example in **Fig. 10.1** and **Fig. 10.2**. It results in a cross section for "Y" which is roughly one order of magnitude smaller than that of OIO. Therefore even though the absorption of "Y" is smaller than that of OIO, due to the smaller cross section it still has a large iodine content, which is a direct measure of its impact on the method of iodine conservation.

	p [mbar]	$[I_2]_0$ [molec/cm^3]	$[O_3]_0$ [molec/cm^3]	$\sigma_{IO(4\leftarrow0)}$ [cm^2/molec]	$\sigma_{IO(3\leftarrow1)}$ [cm^2/molec]	$\sigma_{IO(1\leftarrow2)}$ [cm^2/molec]	$\sigma_{OIO(0,5,1)}$ [cm^2/molec]	σ_Z(340nm) [cm^2/molec]
1	10	1.44E13	5.1E14	3.12±0.08	1.8±0.40	0.95±0.19	1.4±0.4	0.086±0.015
2	10	1.44E13	5.1E14	3.2±0.04			0.91±0.04	0.088±0.003
3	10	1.44E13	5.1E14	3.34±0.06			0.69±0.02	0.088±0.003
4	10	2.9E12	4.9E14	3.61±0.08		0.46±0.03	1.62±0.19	0.036±0.001
5	10	2.9E12	4.9E14	3.4±0.05			1.41±0.11	0.06±0.0014
6	15	2E13	7.4E14	3.95±0.15	0.78±0.07	0.34±0.03	1.2±0.4	0.063±0.018
7	15	2E13	7.4E14	3.51±0.07	1.55±0.13	0.71±0.06	1.5±0.6	0.063±0.015
8	15	2.1E13	7.4E14	3.62±0.11	0.81±0.06	0.47±0.04	1.13±0.11	0.069±0.0012
9	20	3.12E13	1.1E15	3.56±0.12	1±0.1200	0.99±0.12	0.95±0.05	0.088±0.003
10	20	3E13	1.1E15	3.1±0.06		1.5±0.4	0.85±0.05	0.0774±0.0014
11	20	5.7E12	9.8E14	3.86±0.04			1.41±0.05	0.00040.065±
12	20	5.7E12	9.8E14	3.65±0.15		1.3±0.6	1.3±0.3	0.013
13	30	4.2E13	1.5E15	3.59±0.11		0.51±0.06	0.95±0.17	0.078±0.004
14	30	8.5E12	1.5E15	3.56±0.12	1.6±0.50	0.79±0.2	1.9±0.2	0.07860.0009±
15	40	5.4E13	1E15	3.4±0.50	0.59±0.17		1.4±0.5	0.07±0.004
16	40	5.4E13	1E15	3.3±0.17	0.89±0.13	0.4±0.06	0.76±0.07	0.066±0.003
17	40	5.4E13	1E15	3.89±0.17		0.24±0.14	0.71±0.06	0.089±0.002
18	40	1.2E13	2E15	3.58±0.16		0.28±0.03	0.73±0.07	0.078±0.003
19	40	5.4E13	1E15	3.28±0.13	0.72±0.14	0.4±0.07	0.94±0.06	0.072±0.006
20	40	5.4E13	1E15	3.48±0.24		0.31±0.06	1.1±0.23	0.088±0.004
21	40	5.4E13	2E15	3.7±0.30		0.39±0.09	1.2±0.3	0.082±0.003
22	40	5.4E13	1E15	4.0±0.60		0.23±0.08	1.1±0.3	0.0929±0.0016
23	40	5E13	9.1E14	3.9±0.50		0.23±0.07	1.01±0.24	0.0961±0.0017
24	40	5.7E13	2E15	3.2±0.30		0.5±0.3	1.5±0.5	0.097±0.001
25	100	5.4E13	2E15	3.44±0.17		0.23±0.06	1.3±0.4	0.068±0.004
26	100	4.4E13	8.2E14	3.02±0.08			0.81±0.1	0.073±0.003
27	100	5.4E13	2E15	3.79±0.23			0.68±0.09	0.09±0.005
28	150	4.4E13	8.2E14	3.14±0.09			1±0.3	0.085±0.004
29	200	4.4E13	8.2E14	3.24±0.1			1.4±0.4	0.082±0.004
30	200	5.4E13	2E15	3.07±0.07			0.93±0.16	0.0859±0.0015
31	250	4.4E13	8.2E14	3.06±0.08			0.94±0.17	0.098±0.003
32	300	4.4E13	8.2E14	3.1±0.1			1.4±0.4	0.097±0.004
33	300	5.4E13	2E15	3.07±0.15			0.69±0.1	0.0882±0.0013
34	400	5.4E13	2E15	3.61±0.11			1.6±0.3	0.1106±0.0008

Table 10.1 For 34 different data sets the method of iodine conservation could be successfully applied. Calculations were performed with either IO(3←1) or IO(1←2) to overcome collinearity problems. Wherever both produced a set of results, those obtained for the remaining absorbers were averaged. At higher pressure vibrationally excited IO was suppressed by quenching, why in these data sets no estimate was obtained for them. In a number of low pressure experiments radical concentrations were too low to produce a usable signal for vibrationally excited IO, why there as well no estimate for excited IO was obtained.

Having to compromise again on the number of absorbers, "Y" was excluded from the analysis of the remaining data sets. In spite of the limitations by collinearity solution of the reduced set

enables an independent, simultaneous and consistent determination of cross sections of ground state IO, excited IO^* along with OIO and "Z". The fact that for some data sets convergence to horizontal plateaus is achieved and in others not illustrates that collinearity is also linked to the chemical mixture, which changes the relative shape and the relative importance of individual time curves of absorbers. As stated earlier, alternative possibilities to solve the system of linear equations iteratively need to be investigated. Solution in the sense of perturbation theory could provide a means to overcome problems caused by collinearity. In the present work this is not pursued further, but left to future studies.

From the originally prepared 59 data sets (see **Tab. 6.1**) it was possible to obtain reliable solutions to the method of iodine conservation for 34 data sets, while for the remaining ones no satisfactory convergence to horizontal plateaus was achieved. The former ones cover a wide range of mixing ratios and pressure. Initial $[I_2]$ ranged from $2.9 \cdot 10^{12}$ to $5.7 \cdot 10^{13}$molec·cm^{-3}, initial $[O_3]$ from $1.5 \cdot 10^{13}$ to $2 \cdot 10^{15}$molec·cm^{-3} and pressure from 10 to 400 mbar. Results obtained for the individual data sets are listed in **Tab 10.1**. Their averages are summarised in **Tab. 10.2**, where MIntAS-correction for effects of resolution and binning is also applied to produce the final estimates.

Molec.	**λ(vac) [nm]**	**σ [a] [cm²/molec]**	**MIntAS scaling**	**σ [cm²/molec]**	**FWHM [nm]**
IO	427.19±0.05 (4←0)	(MIntAS correction before iodine conservation)		$(3.5 \pm 0.3) \cdot 10^{-17}$	0.12 [b]
IO^*	449.3±0.2 (3←1)	(1.1±0.4)	1.82 ± 0.21	$(2.0 \pm 0.8) \cdot 10^{-17}$ $(4.5 \pm 0.5) \cdot 10^{-17}$ [d]	0.35 [b] 0.12 [b,d]
IO^{**}	484.9±0.2 (1←2)	(0.5±0.4)	1.82 ± 0.21	$(0.9 \pm 0.7) \cdot 10^{-17}$	0.35 [b]
OIO	549.1±0.1 (0,5,1←0,0,0)	(1.13±0.31)	1.14 ± 0.05	$(1.3 \pm 0.3) \cdot 10^{-17}$	0.35 [b]
"Z"	340±0.2 continuum			$(1.0 \pm 0.2) \cdot 10^{-18}$ [c]	1.3
"Y"	322±0.2 continuum			$(1 \text{ to } 3) \cdot 10^{-18}$ [c]	1.3

Table 10.2: Absorption cross sections obtained in this work. The measured OD for IO(4←0) was MIntAS-corrected for effects of resolution and binning to an effective FWHM of 0.12nm before usage of the method of iodine conservation. IO^*, IO^{**}, and OIO were corrected afterwards with the appropriate scaling factors determined in **Chapter 6**. For "Y" and "Z" no resolution or binning dependent correction was applied as they are continuous smooth absorptions.)[a]: result from iodine conservation with MIntAS correction to be applied afterwards by scaling.)[b]: FWHM of MIntAS corrected cross section.)[c]: cm²/iodine atom, as stoichiometry is not determined yet.)[d]: Based on the cross section for (4←0) at 0.12nm FWHM and the Franck-Condon factors by Rao et al.

10.3 DISCUSSION

10.3.1 Discussion with respect to the method and to data consistency

The results listed in **Tab. 10.2** were obtained under a variety of different pressures and mixing ratios, see **Tab. 10.1**. To estimate their reliability their dependence on the parameters pressure, initial [I_2] and initial [O_3] were examined, see **Fig. 10.3** to **10.5**. Please note that there cross sections are shown as they resulted from the method of iodine conservation. They are not corrected for resolution and binning. This correction is applied to the averaged results shown in **Tab. 10.2**. Most determinations of σ_{IO} were performed at comparatively low pressure contributing mostly to the obtained result (**Fig. 10.3**). But a number of determinations at larger pressures appear to fall slightly below the range spanned by the low pressure results. In the high pressure measurements vibrationally excited IO was neglected due to low or not measurable signal. This could explain the observed dependence at least partly. Opposed to the behaviour of σ_{IO} that of σ_Z shows a reversed tendency indicating that higher oxides, especially neglected "Y" might play a role in the pressure dependent deviation of the obtained results. The effect amounts to 25 to 30% across the range of pressures. For vibrationally excited IO no statement is possible, as this yielded results only at low pressure due to quenching. For OIO no dependence of obtained results on pressure is present. For all absorbers but "Z" no dependence of obtained results on initial [I_2] is present in the data (**Fig. 10.4**). For "Z" the derived cross sections appears to increase slightly with increasing [I_2]. But the effect is small and if considering the bulk of data points at the high end of [I_2] might well be insignificant. With respect to initial [O_3] (**Fig. 10.5**) for none of the absorbers considered in the iodine conservation method an obvious dependence of results on initial [O_3] can be detected.

So even though absorbers "X" and "Y" and either one or the other of vibrationally excited IO($\nu' \leftarrow 1$) or IO($\nu' \leftarrow \nu''$), $\nu''>1$ had to be neglected from the iodine conservation algorithm because of collinearity problems, the obtained results are surprisingly consistent and stable across the range of considered conditions. Due to the concept of iodine conservation the algorithm will compensate the content of each neglected species in that curve of OD - and therefore in the corresponding cross section - within the approach, which shows the largest similarity to the neglected curve of OD, compare **Fig. 7.1**. Compensating a higher iodine content within a given curve of OD will lead to underestimation of the cross section. Neglected "X" and neglected vibrationally excited IO are closest to the corresponding curve

of excited IO considered in the solution. Therefore the cross section estimate obtained in any of the two alternative solutions (either with OD of IO(3←1) or IO(1←2)) will underestimate the true cross section.

With respect to the neglected absorber "Y" the situation is somewhat comparable. As in the case of vibrationally excited IO and "X" also between "Y" and "Z" a similarity of temporal behaviour occurs, not withstanding the fact that the collinearity problems were linked to OIO. Therefore it can be expected that missing contributions from "Y" are partly compensated in "Z" leading to an underestimation of its cross section.

Effects of limited resolution have been corrected in the data to the FWHM stated in **Tab. 10.2**. For IO deviations between FWHM=0.12nm and higher resolution are of the order of a few percent and below the uncertainty of the present result. The same is expected for OIO. For vibrationally excited IO somewhat larger effects of resolution and binning have to be present, as the band shape is similar to that of ground state IO and FWHM could only be corrected to 0.35nm. The continuous absorption of "Z" is independent of resolution and binning. It has to be noted that the spectra determined in **Chapter 7** were recorded at 1.3nm FWHM. Before scaling them to absolute cross sections listed in **Tab. 10.2**, the cross sections must be downscaled to the appropriate and possibly OD dependent apparent cross sections, according to the non-linearity found in **Chapter 9**.

On that basis it is therefore concluded that cross sections obtained in the present work for ground state IO and OIO are reliable within the given standard deviation. Those for "Z" and for vibrationally excited IO are considered as lower limits to the true cross sections. The latter is in line with the Franck-Condon factors determined by Rao et al. as well as those determined in this work in Morse approximation. Assuming comparable band shape for (4←0) and (3←1) the cross section for excited IO(3←1) should be at about 0.116/0.091 ≈ 4/3 larger than that of (4←0). This yields an estimated cross section of $\sigma_{IO(3\leftarrow1)} = 4.5 \cdot 10^{-17} cm^2 \cdot molec^{-1}$.

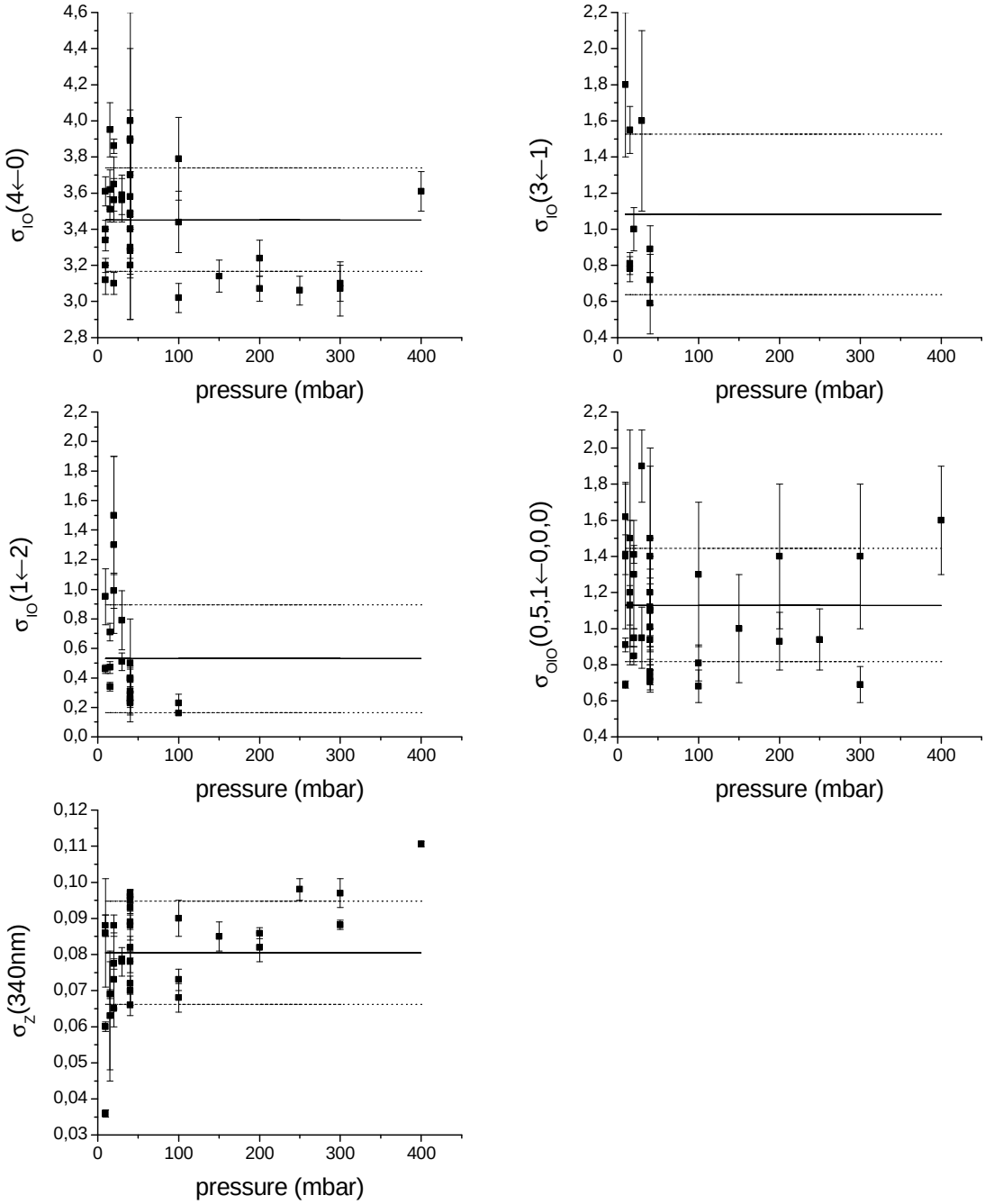

Figure 10.3 Results for cross sections obtained from individual data sets by the method of iodine conservation are plotted against overall pressure present in the individual experiment. This provides a measure for sensitivity of the method to changed conditions. To avoid misunderstandings: Even though cross sections under certain conditions can display a pressure dependence as such, in the present context this is not of concern. Here the dependence of the method and its results on changed chemical and physical conditions, which in turn influences the partitioning between different species is of concern. Vibrationally excited IO was only found at sufficient signal to noise in experiments with lowest pressures. This could partly explain the small pressure dependence observed for IO. The solid horizontal line indicates the average and the dotted lines the interval of standard deviation of each cross section.

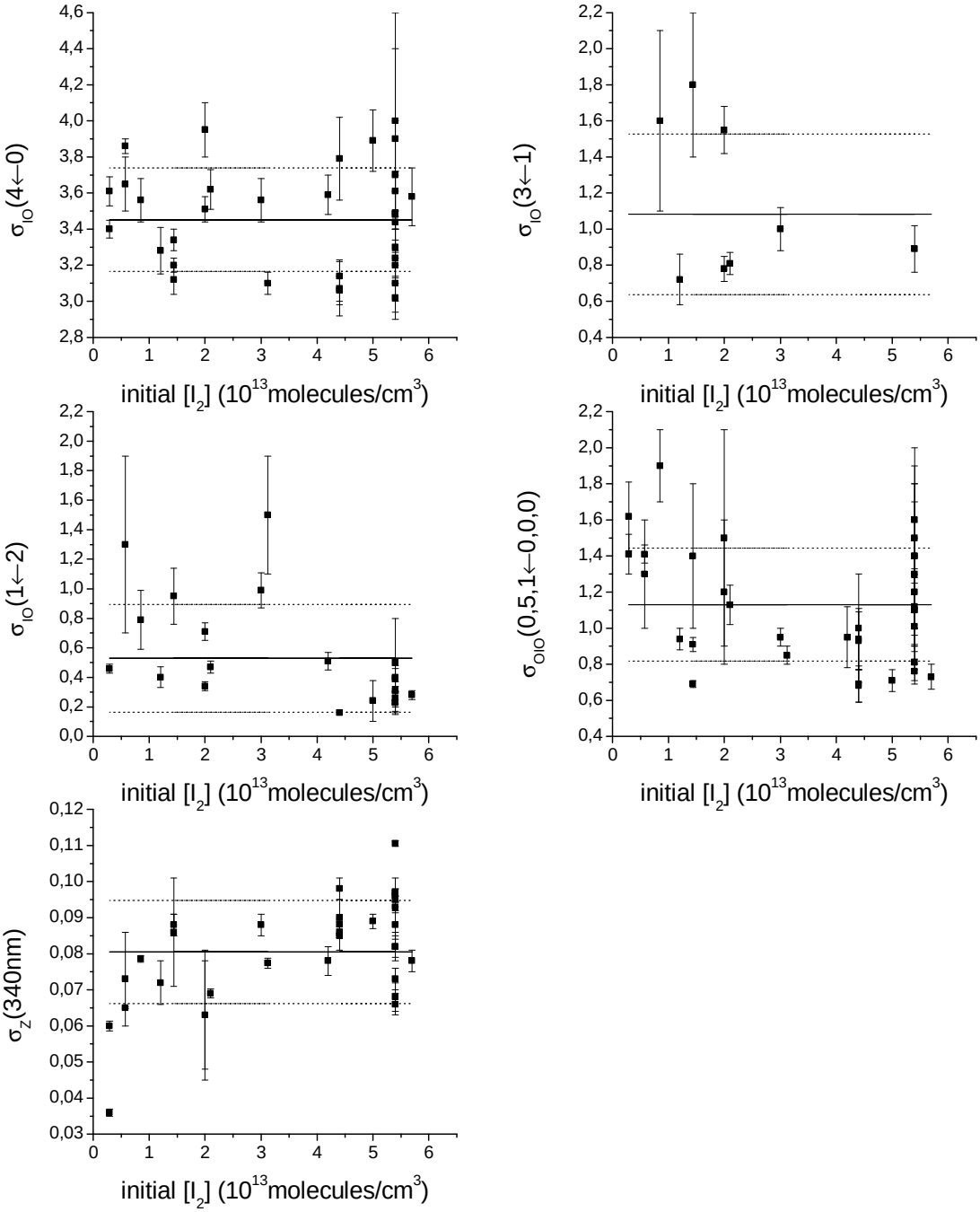

Figure 10.4 The dependence of cross section results obtained for the individual data sets on initial [I_2] concentration present in the experiment is examined. Only in "Z" appears to be a positive tendency in cross section with increasing initial [I_2]. But the effect is not large and considering the bulk of data points at the high end of [I_2] is held to be insignificant. The solid horizontal line indicates the averaged cross section while standard deviation is indicated by the dotted lines.

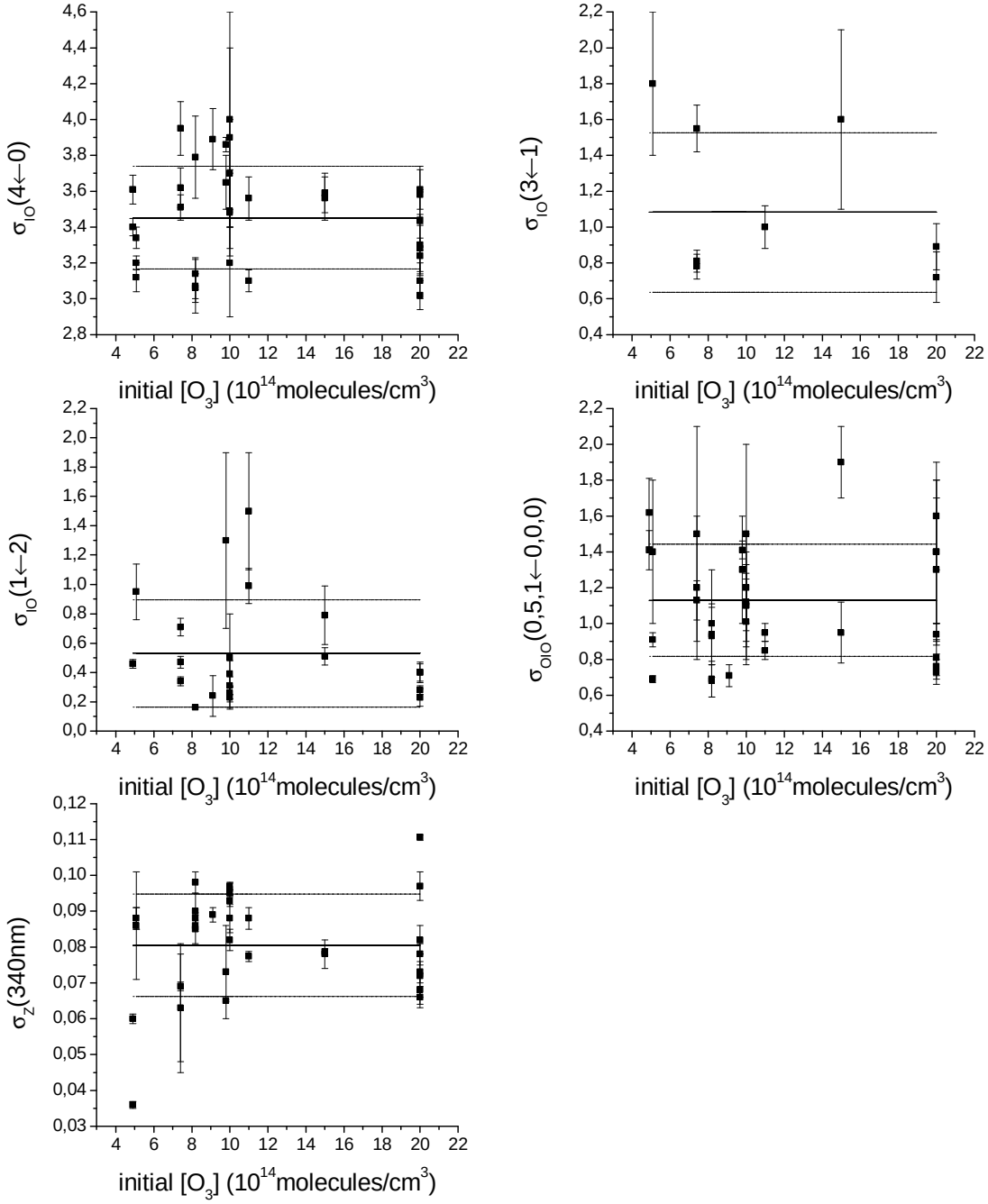

Figure 10.5 With respect to initial [O_3] no dependence of results is found for any of the considered species. The solid horizontal line indicates the averaged cross section while standard deviation is indicated by the dotted lines.

10.3.2 Discussion with respect to previously published results

Over the years a large number of measurements for the absorption cross section of IO have been published. But the scatter among them is considerable. Speculations that this scatter might be due to different resolution proved to be incorrect, see **Fig. 10.6**. There the available results are plotted as a function of resolution, which was used in their determination. In the context of **Chapter 9** the effect of resolution on the apparent peak height of the IO(4←0) transition was determined by direct measurement (black line with open circles). The line shows the relative change of peak height with resolution. It was scaled such that with respect to the available data it is roughly centred. In this sense its vertical position is arbitrary. But its shape demonstrates clearly that the effect of resolution does not explain the scatter of the available data. In **Tab. 10.3** the results from previous publications are summarised.

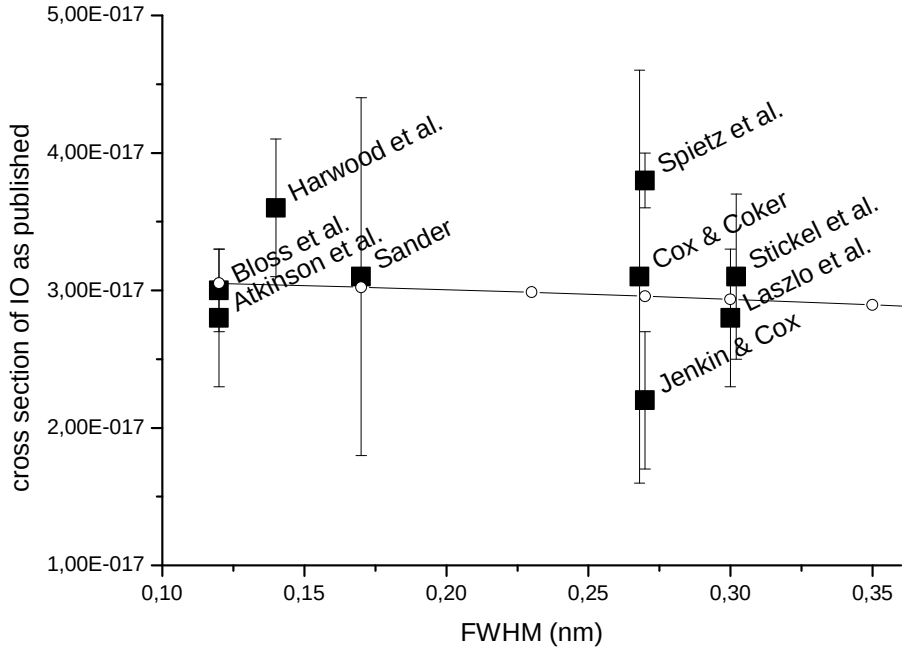

Figure 10.6 Effects of resolution and binning can not explain the scatter among the published results for the IO ground state absorption cross section. The slightly inclined line with open circles shows the effect of resolution and binning on the IO(4←0) band as determined in our measurements. The filled squares are a collection of published cross sections along with error bars and reference.

Dependence on different I_2 cross section reference data

Among the lower results those of Laszlo et al., Huie et al. and Atkinson et al. are systematically linked: The publications by Laszlo et al. and Huie et al. report results from the same experiment and therefore have to be counted as one independent result. Atkinson et al.

published a cross section for the by CRD spectroscopy rotationally resolved IO(2←0) band. This was obtained by transferring the cross section of Laszlo et al. of $(2.7\pm0.5)\cdot10^{-17}cm^2\cdot molec^{-1}$ via the characteristic function of the monochromator used in Laszlo's study. Therefore all three results depend on the same original determination.

Within the validation for the MIntAS approach this link was indirectly confirmed: The CRD spectrum used by Atkinson et al. [1999] is the one published by Newman et al. [1998]. With this spectrum and a sufficiently high resolved FTS spectrum of our Xenon lamp an absorption measurement with our set-up was simulated. In the convolution of the intensity spectra a gaussian was used as an approximation to the instrument's function of our set-up. The convoluted spectrum was then numerically binned on a grid resembling our CCD camera. This procedure produced the down scaling of 9.9±1 reported in **Section 9.8.4** with which the absolute cross section by Atkinson et al. could be transferred to the conditions of our measurements. In **Chapter 7** the relative strength of the IO(2←0) to the IO(4←0) was determined, see **Fig. 7.4** enabling the transfer of cross section to the (4←0) band. Applying MIntAS with an a-priori spectrum of IO(4←0) at 0.12nm FWHM produced an absolute cross section of $(2.6\pm0.8)\cdot10^{-17}cm^2\cdot molec^{-1}$, which after three transfers for resolution and one transfer between different bands is in good agreement with the value Atkinson et al. originally fed into their calculations. This result is also listed in **Tab. 10.3**.

In the determination of an absolute cross section for IO Laszlo et al. calibrated the concentration of IO in their experiment by using a cross section for I_2 of $\sigma_{I_2,C+P}(530nm)=2.56\cdot10^{-18}cm^2\cdot molec^{-1}$ published by Calvert and Pitts [1966]. Our own determination of the iodine cross section proved the results by Tellinghuisen to be highly reliable (see **Chapter 5**). At 530nm Tellinghuisen reports a significantly larger iodine cross section of $\sigma_{I_2}(530nm)=(3.1\pm0.1)\cdot10^{-18}cm^2\cdot molec^{-1}$ at low resolution. This changes the calibration of IO concentration in the data by Laszlo et al. and after rescaling their result accordingly this yields $(3.4\pm0.6)\cdot10^{-17}cm^2\cdot molec^{-1}$. In the same way the results of Huie et al. and Atkinson et al. can be corrected, thereby resolving part of the scatter among the different results. Apart from that the determination of I_2 concentration in the ro-vibronic region above 500nm is critical due to its rich ro-vibronic structure. Results are prone to effects of insufficient resolution as well as pressure. Therefore even after correction of the I_2 cross section the results have to be used with care.

Similar as the work of Laszlo et al. also the cross section obtained by Cox and Coker used an I_2 cross section by Calvert and Pitts. The latter used a cross section at 500nm, which is approximately 5% smaller than that by Tellinghuisen and the one determined in this work. Correcting this increases their cross section from $(3.1^{+2}_{-1.5})\cdot10^{-17}cm^2\cdot molec^{-1}$ to $(3.3^{+2.1}_{-1.6})\cdot10^{-17}cm^2\cdot molec^{-1}$, see **Tab. 10.3**.

Effects of vibrationally excited IO

Among the remaining results a number was obtained under conditions for which the simultaneous observation of vibrationally excited IO was reported. A conclusion of the present work is that the existence of excited IO in the determination of an IO cross section is one of the main problems causing the large scatter among the previously published results. And according to the available observations, at least one publication exists for each used chemical system, which showed the presence of excited IO.

As quenching of vibrationally excited IO depends on pressure, the low pressure experiments are more likely to having contained larger amounts of it. In so far – wherever excited IO was reported or the pressure had been low - the reported cross sections have to be regarded not in the sense of an absolute absorption cross sections for *ground state* IO(4←0), but rather as an overall measure for IO contained simultaneously in both ground state and excited states ad without being at thermal equilibrium. With respect to the studies by Cox and Coker and that by Jenkin and Cox this appears to be quite obvious: The study at high pressure (Cox and Coker, 1013mbar) yields a larger cross section of $3.3\cdot10^{-17}cm^2\cdot molec^{-1}$ (after correction of σ_{I_2}, see below), whereas that at low pressure (Jenkin and Cox, 10 to 100mbar, even though they did not mention the observation of IO^*) yielded a significantly smaller cross section. In the context of the simultaneous existence of ground state and vibrationally excited IO such a pressure dependence can be plausibly understood.

The effect can be quantified using the estimated relative magnitude of cross sections for (3←1) relative to (4←0) of ≈4/3, see above. Therefore observation of OD of excited IO(3←1) of no more than 13% relative to the IO(4←0) absorption will already cause an underestimation of the sought cross section by 10%. In our experiments especially at low pressure excited IO reached as much as 30%. This illustrates the sensitivity of determination of a ground state cross section to traces of excited IO. In those cases, where excited IO was present, the published cross sections therefore have to be smaller than a pure ground state

absorption cross section and have to be considered as lower limits to the true $\sigma_{IO}(4\leftarrow0)$ ground state cross section. This affects the results of Clyne and Cruse, Jenkin and Cox, to a certain degree Sander, also Laszlo et al. and the dependent results of Huie et al. and Atkinson et al., also Spietz et al [1998]. In the work of Harwood et al. it is stated that pressure was >420mbar, which indicates that their result could be less affected by excited IO, but their spectrum shows traces of it. The studies of Cox and Coker, Stickel et al., and Bloss et al. were all performed at 1013mbar, at which pressure the effect of IO^* is the smallest. Nevertheless the spectra by Cox and Coker as well as by Stickel et al. show bands of $IO(\nu'\leftarrow1)$ of the order of 10%. At thermal equilibrium optical density of only 5% relative to $(4\leftarrow0)$ should be expected, see above. In the quite clear spectrum of Bloss et al. only traces of it can be found. Therefore all but the last are regarded as lower limit estimates and are marked correspondingly in **Tab. 10.3**. In this context it has to be kept in mind that only two rough criteria could be used in this discussion, which were pressure and occurrence of excited IO in the spectrum. This leaves this discussion more of a qualitative than a quantitative argument.

Effects of wavelength calibration

The studies by Jenkin and Cox and that by Cox and Coker determined the IO cross section at 426.9nm, which could mean that their cross section is low due to containing the steep band head within the measured interval. But whether it really was determined at the wrong wavelength or just the wavelength calibration was off can not be decided. Durie, Legay and Ramsay [1960] determined the band head of IO *in emission* to be at 426.82nm, i.e. the "foot" of the *absorption* structure and not the maximum absorption. After the publication by Jenkin and Cox [1985] Sander determined the cross section at 427.2nm, after he had made sure that this was the maximum absorption of IO [1986]. All following studies used that wavelength. The CRD spectra by Newman et al. report its maximum to be at 427.20nm (vac.) in agreement with our observations.

Reference	$\sigma_{IO}(4\leftarrow0)\cdot10^{-17}$ ($cm^2\cdot molec^{-1}$)	$\sigma_{OIO}\cdot10^{-17}$ ($cm^2\cdot molec^{-1}$)	source	hot bands rel. to (4←0)	(2←0) reduced?	FWHM (nm)	T (K)
Clyne and Cruse [1970]	>0.5		$I+O_3$	(ν'←1), 30% 1 to 2mbar(?)		0.25	293
Cox and Coker [1983]	$3.1^{+2}_{-1.5}$ [j] **($3.3^{+2.}_{-1.6}$ [f])**		$I+O_3$	(ν'←1), weak 1013mbar	unclear	0.27	303
Jenkin and Cox [1985]	>2.2±0.5 [j]		$O+I_2$	? 10 to 100mbar		0.27	306
Sander [1986]	**(>)3.1±0.3**		$O+I_2$	? 470mbar		0.17	298
Stickel et al. [1988]	**>3.1±0.6**[g]		$O+I_2$ and $I+O_3$ simultaeously	(3←1), weak 1013mbar	unclear	0.3	300
Lazlo et al. [1995]	>2.7±0.5[a] (**>3.3±0.6** [e])		$O+I_2$	none 267 mbar	no	0.3	295
Huie et al. [1995]	>2.7±0.5 (>3.3±0.6 [e])		$O+I_2$	none 267 mbar	no	0.3	295
Turnipseed et al. [1995]			$I+O_3$	(2←1)	strong (LIF)		298
Himmelmann et al. [1996]			$I+O_3$	(ν'←1), 10%, late	no (late)		293
Harwood et al. [1997]	(>)**3.6±0.5**		$O+CF_3I$	weak >420mbar	not clear	0.14	203-373
Spietz et al. [1998]	>3.8±0.2 (**>3.4±0.8** [h])	>0.4 (0,5,1) (range: 2 to 5)	$O+I_2$ and $I+O_3$ simultaeously	(ν'←ν''), ν''>0 40 to 100 mbar	strongly	0.27	293
Atkinson et al. [1999]	>7.3±0.7 (2←0) CRDS (>2.6±0.8 (4←0), 0.12nm [b]) (**>3.1±1.0** (4←0), 0.12nm [e])		$O+CF_3I$	(ν'←1) (Newman et al. 1998)		0.0013 CRDS	295
Ingham et al. [2000]		(0,5,1) >2.7	$O+I_2$	(ν'←1), weak	no	0.16	
Bloss et al. [2001]	1.9±0.2 (1.13nm) (**3.3±0.3** (0.12nm)[c])	$0.87\pm0.15<\sigma_{OIO}<1.29\pm0.22$ (0,5,1) $0.83\pm0.14<\sigma_{OIO}<1.23\pm0.21$ (0,4,1)[d]	$O+CF_3I$	(ν'←1), weak 1013mbar	no	1.13	
Plane et al. [2005]		(0,4,1) 1.5±0.20	$O+CF_3I$			0.4 CRDS	
Dillon et al. [2005]		(0,5,1) 1.2					
This work	**3.5±0.3** (0.12nm)	(0,5,1) 1.3±0.3 (0,4,1) 1.24±0.3 [k]	$O+I_2$ and $I+O_3$ simultaeously	(ν'←ν''), ν''>0 10 to 400 mbar	strongly	0.12/1.3	298

Table 10.3 The results obtained for the IO and OIO absorption cross section in the previous studies are compared. Data in brackets indicates data obtained in this work by applying corrections to the original data, see footnotes. As the ground state cross section depends critically on the possible existence of vibrationally excited IO, this is considered as well. The chemical system in which the cross section was determined in is listed as well as the (approximate) pressure, resolution (FWHM) and temperature of the experiments. Chemiluminescence of the IO(2←0) band was observed. The available reference data was examined for that. Cross sections for OIO by Plane et al. 2005 and Dillon et al. 2005 are private communication.

Footnotes:
[a]: used σ_{I2} by Calvert and Pitts at λ>500nm in ro-vibronic region. In abstract 2.8±0.5, in body of text 2.7±0.5, as in Huie et al..
[b]: convoluted and binned to FWHM=1.3nm, 0.32nm/pixel, transferred to (4←0) by relative scaling, MIntAS correction to FWHM=0.12nm
[c]: MIntAS correction to convert from 1.13nm to 0.12nm, only scaling factor applied. 10% upward correction based on estimation of loss in Harwood et al. in same system.
[d]: transferred to (0,4,1) using the spectrum obtained in this work for comparability with Joseph et al. [2002]
[e]: after correction of σ_{I2} (21%) in Laszlo et al.
[f]: after correction of σ_{I2} (5%)
[g]: relies upon $k_{IO+IO}=6\cdot10^{-11}cm^3\cdot molec^{-1}\cdot s^{-1}$.
[h]: after re-evaluation of systematic errors (deposit) and re-weighting
[j]: IO cross section stated at λ=426.9nm
[k]: transferred to (0,4,1←0,0,0) for comparability with Joseph et al.

Mechanistic approaches: Possible effects of parameterisation or dependence on kinetic reference data

The cross section, which had been determined earlier in this lab [Spietz 1998] was the result of a complex fit to curves of temporal behaviour of IO, OIO, I_2 and O_3. These had been recorded one after another with up to 10 hours between the first and last recording. In spite of the well known deposition of deposit in the course of reaction, the chemical conditions in this system had to be assumed to be constant during that period to enable analysis. Our recent studies demonstrated that due to the accumulation of deposit and also to photolysis of deposit this assumption is a critical issue. In so far the error limit of 0.2 has to be regarded as too optimistic as it does not reflect the systematic errors caused by that. Re-evaluation of the data with systematic weighting by the available error estimates yields $(3.4 \pm 0.8)\cdot10^{-17}cm^2\cdot molec^{-1}$.

The cross sections determined in that study were the result of complex mechanistic studies based on the described curves of temporal behaviour. They were conducted using the commercial FACSIMILE software package and contained a large number of reactions. Therefore either the dependence on a comparatively large number of kinetic rate coefficients or on the other hand the risk of over-parameterisation limit the weight of this result. Also the effect of vibrationally excited IO had not been taken into account so that this result also has to be regarded as a lower limit. The lower limit estimate for OIO had been determined with a very simple predecessor of the method of iodine conservation presented in this work and is

therefore not affected by this. The work of Stickel et al. relied on a number of rate coefficients among which the overall rate coefficient for the IO+IO self reaction was used at $6 \cdot 10^{-11} cm^3 \cdot molec^{-1} \cdot s^{-1}$. According to more recent studies a larger value appears more realistic. This would increase the result by Stickel et al. correspondingly making it also a lower limit estimate.

The work of Harwood et al. [1997] was an intensive study which tested different sources for IO as well as different detection schemes. With a tuneable diode laser the shape of the IO(4←0) band and the wavelength of maximum absorption were determined. The cross section was determined in three different chemical systems ($(N_2O+h\nu)+CF_3I$, $(O_3+h\nu)+I_2$, $(N_2O+h\nu)+I_2$) but the first was found to produce the results with the smaller uncertainty. This system relies on the knowledge of the yield Φ of the reaction of $O+CF_3I$ producing IO. In the analysis of their experimental data obtained at 420mbar Harwood et al. used a value of $\Phi=0.86\pm0.06$ published by Gilles et al., which was obtained at 130mbar (100torr) and found to be independent of temperature. Bloss et al. examined the dependence of this yield on pressure and temperature and found no significant pressure dependence at 295K. The data at that temperature shows a negative trend of approx. 5% per 930mbar (700torr) but which is not significant with respect to the scatter of the data. For lower temperatures a clear negative trend of approx. 20% per 930mbar (700torr) was found. This could indicate that the 5% trend at room temperature might have at least some significance. In that case the cross sections obtained by Harwood et al. for temperatures below 298K would have to be corrected upwards corresponding to a smaller yield in the IO formation. Above 298K the data by Bloss et al. favours only small or no pressure dependence at all.

If one assumes the reduction of Φ of 5%/930mbar at 295K observed by Bloss et al. to be significant, it is possible to interpolate between this and the 20%/930mbar at 220K an estimate for a combined temperature and pressure dependence of Φ. With this the temperature independent value by Gilles et al. of 0.86 at 133mbar (100 torr) could be transferred to a higher pressure to account for p>420mbar in the Harwood et al. experiments. For higher temperatures the pressure dependence is assumed to tend to zero leaving the results unchanged. After this correction the cross section by Harwood et al. should be consistent with the findings of Bloss et al. about the combined temperature and pressure dependence of Φ. See result for this are listed in **Tab. 10.3**.

T (K)	σIO(4←0)·10-17 (cm2·molec-1)	pressure dependence of Φ	Φ	corrected σIO(4←0)·10-17 (cm2·molec-1)
373	3.9±0.1		0.86	3.9
353	3.4±0.1		0.86	3.4
323	3.3±0.1		0.86	3.3
298	3.4±0.1	**-5%/930mbar**	0.84	3.5
250	3.7±0.2	-14.2%/930mbar	0.80	4.0
220	3.7±0.1	**-20%/930mbar**	**0.78**	4.1
203	3.6±0.2	-23.3%/930mbar	0.77	4.0

Table 10.3 The original results obtained by Harwood et al. in the O+CF_3I system are shown in column two. From Bloss et al. a pressure and temperature dependence of the yield of IO in this system is inferred and applied to the former's data. The consistency of the data by Harwood et al. is reduced by that indicating problems in correctly determining the yield of IO and consequently also in deriving its cross section.

But within the Harwood data the former consistency of the cross sections at different temperatures is reduced by this. This could be interpreted such that the behaviour of Φ under different conditions is insufficiently understood. As a consequence the IO cross section depending on this yield would be likewise affected. Also the increased values for σ_{IO} of up to $4.1 \cdot 10^{-17} cm^2 \cdot molec^{-1}$ are somewhat discomforting in the context of the other results.

This is further supported by the fact, that the resolution corrected cross section of $(3.0 \pm 0.3) \cdot 10^{-17} cm^2 \cdot molec^{-1}$ (MIntAS: 0.12nm FWHM) obtained by Bloss et al. in exactly the same system does not reproduce the result of Harwood et al., see **Tab 10.2** and foot note. The differences between their studies were firstly significantly larger concentrations of IO in the study of Bloss et al. and consequently faster losses to the self reaction. Bloss et al. did not model losses near the initial peak absorption of IO as it was done in Harwood et al. Therefore their result should underestimate the true cross section. In the work of Harwood et al. the modelling of possible losses opposed to the simple stoichiometric conversion assumption led to changes of less than 10% (but it is not stated whether these corrections were always systematically in the same direction, as one would expect). In the work by Bloss et al. concentrations were larger and loss processes possibly larger. But even after a 10% correction, the Bloss et al. cross section would in comparison to Harwood et al. still be low at $3.3 \cdot 10^{-17} cm^2 \cdot molec^{-1}$.

After consideration of various effects the scatter between the available cross section data for IO could be reduced resolving some of the inconsistencies. On the scale of the stated

uncertainties most of the published results agree. Only the results by Clyne and Cruse and by Jenkin and Cox (which due to the argument above have also to be regarded as lower limits) fall significantly low with respect to the majority. With respect to all but the latter two the result of our study is in agreement within the error limits. It has to be noted that our result is larger than all others but that by Harwood et al. On the other hand all of them had to be considered as lower limits for reasons discussed above. The insensitivity of our method to experimental conditions, the dedicated consideration of vibrationally excited IO in our approach as well as the discussion of the compensation pattern for neglected absorbers led us to the conclusion that our result should underestimate the true value only to a very small extent (less than the stated uncertainty) if at all.

Therefore averaging the (corrected) results (bold face, **Tab. 10.2**) yields $3.3 \cdot 10^{-17} cm^2 \cdot molec^{-1}$. Considering only scatter of data used for the average produces a standard deviation of $\pm 0.2 \cdot 10^{-17} cm^2 \cdot molec^{-1}$. Regarding this nevertheless as a lower limit, this result is in good agreement with the cross section determined in this work. Both together indicate the true cross section to be between 3.3 and $3.5 \cdot 10^{-17} cm^2 \cdot molec^{-1}$ with a tendency towards the larger of the two.

The only other cross section, for which results have been published is that of OIO, mostly for the (0,5,1←0,0,0) transition. Bloss et al. published a range of $0.87 \cdot 10^{-17} cm^2 \cdot molec^{-1} < \sigma_{OIO} < 1.29 \cdot 10^{-17} cm^2 \cdot molec^{-1}$, which is in good agreement with our estimate of $1.3 \cdot 10^{-17} cm^2 \cdot molec^{-1}$. As for IO this is also not regarded as a lower limit but an absolute value. A previous lower limit estimate from this laboratory [Spietz et al. 1998] was $0.4 \cdot 10^{-17} cm^2 \cdot molec^{-1}$ with an expected range of 2 to $5 \cdot 10^{-17} cm^2 \cdot molec^{-1}$. This was obtained from a complex fit, see discussion for σ_{IO}. The weight of the expected range is therefore considered low, while the lower limit is still in agreement with the present determination. Ingham et al. reported a lower limit, which is substantially larger than the absolute value found in this work. It was based on a comparison of cumulative throughput of iodine through IO into OIO and the observed OD of OIO. As only one point in time was considered, its weight is regarded as low. Plane et al. (private communication 2005) report a value of $(1.5 \pm 0.2) \cdot 10^{-17} cm^2 \cdot molec^{-1}$ at (0,4,1←0,0,0) obtained with a 0.4nm FWHM binned CRDS system while Dillon et al. (private communication 2005) report $(1.2 \pm 0.3) \cdot 10^{-17} cm^2 \cdot molec^{-1}$. Both values are in good agreement with the result from our study with the deviations being within the error limits.

10.4 CONCLUSION

The method of iodine conservation was successfully applied in the determination of absorption cross sections from time resolved absorption spectroscopy measurements. Being independent of assumptions on chemical kinetics makes it a tool complementary to standard chemical models and fitting procedures.

Results were obtained for ground state IO, vibrationally excited IO, OIO and a yet unidentified absorber "Z":

$$\sigma_{IO}(4\leftarrow 0) = (3.5\pm 0.3)\cdot 10^{-17} cm^2\cdot molec^{-1} \text{ at 0.12nm FWHM.}$$

This is in good agreement with the recent understanding and interpretation of the published data. But it has to be pointed out, that the result presented here is a cross section for the *ground state* IO(4←0) progression. It is not – as it has to be inferred from determinations, where vibrationally excited IO was observed but not considered in the calculations – an effective and "over-all" cross section accounting for IO in the electronic ground state ignoring the vibrational excitation. Likewise it is not an "over-all" cross section for IO in thermal equilibrium. Consequently also an *effective* absorption cross section for excited IO was determined relative to the (3←1) transition. Its value accounts *simultaneously for all* IO(ν'←ν''), with ν''>0:

$$\sigma_{IO,eff}(3\leftarrow 1) = (2.0\pm 0.8)\cdot 10^{-17} cm^2\cdot molec^{-1} \text{ at 0.35nm FWHM}$$

Based on Franck-Condon factors by Rao et al. an absolute cross section for IO(3←1) valid for the ν''=1 progression was determined relative to $\sigma_{IO}(4\leftarrow 0)$, 0.12nm FWHM

$$\sigma_{IO}(3\leftarrow 1) = (4.5\pm 0.5)\cdot 10^{-17} cm^2\cdot molec^{-1} \quad \text{at 0.12nm FWHM}$$

The cross section of OIO resulted to be

$$\sigma_{OIO}(0,5,1\leftarrow 0,0,0) = (1.3\pm 0.3)\cdot 10^{-17} cm^2\cdot molec^{-1} \quad \text{at 0.35nm FWHM}$$

being in good agreement with two previous determinations, which yielded an expected range. It is also in agreement with two recent results for absolute cross section, which provided an absolute value rather than a range. For the yet unidentified absorber "Z" it was found:

$$\sigma_{"Z"}(340nm) = (1.0\pm 0.2)\cdot 10^{-18} cm^2\cdot atom^{-1} \quad \text{at 1.3nm FWHM.}$$

The latter is give in units cm^2 per iodine atom contained in the molecule "Z". For another unidentified absorber, labelled "Y" an estimate was determined of

$$\sigma_{"Y"}(322nm) = (1 \text{ to } 3)\cdot 10^{-18} cm^2 \cdot atom^{-1} \quad \text{at 1.3nm FWHM.}$$

This was obtained from only one data set, why its uncertainty is considered large. Units are the same as for "Z". Plausible candidates for these two are I_2O_2 as the expected product from the self reaction of IO as well as I_2O_3 from reaction of IO and OIO.

The main limitation to the method of iodine conservation is collinearity between curves of temporal behaviour of absorbers. It appears promising to consider regularisation methods [Kowalski 1983, Martens and Naes 1989, Neumaier unpubl. material, Tikhonov 1963] as well as approaches similar to perturbation theory to overcome this limitation.

11 SUMMARY AND CONCLUSION

Absorption spectra and absorption cross sections of iodine oxides relevant to atmospheric chemistry and laboratory studies have been studied by flash photolysis and synchronised molecular absorption and resonance absorption spectroscopy. Studied were mixtures of I_2 and O_3 in bath gases N_2 and/or O_2. In preparatory experiments the oscillator strength and absorption cross section of ground state $I(^2P_{3/2})$ in the 183.038nm transition have been determined to be

$$(2.34\pm0.3)\cdot10^{-14}\text{cm}^2\cdot\text{atom}^{-1} < \sigma < (5.42\pm0.8)\times10^{-14}\text{cm}^2\cdot\text{atom}^{-1} \quad \text{and}$$

$$(1.67\pm0.23)\times10^{-3} < f < (3.87\pm0.57)\cdot10^{-3}$$

with the lower limit determined by Clyne and Townsend and the upper limit from this work. The absorption cross section of I_2 at 500.0 nm (in standard air) was determined in an independent measurement to be

$$\sigma_{I_2}(500\text{nm}) = (2.18_6\pm0.021)\cdot10^{-18}\text{cm}^2\cdot\text{molec}^{-1}$$

which is in very good agreement with previously published data and where the uncertainty could be reduced by more than 50%. A weighted average of the recent determinations is suggested as the best estimate for the absolute absorption cross section

$$\sigma_{I_2}(500\text{nm}) = (2.19_1\pm0.02)\cdot10^{-18}\text{cm}^2\cdot\text{molec}^{-1}$$

Time resolved multi channel recordings obtained from absorption spectroscopy measurements with a grating spectrometer and a CCD camera were analysed. Use of methods from multivariate statistical analysis was studied. Independent Component Analysis, Principal Components Analysis and Multiple Multivariate Linear Regression techniques proved to be powerful tools for separating curves of temporal behaviour and for extracting spectra of individual absorbers from time resolved overlapped absorption data. For about 60 data sets recorded under various conditions of pressure and mixing ratios the curves of temporal behaviour of absorbers could be separated from each other. They could be shown to be free of other absorptions to better than ±3%. The sets of separated time curves provide the necessary data for subsequent kinetic analysis of the reaction system under study. Within this study

these curves provide the input data for the method of iodine conservation to produce estimates of absorption cross sections, which are independent of kinetic reference data.

Likewise spectra of individual absorbers could be extracted with the same accuracy of ±3%. For the first time the overlapping absorption spectra of ground state IO, vibrationally excited IO(ν'←ν''), ν''>0 with ν'' up to 7 and of OIO could be separated from each other. The absorption continuum of IO(ν'←0) could be accurately determined to its UV end. Also spectra of three yet unidentified absorbers were extracted. Resolution is 1.3nm FWHM. The spectra are available as reference data.

Given the accuracy of the extracted spectra an analysis of band strength of transitions in the IO molecule was possible. Examination of the absorption continuum of IO provided evidence for two optically active bound-free transitions. Tangents to the repulsive potentials were determined by the reflection method. Extrapolation from the tangents to plausible dissociation products provided estimated shapes of the repulsive potentials, which are in agreement with findings by Newman et al. based on ab initio work on ClO, Wigner-Witmer correlation rules and CRDS measurements of IO transitions.

An absorption feature, which was extracted with the spectrum of vibrationally excited IO could be shown to belong not to excited IO but to a different and up to now not observed molecule. There is evidence that this molecule is the weakly bound IOO.

Band strength of bound-bound transitions of ground state and vibrationally excited IO were determined and – after appropriate scaling - found to be in good agreement with Franck-Condon factors published by Rao et al. as well as factors calculated in Morse approximation.

Anomalous behaviour of the IO(2←0) transition was observed. The observed behaviour could be interpreted as result of chemiluminescence from IO($A^2\Pi_i$), ν'=2 to IO($X^2\Pi_i$), ν'=0. Different sources for IO in the upper electronic state are discussed. O(^{1}D)+I_2 is the only known source providing enough energy, but according to our present understanding only insufficient concentrations of O(^{1}D) should be present in the studied mixtures due to quenching. Therefore the source of the anomalous behaviour of IO(2←0) remains unclear.

Effects of low resolution and coarse binning on apparent optical density and apparent cross section were studied. A method was developed, which allows compensation of such effects, if an absorption spectrum recorded at the higher target resolution is available. The method is referred to as "Multichannel Integrated Absorption Spectroscopy", or – more shortly –

"MIntAS". Apart from simple scaling also non-linear behaviour of optical density relative to concentration was found. For the absorbers under study the effects wee determined and corrected. Thereby it is possible to quantitatively deduce absorption cross sections at nominally higher resolution and finer binning from low resolution experimental data.

Based on the separated curves of optical density obtained above, a method was developed to determine simultaneous estimates for all absorption cross sections observed in an experiment. It considers the available amount of iodine atoms after photolysis and the partitioning of iodine over all observed absorbers at different times after photolysis. Tackling the problem in form of a multivariate linear regression model enables determination of cross section estimates independent of kinetic reference data and independent of mechanistic assumptions. The method is referred to as the method of iodine conservation. Prerequisite to it is that all absorbers of significant iodine content are observed and accounted for. Criteria to check this assumption are formulated. Numerical problems caused by collinearity are encountered and solved by approximate solutions. Improvements to these approximations by methods used in perturbation theory appear promising.

The method was successfully applied to the separated and MIntAS corrected curves of temporal behaviour of absorbers in the I_2+O_3 photolysis. Obtained are cross sections for IO, vibrationally excited IO, OIO and a yet unidentified higher oxide "Z". The results show a good consistency over the available data sets. For ground state IO a cross section of

$$\sigma_{IO}(4\leftarrow 0) = (3.5\pm 0.3)\cdot 10^{-17}\,cm^2\cdot molec^{-1} \text{ at } 0.12nm \text{ FWHM}$$

was obtained, which is in good agreement with the recent understanding and interpretation of the published data. This result is a cross section for *ground state* IO(4←0). It is not an effective and "over-all" cross section accounting for IO in the electronic ground state ignoring the vibrational excitation. Likewise it is not a cross section for IO being in thermal equilibrium. This proved to be of importance as the IO population was found to bestrongly inverted. Consequently for the first time vibrationally excited IO(ν'←1) was considered and the accuracy of the ground state cross section thereby improved. A separate *effective* absorption cross section for excited IO relative to the (3←1) transition was determined, which accounts *simultaneously for all* IO(ν'←ν''), with ν''>0:

$$\sigma_{IO,eff}(3\leftarrow 1) = (2.0\pm 0.8)\cdot 10^{-17}\,cm^2\cdot molec^{-1} \text{ at } 0.35nm \text{ FWHM}$$

Based on Franck-Condon factors by Rao et al. also an absolute cross section for IO(3←1) valid for the ν"=1 progression was determined relative to σ_{IO}(4←0), 0.12nm FWHM

$$\sigma_{IO}(3\leftarrow1) = (4.5\pm0.5)\cdot10^{-17}cm^2\cdot molec^{-1} \quad \text{at 0.12nm FWHM}$$

The cross section of OIO is determined to be

$$\sigma_{OIO}(0,5,1\leftarrow0,0,0) = (1.3\pm0.3)\cdot10^{-17}cm^2\cdot molec^{-1} \quad \text{at 0.35nm FWHM}$$

which is in good agreement with two previous determinations, which yielded an expected range and also with two recent results for absolute cross section. For two further and yet unidentified absorbers "Z" and "Y" the cross section could also be determined:

$$\sigma_{"Z"}(340nm) = (1.0\pm0.2)\cdot10^{-18}cm^2\cdot atom^{-1} \quad \text{at 1.3nm FWHM.}$$

$$\sigma_{"Y"}(322nm) = (1 \text{ to } 3)\cdot10^{-18}cm^2\cdot atom^{-1} \quad \text{at 1.3nm FWHM.}$$

Units are cm^2 per iodine atom contained in the molecule. The latter was obtained from only one data set, why its uncertainty is considered large.

For future work it appears promising to consider regularisation methods for overcoming collinearity problems in the solution of the iodine conservation algorithm. Also concepts similar to perturbation theory seem suited to solve the model iteratively.

REFERENCES

Allan, B.J., G. McFiggans, and J.M.C. Plane (2000): **Observation of iodine monoxide in the remote marine boundary layer.** *J. Geophys. Res.*, Vol. 105, pp. 14363-14369

Allan, B.J., J.M.C. Plane, and G. McFiggans (2001): **Observations of OIO in the remote marine boundary layer.** *Geophys. Res. Lett.*, Vol. 28, pp. 1945-1948

Allicke, B., K. Hebestreit, J. Stutz, and U. Platt (1999): **Iodine oxide in the marine boundary layer.** *Nature*, Vol. 397, pp. 572-573

Atkinson, D.B., J.W. Hudgens, ad A.J. Orr-Ewing (1999): **Kinetic Studies of the Reactions of IO Radicals Determined by Cavity Ring-Down Spectroscopy.** *J. Phys. Chem. A*, Vol. 103, pp.6173-6180

Barrie, L.A., J.W. Bottenheim, R.C. Schnell, P.J. Crutzen, R.A. Rasmussen (1988): **Ozone destruction and photochemical reactions at polar sunrise in the lower Arctic atmosphere.** *Nature*, Vol. 334, pp. 138

Barrie, L.A., R. Staebler, D. Toom, B. Georgi, G. Denhartog, S. Landsberger, D. Wu (1994): **Arctic aerosol size-segregated chemical observations in relation to ozone depletion during Polar Sunrise Experiment 1992.** *J. Geophys. Res.*, Vol. 99, pp. 25439-25452

Bates, D.R., and M. Nicolet (1950): **Atmospheric Hydrogen.** *Publ. Astron. Soc. Pac.*, Vol. 62, pp. 106-110

Bauer, D., T. Ingham, and J.N. Crowley (2004): **Interactive comment on "Absolute absorption cross section and photolysis rate of I_2" by A. Saiz-Lopez et al..** *Atmos. Chem. Phys. Discuss.*, Vol. 4, S741-S743

Bedjanian, Y., G. Le Bras, G. Poulet (1997): **Kinetics and mechanism of the IO + ClO reaction**, *J. Phys. Chem. A*, Vol. 101, pp. 4088 - 4096

Bedjanian, Y., G. Poulet (2003): **Kinetics of Halogen Oxide Radicals in the Stratosphere.** *Chem. Rev.*, Vol. 103, pp. 4639-4655

Beine, H. J., R.E. Honrath, F. Domine, W.R. Simpson, M.D. King, J.D. Fuentes (2001): **NOx during background and ozone depletion periods at Alert: Fluxes above the snow surface.** *J. Geophys. Res.*, 10.1029/2002JD002082.

Bloss, J.W., D.M. Rowley, R.A. Cox, and R.J. Jones (2001): **Kinetics and Products of the IO Self-Reaction.** *J. Phys. Chem.*, Vol. 105, pp.7840-7854

Bottenheim, J.W., L.A. Barrie, E. Atlas, L.E. Heidt, H. Niki, R.A. Rasmussen, P.B. Shepson (1990): **Depletion of lower tropospheric ozone during Arctic spring: The polar sunrise experiment 1988**, *J. Geophys. Res.*, Vol. 95, pp. 18555

Boumans, P.W.J.M (1972): **Excitation of Spectra.** in *E.L.Grove (Ed.): Analytical Emission Spectroscopy Part II*, Marcel Dekker, New York, Chap. 6

Burkholder, J.B., C. Curtius, A.R. Ravishankara, and E.R. Lovejoy (2004): **Laboratory studies of the homogeneous nucleation of iodine oxides.** *Atmos. Chem. Phys.*, Vol. 4, pp. 19-34

Canosa-Mas, C.E., M.J. Scott, D. Shah, A. Vipond, K. Wagner, and R.P. Wayne (1999): **Laboratory investigation of kinetics of reactions of IO radicals**, *Central Laser Facility Annual Report 1999/2000*

Calvert, J.G. and J.N. Pitts (1966): **Photochemistry**. John Wiley and Sons, New York

Carpenter, L.J. (2003): **Iodine in the Marine Boundary Layer.** *Chem. Rev.*, Vol. 103, pp. 4953-4962

Carpenter, L.J., G. Malin, F. Kuepper, P.S. Liss (2000): **Novel iodine-containing trihalomethanes and other reactive halocarbons in the Coastal East Atlantic.** *Global Biogeochem. Cycles*, 14(4), pp. 1191-1204

Carpenter, L.J., K. Hebestreit, U. Platt, P.S. Liss (2001): **Coastal zone production of IO precursors: A 2-dimensional study.** *Atmos. Chem. Phys.*, Vol. 1, pp. 9-18

Carpenter, L.J., W.T. Struges, P.S. Liss, S.A. Penkett, B. Allicke, K. Hebestreit, U.Platt (1999): **Short-lived alkyl iodides and bromides at Mace Head, Ireland: Links to biogenic sources and halogen oxide production.** *J. Geophys. Res.*,Vol. 104, pp.1679-1689

Chameides, W.L. and D.D. Davis (1980): **Iodine: Its Possible Role in Tropospheric Photochemistry.** *J. Geophys. Res.*, Vol. 85, pp. 7383-7398

Chapman, S. (1930): **A theory of upper-atmosphere ozone.** *Mem. Roy. Meteorolog. Soc.*, Vol. 3, pp. 103

Chase, M.W., Jr. (1996): **NIST-JANAF Thermochemical Tables for the Iodine Oxides.** *J. Phys. Chem. Ref. Data*, Vol. 25, No. 5, pp. 1297-1339

Chase, M.W., Jr. (1998): **NIST-JANAF Thermochemical Tables, Fourth Edition.** *J. Phys. Chem. Ref. Data, Monograph 9*, pp. 1-1951

Clyne, M.A.A. and H.W. Cruse (1970): **Rates of elementary reactions involving the BrO($X^2\Pi$) and IO($X^2\Pi$) radicals. Part 2. Reactions of the BrO and IO radicals.** *Trans. Faraday Soc.*, Vol. 66, pp. 2227-2236

Clyne, M.A.A. and L. W. Townsend (1974): **Determination of atomic oscillator strengths using resonance absorption with a Doppler line source: Transitions of Br and I(n+1)s-np^5.** *J. Chem. Soc. Faraday Trans. II*, Vol. 70, pp. 1863–1881

Cox, R.A. and G.B. Coker (1983): **Absorption Cross Section and Kinetics of IO in the Photolysis of CH_3I in the Presence of Ozone.** *J. Phys. Chem.*, Vol. 87, pp. 4478-4484

Crutzen, P.J. (1970): **The influence of nitrogen oxide on the atmospherc ozone content.** *Q.J.R. Meteorol. soc.*, Vol. 96, pp. 320-327

Crutzen, P.J., and P.H. Zimmermann (1991): **The changing photochemistry of the troposphere**. *Tellus*, Vol. 43AB, pp. 136-151

Dahlquist, A., A. Björk and N. Anderson (1974): **Numerical Methods.** Prentice Hall, Englewood cliffs, N.J.

Davis, D., J. Crawford, S. Liu, S. McKeen, A. Bandy, D. Thornton, F. Rowland, and D. Blake (1996): **Potential impact of iodine on tropospheric levels of ozone and other critical oxidants.** *J. Geophys. Res.*, Vol. 101, pp. 2135-2147

Dobson, G.M.B. (1968): **Forty Years' Research on Atmospheric Ozone at Oxford: A History**. Applied Optics, Vol. 7, No. 3, pp. 387-405

Durie, R.A. and D.A. Ramsay (1958) **Absorption Spectra of the Halogen Monoxides**. *Canadian Journal of Physics*, Vol. 36, pp. 35-53

Durie, F. Legay and D.A. Ramsay (1960): **An emission system of the IO molecule**. *Canadian Journal of Physics* 38, 444-452

Fan, S. and D. Jacob (1992): **Surface ozone depletion in Arctic spring sustained by bromine reactions on aerosols.** *Nature*, Vol. 359, pp. 522-524

Farman, J.C., B.G. Gardiner, and J.D. Shanklin (1985): **Large losses of total ozone in Antarctica reveal seasonal ClO_x/NO_x interaction.** *Nature*, Vol. 315, pp. 207-210

Fickert, S., J.W. Adams, and J.N. Crowley (1999): **Activation of Br_2 and BrCl via uptake of HOBr onto aqueous solutions.** *J. Geophys. Res.*, Vol. 104, pp.23719-23727

Finlayson-Pitts, B.J. and J.N. Pitts Jr. (2000): **Chemistry of the Upper and Lower Atmosphere.** Academic Press, New York

Fishman, J. and P. Crutzen (1978): **The origin of ozone in the troposphere.** *Nature*, Vol. 274, pp. 855-858

Gilles, M.K., A.A. Turnipseed, M.K., J.B. Burkholder and A.R. Ravishankara (1997): **Kinetics of the IO radical: 1. Reaction of IO with ClO**, J. *Phys. Chem. A*, Vol. 101, pp. 5526-5534

Gómez Martín, J.C., P. Spietz, J. Orphal and J. P. Burrows (2004): **Principal and Independent Component Analysis of Overlapping Spectra in the Context of Mulichannel Time-resolved Absorption Spectroscopy**. *Spectro. Chim. Acta A*, Vol. 60, pp. 2673-2693

Gross, U., A. Ubelis, P. Spietz, and J.P. Burrows (2000): **Iodine and mercury resonance lamps for kinetics experiments and their spectra in the far ultraviolet.** *J. Phys.D: Appl. Phys.*, Vol. 33, pp. 1588-1591

Hartley, W.N. (1881): **On the absorption of solar rays by atmospheric ozone.**

J.Chem.Soc., Vol. 39, pp.111

Harwood, M., J. Burkholder, M. Hunter, R. Fox, and A. Ravishankara (1997): **Absorption Cross Sections and Self-Reaction Kinetics of the IO Radical.** *J. Phys. Chem. A*, Vol. 101, pp. 853-863

Haussmann, M., and U. Platt (1994): **Spectroscopic measurement of bromine oxide and ozone in the high Arctic during Polar sunrise Experiments 1992.** *J. Geophys. Res.*, Vol. 99, pp. 25399-25413

Herzberg, G. (1950): **Moleculat Spectra and Molecular Structure, Vol. I. Spectra of Diatomic Molecules**, Krieger Publishing Company, Malabar, Florida

Himmelmann, S., J. Orphal, H. Bovensmann, A. Richter, A. Ladstaetter-Weissenmayer and J.P. Burrows (1996): **First observation of the OIO molecule by time-resolved flash photolysis absorption spectroscopy**, *Chem. Phys. Lett.*, Vol. 251, pp. 330-334

Hoffmann, T., C.D. O'Dowd, and J.H. Seinfeld (2001): **IO homogeneous nucleation: An explanation for coastal new particle formation.** *Geophys. Res. Lett.*, Vol. 28, pp. 1949-1952

Holand, H.D. (1978): **The chemistry of the atmosphere and oceans.** New York, John Wiley & Sons

Houzeau, A. (1858): **Preuve de la présence dans l'atmosphere d'un nouvea principe gazeux, l'oxygène naissant.** *C.R. Acad. Sci. Paris*, Vol. 46, pp.89

Huie, R.E., B. Laszlo, M.J. Kurylo, S.N. Buben, E.M. Trofimova, A.I. Spassky, N.A. Messineva, D. Nevozhai, A.W. Miziolek (1995): **The atmospheric chemistry of iodine monoxide.** Presented at the Halon Options Technical working conference, Albuquerque, N.M.

Hunter, T.F. and C.M. Leong (1987): **Absolute Yields of $I(^2P_{1/2})$ in I_2 Photodissociation using a Laser Optoacoutstic Technique.** *Chemical Physics*, Vol. 111, pp. 145-153

Ingham, T., M. Cameron and J.N. Crowley (2000) **Photodissociation of IO (355 nm) and OIO (532 nm): Quantum yields for $O(^3P)$ and $I(^2P_J)$ Production**, *Journal of Physical Chemistry A*, 104, pp. 8001-8010.

Ingle, J. D. Jr. and S. R. Crouch (1988): **Spectrochimical Analysis.** Prentice Hall International Editions, London, App.F, pp.563

Itoh, N., M. Tsujita, T. Ando, G. Hisatomi, T. Higashi (1997): **Formation and emission of monohalomethanes from marine algae.** *Phytochemistry*, Vol. 45, pp.67-73

IUPAC, Subcommittee for Gas Kinetic Data Evaluation (2003): **Supplementary Data: Thermodynamic Data**, http://www.iupac-kinetic.ch.cam.ac.uk/

Jenkin, M.E., and R.A: Cox (1985): **Kinetics Study of the Reactions IO + NO_2 + M → $IONO_2$ + M, IO + IO → Products, and I + O_3 → IO + O_2.** *J. Phys. Chem.*, Vol. 89, pp. 192-199

Jenkin, M.E., R.A. Cox, and G.D. Hayman (1991): **Kinetics of the reaction of IO radicals with HO_2 radicals at 298K**, *Chem. Phys. Lett.*, Vol. 177, No. 3, pp. 272-278

Johnston, H.S. (1971): **Reduction of stratospheric ozone by nitrogen oxide catalysts from supersonic transport exhaust.** *Science*, Vol. 173, pp. 517-522

Johnston, P.V. (1996): **Studies on the I_0-effect.** unpublished manuscript

Jones, A.E., and J.D. Shanklin (1995): **Continued Decline of total ozone over Halley, Antarctica, since 1985.** *Nature*, Vol. 376, pp. 409-411

Jones, A.E., R. Weller, A. Minikin, E.W. Wolff, W.T. Sturges, H.P. McIntyre, S.R. Leonard, O. Schrems, and S. Bauguitte (1999): **Oxidized nitrogen chemistry and speciation in the Antarctic troposphere.** *J. Geophys. Res.*, Vol. 104, pp. 21355-21366

Joseph, D.M., S.H. Ashworth, B.J. Allan and J.M.C. Plane (2002): **Laboratory studies of OIO radical chemistry**. Proceedings of the 17th International Symposium on Gas Kinetics, Essen, Germany

Junge, C.E. (1963): **Global Ozone Budget and Exchange between Stratosphere and Troposphere.** *Tellus*, Vo. 14, pp. 363-377

Klick, S., K. Abrahamsson (1992): **Biogenic volatile iodated hydrocarbons in the ocean.** *J. Geophys. Res.*, Vol. 97, pp. 12683

Kortüm, G. and G. Friedheim (1947): **Lichtabsorption und Molekularzustand des Jods als Dampf und Lösung.** *Zeitschrift für Naturforschung*, Vol.2a, pp. 20-27

Kowalski, B.R. (ed.)(1983): **Chemometrics and Statistics in Chemistry.** Reidel, dordrecht, Holland

Kreher, K., P.V. Johnston, S.W. wood, and U. Platt (1997): **Ground based measurements of tropospheric and stratospheric BrO at Arrival Heights (78°S), Antarctica.** *Geophys. Res. Lett.*, Vol. 24, pp. 3021-3024

Lafferty, W.J., A. M. Solodov, C. L. Lugez, and G. T. Fraser (1998): **Rotational Line Strengths and Self-Pressure-Broadening Coefficients for the 1.27- m, $a^1\Delta_g$ - $X^3\Sigma_g^-$, v 0 0 Band of O_2**, *Appl. Opt.*, Vol. 37, pp. 2264-2270.

Laidler, K.J. (1987): **Chemical Kinetics, 3rd Edition.** *Harper Collins Publishers Inc.*, New York

Larin, I.K., D.V. Nevozhai, A.I. Spasskii, E.M. Trofimova, and L.E. Turkin (1999): **Measurement of rate constants for the reaction of iodine monoxide with ozone**, *Kinetics and Katalyis (Kinetika i Kataliz)*, Vol. 40, No. 4, pp. 435-442

Laszlo, B., M.J. Kurylo, and R.E. Huie (1995): **Absorption Cross Sections, Kinetics of Formation, and Self Reaction of the IO Radical Produced via the Laser Photolysis of $N_2O/I_2/N_2$ Mixtures.** *J. Phys. Chem.*, Vol. 99, pp. 11701-11707

Lawrence G. M. (1967): **Resonance transition probabilities in intermediate coupling for some neutral non-metals.** *Astrophys. J.*, Vol. 148, pp. 261

Lide, D.R., ed. (1993): **CRC Handbook of Chemistry and Physics, 73. Ed.**, CRC Press Inc.

Maier and Bothur (1997): **Matrix-Isolation of Iodine Superoxide and Iodine Dioxide.** *Chem. Berichte*, Vol. 130, pp. 179-181

Manley, S.L, J.L de la Cuesta (1997): **The production of methyl iodide by phytoplankton in culture.** *Limnol. Oceanogr.*, Vol. 42, pp.142-147

Martens, H. and T. Naes (1989): **Multivariate calibration.** Wiley, New York.

Marter, T.v., M.C. Heaven, and D. Plummer (1996): **Measurement of the rate constant for the quenching of $I(^2P_{1/2})$ by $O_2(X)$ at 150K**. *Chem. Phys. Lett.*, Vol. 260, pp. 201-207

Martinez, M., T. Arnold, and D. Perner (1999): **The role of bromine and chlorine chemistry for arctic ozone depletion events in Ny-Alesund and comparison with model calculations.** *Ann. Geophys.*, Vol. 17, pp. 941-956

McElroy, C., C. McLinden, and J. McConnell (1999): **Evidence for bromine monoxide in the free troposphere during the Arctic polar sunrise.** *Nature*, Vol. 397, pp. 338-341

McElroy, M.B., R.J. Salawich, S.C. Wofsy, and J.A. Logan (1986): **Reduction of Antarctic ozone due to synergistic interactions of chlorine and bromine.** *Nature*, Vol. 321, pp. 759-762

McFiggans, G., J.M.C. Plane, B.J. Allan, and L.J. Carpenter (2000): **A modeling study of iodine chemistry in the marine boundary layer.** *J. Geophys. Res.*, Vol. 105, pp. 14371-14385

McGrath, W.D. and R.G.W. Norrish (1958): *Z. Phys. Chem.*, Vol. 15, pp. 245; (1960): *Proc. Roy. Soc. A*, Vol. 254, pp. 317

Miller, C.E. and E.A. Cohen (2001): **Rotational spectroscopy of IO $X^2\Pi_i$.** *J. Chem. Phys.*, Vol. 115, No. 14, pp. 6459-6470

Miller, C.E. and E.A. Cohen (2003): **The rotational spectrum of iodine dioxide OIO**, *J. Chem. Phys.*, Vol. 118, No. 10, pp., DOI: 10.1063/1.1540107

Misra, A., P. Marshall (1998): **Computational investigations of iodine oxides.** *J.Phys.Chem. A*, Vol. 102, pp.9056-9060

Mitchell, A.C.G., M.W. Zemansky (1972): **Resonance Radiation and Excited Atoms.** Cambridge Univ. Press

Molina, L.T., and F.S. Rowland (1974): **Stratospheric sink for Chlorofluoromethanes: chlorine atom catalyzed destruction of ozone.** *Nature*, Vol 249, pp. 820-822

Molina, L.T., and M.J. Molina (1987): **Production of Cl_2O_2 from the self reaction of the ClO radical.** *J. Phys. Chem.*, Vol. 91, pp. 433-436

Molina, M. J., T.-L. Tso, L.T. Molina, and F. C.-Y. Wang (1987): **Antarctic Stratospheric Chemistry of Chlorine Nitrate, Hydrogen Chloride, and Ice: Release of Active Chlorine.** *Science*, Vol. 238, pp. 1253-1257

Molina, M.J. (1991): **Heterogeneous Chemistry on Polar Stratospheric Clouds.** *Atmos. Environ.*, Vol.25A, pp. 2535-2537

Moore, R.M., and R. Tokarczyk (1993): **Volatile biogenic halocarbons in the north-west Atlantic.** *Global Biogeochem. Cycles*, Vol. 7, pp. 195-210

Morse, P.M. (1929): **Diatomic molecules according to the wave mechanics. II. Vibrational levels**. *Phys. Review*, Vol. 34, pp 57-64

National Reseach Council (1979): **Stratospheric Ozone Depletion by Halocarbons: Chemistry and Transport.** Panel on Chemistry and Transport, Committee on

Impacts of Stratospheric Change, Assembly of Mathematical and Physical sciences, National academy of Sciences, Washinton, DC

Neumaier, A.: **Solving ill-conditioned and singular linear systems: A tutorial on regularization.** manuscript available at: http://solon.cma.univie.ac.at/~neum

Newman, S.M., W. H. Howie, I. C. Lane, M. R. Upson and A. J. Orr-Ewing (1998). **Predissociation of the A $^2\Pi_{3/2}$ state of IO studied by cavity ring-down spectroscopy**. *J. Chem. Soc., Faraday Trans.*, Vol. 94, 2681-2688

Newman, S. M., I. C. Lane, A.J. Orr-Ewing, D.A. Newnham, J. Ballard (1999). **Integrated absorption intensity and Einstein coefficients for the O_2 *a* $^1\Delta_g$–*X* $^3\Sigma_g^-$ (0,0) transition: A comparison of cavity ringdown and high resolution Fourier transform spectroscopy with a long-path absorption cell**. *J. Chem. Phys.*, Vol. 110, 10749-10757.

NIST Online Databases (2003): http://webbook.nist.gov

NIST: National Institute of Standards and Technology, Reference Data Program (1998):

NIST Chemical Kinetics Database, NIST Standard Reference Database 17 2Q98,

Gaithersburg, U.S. Secretary of Commerce, United States of America

Norrish, R.G.W. (1967): **Some Fast Reactions in Gases Studied by Flash Photolysis and**

Kinetic Spectroscopy, Nobel Lecture, Cambridge University

Norrish, R.G.W., G. Porter (1949): Nature, Vol.164, pp.658

Notholt, J., F. Cappellani, H. Roesdahl and G. Restelli (1991): **Absolute infrared band intensities and air broadening coefficient for spectroscopic measurements of formic acid in air.** *Spectrochimica Acta Part A*, Vol. 47, No.3/4, pp. 477-483

O'Dowd, C.D. (2001): **Biogenic coastal aerosol production and it influence on aerosol radiative properties.** *J. Geophys. Res.*, Vol. 106, pp. 1545-1549

O'Dowd, C.D., J.L. Jimenez, R.Bahreini, R.C. Flagan, J.H. Seinfeld, K. Hameri, L. Pirjola, M. Kulmala, S.G. Jennings, and T. Hoffmann (2002): **Particle Formation in the Marine Atmosphere Controlled by Biogenic Iodine Emissions.** *Nature*, Vol. 417, pp. 632-636

Okabe, H. (1978): **Photochemistry of small molecules**, Wiley and Sons Inc.

Pinta, M. (1975): **Atomic Absorption Spectrometry.** Adam Hilger, London, Chap. 1.1.4, pp.7-8

Plane, J.M.C., B.J. Allan, and S.H. Ashworth (2001): **On the chemistry of iodine oxides in the Marine Boundary Layer.** *Geophys. Res. Abs.*, Vol. 3, pp. 6498

Porter, G., F.J. Wright (1953), **Studies of Free Radical Reactivity by the Methods of Flash Photolysis**, *Discuss. Faraday Soc.*, Vol.14, pp.23

Press, W.H., B.P. Flannery, S.A. Teukolsky, W.T. Vetterling (1986): **Numerical Recipes in C: The Art of Scientific Computing**. Cambridge University Press, Cambridge, U.K.

Prinn, R.G., B. Fegley (1987): **The Atmospheres of Venus, Earth and Mars: A critical comparison.** *Annual Review of Earth and Planetary Sciences*, Vol 15, pp. 171-212

Rabinowitch, E. and W.C. Wood (1936): **The extinction coefficients of iodine and other halogens.** *Trans. Faraday Soc.*, Vol. 32, pp. 540-546

Rao, M.L.P., D.V.K. Rao, and P.T. Rao (1974): **Dissociation Energies, r-Centroids and Franck-Condon Factors of IO Molecule.** *Physics Letters*, Vol. 50A, No. 5, pp. 341-342

Revalde, G. and A. Skudra (1998): **Optimization of mercury vapour for high-frequency electrodeless light sources.** *J. Phys. D: Appl. Phys.*, Vol. 31, pp. 3343-3348

Richter, A.(1997): **Absorptionsspektroskopische Messungen stratosphärischer Spurengase über Bremen, 53°N.** *Cuvillier Verlag*, Göttingen, Germany

Richter, A., F. Wittrock, M. Eisinger, and J.P. Burrows (1998): **GOME Observations of Tropospheric BrO in Northern Hemisphere Spring and Summer 1997.** *Geophys. Res. Lett.*, Vol. 25, pp. 2683-2686

Richter, A. (1996): unpublished work, Institute of Environmental Physics, University of Bremen, Germany

Rowley, D.M., M.H. Harwood, R.A. Freshwater, and R.L. Jones (1996): **A novel Flash Photolysis/UV Absorption System Employing Charge-Coupled Device (CCD)**

Detection: A Study of the BrO + BrO Reaction at 298K. *J. Phys. Chem.*, Vol. 100, pp. 3020-3029

Rowley, D.M., J.C. Mössinger, R.A. Cox, and R.L. Jones (1999): **The UV-visible absorption cross-sections and atmospheric photolysis rate of HOI**, *J. Atmos. Chem.*, Vol. 34, pp. 137-151

Saiz-Lopez, A. and J.M.C. Plane (2004): **Novel iodine chemistry in the marine boundary layer.** *Geophys. Res. Lett.*, Vol. 31, L04112, doi: 10.1029/2003GL019215

Saiz-Lopez, A. R.W. Saunders, D.M. Joseph, S.H. Ashworth and J.M.C. Plane (2004b): **Absolute absorption cross section and photolysis rate of I_2.** *Atmos. Chem. Phys.*, Vol. 4, pp. 1443-1450

Sander, S.P. (1986): **Kinetics and Mechanism of the IO + IO Reaction.** *J. Phys. Chem.*, Vol. 90, pp. 2194-2199

Sarkissian, A., J.P. Pommereau, and F. Goutail (1991): **Identification of Polar Stratospheric Clouds from the Ground by visible Spectrometry.** *Geophys. Res. Lett.*, Vol. 18 pp. 779-782

Schall, C. K.G. Heumann, G.O. Kirst (1997): **Biogenic volatile organoiodine and organobromine hydrocarbons in the Atlantic Ocean from 42° N to 72° S.** *Fresenius J. Anal. Chem.,* Vol. 359, pp. 298

Schoeberl, M. R., and D.L. Hartmann (1991): **The dynamics of the stratospheric polar vortex and its relation to springtime ozone depletions.** *Science, Vol. 251, pp. 46-52*

Schoeberl, M.R., L.R. Lait, P.A. Newman, and J.E. Rosenfield (1992): **The structure of the polar vortex.** *J. Geophys. Res.*, Vol. 97, pp. 7859-7882

Schönbein, C. (1840): **Recherches sur la nature de l'odeur qui se manifeste dans certaines actions chimiques.** *C.R. Acad. Sci. Paris*, Vol. 10, pp.706

Schubert, G., A.D. Del Genio, L.S. Elson, G. Keating, A. Seiff, R.E. Young, J. Apt, C.C. Counselman III, A.J. Kliore, S.S. Limaye, H.E. Revercomb, L.A. Stromovsky, V.E. Suomi, F. Taylor, R. Woo, U. von Zahn (1980): **Structure and Circulation of the Venus Atmosphere.** *Journal of Geophysical Research*, Vol. 85, pp. 8007-8025

Shirley, D.A. and W.F.Giauque (1959): **The entropy of Iodine, Heat Capacity from 13 to 327K, Heat of Sublimation**, J. Am. Chem. Soc., Vol. 81, pp. 4778-4779

Sirois, A., L.A. Barrie (1999): **Arctic lower tropospheric aerosol trends and composition at Alert, Canada: 1980-1995.** *J. Geophys. Res.*, Vol. 104, pp. 11599-11618

Solomon, S., A.L. Schmeltekopf, and W.R. Sanders (1987): **On the interpretation of zenith sky absorption measurements.** *J. Geophys. Res.*, Vol. 92, pp. 8311-8319

Solomon, S., R.R. Garcia, and A.R. Ravishankara (1994): **On the role of iodine in ozone depletion.** *J. Geophys. Res.*, Vol. 99, pp. 20491-20499

Spietz, P. (1997): **Spektroskopische und kinetische Untersuchung der Photolyse von Jod in Anwesenheit von Ozon im Rahmen atmosphärenphysikalisch-chemischer Fragestellungen.** Diplomarbeit im Studiengang Physik, Institut für Umweltphysik, Universität Bremen (Diploma Thesis at the Department of Physics, Institute of environmental Physics, University of Bremen)

Spietz, P., J.C. Gómez Martín, and J.P. Burrows (2004): **Quantitative treatment of insufficiently resolved and/or coarsely binned optical multichannel recordings in molecule absorption spectroscopy**, Manuscript, submitted to Spectrochimica Acta Part A, Molecular and Biomolecular Spectroscopy, October 2004

Spietz, P., J.C. Gómez Martín, and J.P. Burrows (2005): **Effects of column density on I_2 spectroscopy and a determination of I_2 absorption cross section at 500 nm**. Manuscript, submitted to ACPD, March 2005

Spietz, P., S. Himmelmann, U.Gross, J. Bleck-Neuhaus, and J.P. Burrows (1998): **A complex approach to investigate the chemistry and kinetics of IO_x using flash photolysis and time resolved absorption spectroscopy.** 15th Int. Symp. Gas Kinetics, Bilbao, Spain.

Stickel, R.E., A. J. Hynes, J. D. Bradshaw, W. L. Chameides and D. D. Davies (1988): **Absorption Cross Sections and Kinetic Considerations of the IO Radical As Determined by Laser Flash Photolysis/Laser Absortption Spectoscopy**, *Journal of Physical Chemistry*, 92, 1862.

Stolarski, R.S. and R. Cicerone (1974): **Stratospheric Chlorine: A possible sink for ozone.** *Can. J. Chem.*, Vol. 52, pp. 1610-1615

Stule, D.R. ed.(1961): **Thermochemical Tables**, Dow Chemical, Midland, Mich., USA

Sulzer, P. and K. Wieland (1952): **Intensitätsverteilung eines kontinuierlichen Absorptionsspektrums in Abhängigkeit von Temperatur und Wellenzahl.** *Helv. Phys. Acta*, Vol. 25, pp. 653-676

Tang, T. and J.C. McConnell (1996): **Autocatalytic release of bromine form Arctic snow pack during polar sunrise.** *Geophys. Res. Lett.*, Vol. 23, pp. 2633-2636

Tellinghuisen, J. (1973): **Resolution of the visible-infrared absorption spectrum of I_2 into three contributing transitions.** *J. Chem. Phys.*, Vol. 58, pp. 2821-2834

THALOZ (2001): **Tropospheric Halogens - Effect on Ozone**. A European Union Fifth Framework Research and Technology Development Programme, Contributing to the implementation of the Key Action "Global change, climate and biodiversity" within Energy, Environment and Sustainable Development: Contract No. EVK2 CT2001 - 00104, at http://www.atm.ch.cam.ac.uk/~thaloz/

Thorne, A., U. Litzén, S. Johansson (1999): **Spectrophysics: Principles and Applications.** Springer, Berlin, Heidelberg, New York, Chap. 7.8, pp.175-179

Tikhonov, A.N. (1963): Solution to incorrectly formulated problems and the regularization method. *Soviet. Math Dokl.* 4, pp.1035-1038

Tuckermann, M., R. Ackermann, C. Gölz, H. Lorenzen-Schmidt, T. Senne, J. Stutz, B. Trost, W. Unold, and U. Platt (1997): **DOAS-observation of halogen radical-catalysed Arctic boundary layer ozone destruction during th ARCTOC campaign 1995 and 1996 in Ny-Alesund, Spitsbergen.** *Tellus*, Vol. 49b, 533-555

Turnipseed, A.A., M.K. Gilles, J.B. Burkholder and A.R. Ravishankara (1995): **LIF detection of IO and the rate coefficients for $I+O_3$ and IO+NO reactions**, *Chemical Physics Letters*, Vol. 242, pp. 427-434

Turnipseed, A.A., M.K. Gilles, J.B. Burkholder and A.R. Ravishankara (1997): **Kinetics of the IO radical: 1. Reaction of IO with ClO**, J. *Phys. Chem. A*, Vol. 101, pp. 5517-5525

Vaidya, W.M. (1937): **The flame spectra of some aliphatic halides. Part I Methyl Iodide**, *Proc. Ind. Acad. Sci.*, Vol. A6, pp. 122-128

Vikis, A.C. and R. MacFarlane (1985): **Reaction of Iodine with Ozone in the Gas Phase**, *J. Phys. Chem.*, Vol. 89, pp. 812-815

Vipond, A., C.E. Canosa-Mas, M.L. Flugge, D.J. Gray, D.E. Shallcross, D. Shah, and R.P. Wayne(2002): **A discharge flow study of the self reaction of IO**. *Phys. Chem. Chem. Phys.*, vol. 4, 3648-3658

Vogt, R., P.J. Crutzen, and R. Sander (1996): **A mechanism for halogen release from sea-salt aerosol in the remote boundary layer.** *Nature*, Vol. 383, pp. 327-330

Vogt, R., R. Sander, R. Von Glasow and P.J. Crutzen (1999): **Iodine Chemistry and its Role in Halogen Activation and Ozone Loss in the Marine Boundary Layer: A Model Study,** *Journal of Atmospheric Chemistry*, Vol. 32, pp. 375–395

von Glasow, R. and P.J. Crutzen (2004): **Tropospheric halogen chemistry**. In: **Treatise on Geochemistry**, edited by K. K. Turekian and H. D. Holland, pp. 21 - 64

Volkamer, R., T. Etzkorn, A. Geyer and U. Platt (1998): **Correction of the oxygen interference with uv spectroscopic (DOAS) measurements of monocyclic aromatic hydrocarbons in the atmosphere**. *Atmospheric Environment*, Vol. 32, No. 21, pp. 3731-3747

White, J.U. (1942): **Long Optical Paths of Large Aperture.** *J. Opt. Soc. Am.*, Vol. 32, pp. 285-288

White, J.U. (1976): **Very long optical paths in air.** *J. Opt. Soc. Am.*, Vol. 66/5, pp. 411-416

Wittrock, F., M. Eisinger, A. Ladstätter-Weißenmayer, A. Richter, and J.P. Burrows (1996): **Ground based UV/vis measurements of O_3, NO_2, BrO, and OClO over Ny Alesund (78°N)**, in *Proceedings of XVIII Ozone Symposium in L'Aquila*

Wofsy, S.C., M.B. McElroy, and Y.L.Yung (1975): **The Chemistry of Atmospheric Bromine.** *Geophys. Res. Lett.*, Vol. 2, pp. 215-218

World Meteorological Organisation (WMO) (1995): **Scientific Assessment of Ozone Depletion: 1994.** Global Ozone Research and Monitoring Project, Report No. 37, published February 1995, 1998 update, Report No. 44, published February 1999

World Meteorological Organisation (WMO) (2003): **Scientific Assessment of Ozone Depletion: 2002.** Global Ozone Research and Monitoring Project, Report No. 47, published March 2003